

Stretch activation in insect fibrillar flight muscle.

Submitted for the degree of Doctor of Philosophy

Nicholas James Carter

Department of Biology,
University of York.

March 1995

Table of Contents

1. INTRODUCTION	
1.1 THE STRUCTURE OF STRIATED MUSCLE	1
1.1.1 <i>Muscle fibres, myofibrils and sarcomeres</i>	1
1.1.2 <i>Sliding filaments</i>	2
1.2 THE CROSS-BRIDGE THEORY OF MUSCLE CONTRACTION	3
1.2.1 <i>The Huxley two state model</i>	3
1.2.2 <i>Huxley and Simmons model (1971)</i>	4
1.2.3 <i>Muscle biochemistry</i>	6
1.3 STRETCH ACTIVATION	7
1.4 THE MECHANISM OF STRETCH ACTIVATION.....	8
1.4.1 <i>The Wray 'match-mismatch' model</i>	9
1.4.2 <i>Connecting filaments</i>	13
1.4.3 <i>Troponin mediated activation</i>	13
1.5 MODELLING STRETCH ACTIVATION.....	14
1.6 MUSCLE FIBRE MECHANICAL ANALYSIS.....	15
2. HARDWARE	17
2.1 INTRODUCTION	18
2.2 POSITION MOTOR AND DRIVER CIRCUITRY	19
2.2.1 <i>Requirements</i>	20
2.2.2 <i>Position motor designs</i>	21
2.2.3 <i>The loudspeaker motor</i>	22
2.2.4 <i>Motor driving circuitry</i>	24
2.2.5 <i>Tuning</i>	26
2.2.6 <i>Calibration</i>	27
2.2.7 <i>Performance</i>	28
2.3 RECORDING TENSION	29
2.3.1 <i>Requirements</i>	29
2.3.2 <i>Micro-Newton strain gauge designs</i>	30
2.3.3 <i>The Akers gauge</i>	32
2.3.4 <i>Tension circuitry</i>	32
2.3.5 <i>Calibration and performance</i>	33
2.3.6 <i>Temperature controlled bath</i>	35
2.4 DATALAB WAVEFORM RECORDER (DL1200)	37
2.5 COMPUTER INTERFACE.....	38
2.6 FUTURE WORK.....	38
3. SOFTWARE	40

3.1 INTRODUCTION	41
3.1.1 <i>Programming Language</i>	42
3.1.2 <i>Source files</i>	43
3.1.3 <i>Overview of muscle program</i>	43
3.2 RECORDING TRACES	45
3.2.1 <i>Introduction</i>	45
3.2.2 <i>Motor Set-up Routine</i>	46
3.2.3 <i>Machine code control of recordings (Sweep)</i>	48
3.2.3.1 <i>Introduction</i>	48
3.2.3.2 <i>Recording phases</i>	50
3.2.3.3 <i>The DAC signal array</i>	50
3.2.3.4 <i>Machine code details</i>	51
3.2.4 <i>Step length change recordings</i>	52
3.2.5 <i>Nyquist recordings</i>	52
3.2.5.1 <i>Nyquist amplitude correction</i>	54
3.2.6 <i>Other recordings</i>	55
3.2.7 <i>Datalab communication</i>	56
3.2.8 <i>Trace Averaging</i>	57
3.2.9 <i>Finding zero tension</i>	57
3.3 VIEWING TRACES.....	58
3.3.1 <i>Plotting the data to screen</i>	58
3.3.2 <i>Printing routines</i>	61
3.3.3 <i>Data smoothing</i>	61
3.4 SAVING AND LOADING TRACES	63
3.5 EXPONENTIAL FITTING.....	63
3.5.1 <i>Introduction to Linear and nonlinear regression</i>	64
3.5.2 <i>Non-linear curve-fitting algorithms</i>	65
3.5.3 <i>Exponential fitting procedure</i>	67
3.5.4 <i>Exponential fitting software</i>	69
3.5.5 <i>Data Weighting</i>	70
3.5.6 <i>Exponential fitting problems and considerations</i>	70
3.6 SINUSOIDAL ANALYSIS	70
3.7 FUTURE WORK	72
3.7.1 <i>Curve Fitting to Nyquists</i>	72
3.7.2 <i>High frequency correction</i>	72
4. MATERIALS, METHODS AND CONTROLS	74
4.1 INTRODUCTION	75
4.2 MUSCLE FIBRES	75
4.2.1 <i>Flight muscle dissection</i>	75

4.2.2	<i>Fibre size</i>	76
4.2.3	<i>Attaching fibres to the apparatus</i>	77
4.2.3.1	T-clips.....	77
4.2.3.2	Cellulose nitrate glue.....	78
4.2.4	<i>Rest length</i>	79
4.2.5	<i>Mounted fibre lifetime</i>	80
4.3	SOLUTIONS.....	81
4.3.1	<i>Constituents</i>	81
4.3.2	<i>Changing solutions</i>	82
4.4	NYQUIST RECORDINGS.....	83
4.4.1	<i>Pre-recording oscillation</i>	83
4.4.2	<i>Temperature</i>	85
4.4.3	<i>Oscillation amplitude</i>	87
4.4.4	<i>Pre-stretch</i>	89
4.5	STEP LENGTH CHANGE RECORDINGS.....	91
5. THE EFFECTS OF MILD CALPAIN DIGESTION ON <i>LETHOCERUS</i> INDIRECT		
FLIGHT MUSCLE.....93		
5.1	INTRODUCTION.....	94
5.1.1	<i>Troponin-H</i>	94
5.1.2	<i>Calpain</i>	96
5.1.3	<i>Calpain specificity</i>	97
5.2	MATERIALS AND METHODS.....	97
5.2.1	<i>Digestion conditions and solutions</i>	97
5.2.2	<i>Fibre mechanics</i>	98
5.2.3	<i>Digestions for PAGE and the Western Blot</i>	99
5.2.4	<i>SDS Poly-acrylamide gel electrophoresis (PAGE)</i>	99
5.2.5	<i>Western Blot</i>	100
5.3	RESULTS.....	101
5.3.1	<i>Electrophoresis</i>	101
5.3.2	<i>Western Blot</i>	102
5.3.3	<i>Step length changes</i>	102
5.3.4	<i>Sinusoidal analysis</i>	104
5.3.5	<i>Electron micrographs</i>	105
5.4	DISCUSSION.....	107
5.4.1	<i>Passive stiffness and stretch activation</i>	108
5.4.2	<i>Possible roles for Tn-H in stretch activation</i>	109
5.4.2.1	Tn-H and the Wray model.....	109
5.4.2.2	Tropomyosin displacement.....	110
5.4.2.3	Direct interaction with the Cross-bridge.....	110

6. INSECT FLIGHT MUSCLE CROSS-BRIDGE KINETICS.....	112
6.1 INTRODUCTION	113
6.2 MATERIALS AND METHODS	113
6.2.1 T_1 - T_2 with passive component subtracted	114
6.2.2 Changes in r_2 , r_3 and r_4 with step size and $[P_i]$	114
6.2.3 Comparison of kinetics at 0% and 1% strain	115
6.3 RESULTS	116
6.3.1 T_1 - T_2 Active minus passive	116
6.3.2 Step size and r_2 , r_3 and r_4	121
6.3.3 The effect of P_i on the step size dependence of r_2	121
6.3.4 The effect of P_i on the T_1 - T_2 curves	121
6.3.5 The effect of P_i on the step size dependence of r_3 and r_4	124
6.3.6 The Effect of P_i on the Nyquist plot.....	124
6.3.7 The kinetics of <i>Lethocerus</i> flight muscle at 0% and 1% strain	124
6.4 DISCUSSION	133
6.4.1 The active component T_1 - T_2	133
6.4.2 Phosphate and the step size dependence of r_3 and r_4	135
6.4.3 Phosphate and the step size dependence of r_2	136
6.4.4 The effect of P_i on the fibre stiffness.....	137
6.4.5 Fibrillar muscle kinetics at 0% and 1% strain.....	137
7. A STOCHASTIC MODEL OF CROSS-BRIDGE CYCLING AND STRETCH	
ACTIVATION	138
7.1 INTRODUCTION	139
7.1.1 Cross-bridge models	139
7.2 A NOVEL ALGORITHM FOR STOCHASTIC MODELLING.....	140
7.2.1 Storing time information for each element in the model	142
7.2.2 Verification of the model mechanism	143
7.3 SOFTWARE	147
7.3.1 The Stoch subroutine	147
7.3.2 The model run screen.....	150
7.4 MODEL PARAMETERS.....	151
7.4.1 Free energy profiles.....	154
7.4.2 Rate constant values	155
7.4.3 Cross-bridge distortion distribution	159
7.4.4 ATPase	160
7.5 MODEL OUTPUT.....	160
7.5.1 Model T_1 - T_2 curves	160
7.5.2 Step length changes	164
7.5.3 Force-velocity.....	165

7.5.4 Lombardi Staircase Experiment.....	165
7.5.5 Stretch activation.....	169
7.6 DISCUSSION	170
7.6.1 Huxley and Simmons (1971) characteristics.....	170
7.6.2 Step length changes	172
7.6.3 Muscle shortening and ATPase	173
7.6.4 Stretch activation.....	175
7.6.5 Future work.....	176

Acknowledgements

I would like to thank David White for the help and encouragement he gave throughout this work. Thanks to Justin Molloy for his technical expertise and help. Thanks to John Sparrow for the use of his laboratory for some of the biochemistry and for helpful discussions about Troponin-H. Thanks to Jody Dantzig for her enthusiasm and assistance with the calpain work.

Also many thanks to my family and friends for their support throughout this work.

Special thanks to Alessandra for her support and patience all the time that I was “nearly” finished.

Declaration

Unless otherwise stated in the text, the work described in this thesis is my own. None of this work has been accepted in any previous application for a degree. Some of the calpain digestion mechanical experiments were performed in collaboration with Jody Dantzig. Electron micrographs in the Chapter 5 were made by Meg Stark.

Nick Carter

March 1995

Abstract

An apparatus was built to perform mechanical experiments on single skinned muscle fibres. Fibre length was controlled using a purpose built motor capable of applying rapid ($<180\mu\text{s}$) length changes. Tension was measured using a strain gauge with a high frequency response. The muscle bath was held at a constant temperature using a Peltier effect heat pump.

The software written to control the apparatus had several important features that provided the means for recording better quality data. The ability to change sample rate in mid-recording enabled the optimal capture of processes of different rates in the same trace. Fast machine code routines allowed very high sample rates where needed and very rapid data plotting. On-line Fourier analysis and exponential fitting routines gave immediate feedback during the course of experiments. Signal averaging and data smoothing routines increased the signal to noise ratio of recorded traces.

Selective digestion of the thin filament protein troponin-H by the enzyme calpain, resulted in a decrease in the amplitude of delayed tension. The changes were not accompanied by a change in relaxed or rigor stiffnesses. It was concluded that troponin-H is associated with the mechanism of stretch activation.

The insect fibrillar muscle cross-bridge was characterised in a T_1 - T_2 plot by subtracting the passive component from the active traces. By modelling using the Huxley-Simmons equations and also the stochastic cross-bridge model, it was concluded that the size of the working stroke of the insect muscle is longer than that of vertebrate striated muscle, in the region of 10nm. The kinetics of the delayed tension change in insect muscle was investigated under varying concentrations of inorganic phosphate and varying step size.

A stochastic multi-state cross-bridge model was developed. The rate constants were manipulated to investigate what is required to reproduce the non-linear characteristics of the tension phases observed in mechanical fibre experiments. Two mechanisms for stretch activation in insect fibrillar muscle are also modelled.

Abbreviations

A	actin
A_2, A_3, A_4	amplitudes of exponentials in transient phases 2, 3 and 4
ADC	analogue to digital converter
ADP	adenosine-5'-diphosphate
ATP	adenosine-5'-triphosphate
ATPase	adenosine-5'-triphosphatase
DAC	digital to analogue converter
DLM	dorsal longitudinal muscle
GPIB	General Purpose Interface Bus
HMM	heavy meromyosin
LED	light emitting diode
LMM	light meromyosin
M	myosin
PAGE	Polyacrylamide gel electrophoresis
P_i	Inorganic phosphate
r_2, r_3, r_4	mechanical rate constants for transient phases 2, 3 and 4
S1, S2	Myosin subfragments 1 and 2
SDS	sodium dodecyl sulphate

1. Introduction

In order to drive the wing-beat cycle in flight, the flight muscles of many insects are stretch activated. Rather than initiating each contraction with a nerve impulse, the muscle contraction is activated by the stretch that occurs with each wing-beat. This type of muscle is referred to as insect fibrillar flight muscle. The delayed rise in tension following a stretch is not peculiar to insect flight muscle. Under the right conditions many types of muscle can be made to behave in this way. However in insect muscle the size of the tension rise is very large.

The mechanism of stretch activation in insect fibrillar flight muscle is not understood, although several models have been suggested. The aim of the work described in this thesis was to investigate the mechanical properties of active insect fibrillar flight muscle, with particular attention to the large amplitude stretch activation seen in this muscle.

1.1 The structure of striated muscle

1.1.1 Muscle fibres, myofibrils and sarcomeres

All types of striated muscle, including insect fibrillar flight muscle, have the same basic structure. The cellular unit of striated muscle is the muscle fibre. Fibres are unbranched and can span the whole length of the muscle. The diameter of most striated muscle fibres lies in the range 30 μm and 100 μm , though some insect muscle fibres can be over 200 μm .

The contractile organelles within the fibre are the myofibrils. A single fibre can contain a thousand or more myofibrils, which run the entire length of the fibre. Myofibrils are between 1 μm and 3 μm in diameter. Often the second most abundant fibre organelles, after the myofibrils, are the mitochondria. The volume ratio of mitochondria to myofilaments is an indication of the metabolic activity or work performed by that fibre (Pennycuik and Rezende, 1984). Because of the high metabolic cost of insect flight, insect fibrillar flight muscle contains roughly equal volumes of mitochondria and myofilaments.

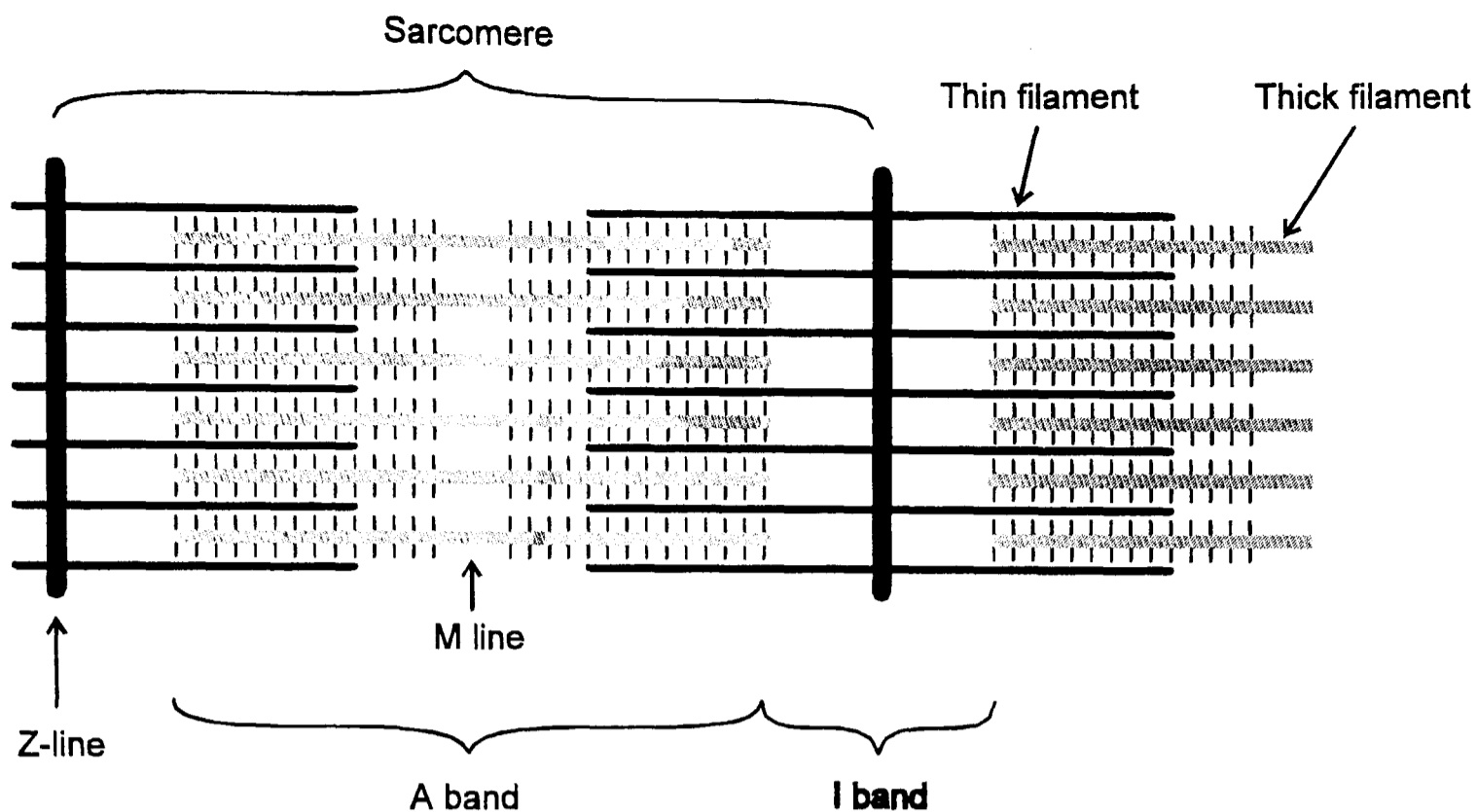


Figure 1.1: A schematic illustration describing the striated muscle sarcomere and its major structures. The striations are the result of alternating A and I bands. The A-band is the region containing the whole length of the thick filaments. The I band is the region between A bands consisting of part of the length of the thin filaments, with the Z-line at the centre.

1.1.2 Sliding filaments

The banding in striated muscle is composed of alternating bands of varying refractive index called A-bands and I-bands. Using electron microscopy H. E. Huxley (1953) made the observation that these bands consist of two types of interdigitating filaments (thick and thin). Huxley also made the suggestion that the two major muscle proteins actin and myosin were situated in the thin and thick filaments respectively.

H. E. Huxley suggested that during active shortening, the two sets of filaments slide past on another, rather than undergo any change in filament length. This view of muscle contraction was supported by work by A. F. Huxley and Niedergerke (1954). Using interference microscopy, Huxley and Niedergerke were able to show that during active contraction the width of the A bands remained constant whilst the I bands shorten. An observation consistent with the sliding filament model.

A schematic diagram showing the main structures that make up a striated muscle sarcomere is shown in Figure 1.1. The sarcomere is the contractile unit of the muscle composed of the thick and thin interdigitating filament.

1.2 The Cross-bridge theory of muscle contraction

Given the information that the two sets of filaments slide past each other during length changes, it became quite plausible that the mechanism by which muscle produces force involves interaction of the proteins contained in the two types of filament. One of the predictions of a model in which force is produced at the region of overlap is that force should be proportional to the degree of overlap. This was shown to be the case by Gordon *et al* (1966).

1.2.1 The Huxley two state model

In 1957 A. F. Huxley proposed a mechanism of muscle contraction in which projections from the thick filaments interacted cyclically and independently with sites on the thin filaments. The projections are now referred to as cross-bridges, and most models of muscle contraction since then have incorporated the idea of cross-bridges cycling in this way.

In his model, Huxley considered the cross-bridges to exist in just two states, attached to the thin filament or detached (see Figure 1.2). The rate constants for transition between the two states are f for attachment and g for detachment. The fraction of the total population of cross-bridges attached is n , leaving a total of $1-n$ detached.

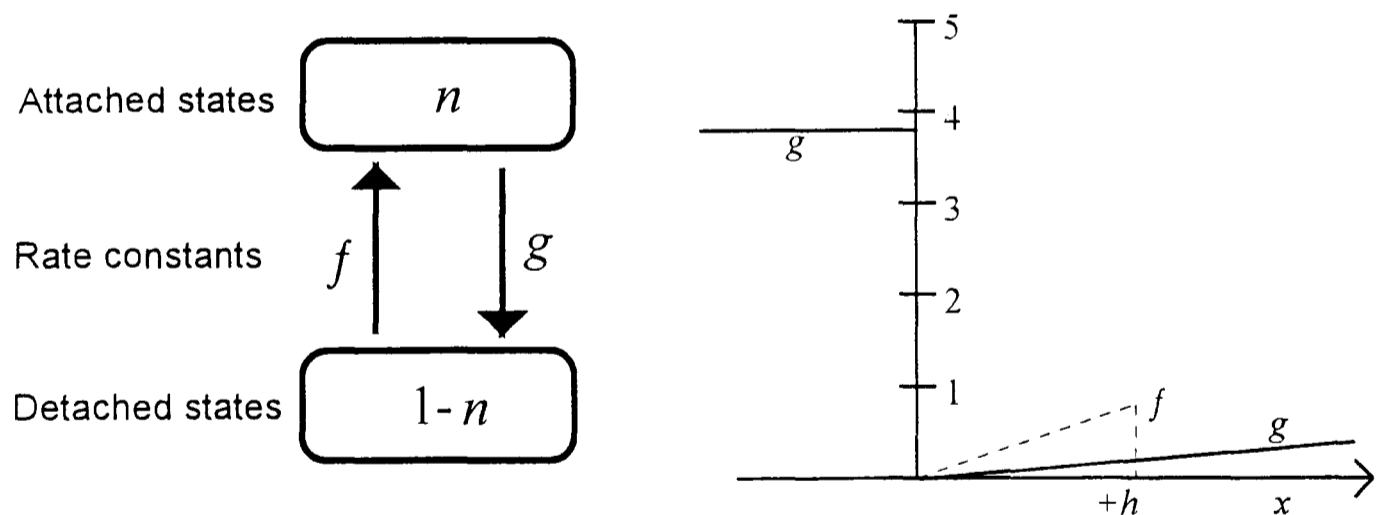


Figure 1.2: Schematic diagram of Huxley 1957 two-state model. Proportion n of the total cross-bridge population are in the attached force-producing state, $1-n$ are detached. The graph shows the dependence of the rate constant for attachment (f , dashed line) and detachment (g , solid line) on cross-bridge distortion (x).

Huxley suggested that the attached cross-bridges behave elastically, the force produced by an attached cross-bridge being proportional to its distortion. Also that such distortion affects the values of f and g . For negative distortions $f=0$ and g is very large. For positive distortions both increase proportionally with

displacement, with f approximately eight times the magnitude of g . In this scheme, random thermal motion makes it possible for cross-bridges to attach with positive distortion, and hydrolysis of a single ATP molecule is necessary for detachment.

With this simple two state model, Huxley was able to account for the findings of Hill (1938), for tension, contraction velocity and heat production. This model does not however account for the results of transient experiments, in which tension is recorded during a rapid change in length.

1.2.2 Huxley and Simmons model (1971)

In 1971, Huxley and Simmons published a paper in which they studied the tension response to rapid step changes in length. Using apparatus with greatly improved temporal resolution they were able to record previously unnoticed features on the tension response. Using such results they proposed a model in which generation of force occurs after attachment, rather than relying on thermal motion for attachment in a positive distortion position.

The response of a muscle to a rapid release follows a characteristic sequence. A diagram describing this sequence is shown in Figure 1.3. Firstly a rapid tension change occurs which is in phase with and in the same direction as the length change. This elastic part of the response is referred to as phase 1. Creating a length-tension plot for this part of the curve allows the instantaneous stiffness of the muscle to be calculated. Huxley and Simmons (1971) showed that in active vertebrate muscle, stiffness measured in this way is proportional to the degree of filament overlap and therefore to the number of cross-bridges attached.

Phase 2 is the rapid recovery in tension towards the starting tension. Two possible reasons are suggested for this recovery. Firstly that during phase 2 there is a redistribution of attached and detached cross-bridges resulting in a recovery of force (Podolsky *et al*, 1969). Secondly the cross-bridges remain attached throughout phase 2 and undergo a conformational change between different attached states. It was the second case that Huxley and Simmons suggested in their model. Evidence in favour of the second explanation is that a second length change occurring at the end of phase two demonstrates the same stiffness as the first length change. This indicates that the same number of cross-bridges are attached at this stage in the tension transient.

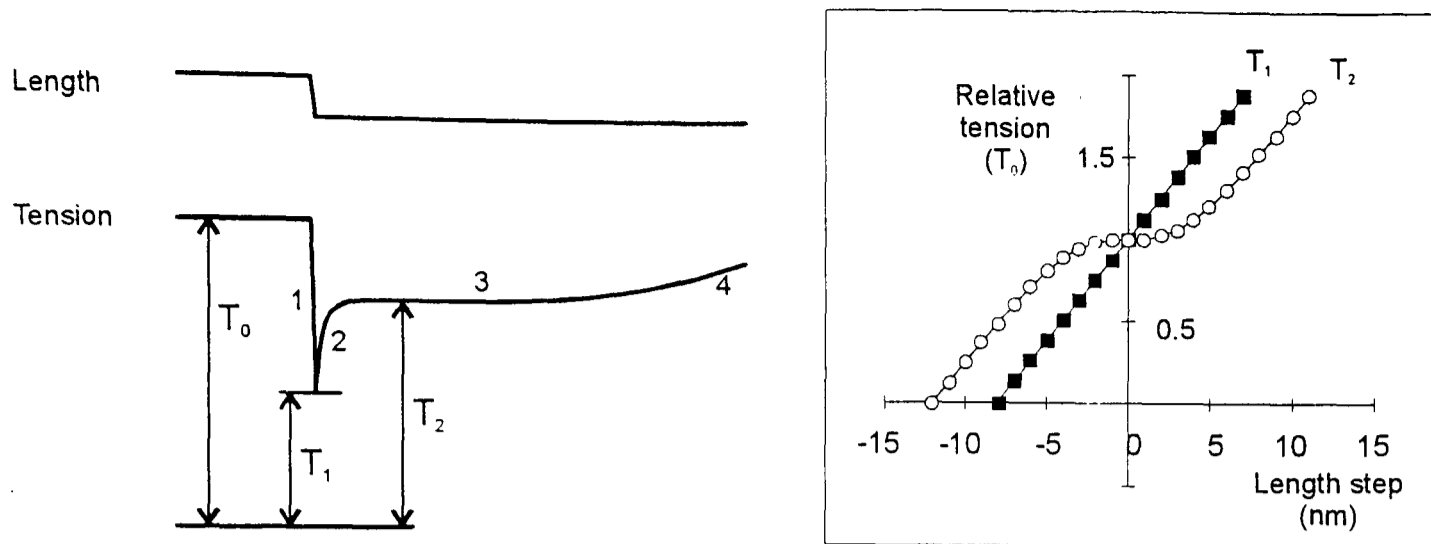


Figure 1.3: Diagram to explain the derivation of the T_1 - T_2 curves (Huxley and Simmons, 1971). The tension response to a rapid length change can be separated into four distinct phases. Phase 1 is the elastic phase showing the tension changes that are in phase with the length change. The plotted value of T_1 is the ratio of the tension at the end of phase 1 to the starting tension T_0 . Phase 2 is a rapid process in which tension recovers towards T_0 . The value of T_2 is the ratio of tension at the end of phase 2 to T_0 . Phases 3 and 4 are slower processes not considered in the model. The T_1 - T_2 curves shown are the output from the mathematical model of a cross-bridge moving between two attached states.

Huxley and Simmons (1971) measured the tensions at the end of phases 1 and 2, and showed the results in a T_1 - T_2 plot. The units of the applied length step are shown in nanometres. This refers to nanometres per half sarcomere, meaning the relative displacement of the filaments. A T_1 - T_2 plot is shown in Figure 1.4. This plot is not real data but was generated from the Huxley and Simmons mathematical model. In active muscle the T_1 curve describes the behaviour of an elastic element, with a linear relationship with the applied length change. The T_2 curve however has a non-linear relationship with the applied step size. With very small step sizes the phase 2 recovery returns tension to the level of starting tension (T_0).

The explanation for the shape of the T_2 curve is that at these small step length changes the cross-bridges move through the working stroke. In the mathematical modelling section, two cross-bridge positions are considered. At steady state it is assumed that equal numbers of cross-bridges exist in both states. On releases the cross-bridge populations are redistributed with the tendency to move into the second state. Conversely stretches have the tendency to move cross-bridges into the first state. In the linear regions of the T_2 curve at the larger step sizes, the cross-bridges are all in one or the other state.

This model of cross-bridge action is an improvement on the Huxley (1957) scheme because force generation occurs after binding to actin, rather than relying on binding in a strained state. Using the model, Huxley and Simmons were able to estimate that the size of the working stroke of the cross-bridge was in the region of 8nm.

1.2.3 Muscle biochemistry

The most abundant proteins in muscle are myosin and actin. Monomeric actin is a globular protein (G-actin) of molecular weight 42 000Da. Under physiological conditions actin form into a double helix which makes up the majority of the thin filaments (F-actin). The helical nature of the thin filament is evident from both electron microscopy and X-ray diffraction studies of whole muscle. The atomic structure of G-actin complexed with DNase 1 has been solved by Kabsch *et al* (1990) using X-ray crystallography. The molecule consists of two domains. It is thought that the larger of the domains is situated towards the centre of the filament, while the myosin binds to the smaller domain.

Myosin is a high molecular weight protein (MW 520 000Da), which like actin polymerises at physiological ionic strengths. When denatured, myosin dissociates into two heavy chains (MW 220 000Da) and four light chains (MW 20 000Da). Mild digestion with chymotrypsin will cleave the myosin molecule into two fragments, heavy meromyosin (HMM) and light meromyosin (LMM). The LMM is a rod-like α -helical region of the heavy chain. In the whole molecule, the LMM of the two heavy chains form a coiled coil. This coiled-coil region of the myosin links with other myosin molecules in the formation of the back-bone of the thick filament. The HMM can be further cleaved into subfragments 1 (S1, MW 120 000Da) and 2 (S2, MW 100 000Da) using papain or chymotrypsin.

S1 is the globular head of the myosin molecule which attaches to actin during contraction. The S1 head is also the location of the myosin light chains. In vertebrate skeletal muscle the light chains do not perform a regulatory role. However in the majority of invertebrate muscles, including insect flight muscle, the light chains are regulatory Lehman (1977).

Many of the major muscle proteins are present in the cytoskeleton of non-muscle cells as well as the myofibrils of muscle cells. An example of such a protein is tropomyosin. Tropomyosin is an α -helical coiled coil dimer which extends across 7 actin monomers. Tropomyosin sits in the groove of the actin filament, slightly overlapping the neighbouring tropomyosin molecule. Thin

filament regulation requires both the tropomyosin and another complex called troponin.

Troponin consists of three subunits Troponin-C (calcium binding), Troponin-I (inhibitory) and Troponin-T (tropomyosin binding). When calcium binds to troponin-C, the whole tropomyosin-troponin complex shifts in position. The tropomyosin moves out of the thin filament cleft, in the process revealing myosin binding sites.

Besides these force producing and regulatory muscle proteins there are a number of proteins with structural roles in the sarcomere. One such protein is titin, an enormous protein with a molecular weight close to 3 000 000Da. Titin connects the thick filament to the Z-line. It is responsible for the passive stiffness in striated muscle (Wang *et al*, 1993) and probably helps keep the thick filaments towards the centre of the sarcomere.

Another large myofibrillar protein is nebulin (MW 600 - 800KDa). Immunological studies show that nebulin lies parallel to the thin filament, extending from the Z-line to the end or possibly just beyond the end of the thin filament. (Wang & Wright, 1988). There are 3 or 4 nebulin molecules per thin filament. Nebulin may have a role as a template controlling thin filament length.

1.3 Stretch activation

In muscles which exhibit stretch activation, fully calcium-activated fibres can be activated further by applying a small stretch. In insect fibrillar flight muscle stretch activation is a property of the myofibrillar proteins, rather than a membrane mediated response (Jewell and Rüegg, 1966).

In order to avoid confusion, it is necessary to clarify the meaning of the word activation used here. In terms of stretch activation, the word 'activation' can refer to any of three properties demonstrated in insect fibrillar flight muscle. Following a small stretch the muscle shows

- (1) a delayed tension rise,
- (2) a maintained increase in tension and
- (3) a maintained increase in ATPase activity.

These three observations can be categorised as transient (1) and maintained (2 and 3) effects.

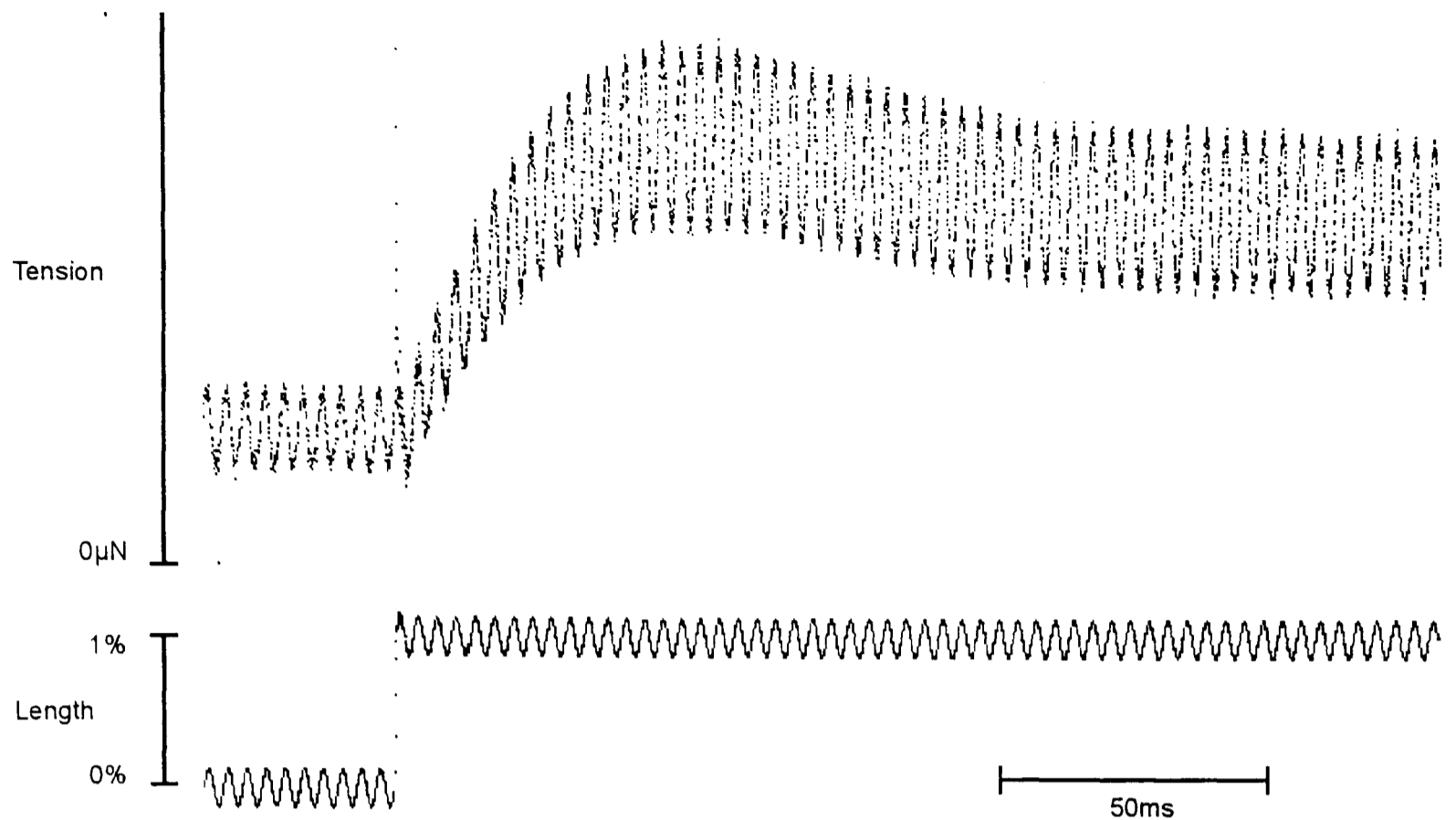


Figure 1.4: The change in stiffness during the delayed tension rise of stretch activation. A low amplitude (0.2%) high frequency (280Hz) oscillation is superimposed over a 1% step stretch of a single insect flight muscle fibre (*Tipula* dorsal longitudinal muscle).

The delayed tension rise following stretch is not a response only found in insect fibrillar flight muscle. Under certain conditions vertebrate skeletal muscle can show a delayed tension rise after stretch (Rüegg *et al*, 1970) and given sinusoidal oscillations perform work on the apparatus (Kawai & Brandt, 1980). In comparison to insect fibrillar muscle however, the stretch activation shown in vertebrate skeletal muscle is low in amplitude and shows none of the maintained observations seen in insect fibrillar muscle and cardiac muscle.

Cardiac muscle gives delayed tension which is as large as that in insect fibrillar muscle (Steiger, 1977). This stretch activation is also similar to that in insect fibrillar muscle in that the steady state tension remains high after the stretch.

1.4 The Mechanism of Stretch Activation

In both insect fibrillar flight muscle (see Figure 1.4) and vertebrate cardiac muscle (Steiger, 1977 in Figure 27), the tension rise following stretch is accompanied by an increase in high frequency stiffness. It is accepted that stiffness measured in this way gives an indication of the number of cross-bridges attached. The increase in stiffness which accompanies the rise in tension

indicates that the mechanism of stretch activation must be one of *recruitment*. Any model proposed to explain the mechanism of stretch activation must show how stretch of the sarcomere increases the number of the cross-bridges that are attached and producing force.

A structural basis to the mechanism of stretch activation in insect fibrillar muscle is yet to be determined, though several possible mechanisms have been proposed. The mechanism which has received most attention is that of Wray (1979b) which is based on the observed geometry of the myofilaments. In other mechanisms people have focused their attention on proteins that are peculiar to this muscle. Mechanical strain on these novel or modified proteins in some way changes the interaction of actin and myosin. Connecting filaments which attach the thick filaments to the Z-line in insect muscle could directly activate the thick filament (Thorson & White, 1969). Finally, the unusually large troponin complex in insect flight muscle (Bullard, 1984) may detect relative displacement of the two filament types. There follows a more detailed description of these mechanisms.

1.4.1 The Wray 'match-mismatch' model

Using X-ray diffraction Wray (1979a) suggested that in *Lethocerus* flight muscle, the thick filament consists of a four start helix with 38.5nm helicity. Wray (1979b) suggested that it was no coincidence that 38.5nm was also the distance between preferred myosin binding sites on the thin filament, rather that this filament geometry was the structural basis for the high degree of stretch activation found in this muscle.

If Wray's interpretation of the X-ray data is correct, it is possible to show that a small displacement of the two filaments can result in a large change in the population of cross-bridges that can attach and produce force. Figure 1.5 shows a pictorial representation of this model.

The six thin filaments that surround a single thick filament are shown "unrolled" in **(a)**. Each half turn of the thin filament is 38.5nm long. The half turn consists of an active region where cross-bridges can bind (black) and the remainder (white) where binding is unfavourable. The opposing pairs of filaments surrounding a thick filament share the same orientation. This arrangement of the thin filaments has been shown to exist in insect flight muscle in rigor (Reedy, 1968).

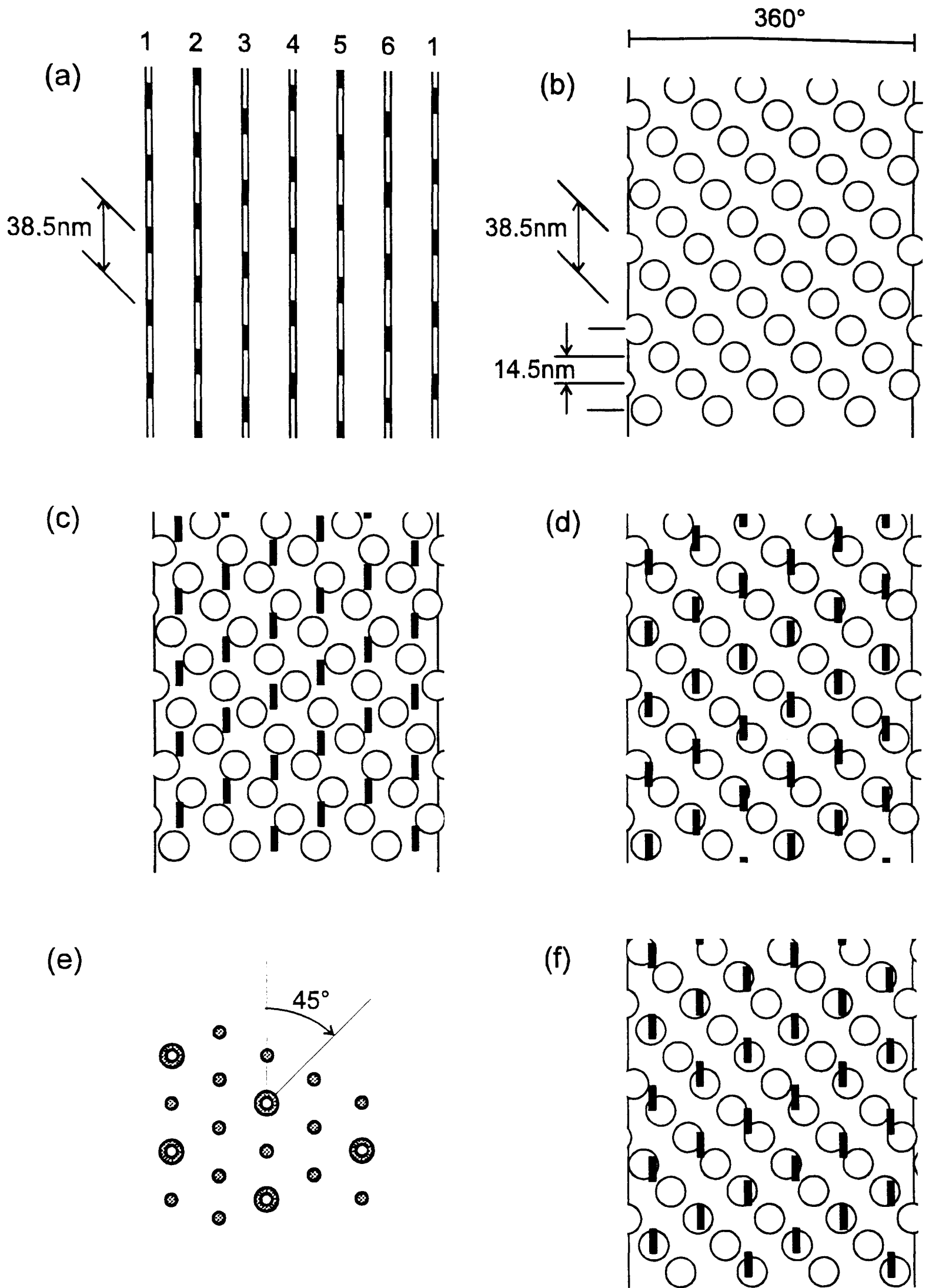


Figure 1.5: The Wray model of stretch activation in insect fibrillar flight muscle. The potential cross-bridge binding sites (a, black regions) are superimposed over the cross-bridge binding ranges (b, circles). In the state shown in (c), the muscle is at rest length. In (d) a small longitudinal displacement (muscle stretch) greatly increases the proportion of cross-bridges that can attach. However the same level of activation can be achieved by a small twist in the filament. In (f) the low activation state (c) has been modified by a small 45° rotation as shown in (e). (Modified from Wray, 1979).

The myosin thick filament itself is also shown unrolled (**b**). The circles represent an assumed range for possible attachment of a cross-bridge pair. The four myosins per 14.5nm repeat was suggested by Reedy (1968). As drawn, the potential binding sites in (a) and the cross-bridge ranges in (b) share a helix in common. That is a four start helix with an axial separation of 38.5nm for each track.

When the drawings in (a) and (b) are superimposed, the tracks of the four start helices may be in or out of phase. This phase relationship has a very large effect on the proportion of cross-bridges that may attach and produce force. In (c) the phase relationship is such that a minimum number of interactions are occurring. Applying a small stretch to the muscle (d), brings the tracks into phase. Here the maximum number of cross-bridges can interact with the actin active sites.

Assuming a sarcomere length of $2.7\mu\text{m}$ for active *Lethocerus* muscle, the 38.5nm axial repeat corresponds to a 2.85% length change of the whole muscle. There is some evidence from work on whole fibres that supports this inherent periodicity in the muscle. Abbott and Cage (1978) demonstrated a 3% periodicity in the in-phase and quadrature stiffness on stretching a sub-maximally activated *Lethocerus* flight muscle fibre. In their experiment, a single fibre was stretched in 0.25% increments from 0% to more than 8%. At each increment, an oscillation of 0.07%, 5Hz was applied and in-phase and quadrature stiffness measured. Throughout the stretch from 0% to 8% the tension increases in an almost linear fashion. However, the stiffness measurements rise from almost zero at the 0% level to a peak at roughly 4%. The stiffnesses then decrease and rise to another peak at near 7%.

To date this is the only mechanical evidence in support of Wray's model. The observed 3% periodicity does fit with the inter filament sliding distances suggested by the Wray model. On closer inspection the Abbott and Cage result has some features which would not be predicted by the Wray model.

The observed periodicity is not observed at saturating levels of calcium. The authors claim that this is due to heterogeneity of sarcomere lengths at full activation. In terms of the Wray model this is an unsatisfactory explanation. Since stretch activation increases with calcium concentration right up to saturation, then so should such an observation that claims to explain the mechanism of stretch activation.

The shapes of the stiffness curves is not that predicted by the Wray model. There is a maximum at 7% and one at 4% stretch. Wray's geometric

interpretation, with its 3% repeat suggests that a further peak should exist in the 1% region. There is no peak at 1%.

In the Abbot and Cage results, it is surprising that no periodicity is apparent in the tension signal itself. It is not the case that stretch activation is a transient phenomenon detectable only by oscillation or in the short period of time following a stretch. The maintained characteristics, the increased ATPase and tension, should also show a 3% repeat. No such relationship is apparent here in the tension signal, or has been demonstrated in ATPase.

In order for Wray's model to work, several assumptions must be made about the proteins involved. As drawn in his diagram (reproduced in Figure 1.5 part (a)), Wray assumes that approximately 36% of the thin filament half-turn has available actin sites. Wray does not explain why this value was chosen. The proportion is equivalent to 2.5 actin monomers out of the 7 in a half turn of the filament. The real value is difficult to determine. In rigor it is thought that 70% of cross-bridges are attached (Lovell *et al.*, 1981), though whether this reflects the proportion of cross-bridges which can bind and produce force in active muscle is difficult to say.

Similarly the range of movement of individual cross-bridges (circles in Figure 1.5, part (b)) is difficult to determine. As drawn, the circles in the Wray model correspond to a longitudinal attachment range of 15nm and an axial attachment range of 33°.

One critical factor which is not accounted for in the explanation of the model is that described in (e) and (f) of Figure 1.5. If the thick filament is allowed to rotate through 45° as described in (e) then the resulting helix overlap picture is that shown in (f). That is the same amount of activation which previously required a 1.5% stretch of the muscle can also be achieved by a very small twist in the thick filament. Indeed the state drawn in (c) is energetically a highly unstable one. Once cross-bridges attach and favour a twist in one direction, yet more cross-bridges attach and twist the filament till the helices fully overlap. Present knowledge about filament structure suggest that there is no reason why filaments are not free to twist in this way.

This criticism considers the possibility of a small twist in only one of the filament types. When one also takes into account the possibility that the thin filaments may also twist to favourable positions, the idea that the filaments would remain in state (c) becomes less believable.

For the Wray model to discount this possibility, it is necessary to show that the filaments are not free to twist in this way. It is very unlikely that the filaments themselves have a high enough torsional stiffness to prevent such twisting.

Instead, the model requires that a protein physically prevents such twist from occurring.

1.4.2 Connecting filaments

Insect fibrillar flight muscle has very short I-bands. The thick filaments extend almost all the way to the Z-lines. This distance does not alter very much, since the amplitude of the length change in the flying insect is very small.

Auber and Couteaux (1963) saw a link between the thick filaments and the Z-line in electron micrographs of insect flight muscle. These protein links are called C-filaments or connecting filaments.

The protein responsible for these links has been isolated and shown to be a large protein referred to as p800 because of its molecular weight of 800KDa (Lakey *et al*, 1990). This is the same protein as projectin, a large protein shown to be present in the locality of the Z-lines (Saide *et al*, 1990).

Immunofluorescence and electron microscopy showed that projectin spanned the gap between the thick filament and the Z-line, forming a mechanical link (Lakey *et al*, 1990). Projectin is antigenically related to vertebrate titin (connectin) and nematode twitchin, which occur at the same location in these muscles.

The connecting filaments are thought to be the component in insect flight muscle which give it its high relaxed stiffness (White, 1983). This high stiffness can be accounted for simply by the fact that insect flight muscle C-filaments are much shorter than their non-fibrillar equivalents. It is not necessary that the projectin be any stiffer per unit length than vertebrate titin to explain this observation.

Thorson & White (1969) suggested that strain acting through the C-filaments onto the thick filaments may be involved in stretch activation.

1.4.3 Troponin mediated activation

The troponin complex of insect flight muscle is very much larger than its vertebrate equivalent, with a total molecular weight of approximately 120000Da compared to 70 000Da in vertebrate striated muscle. The difference in size is due to a larger Tn-T (MW 53 000Da compared to 31000-36000Da in rabbit) and to the existence of another heavy component with an apparent molecular weight of 80000Da (Bullard, 1984).

The heavy component is called troponin-H (Tn-H). It is related to the heavy tropomyosins of *Drosophila* flight muscle (Bullard *et al*, 1988). There is good

evidence that the carboxyl end of Tn-H extends away from the thin filament. Firstly, the carboxyl terminus, which has been sequenced in *Drosophila*, has a high proline content. Secondly, the Tn-H molecule is extremely susceptible to digestion by calpain, a calcium activated protease.

Bullard (1984) suggested that the mere size of the troponin complex in insect fibrillar muscle could prevent cross-bridges from binding at certain muscle lengths. The possibility that Tn-H plays a role in stretch activation in fibrillar flight muscle inspired the work described in chapter 5.

1.5 Modelling stretch activation

Using the model proposed by A. F. Huxley (1957), Thorson and White (1969) developed a simple two state model of stretch activation. In this model the tension contributed by all n attached cross-bridges is assumed to be equal. The change in tension on stretch must therefore change n by altering ratio of the attachment (f) and detachment (g) rates.

There follows a brief description of the derivation of this model. From the Huxley 1957 model it can be seen that the change in the value of n can be written as follows:

$$\frac{dn}{dt} = f(1-n) - g.n$$

$$\frac{dn}{dt} = f - n.(f + g) \quad (1.1)$$

In steady state conditions $\frac{dn}{dt} = 0$, therefore:

$$n = \frac{f}{f + g} \quad (1.2)$$

Since all attached cross-bridges are assumed to contribute the same force, this expression describes the relationship between tension and the attachment and detachment rate constants.

In steady state conditions the cycling rate or flux in the model is $n.g$ (or $f.(1-n)$) this can be written:

$$\text{flux} = \frac{f.g}{f + g} \quad (1.3)$$

Assuming that a fixed number of ATP are hydrolysed per cycle, this estimation of flux is proportional to the ATPase of the muscle.

If non-steady state conditions are considered, we have to account for changes in n . This is written as an exponential function.

$$n = A + Be^{-kt} \quad (1.4)$$

Differentiating:

$$\frac{dn}{dt} = -kBe^{-kt}$$

$$\frac{dn}{dt} = kA - kn$$

Equation (1.1) shows that k in the last equation is equal to $f+g$, so the system approaches equilibrium with the rate constant $f+g$.

1.6 Muscle fibre mechanical analysis

To investigate the frequency characteristics of a system, the system must be perturbed in some way, and the response to that perturbation analysed. This type of analysis falls into three main categories. These are step perturbations, sinusoidal analysis and white noise analysis. In a linear system all these methods are equivalent extracting the same information from a system. However it is important to note that active muscle is a nonlinear material, so these different methods of analysis do not always provide the same results.

One of the simplest perturbations that can be applied to a muscle is a length change. In the majority of single muscle fibre experiments, the fibre length is controlled whilst the tension is recorded and analysed. The analysis is complicated because muscle is a nonlinear system. The tension response to a stretch is not necessarily the mirror image of the response to a release. This nonlinearity becomes more apparent as the amplitude of the length change increases.

For the mechanical experiments described in this thesis, I used step perturbations and sinusoidal analysis to extract kinetic information from the muscle fibres. The next two chapters in this thesis describe the apparatus built to perform these types of tests single muscle fibres and the software written to drive the apparatus and analyse the data.

A materials and methods chapter follows this describing the conditions used for most of the single fibre experiments. This chapter also contains some important control experiments which investigate the properties of single insect fibrillar flight muscle fibres under changing physical conditions.

Chapter five describes experiments carried out to investigate the role of a single protein (Tn-H) in the stretch activation of insect fibrillar flight muscle. The relaxed, active and rigor mechanical characteristics of single fibres is recorded before and after mild digestion with the protease calpain.

The change in the amplitude and rate constants of phases 2, 3 and 4 are investigated at various step sizes and at different concentrations of inorganic phosphate (P_i) is studied in Chapter six.

The final chapter introduces a computer model of cycling cross-bridges, in which distortion dependent rate constants are defined in such a way that the model recreates all three phases observed in striated muscle, as well as their relationships to step size described in chapter six. Two different mechanisms of stretch activation are modelled.

2. Hardware

2.1 Introduction

This chapter describes the apparatus built to perform rapid mechanical experiments on single muscle fibres. Following this brief introduction, each part of the apparatus is described and discussed individually.

Figure 2.1 shows a summary of the major components of the apparatus, illustrating how they are interconnected. The muscle fibre is held between two glass hooks in a bath of solution.

The bath solution is held at a constant temperature. A small bead thermistor measures the temperature of the bath solution. The temperature signal controls a feedback circuit that drives a Peltier effect heat pump on the muscle bath. Solutions in the bath can be changed using two syringes in a flow through system. New solutions quickly reach the temperature set by the Peltier circuit.

To the right of the muscle bath is a position motor capable of applying fast length changes. A feedback circuit with velocity compensation controls the motor position. A 170W power amplifier supplies the high currents necessary to accelerate the motor quickly. Under computer control, the motor can perform quick steps or high frequency sinusoidal length changes to the muscle fibre.

The other end of the fibre attaches to a strain gauge on the opposite side of the muscle bath. To complement the fast motor, the strain gauge is also optimised for high frequency response. The strain gauge is mounted on a micromanipulator so it can be moved to accommodate fibres of different length.

The motor position signal and the output of the strain gauge amplifier are displayed in real time on an oscilloscope. For recordings, these signals are digitised and stored temporarily by a Datalab DL1200 waveform recorder. Once recorded, data is dumped from here to the computer over a fast general purpose interface bus (GPIB).

An IBM AT compatible computer controls the recordings made using a Labmaster interface card. A digital to analogue converter (DAC) on the interface card provides the signal that controls the motor position in real time. Accurate programmable timers on the interface card control both the timing of the output of DAC values and also that of the samples taken by the Datalab.

The computer and driving software allow the user to view and analyse the length and tension data dumped from the Datalab. Recorded data, calibration and timing information can be saved to disk.

2.2 Position Motor and driver circuitry

2.2.1 Requirements

This section describes the mechanical and electrical characteristics of a motor used in rapid length change experiments on insect flight muscle fibres.

The range of movement of the motor need not be very great. In comparison to other muscle types, insect muscle is very stiff. Typically, stretches greater than 5% over rest length result in either fibre damage or failure of the fibre attachment. A total range of movement of 1mm allows for a length change range of $\pm 10\%$ of the longest fibres that are likely to be used. The moving mechanism of the motor must be designed such that the hook does not vibrate out of the axis of the muscle fibre.

The quality of the motor position signal is very important. Not only is this signal important in the analysis of the recorded data, but is also used for feedback control of the motor position in a servo loop. This means that noise in the signal will also affect the length of the muscle being tested. For these reasons, position signal noise must be reduced as much as possible. Unfortunately, it is usually the case that reduction of high frequency noise involves a trade off against the frequency response of the position detection circuitry. Low frequency noise or drift is equally undesirable, especially when one considers the stretch sensitivity of the muscle type to be tested. This type of drift is usually caused by temperature changes in the circuitry as it warms up. This low frequency noise can be controlled by choosing low drift components.

The amount of noise that is acceptable is dependent on the experimental conditions. The length of the fibres being tested is important. Obviously the length signal noise has most effect on the shortest fibres used. For example, if it is necessary to analyse 0.2% length changes on *Drosophila* fibres, then length changes of the order of 500nm must be clearly visible.

The type of analysis is also important in determining the effect of noise on the experiments. When measuring high frequency stiffness using step length changes, only a the small number of samples taken during the length change are used in the analysis. Conversely, sinusoidal analysis makes use of all samples taken during the oscillation to extract the stiffness information. This means that stiffness measurements made in step length change experiments are more sensitive to signal noise than those made from sinusoidal analysis.

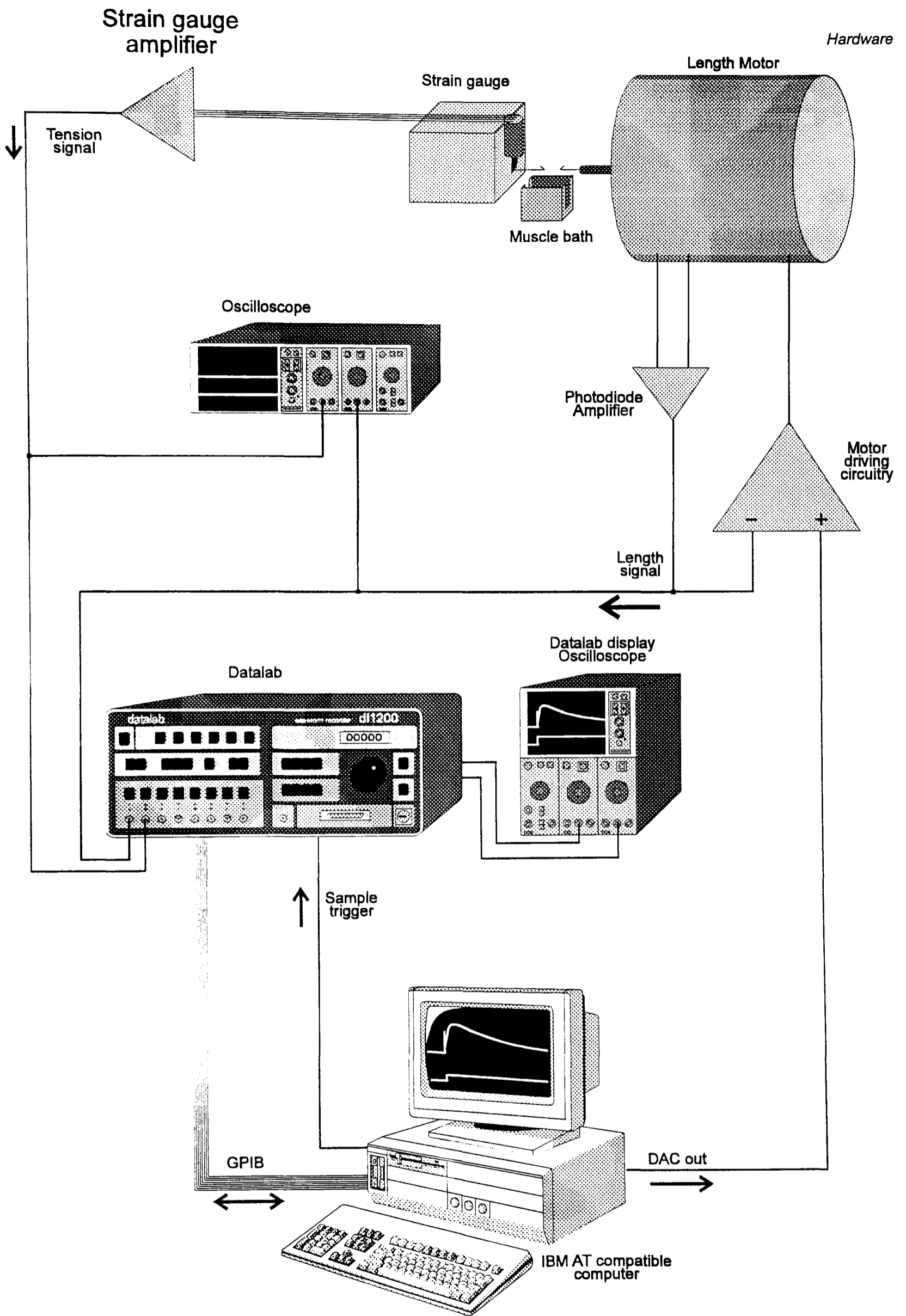


Figure 2.1: Schematic overview of the muscle apparatus, showing the major components and how they are interconnected. Arrows adjacent to some of the lines indicate direction of "information" flow.

Ideally, the position signal should be linear over the range that the motor is used. With a linear output, the computation of motor position is very simple. All that is required is that the analysis software knows the slope of the motor signal response in $\mu\text{m/V}$. A non-linear position signal unnecessarily complicates the computation required. In such cases, a look-up table is necessary to correct the data after or during sampling.

The frequency response of the motor and driving circuitry needs to be high. This property of the motor system is what limits the rate at which steps can be applied and the highest frequency at which the fibre can be oscillated. In some fibre preparations the rapid recovery phase (phase 2) can begin less than $200\mu\text{s}$ after the onset of the length change. There are two reasons why it is undesirable for the tension change of phase 2 to begin before the length change is over. Firstly, it is possible to make stiffness measurements only in the linear part of the tension signal. That is the region before the phase 2 relaxation begins. Secondly, for the analysis of phase 2 it is ideal that the length change is over before this relaxation phase begins. For these reasons, for better analysis of the high frequency properties of the muscle fibres a step length change should be complete within $200\mu\text{s}$.

2.2.2 Position motor designs

Before building this apparatus, two designs of position motor were in use in this laboratory. The older and slower of the two designs is a commercially available electromagnetic vibrator produced by Ling Dynamics (type 101). This type of motor is very robust. It works on the same principle as a loudspeaker. The moving part of the motor contains a coil that sits between the poles of a strong permanent magnet. Current passing through the coil causes deflection of the moving part of the motor. Unfortunately, mass of the moving part of the motor is larger than necessary for this type of experiment. This mass limits the minimum ramp times to 1ms or more.

A faster motor is described by Ford *et al* (1977), and by Molloy (1988). In this motor, the arrangement of the coil and magnet is similar to those in a galvanometer. The muscle attachment hook connects to the coil by way of a light, rigid pyramid constructed from dried grass. This design of motor is capable of completing steps as fast as $200\mu\text{s}$. In this design of motor, the pyramid moves perpendicular to its long axis. Because of the nature of this movement, vibration in the long pyramid supports makes it necessary to have several bracing struts. These add to the mass of the moving part of the motor, increasing its moment of inertia. An increase in the moment of inertia of the moving part of the motor

results in an increase in the current necessary to apply a given angular acceleration.

More recently a motor design that incorporates the best qualities of the two previously described designs has been used in muscle fibre experiments. The simplicity of the linear translational movement of the loudspeaker design is combined with the light dried grass pyramid of Ford *et al.* This is the design of motor I chose to use in my experiments. Both the motor and its driving circuitry are described in the next section.

2.2.3 The loudspeaker motor

The motor built to perform rapid length changes is shown in 'exploded' view in Figure 2.2. The coil and magnet used are those of a 15W loudspeaker (RS 249-902). The speaker coil is wound around an aluminium former. To reduce mass, this former is cut away until the minimum required to hold the coil remains. The dried grass pyramid was constructed on top of this former. The pyramid was assembled and fixed to the coil former using Araldite adhesive. In this design of motor, since acceleration and deceleration occur in the almost the same plane as the long struts, no serious vibration has been detected in these. For this reason no bracing struts were necessary.

The hinge mechanism consists of two sets of four strip hinges. These constrain the pyramid and coil assembly to movement in only one plane. The strip hinges used were 1.5mm wide sections of .15mm gauge phosphor bronze sheet. These were attached to the top of the pyramid and to the aluminium former using Araldite. The other ends of the hinges were fixed to the motor casing, a section of 65mm aluminium tubing.

An optical system is used for position detection. The light beam from a bright light source shines onto a mask on the pyramid assembly. This mask casts a band of light onto a pair of photodiodes (Farnell BPW34-B). A difference amplifier detects changes in the relative illumination of the two photodiodes. When no current passes through the coil, the motor remains in its central position. Here light falls equally on the two photodiodes resulting in a motor position signal of approximately 0V. Small movement of the pyramid assembly changes the relative illumination of the photodiodes, and therefore the voltage of the motor position signal.

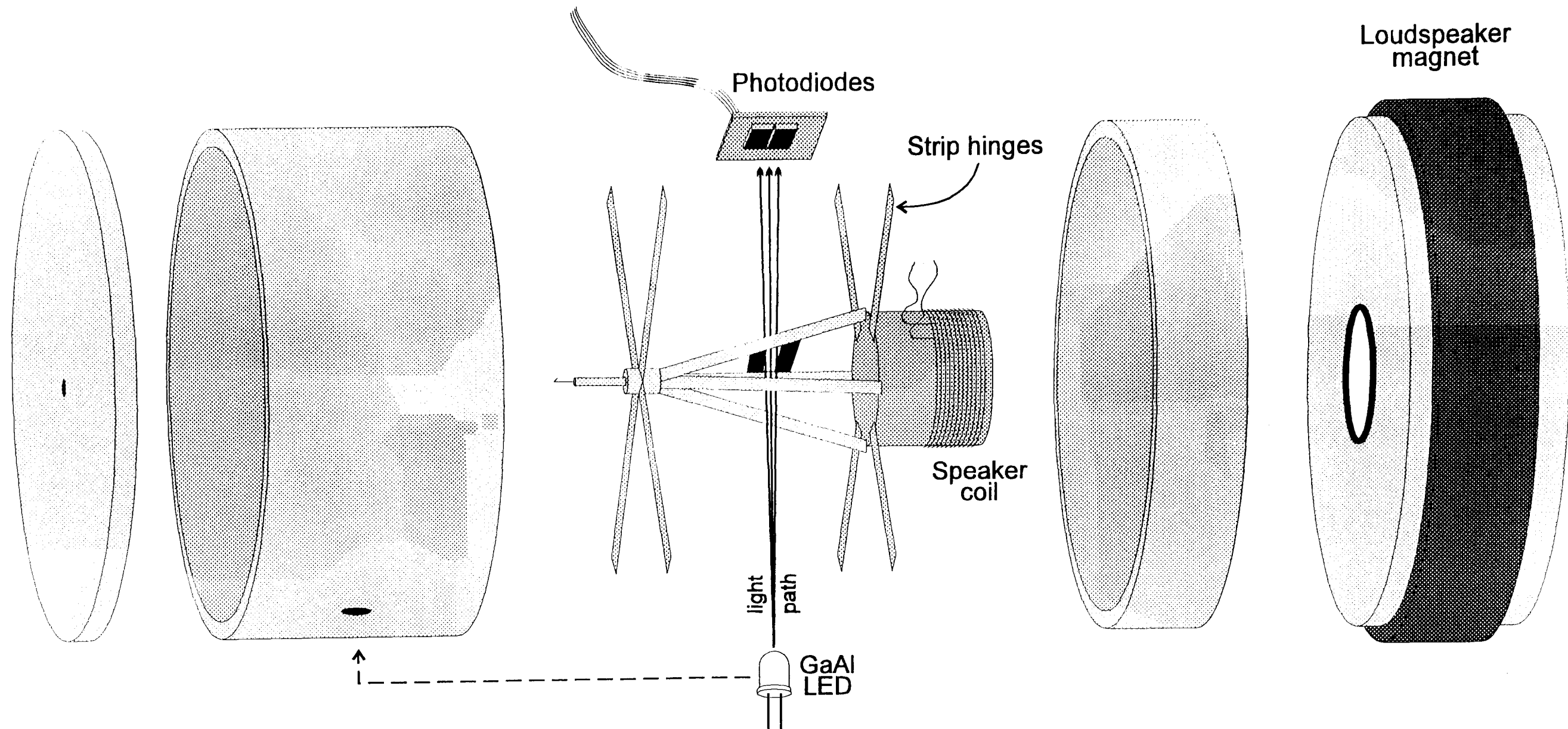


Figure 2.2: An exploded view of the position motor. The motor uses the coil and magnet from a small 15W speaker (RS 249-902). The coil is connected to the hook by a very light and rigid pyramid of grass straws, glued together with Araldite. Phosphor bronze strip hinges constrain the coil and pyramid assembly to one plane of movement.

The choice of light source is an important consideration. For a low noise position signal, the voltage output of the photodiodes must be large compared to the noise of the photodiodes. To do this a bright light source is necessary. Until recently the only convenient solution was to use a filament light bulb. In some instances this caused problems due to the tendency for the lamp filament to oscillate after a motor step. This oscillation does not necessarily appear on the circuit position out signal, since the motor may oscillate to compensate. In the late 1980s cheap and very bright GaAl light emitting diodes (LEDs) became available. This is the light source used in the position motor (RS 577-730). These LEDs have the advantage of a bright narrow beam of light without the problem of filament vibration.

The light emitted by the LED must be constant. Any variation here will alter the calibration of the position signal. The voltage driving the LED is regulated by the circuit shown in part (c) of Figure 2.3. The power supply feeding this LED driver circuit can vary between 5V and 7V. Under these conditions the output voltage remains within 1mV of 2.35V.

2.2.4 Motor driving circuitry

Figure 2.3 shows the position signal and feedback circuits built to drive the length motor. The position signal is generated by the circuit (a). The signal from the photodiodes is put through a difference operational amplifier (op-amp) circuit. The position signal circuit uses low noise op-amps (Burr Brown OPA606KP and OPA37GP). The second (upper) op-amp circuit in (a) amplifies the position signal further into a range suitable for input into the Datalab waveform recorder ($\pm 0.5V$). This op-amp circuit also prevents the potentially disastrous consequences of the Datalab or other monitoring equipment taking too much current from the signal circuit. This type of leakage could make the feedback circuit unstable, and damage the motor.

The position signal is fed back into the motor driving circuitry, in a signal mixing circuit (b). In the signal mixer op-amp, the position signal is compared to the command position signal from the computer (DAC I/P). In essence, the output from the signal mixer is an error signal that is further amplified and drives the motor. This error signal ensures that the command input from the computer is closely followed by the motor position.

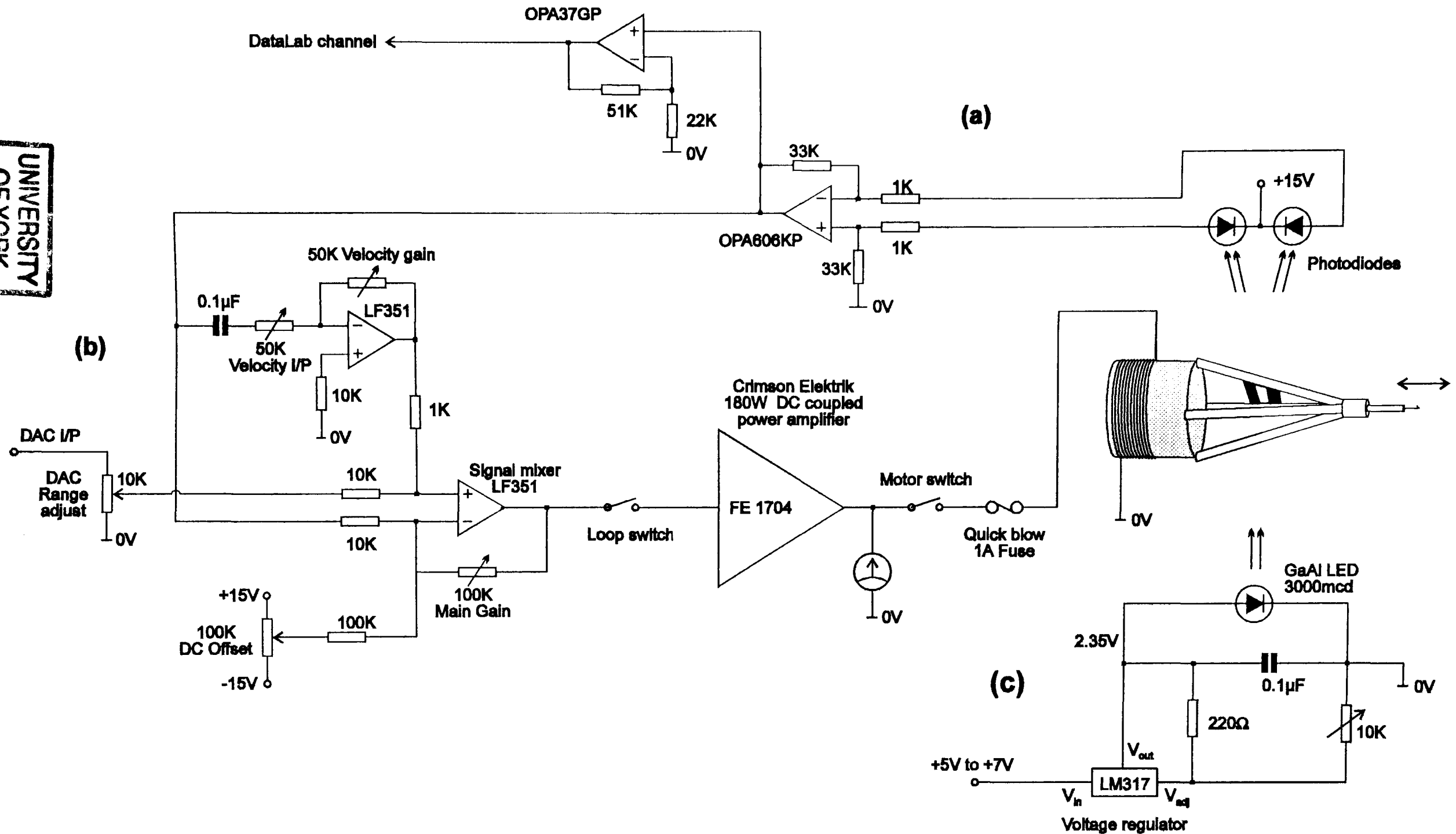


Figure 2.3: Circuit diagram of the position motor servo loop. The motor position signal from circuit (a) is mixed with the command signal from the DAC in circuit (b). Output from the signal mixer circuit (b) is amplified through a power amplifier that drives the motor. The circuit (c) provides a stabilised, regulated voltage for the LED light source.

As an example we will assume that the computer DAC is giving out a continuous square wave. The rate at which the motor is able to reach a new position set by the computer is partly a function of the gain ("Main gain") of the signal mixer circuit. Increasing the gain of this circuit increases the rate at which the motor is able to reach the new position. Unfortunately, this rate increase has an upper limit. As the gain is increased to high levels, overshoot begins to occur. Beyond this damped ringing starts, further still and positive feedback causes the system to go into permanent oscillations.

This high frequency instability of the system introduces the reason for the second op-amp in the circuit. This velocity compensation circuit allows the circuit to be tuned to reduce ringing and overshoot at high step rates. The capacitor on the input line allows the op-amp to detect the rate of change of the position signal. The variable resistor in series with the capacitor allows the frequency characteristics of the velocity circuit to be adjusted. The op-amp gain can be adjusted (velocity gain) to vary the effect of velocity compensation on the signal mixing circuit.

The error signal with velocity compensation drives a large power amplifier. This amplifier is a DC coupled power amplifier that provides the large currents necessary to drive the motor. The amplifier is a commercially available unit (Crimson Elektrik CE1704) originally designed for public address systems. The maximum output of 170W is more than enough to run the motor at its maximum speeds.

Although the coil in the motor is from a 15W loudspeaker, the coil itself can withstand very high currents provided that they are brief. For a step length change the motor is sent a two opposing voltage spikes to accelerate and decelerate the motor. These large currents pass through the coil only during the length change. After the step a very small current flows through the coil, that being the current necessary to oppose the forces of the strip hinges to hold the new motor offset. For protection from high currents that may damage the motor a 1A quick blow fuse lies between the power amplifier and the motor.

2.2.5 Tuning

The fine tuning of the motor and the motor driver circuit is done each time it is used. The motor driving software is written in such a way that it is not possible to drive the motor without first executing a motor set-up and self-calibration routine. This procedure includes a continuous square wave output from the DAC. This enables the main gain and velocity adjustments to be set.

The loop is switched on with the main gain set very low. This caution ensures that if there is any error in the circuit, only small currents should be sent to the motor. The shape of the motor step response can be viewed on the oscilloscope or the computer screen. The computer also provides information about the present ramp time (5% to 95%). The main gain and velocity controls are adjusted so that the step time is at its fastest, without any overshoot or ringing after the step.

In the set up procedure, it is also possible to adjust the range of the DAC. It is useful to vary this according to the length of the present fibre and the type of analysis that is to be done on the fibre. In all cases it is desirable to have the full scale of the 12 bit DAC (4096 values) to correspond to just more than the maximum length change required. If only a small part of the full 12 bit scale is used, the staircase nature of the DAC output signal becomes visible in the length signal. This is not purely an issue about the appearance of the length signal. The tension response of a fibre to a length change that consists of large discrete steps is different from that in which the will steps are a small proportion of the signal. This "bit noise" introduces high frequency harmonics into the system. These harmonics can be a source of error during the analysis of the traces.

When setting up the motor DAC range the software is self calibrating. During the motor set up procedure, the computer continuously sends out steps. The motor response to these steps is dumped back to the computer so that a calibration value for the DAC can be set. The DAC range is printed to the screen as a percentage of the present fibre length. It is important that the software includes this self calibration. The length change per DAC unit is also sensitive to the current settings of the main gain and velocity compensation circuits.

2.2.6 Calibration

The calibration procedure involves setting a single value in the muscle program software. The value of the variable **Lcal!** (in μm per length unit) contains the current setting for the length calibration of the motor position detection circuitry.

To measure the actual motor displacement, a travelling microscope is positioned over the hook where the fibre is attached. The eyepiece reticle has units of $10\mu\text{m}$. The motor could be calibrated by measuring the voltage of the "position out" signal at various motor positions. The calibration value ($\mu\text{m}/V$) could then be used to set the value of **Lcal!** (μm / length unit). A more simple calibration is to set the software to output a slow staircase of $10\mu\text{m}$ step size. These steps can be observed through the eyepiece. If the observed steps do not

follow the reticle units then the calibration value can be adjusted accordingly. The staircase can be applied in both directions. This simple, fast and accurate method of calibration also detects any nonlinearity in the position detection system. Although unlikely, a calibration error in the Datalab would not affect the accuracy of this type of motor calibration.

2.2.7 Performance

The amplitude of the high frequency noise in the position signal is equivalent to 50nm of hook movement. This level is acceptable for most recordings made. However it is too much for accurate small signal sinusoidal analysis of the shortest fibres. This can be overcome by averaging several traces.

Another type of noise which can be easily overlooked is that of the hook position itself. The most common source of this type of noise is mains interference in the position detection circuitry, but may be elsewhere in the feedback circuit. It is important to check for this type of noise because it is not visible in the position signal. When the loop is switched on the feedback circuit will cancel the noise by moving the motor. Any mains hum or other interference in the position signal can be seen by looking at the signal when the loop is not switched on. This does not account for any noise in the other amplifiers circuits.

When the loop is switched on, hook movement noise can be detected by attaching a very stiff material to the apparatus and recording the tension signal. A fine hair can be attached to the apparatus using the same type of clips used for muscle experiments. Presently some 50Hz (mains noise) movement is detected which has an amplitude of 7nm. This size of movement is a very small proportion of the typical length changes used in muscle experiments. This movement can be a source of error when performing small signal sinusoidal analysis on short fibres, especially at frequencies close to 50Hz. However in such experiments it is necessary to average several traces to get a clear signal in both the length and tension channels. Trace averaging reduces both high and low frequency noise.

Presently the motor is capable of performing a complete step without any overshoot or ringing within 180 μ s (5% to 95% in 160 μ s).

2.3 Recording tension

2.3.1 Requirements

The compliance of the gauge itself must be very small. Some movement will always be present since this is how strain gauges detect the applied force. However a large deflection in the strain gauge would make the measurement of the applied length change inaccurate. The compliance of the gauge should not be more than 40nm/mN.

The maximum tension that a single insect muscle fibre can produce is very rarely greater than 500 μ N. This is a suitable value for the full scale range of the output circuitry. Unfortunately it is by no means a suitable upper limit for the failure value of the transducer. When mounting the fibres on the apparatus touching the strain gauge hook may apply forces that are orders of magnitude higher than a single fibre could exert.

The acceptable level of high frequency noise in the output signal is dependent on the type of recording that is to be made. For example when performing small signal sinusoidal analysis on a relaxed fibre (low stiffness fibre), then the amplitude of the tension signal may be as small as 10 μ N. In this situation the noise must be much less than 10 μ N. It is not always necessary that this noise reduction be performed by the strain gauge amplifier. After capture the computer can do trace averaging and digital filtering.

The low frequency noise is very often a problem with very sensitive strain gauges. Since the mechanism relies on detecting a tiny movement in the gauge itself, they can be very sensitive to temperature change. During experiments, a small amount of slow drift in the output signal can be corrected for by performing frequent releases to find zero tension.

The frequency response of the strain gauge is a very important consideration. As the mechanical frequency response of the strain gauge increases, the more rapid are the tension changes which can be measured accurately. The most rapid tension changes to be analysed are those which occur during step length changes, and the rapid recovery phase (phase 2) in step release experiments. However in practice, increasing the frequency response of the gauge can introduce other unwanted factors. For example reducing the length of the transducer lever, reduces both the signal to noise ratio and also the freedom of movement that the hook has within the muscle bath.

2.3.2 Micro-Newton strain gauge designs

The most popular type of strain gauge used in single muscle fibre experiments is the Akers 801. This strain gauge consists of a small beam of silicone. Two piezo-resistive elements are etched onto opposite sides of the beam. The resistance of these elements is sensitive to the stretch or compression that results from flexing in the silicon beam. Applying a force to the end of the beam increases the resistance of one element and decreases the resistance of the opposite one. The two elements in the gauge are connected in a Wheatstone bridge circuit and fed through a difference amplifier. The presence of two elements not only doubles the sensitivity of the transducer, but also reduces the sensitivity of the strain gauge to changes in temperature. To attach the muscle fibre to the gauge, an extension piece with a hook (made from a glass capillary) is fixed to the end of the beam. The normal gauge without any extension piece has an undamped resonant frequency in the region of 12kHz. The addition of the glass extension, hook and the fixative typically reduces this to 4 to 5kHz.

A much higher frequency response has been achieved in purpose built capacitance strain gauges (Huxley & Lombardi, 1980). The muscle hook is attached to the centre of a small, thin quartz strip. This strip lies over another piece of quartz, supported at both ends to leave a 6 μ m gap between the two. The surfaces of the quartz are metallized and act as a capacitor. A force acting on the hook causes the attached quartz strip to flex slightly. This increases the size of the gap enough to be detected as a change in the capacitance of the gauge. Such strain gauges have been constructed with a resonant frequencies as high as 50kHz. These gauges do not require further damping since sufficient damping is provided by the air in the gap of the gauge.

However these gauges do have problems. Expansion and contraction of the quartz due to temperature changes cause the gauge to drift. Though this can be reduced by using fused quartz which has a higher thermal stability, it still remains a problem. A more serious problem is that of drift caused by humidity changes. The dielectric property of the air in the capacitor gap is very sensitive to humidity change. Humidity changes in the environment close to the muscle bath are difficult to avoid. To reduce this drift it is necessary to isolate or at least distance the gauge from the bath solution. This has the unavoidable consequence of reducing the resonant frequency of the gauge.

To measure tension I chose to use the Akers gauge. Though it typically has a lower resonant frequency, it does not suffer from drift problems associated with the capacitance gauge.

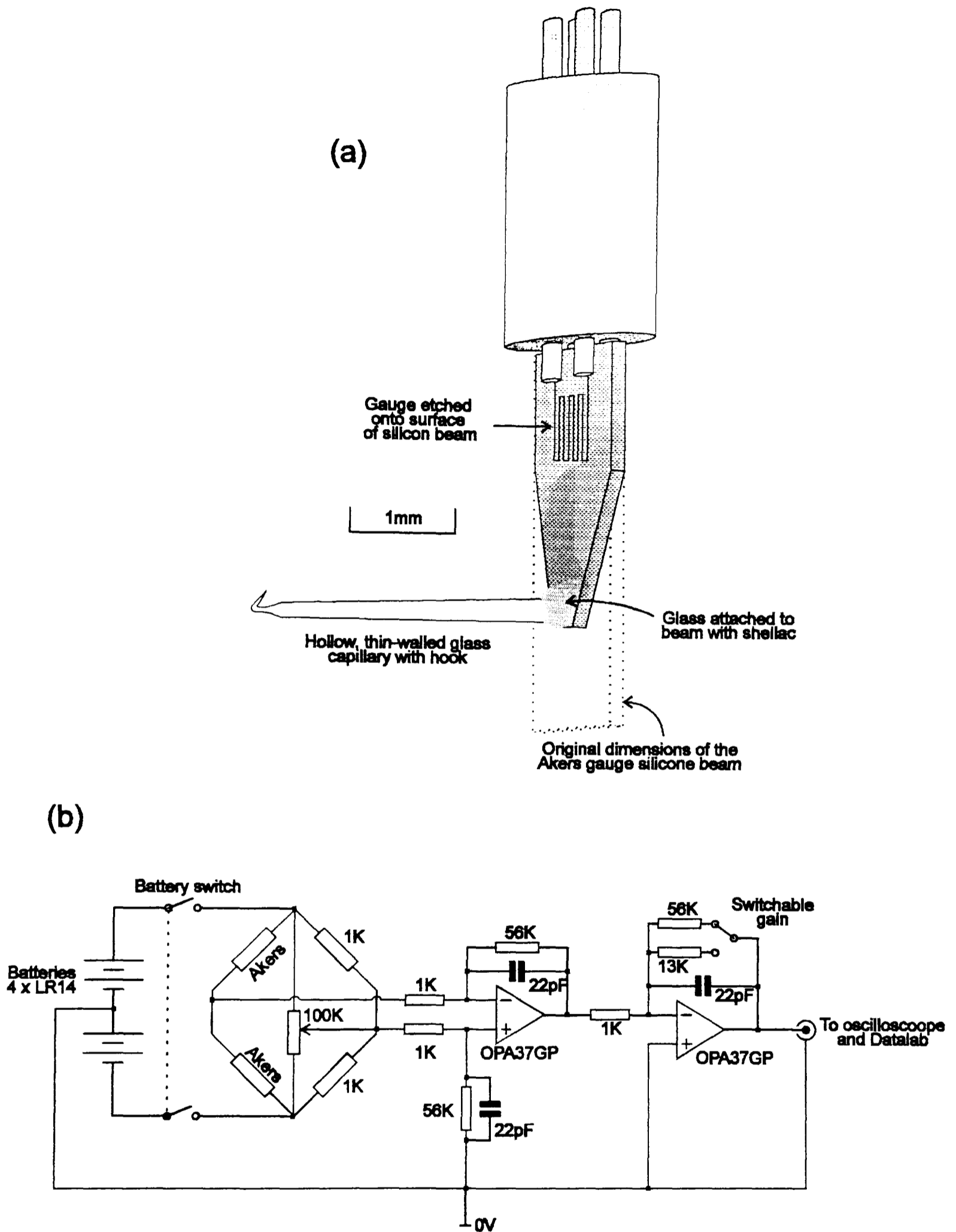


Figure 2.4: Strain gauge apparatus optimised for high frequency tension measurement at the micronewton level. (a) Akers gauge, shortened and ground to a wedge shape to increase the frequency response. (b) Diagram of the circuit used, showing the Wheatstone bridge and low noise, low drift operational amplifiers.

2.3.3 The Akers gauge

The strain gauge and circuitry are shown in Figure 2.4. To increase the resonant frequency of the gauge, the silicone beam was ground down to a wedge shape. The glass capillary was pulled out using a Bunsen flame. The hook on the end was shaped using a small electric heating element. The length of the glass capillary is the minimum which will allow a range of movement of 2mm inside the muscle bath. Also a minimal amount of shellac was used to attach the hook.

The gauge is mounted in an aluminium block. A brass flat ended screw lies behind the gauge. This screw allows adjustable oil damping to be applied if necessary. The front of the gauge is shielded with a piece of aluminium foil. The gauge hook passes through a small hole in the foil. The Akers gauge is very sensitive to ambient light changes. The foil shields the gauge so that sunlight changes and the 100Hz of the illuminating lamp do not affect the tension signal. The foil also reduces the sensitivity of the gauge to local changes in air temperature.

2.3.4 Tension circuitry

The Akers gauge is incorporated into a Wheatstone bridge circuit. A variable resistor allows the bridge to be balanced at 0V when no load is applied to the gauge. The bridge voltage is supplied by four batteries. Batteries are used because they are a cheap way to supply the bridge with a stable, low noise voltage source.

A difference op-amp circuit amplifies changes in the bridge balance. A second op-amp circuit serves two functions. Firstly it amplifies the signal further into a range which the Datalab can record ($\pm 0.5V$). Secondly it allows gain of the tension circuit to be switchable. Having a switchable gain is necessary when the circuit is to be used for other gauges which are not optimised for a high frequency response. The op-amps used in the circuit are Burr Brown OPA37GP. They were selected for their low noise, low drift and high frequency characteristics.

The voltage gain on the tension amplifier is adjusted to give a final value in the region of $600\mu N/V$. A value lower than this would risk the signal going off-scale in some recordings. Higher range values would be of no benefit since the fibre preparation used does not withstand forces higher than this. A larger range value would result in a reduction of resolution in the recordings.

The small capacitors on the feedback resistors reduce some of the high frequency noise in the circuit. Increasing the value of the capacitors used would

further reduce the high frequency noise in the output. Unfortunately this also has the effect of reducing the frequency response of the circuit. The amount of electronic filtering used is always a compromise between noise reduction and reduced frequency response.

To detect the effect of the feedback capacitors on the frequency response of the circuit, a waveform generator was used to apply a high frequency signal to the input of the first amplifier in the tension circuit. By maintaining the same input voltage amplitude but changing the input frequency, it is possible to determine the frequency characteristics of the tension circuit. The capacitors chosen were those with which the high frequency amplitude remained constant at frequencies below 15kHz. Further filtering is done by software.

2.3.5 Calibration and performance

A calibration curve for the strain gauge is shown in Figure 2.5, part (a). The strain gauge is calibrated by positioning the strain gauge hook so that the glass capillary hangs down vertically. A range of small weights are hung from the hook and the change in the output voltage recorded as they are removed. It is more accurate to record the voltage change when removing the weight. This takes less time than adding the weight, allowing less time for drift. The range of small weights added correspond to a force range similar to that applied by the muscle fibres. Any non-linearity of the gauge outside this range should not alter the calibration. Recording the tension output for a range of forces shows the linearity of the gauge and its circuitry.

Generally Akers gauges prove to be quite linear output over the range that they are used in muscle fibre experiments. Calibration results remain true for a long period of time. Any change in sensitivity is usually due to the a lowering to the battery voltage. At this time the batteries must be replaced, since they can lose there charge at different rates causing the tension output to drift quite quickly.

The resonant frequency of the strain gauge is 13.2kHz (Figure 2.5 parts (b) and (c)). Such a high resonant frequency is very important for recording the high frequency characteristics of the muscle fibre. This frequency describes the oscillation of the free transducer. This is quite different from the expected resonant frequency of the gauge when a muscle fibre is attached in experiments. Because of the added mass of the fibre and the damping effects of the surrounding solution the experimental resonant frequency is in the region of 6 to 8kHz. The exact value is difficult to determine and is dependent on how the fibres are mounted.

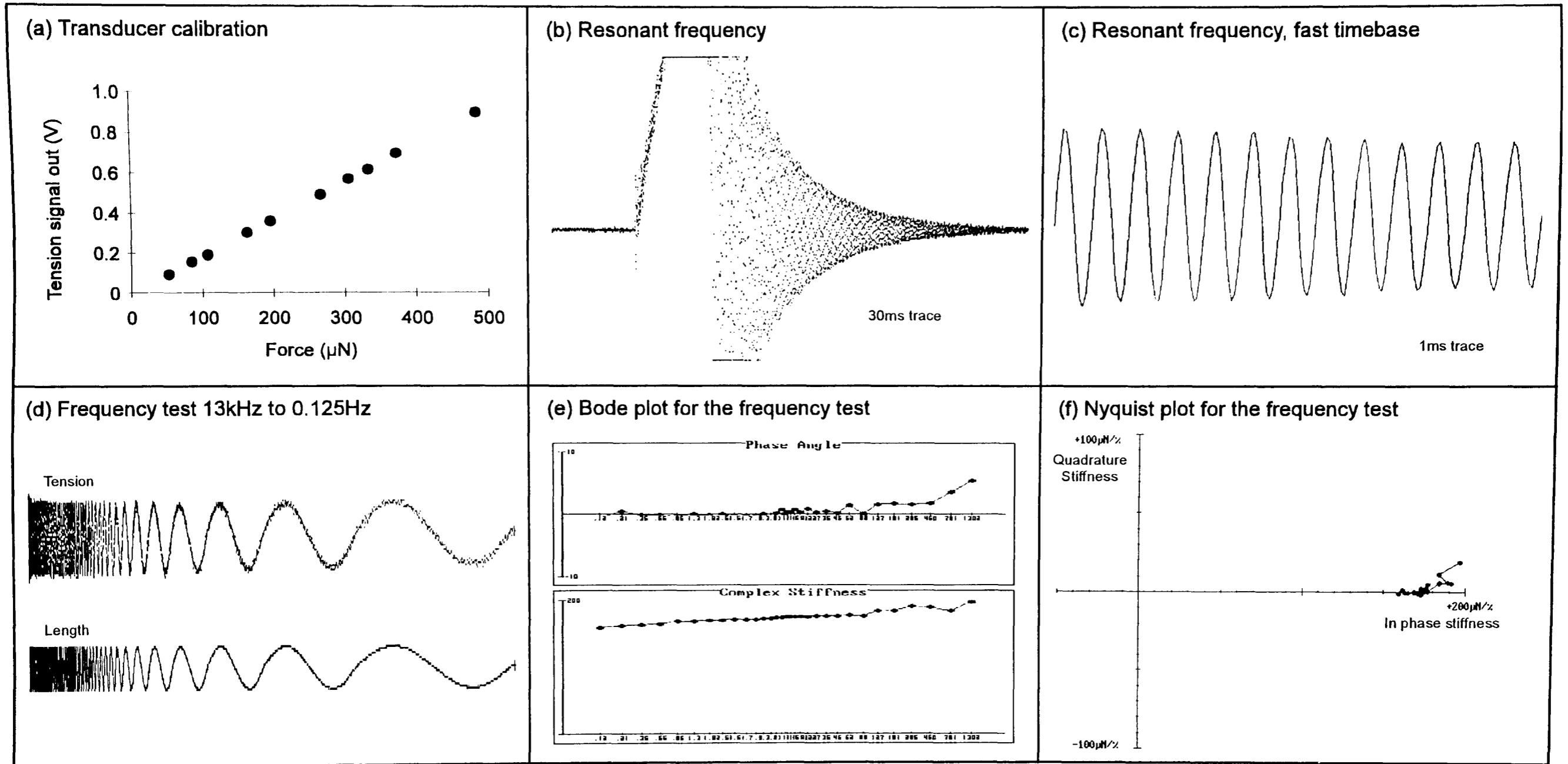


Figure 2.5: The mechanical characteristics of the strain gauge. (a) Gauge calibration showing that the output is linear with applied force ($530.3\mu\text{N/V}$, $r=0.999948$). (b) Touching the unloaded undamped strain gauge can cause it to ring. (c) The same recording on a faster time base showing a resonant frequency of 13kHz. (d) An elastic material is oscillated at 32 frequencies from 1.3kHz to 0.125Hz. (e) A Bode plot for the data shown in (c). The phase angle is zero at the lower frequencies, increasing to a maximum of 5° at the highest frequency recorded. (f) The Nyquist plot for the same data.

To accurately characterise the frequency response of the tension recording system an elastic material is attached to the apparatus in the same way as fibres are mounted. Of several materials were tested for their elasticity, condom rubber is the most perfectly elastic under the conditions used. A strip of rubber is mounted in the same type of aluminium clips used in fibre experiments. The bath is filled with solution, since this has a small damping effect on the gauge. The results of a Nyquist series on the rubber fibre are shown in Figure 2.5 (parts (d), (e) and (f)). From the tension plot in (d) it can be seen that the tension amplitude remains quite consistent throughout all the frequencies tested. The change in phase angle remains very small, even at the highest frequency of 1.3kHz.

2.3.6 Temperature controlled bath

In previous muscle experiments in this laboratory, muscle bath temperature was controlled by water from a constant temperature tank passing close to the muscle bath. This method of temperature control has several problems. Because there is no feedback from the muscle bath, the bath temperature is sensitive to changes in room temperature and must be checked regularly. Temperature changes can take a long time. This affects the length of time it takes to start an experiment and makes temperature change experiments difficult.

Because the amount of solution in a typical muscle bath is small (10 to 100 μ l) it is possible to use Peltier effect heat pump to control its temperature. Peltier effect heat pumps are small, cheap devices which transfer heat from one surface to the other. The direction of heat transfer is dependent on the direction of the current passing through them. In this way the same device can be used as a heating or a cooling element depending on the direction of the applied current.

The circuit designed to drive the Peltier effect heat pump is shown in Figure 2.6. Two Peltier devices (0.32W mini module, RS 618-718) are wired in series. One side of the pumps is fixed to a very thin piece of aluminium which makes up one wall of the muscle bath. The other side of the pumps is attached to a small block of aluminium (10mm x 10mm x 30mm). This block acts as a "heat reservoir". Bath temperature is detected by a miniature bead thermistor in the muscle bath. A variable resistor allows the user to set the temperature. The "set temperature" signal is compared to the "present temperature" signal in the op-amp LM759. The error signal drives two FET transistors which supply the current to drive the Peltier pump.

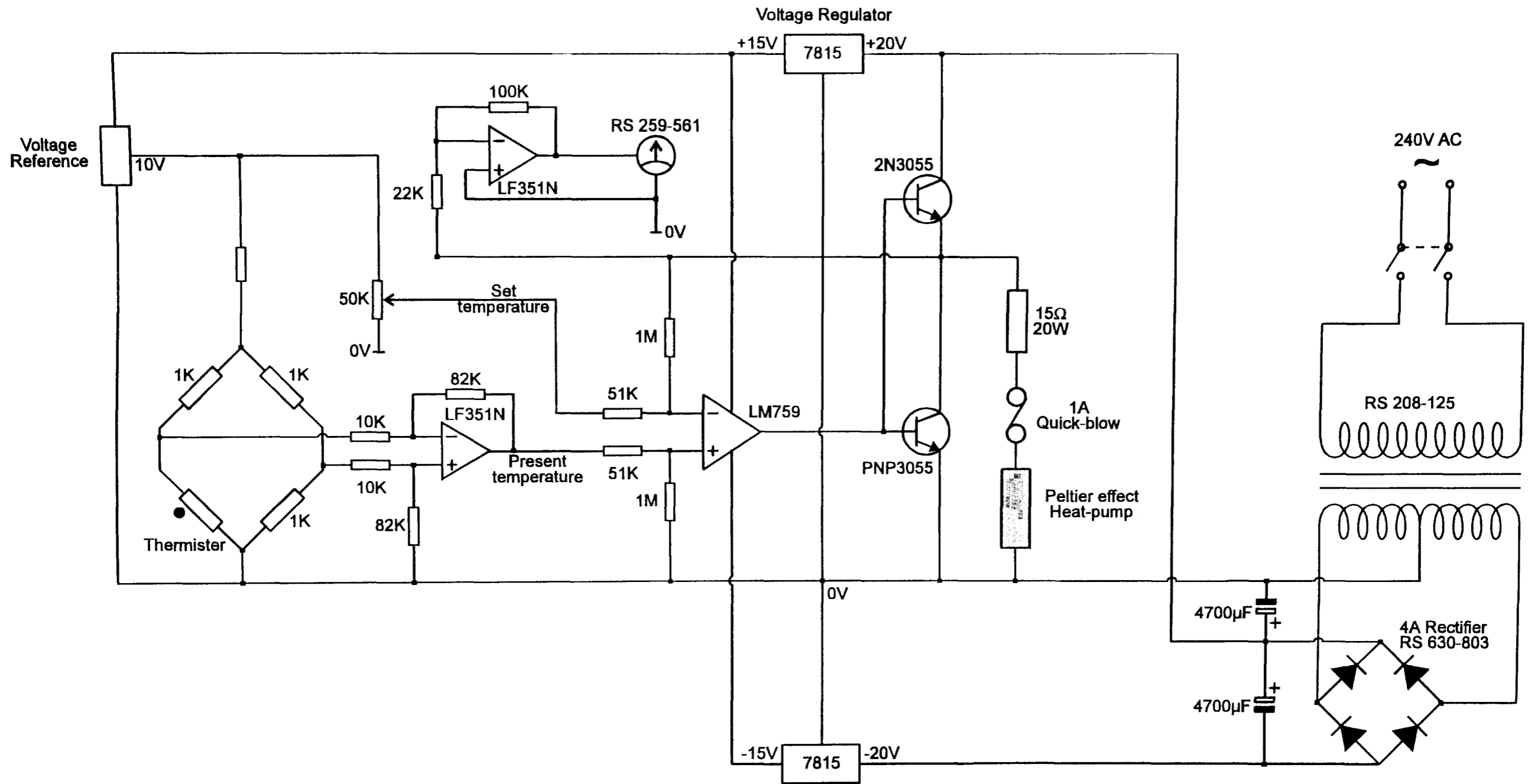


Figure 2.6: The peltier heat pump driver circuit. The bath thermistor in a Wheatstone bridge circuit provides the temperature signal. The bath temperature is compared to the pre-set temperature in a difference amplifier. The amplified error signal drives two large transistors that provide the current to drive the peltier heat pump.

Two related and important variables in this system are the gain of the feedback circuit and the position of the thermistor in the muscle bath. A high gain setting ensures that temperature clamping is accurate and rapid. Unfortunately setting the gain too high introduces oscillation into the circuit due to the delay between passing current through the Peltier and the thermistor detecting any temperature change. This delay can be reduced (allowing a higher gain setting) by positioning the thermistor close to the Peltier pump in the muscle bath. When the thermistor is very close to the Peltier another problem is introduced. The solution in the region of the Peltier is perfectly well temperature clamped, however there is now a temperature gradient (possibly of several degrees centigrade across the bath). For these reasons, position of the thermistor and the insulation of the bath are important factors in the design of a temperature feedback system.

In the muscle bath used, the bath solution is surrounded by insulating material (plastic and silicone rubber glue). This increases the speed at which temperature changes can be made, and decreases the effect of temperature gradients across the bath. The bath volume is low (30 μ l). The mounted fibre lies in parallel with and close to (1.5mm) the surface of the Peltier device. The thermistor lies slightly below the fibre 0.5mm from the surface of the Peltier device.

The temperature controlled bath is capable of maintaining constant temperatures in the range 5° to 48°. Temperatures lower than 5° are possible if cold water is passed through the aluminium block close to the Peltier device. Heating occurs at approximately 2.5° per second and cooling at 1° per second. Some oscillation occurs on reaching a new temperature, but is stable within 10s. To reduce evaporative heat loss (and ionic strength changes) at higher temperatures a cover-slip can be placed across the top of the bath. This also reduces temperature gradients at the highest and lowest temperatures.

2.4 Datalab waveform recorder (DL1200)

A Datalab 1200 waveform recorder samples and stores the data during experiments. When used with the muscle program the Datalab is set to 4 channel mode. In this mode it can simultaneously record and store 8192 samples on each of four channels.

The DL1200 multichannel waveform recorder is a sophisticated storage oscilloscope. The recorder used has the ability to record up to 4 channels simultaneously. Each channel has a 12 bit analogue to digital converter (ADC).

All channel data is stored in 64Kb of on board memory. A channel can record 32K, 16K or 8K samples depending on whether 1, 2 or 4 channels are recording simultaneously. On board clocks allow sampling rates as fast as $2\mu\text{s}$ (0.5MHz), although if triggered externally the ADCs can run at $1\mu\text{s}$. Recorded data is displayed separately on an oscilloscope screen.

During muscle experiments the Datalab is configured to record on 4 channels. Although only two channels are used presently (motor position and muscle tension), this still allows 8K samples per channel to be recorded and enables future expansion, if further channels are required.

Two methods of interface are available, the RS232C (serial) and the IEEE-488 or GPIB (parallel). All parameters and front panel switch settings can be set through these interfaces using a simple command language. The GPIB port is used to link the computer and the Datalab. To dump the 32K of recorded data from the Datalab to the computer using the RS-232 would take approximately 40s to complete. Using the GPIB and machine code routines the data is transferred in less than one second.

2.5 Computer interface

An IBM AT compatible computer controls the motor position and triggers samples during recordings. The computer used is a Viglen II (16MHz 80286). The computer contains two commercially available expansion cards. Firstly a CEC 010000 card provides the GPIB interface to the Datalab waveform recorder. Secondly, a general purpose interface card controls the motor position and Datalab sampling.

The interface card is a Labmaster DMA interface card. The card contains two digital to analogue converters (12 bit). One of these DACs generates the motor control signal. Two programmable timers (9513A) accurately control the timing of both the Datalab sampling and the timing of the output of new DAC values. The details the machine code that controls the interface is given in the software chapter.

2.6 Future work

Making the apparatus faster than at present is not a simple task. This would require modifications to both the motor and the strain gauge, since both are working at their limit. A motor capable of steps faster than $150\mu\text{s}$ will require a strain gauge with a higher frequency response than the present one. The motor

could be made faster by rebuilding the moving part of the motor so that it is lighter than at present. The present resonant frequency of 13kHz is probably close to the upper limit of what is possible with an Akers gauge. If more mass is removed from the silicone beam this would lower the leverage the fibre has on the gauge and decrease the signal to noise ratio further. A shorter glass capillary would reduce the range of movement the gauge has in the bath. A faster strain gauge could be constructed using a glass needle with an optical movement detector.

3. Software

3.1 Introduction

The computer performs many functions in muscle experiments. As described in the hardware chapter, the computer controls the position signal and triggers samples during recordings. Once recorded, data is dumped from the Datalab waveform recorder to the computer. Here the data can be displayed, analysed, filtered and also saved to disk.

In this chapter program names and variable names from the software are written in bold Roman text e.g. **CALL NyquistMenu**. Source files, the executable file and some example traces are included on the diskette supplied with this thesis (the diskette format is 3.5", 720K DOS). The executable file will run on an IBM-PC compatible computer running DOS (version 3.3 or later), with an EGA, VGA or Hercules graphics.

3.1.1 Programming Language

Before my work, software to control muscle experiments was already in use in the laboratory. This was originally written by K. Drew (Drew, 1984) in a combination of machine code and BASICA. BASICA is Basic for the IBM PC, and is equivalent to GW-Basic available for IBM compatible computers. For several reasons, BASICA is not the best choice for this application. The most significant of these being its slow speed and its 64Kb limit on program size. These versions of Basic for the IBM PC are not compiled. Instead the program code must be loaded into the Basic editing environment where it is run in an interpreted way.

More recent versions of Basic for the IBM PC are supplied with a compiler and do not have the 64K program limit. I chose to use QuickBASIC (Microsoft, version 4.5) to write most of the control and analysis software. This is the most popular Basic for DOS. A cut-down version of QuickBASIC called QBasic is supplied with versions of DOS from version 5.00 onwards.

In QuickBASIC, like in BASICA, programs can run from the editing environment. Once written, the source code can be compiled to create a stand-alone executable program. The only limit on program size is the amount of available base memory. The language, although almost completely compatible with GW-Basic, has many more advanced features that make programs more simple to write and understand.

Other programming languages are available which would produce faster and smaller code than Microsoft QuickBASIC. The obvious example being the language "C". A further advantage of some C compilers is the ability to write machine code in the same source file. However, some aspects of the C programming language make it less suitable than Basic for this application. The main problem being its apparent complexity to those who are not familiar with the syntax. I have tried to write this code in such a way that future researchers could alter and add to the code without a BSc in computer science. In this respect, since it is the most popular language among non-professional programmers, Basic is an obvious choice.

The parts of the software that are not written in Basic, are written in machine code. Machine code (also known as assembly language) is the language that the microprocessor understands. High level languages like Basic and C must be converted to machine code before the microprocessor can run them. This conversion process is done by the compiler (or an interpreter in the case of BASICA). Unfortunately the compilation process is never as efficient as it could be. Routines that are written directly in machine code are faster than the equivalent code which is compiled from a high level language. The speed enhancement is not trivial, in well written code an improvement of an order of magnitude or more is not unusual.

Obviously there is a price paid for this high speed. In comparison to high level languages, machine code is difficult to learn and write. Machine code programming requires a level of understanding of the computer architecture beyond that necessary to write in a compiled language. Machine code is also very unforgiving. The smallest mistake can result in the computer locking up, the reset switch being the only solution. Finding errors in the code (debugging) can also be a very slow task. Unless written with many descriptive comments the code can be very difficult to understand. Making alterations to code without an abundance of such comments is very difficult. Code without comments can sometimes be quicker to re-write than to decipher.

The muscle program uses several machine code subroutines. In these routines, I used machine code either for its speed of execution or to perform operations that are not available in QuickBASIC. The one routine in which machine code is essential is the routine that controls the trace recordings. Other routines include displaying the data, the Datalab interface commands and various array manipulating functions could have been written in Basic but would make the program considerably slower.

3.1.2 Source files

The software is compiled into one executable file (**MUSCPROG.EXE**) which from here will be referred to as the *muscle program*. Keeping analysis software together with the trace recording software in one program has several advantages. At first sight these seem to be separate functions which could be performed by independent programs. However it is often convenient to see a Nyquist plot or fit an exponential to a trace as soon as it is recorded. Also the routines which control the hardware and the analysis software share common subroutines (called Subprograms in QuickBASIC), such as those which display data and perform array functions.

The QuickBASIC source code is split into three files. This split is necessary because QuickBASIC cannot compile source files which are larger than 64K. The three source files (modules) are **MUSCPROG.BAS**, **MUS-ANLY.BAS** and **MUS-HDWR.BAS**. The first is the main module. It contains the code for the user interface. The second two modules contain the code for trace analysis and hardware control respectively.

The machine code subroutines are assembled and linked into two libraries. Firstly **MPCODE.LIB** is the library which is linked into the muscle program when the program is compiled. The second library **MPCODE.QLB** is a Quick library which makes the machine code subroutines available from within the Basic editing environment. In the editing environment, with the quick library and all three of the Basic source modules loaded, the muscle program can be run just as it would when compiled. This makes editing and debugging much more convenient. It removes the need to compile to detect errors. However, when run from the editing environment, the Basic code runs more slowly than when compiled.

3.1.3 Overview of muscle program

All of the modules begin with the same include file, **MUS-INCL.BAS**. This file contains the declaration statements for the Basic subprograms, the machine code subroutines and all the variables that are to be shared between the modules. The shared variables are declared using the **COMMON SHARED** statement. Some of the variables are declared a second time with a lower case "r" prefix. The first variable stores the current system values. The second with the "r" prefix holds the values for the record which is currently held in memory. Using two sets of variables in this way allows previously recorded traces to be loaded without changing the current system values.

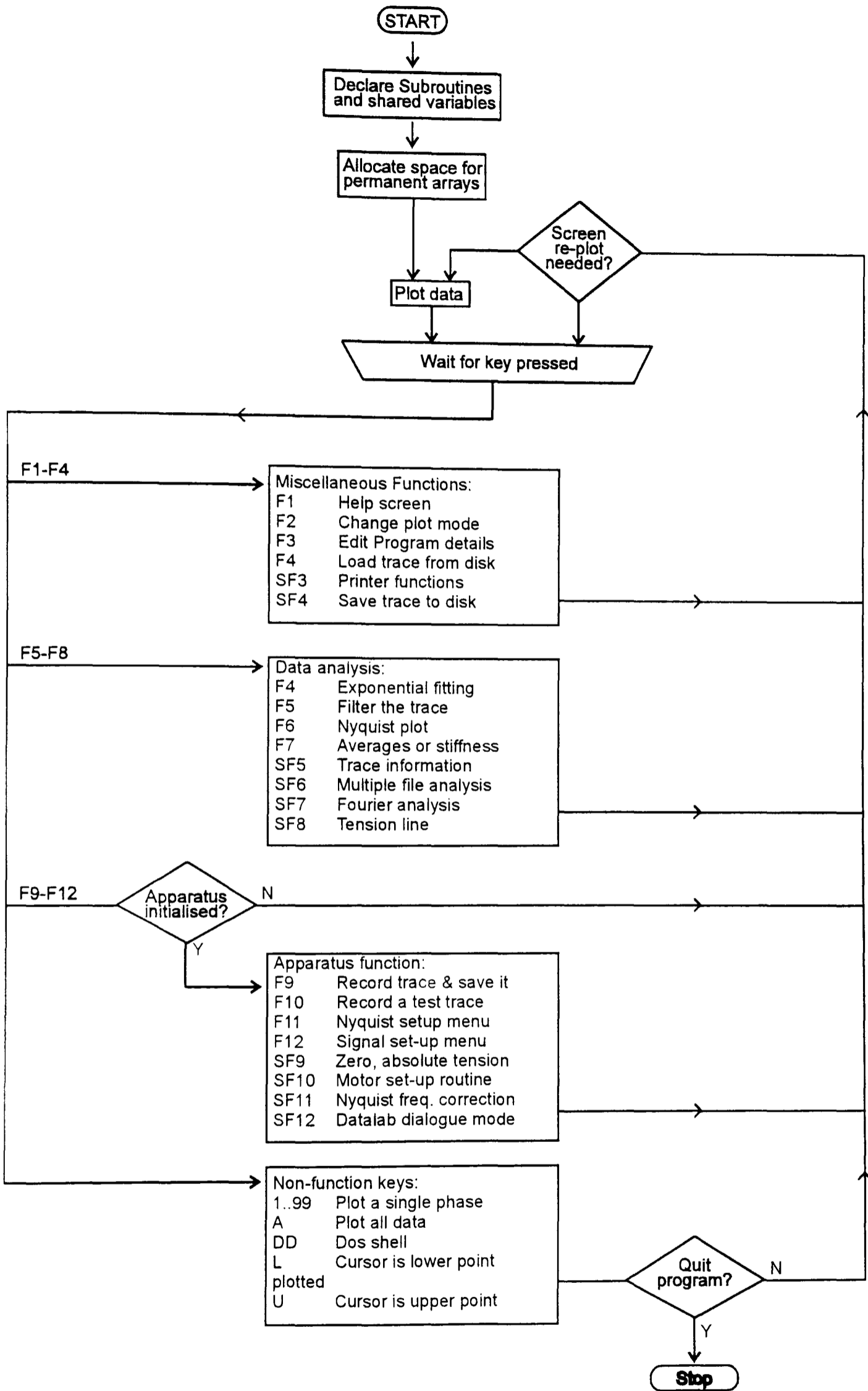


Figure 3.1: Flow chart of the Muscle experiment control program.

A flow chart of the muscle experiment control program is shown in Figure 3.1. Program execution begins in the main module. After the declarations in the include file, memory is allocated for the permanent arrays and other variables.

Before the main muscle program screen is plotted, a set-up routine (**Setup**) is called. This procedure assigns default values to the major program variables. It also detects the type of graphics adapter (VGA or Hercules). If a Microsoft (or compatible) mouse and driver are detected, the driver is initialised.

Once initialised, the program plots the main program screen and waits for a key to be pressed. The majority of the main program screen consists of the plotted length and tension data. The program is now in the main program loop, in which it waits for a key-press, performs the associated function and if necessary re-plots the data screen once complete. All the program functions are accessed from the main screen using the function keys.

In the flow chart the program functions are split into four groups. The first three groups describe the function keys F1 to F4, F5 to F8 and F9 to F12. These groups access the user-interface, trace analysis and hardware functions respectively. With a small number of exceptions these groups correspond to code in the modules **MUSCPROG.BAS**, **MUS-ANLY.BAS** and **MUS-HDWR.BAS** respectively. The final group describes the non-function keys which are primarily for controlling what data is plotted to the screen. Most of the program functions operate by calling one or more subprograms. Though some are small enough to be performed in the main program loop.

3.2 Recording traces

3.2.1 Introduction

All the hardware functions of the muscle program are accessed using the function keys F9 to F12. By default all of these keys are disabled at start-up. This is a safety mechanism which prevents computers without the hardware interface cards from locking up if these keys are pressed. Hardware functions are initialised from the experimental details menu (F3). The apparatus functions can be turned on only if the presence of the GPIB interface card is detected.

Before recordings can be made the motor must be set-up. The motor set-up routine allows the motor driving circuitry to be tuned. Also the motor is calibrated for its sensitivity to the DAC signal. Separate menus are used to select for simple

recordings such as steps and single sinusoids (F12) or for Nyquist recordings (F11). Once the recording type has been selected, it can be recorded using F9 (record and save) or F10 (record without save to disk).

3.2.2 Motor Set-up Routine

The motor set up procedure performs several functions which relate to the tuning the motor circuitry, and the characteristics of the DAC signal which controls the motor position. The **Motorsetup** subprogram must be run at the start of all experiments. The muscle program will not run other trace recording options until this initialisation routine has been done. It can also be run in mid-experiment if the tuning circuitry is changed in any way.

Before any signal is sent to the motor circuitry, the user must select two characteristics of the test output signal. Firstly the size of the step as a percentage of the present muscle fibre length (default 1%). Secondly the duration of the ramp in the step signal (**RampLen%**, default 110 μ s). Sending a fast ramp to the motor produces a more smooth step than a square wave input. That is it reduces the tendency for the motor to ring after the step. The fastest steps with least ringing occur when the DAC ramp is set between half and two thirds of the motor ramp time.

Once these variables are set, a series of steps are sent to the motor. The motor response is recorded on the Datalab, dumped to the computer and plotted on the computer screen. This sequence is repeated continuously. At this time the "main gain", "velocity gain" and "velocity balance" can be adjusted to give the best step response from the motor. See section 2.2.5 for a more detailed description of this process.

With each step motor response dumped from the Datalab, the computer performs a DAC calibration. The variable **DACcal!** stores the amount of motor movement (μ m) produced per DAC unit. The variable is set very accurately by averaging 3800 samples at both zero offset and at the top of the step to do the calculation. This self calibration is performed with each loop of the motor set up procedure. The value in **DACcal!** from each step is used to calculate the DAC values sent in the next step. Once the motor set up is completed, **DACcal!** is used to set all signals that are written to the motor.

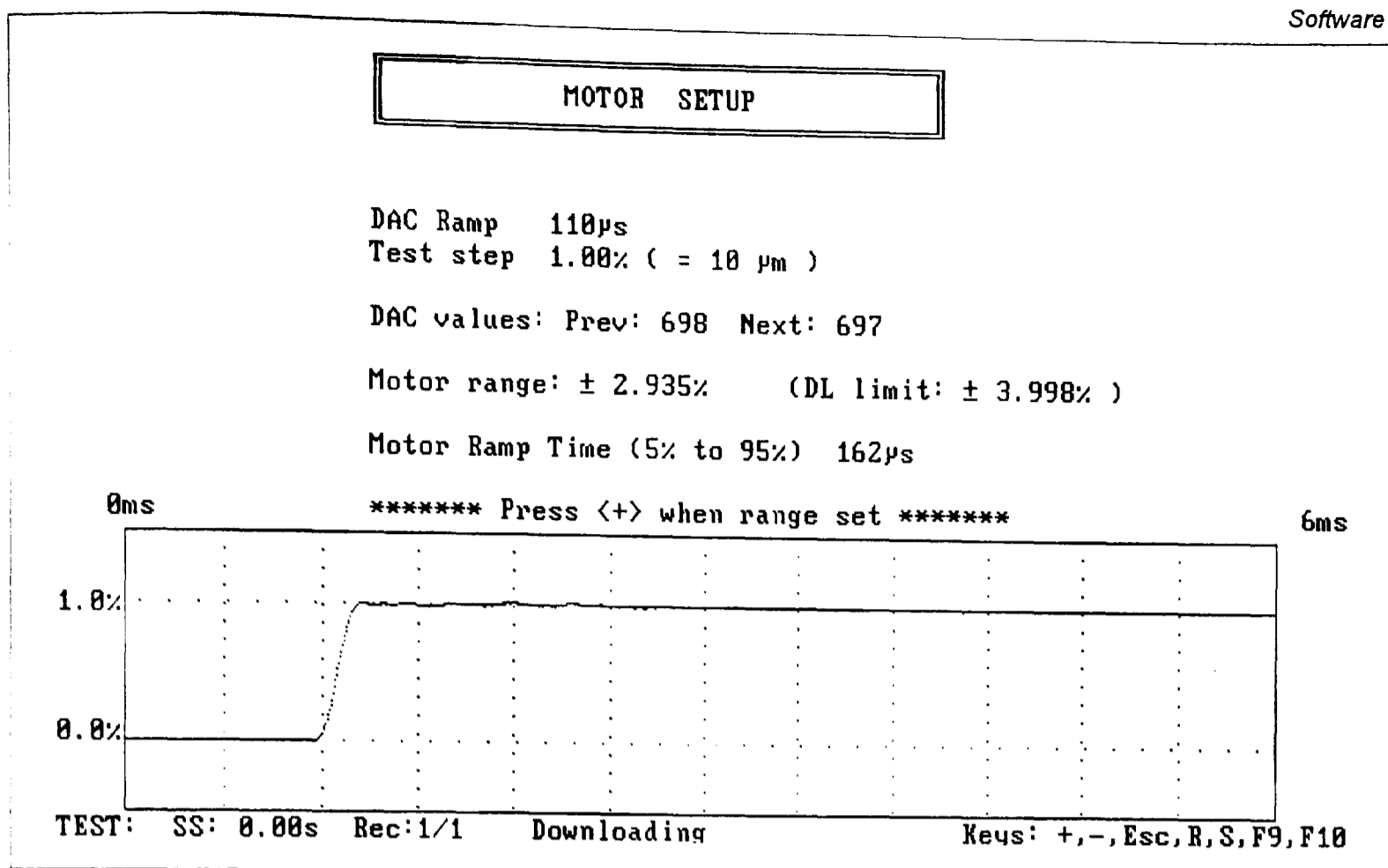


Figure 3.2: A screen image captured during the motor set-up procedure. Test steps are repeated and this screen updated continuously allowing the user to adjust the motor driving circuitry.

The channel data dumped from the Datalab is in the form of unsigned 12 bit words. The values from 0 to 4095 cover the input voltage range from -0.5V to +0.5V. For this reason when the motor is at zero offset, the motor position signal voltage corresponds to a channel output value close to 2048. In the motor set up routine the channel value which represents zero offset is calculated accurately. The value is stored in the variable **zeroL%**. After the motor set-up procedure is completed, this value is subtracted from length channel samples of all recordings. The muscle program stores and saves length channel data as signed integers, in which a value of zero represents a motor offset of zero. Unlike the equivalent tension value (see **zeroT%** in section 3.2.9) the length signal does not drift. For this reason, **zeroL%** need only be set at the start of an experiment.

A captured screen image from this set-up procedure is shown in Figure 3.2. As well as the plotted step, other information about the step response is printed with each repetition. Two motor ranges are given. Firstly the full motor range of the DAC output ("Motor range"). This value is given as a percentage of the current fibre length. The second range is the full range that the Datalab is capable of recording. The motor range can be changed at this point by adjusting a potential divider on the DAC input to the motor circuit. The motor range should be set to a value just above the maximum offset that is expected to be used in the

experiment. This makes optimal use of the full range of the DAC, reducing the affect of bit noise on the recordings.

3.2.3 Machine code control of recordings (Sweep)

3.2.3.1 Introduction

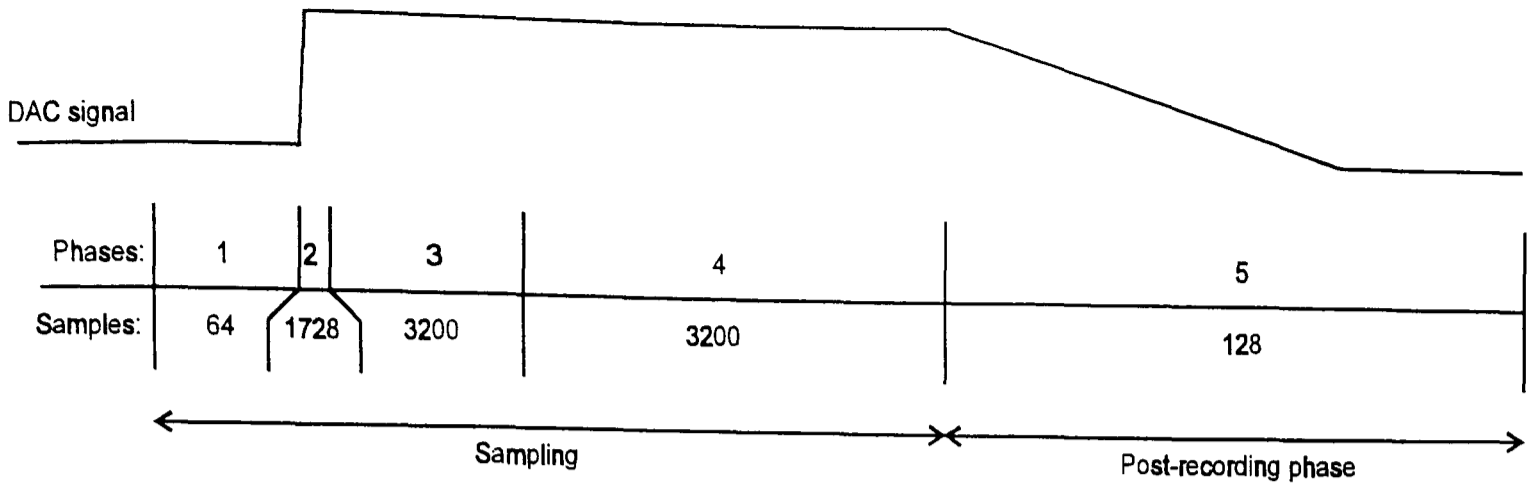
Motor position and Datalab samples are controlled by a single machine code subroutine called **Sweep**. This routine disables the system interrupts and performs an accurately timed loop. In a single loop cycle, three different operations take place. A trigger signal is sent to the Datalab to take a single sample on the length and tension channels. Secondly, a new value is sent to the DAC to control the motor position. Finally, if the sample rate is to change, the new value is placed in the loop timer. These operations are completed in a loop time as short as $6\mu\text{s}$ (limited by the speed of the 286 used). The range of timer values from $6\mu\text{s}$ to $65535\mu\text{s}$ allows complete recordings (8192 samples) to last from less than 50ms to almost 9 minutes.

It is not inconvenient that DAC output and sample triggering are coupled in this way. Rapid changes in motor position occur more smoothly if the controlling signal is made up of many small steps i.e. a fast loop rate. During rapid length changes many samples should be triggered to capture the high frequency stiffness information.

The ability to change sample rate in mid-recording increases tremendously the amount of information that can be recorded in a single trace. For example in step length changes the highest sample rate can capture the ramp and the rapid recovery of the muscle tension and slower rates used to capture the slower tension transients. Similarly, in Nyquist recordings, the whole range of frequencies can be recorded quickly in a single trace. Previously separate recordings at different sample rates were necessary to record all of these processes.

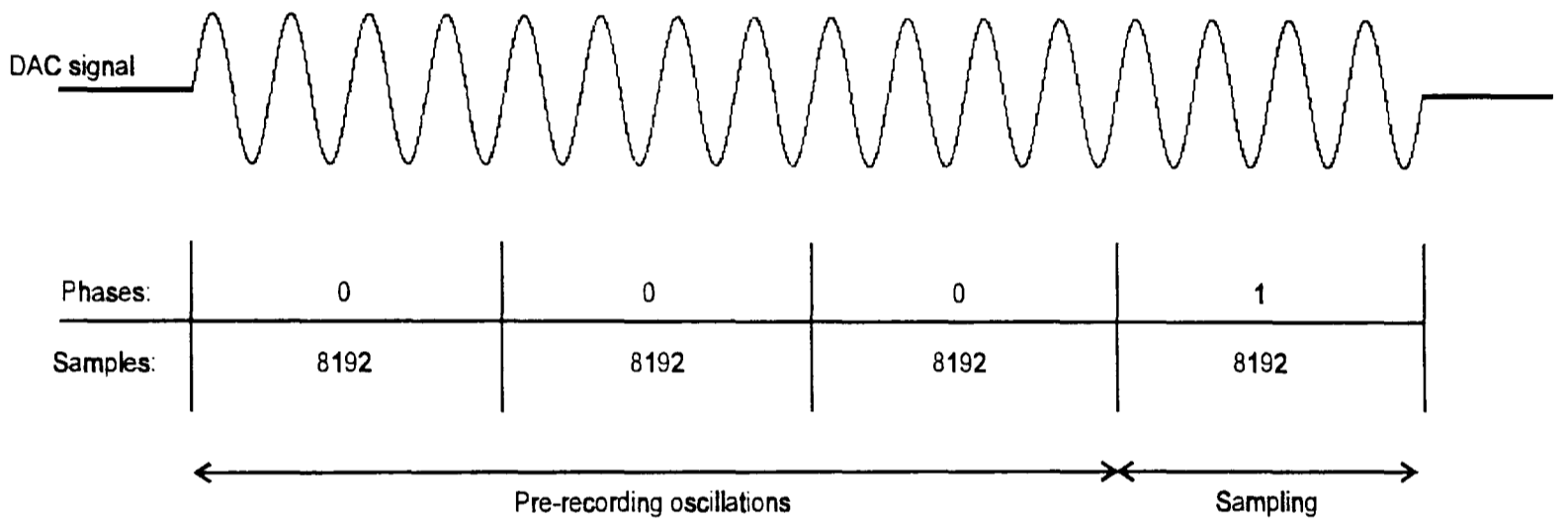
The ability to change sample rate also improves the accuracy of the exponential fitting process. Unlike previous recordings, the sum of all the exponential processes can be fitted in one run of the fitting program. To a certain extent the sample rate changes also give the tension transients a more even weighting. When fitting more than one exponential, the tension transient that contains the most samples will bias the result of the fit. One way to reduce this is to try to have more even numbers of samples in each of the processes by changing the sample rate through the trace.

(a) Example Step:



		Phase	0	1	2	3	4	5	6
Signal description arrays	Snum%		0	64	1728	3200	3200	128	0
	Sint%		-	4000	6	140	2200	1304	-
	Offset!		-	0	1	1	1	0	-
	SgnlS		-	T	T	T	T	R	-

(b) Example oscillation:



Phase	0	1	2
Snum%	3	8192	0
Sint%	-	12	-
Cycles%	-	4	-
Freq!	-	40.69	-
Ampltd!	-	1	-
Offset!	-	0	-
SgnlS	-	S	-

Figure 3.3: Examples showing how trace recordings are split into phases. (a) The table shows the signal description array values for a typical step recording. The sample rate is high during and immediately following the length change, but decreases in each of the two phases which follow this. A post-recording ramp down returns the muscle to rest length. (b) In sinusoidal recordings, the sampling phase is repeated several times before the recording starts. This ensures that a steady state is reached before recording starts. The number of times that phase 1 is repeated before recording starts is stored in Snum%(0).

3.2.3.2 Recording phases

A single recorded trace is made up of one or more recording phases. Recording phases differ according to either the motor position signal or to the sample rate. If a sample rate change or a new motor position is required then a new recording phase must be defined. The **Sweep** subroutine accepts as many phases as there are samples. That is each sample could be recorded at a new sample rate, although in practice between 1 and 32 are used. When the muscle program calls the **Sweep** subroutine, it sends information in three arrays, **Snum%()**, **Sint%()** and **DACout%()**. The former pair of arrays describe each phase in terms of number of samples and sample interval (μs) respectively. The third array contains all of the motor position information (8192 or more values) which is sent to the DAC during the recording.

Figure 3.3 shows how recordings can be made up of one or more phases. Part (a) shows an example step recording. The diagram below the DAC signal shows the relationship between the phases which describe the timing of the recording and the DAC signal itself. The table shows the values in the signal description arrays. A "-" in the table indicates that the actual value in this element of the array is irrelevant to the function of the code. The phases 1 to 4 are the sampling phases, the sum of the sample numbers in these phases is 8192. Phase 5 occurs after all the samples have been recorded, it returns the muscle offset to rest length.

The value in **Snum%(0)** is zero in the step length change example. This is reserved for pre-conditioning in sinusoidal recordings. In sinusoidal recordings, it is often important to give the muscle several oscillations before recording is started. These pre-recording oscillations allow the muscle to reach a steady state before any samples are taken. The array element **Snum%(0)** stores the number of repetitions of phase 1 (described by **Snum%(1)** and **Sint%(1)**) that occur before recording begins. In non-sinusoidal recordings, the value sent in **Snum%(0)** is zero and no pre-recording phases occur.

3.2.3.3 The DAC signal array

As well as **Snum%()** and **Sint%()**, other arrays are shown in Figure 3.3 which describe the DAC signal. These arrays are not passed directly to the **Sweep** subroutine. Instead the signal which these arrays describe is written to a single array **DACout%()** before the machine code is called. The Basic subprogram **WriteDAC** fills the array **DACout%()** with the exact values which are written to the DAC during the recording.

The **WriteDAC** subprogram fills the **DACout%()** array phase by phase. The array **Sgnl\$()** describes the type of signal in each phase using a single character. The character "T" for fast steps and steady values and "S" for simple sinusoids. Phases in a Nyquist series are designated by "N" or "F" depending on whether they use pre-recording oscillation or not.

For rapid steps, a fast ramp is written to the **DACout%()** array as defined in the motor set-up routine. The **Offset!()** array stores the length offset for each phase. The value is stored as a percentage of the total muscle length. In the motor set-up procedure the motor sensitivity is stored in the motor calibration variable **DACcal!**. Using this calibration value and the muscle fibre length (**Mlength!**) the **WriteDAC** subprogram calculates the exact value to achieve the percentage length change specified in the **Offset!()** array.

For sinusoidal phases, several more arrays are required to store the signal description. The number of complete cycles in the **Cycles%()** array, the oscillation amplitude in the **Ampltd!()** array and frequency in the **Freq!()** array. The value in **Offset!()** is taken into account if a non-zero offset is specified.

3.2.3.4 Machine code details

The code that controls the recording process is actually a very small part of the source code. The majority of the source prepares the timers and data arrays for the small timed loop to run as efficiently as possible.

At the start of the subroutine, the system interrupts are stopped. This is essential in a routine such as this where timing is critical to the level of less than one microsecond. When system interrupts are enabled, several precious microseconds of processor time can be used by another routine. An example of such an interrupt is that generated to maintain the value in the time-of-day clock. This routine is called 18.2 times per second on all IBM compatibles. Such interference would not be acceptable, especially during rapid length changes.

Programming references recommend that interrupts are not disabled for longer than a few milliseconds. Despite this, I have noticed no adverse effects even on the longest recordings of several minutes. Caution on the part of these references is probably to avoid problems with other interrupt driven routines such as packet drivers for networks. The value in the time-of-day clock is reset from the value stored in CMOS at the end of the **Sweep** routine (the CMOS clock is that which keeps time when the machine is off). This ensures that the system clock and more importantly the file save times remain accurate.

Two versions of the phase output loop exist in the code, one for each timer on the interface card. The output signal of the Labmaster timer 1 is wired directly

to the sample trigger line of the Datalab waveform recorder. For this reason, a separate control loop and timer 2 are used to perform the timing of any pre-recording repetitions of phase 1 (i.e. when $Snum\%(0)>0$). During the development of the control loop, many different ways of performing the same task were tested, in order to find that which gave the maximum sample rate.

Once written, the code was given rigorous testing. This was to ensure accuracy in the timing events. The accuracy of the timing was tested by recording the signal from an external waveform generator of known frequency. The optimal loop frequency can be found by having the loop output a repeating signal with a small number of samples. The DAC output can be viewed on an oscilloscope, whilst the timer value is reduced. When the computer execution time becomes limiting is shown by sudden irregularity in the output signal. The present minimum loop time is $6\mu s$ on the 286 based computer. On a fast 486 based computer, the maximum sample rate of the Datalab of $1\mu s$ will be possible, though it is debatable whether such a high sample rate is necessary.

3.2.4 Step length change recordings

Simple step recordings can be selected by pressing F12. This calls the subprogram **StepMenu**. A simple menu allows the user to select the size (as a percentage of the muscle length) and duration (seconds) of the step to be applied.

The number of phases can also be altered. The step can be made up of up to 10 phases. The phases have equal numbers of samples (**Snum%()**), but the sample rate (**Sint%()**) increases logarithmically. The values of the sample rates are calculated automatically from the selected step duration.

By default the program will record the return to zero offset after the step is completed. This return to zero is recorded using half the number of samples in the step itself. The return to zero recording can be switched off so that all of the samples are used to record the step. In such recordings, the length offset is returned to zero after the recording has ended. A slow ramp is used for such non-recorded length changes since they do less damage to the fibre.

3.2.5 Nyquist recordings

Although Nyquist recordings use the same phase by phase style of recording as other recording types they have a dedicated menu system. This is because Nyquist recordings have several special requirements. Pressing F11 invokes the **NyquistMenu** subprogram.

(a)

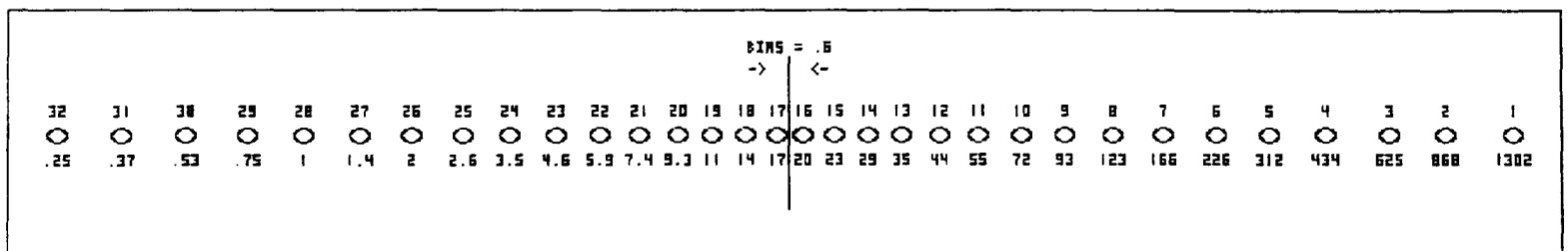
***** NYQUIST *****

Nyq	sInt	Cycles	Frequency(Hz)	Lcorr	Nyq	sInt	Cycles	Frequency(Hz)	Lcorr
1	24	8	1302.0834	1.061	17	470	2	16.6223	1.006
2	36	8	868.0555	1.037	18	564	2	13.8520	1.001
3	50	8	625.0000	1.029	19	684	2	11.4218	1.000
4	72	8	434.0278	1.005	20	842	2	9.2785	0.999
5	100	8	312.5000	1.002	21	1052	2	7.4263	1.004
6	138	8	226.4493	1.003	22	1334	2	5.8564	1.002
7	188	8	166.2234	1.006	23	1714	2	4.5581	1.006
8	254	8	123.0315	1.001	24	2236	2	3.4940	1.006
9	168	4	93.0060	1.002	25	1478	1	2.6429	1.003
10	218	4	71.6743	1.007	26	1984	1	1.9689	1.005
11	282	4	55.4078	0.996	27	2700	1	1.4468	1.005
12	356	4	43.8904	1.005	28	3728	1	1.0478	1.004
13	446	4	35.0336	1.001	29	5222	1	0.7480	1.000
14	548	4	28.5128	1.005	30	7418	1	0.5266	0.996
15	666	4	23.4610	1.006	31	10690	1	0.3654	1.004
16	798	4	19.5802	1.003	32	15624	1	0.2500	1.003

<F1> 4 Freq. Amplitude: 0.200% <F5> to set (137 DAC units)
 <F2> 8 Freq. Nyquist type: Normal <F6> to toggle
 <F3> 16 Freq. Samples: 256 per frequency
 <F4> 32 Freq. <F8> Frequency plot & set bias

(b)

Logarithmic Frequency Plot:



Bias: +0.6 Keys: <->, <+> alter bias to central frequencies
 Left,Right Move the centre for frequency bias
 <L> Toggle logarithmic-linear plot

Figure 3.4: Two screens captured from the Nyquist menu subprogram. (a) The menu itself allows individual frequencies to be edited. The number of frequencies to record in a single sweep is set using the function keys F1 to F4. Pressing F8 shows the set up screen shown in (b). This automatically sets all the frequencies based on the lowest and highest values in menu (a). Frequencies are plotted on a logarithmic scale. Frequencies can be biased towards or away from a specified point on the scale.

A captured screen from the Nyquist set up menu is shown in Figure 3.4, part (a). The number of frequencies to be recorded is selected using the keys F1 to F4. From 4 to 32 frequencies can be recorded in a single sweep. Each frequency is allocated an equal number of samples in a recording. This varies from 2048 samples in 4 frequency recordings to 256 samples in 32 frequency recordings. In the main Nyquist menu, the user can set the number of whole cycles to as well as the frequency itself for each phase. It is necessary to record more than one cycle at the higher frequencies because of the limit on the loop time in the **Sweep** subroutine.

Although all each frequency can be altered individually from this menu, this is a lengthy process. Another set up screen performs this automatically. Pressing F8 calls the subprogram **NyqSetFreq**. This routine (Figure 3.4, part (b)) reads the highest and lowest frequencies set in menu (a). Using these values it automatically calculates the spacing for the intervening frequencies. This spacing can be calculated on a logarithmic or linear scale, the default is logarithmic. The frequencies positions are plotted across the screen, linearly or logarithmically. The phase number is written above each frequency dot, the frequency value is written below.

This procedure allows the user to bias frequencies towards the middle frequencies. This is especially useful for recording active responses, where the frequency characteristics of the muscle can be especially sensitive to frequency changes in the mid-range. The value for "bias" can be altered using the "+" or "-" keys. The actual value of bias is the ratio of the smallest log-frequency interval to the average interval for all frequencies. The left and right cursor keys can be used to move the bias centre to any point in the frequency range. The bias centre is shown as a vertical line on the frequency scale.

3.2.5.1 Nyquist amplitude correction

Once the Nyquist frequency range has been selected, a length correction routine can be performed. At the highest frequencies the motor cannot always match the amplitude output by the DAC. To prevent this change in amplitude with frequency, the correction procedure **NyqCorr** sets the values in the array **NyqLcorr!()**. This array contains the multiplication values for the amplitude of each frequency in the Nyquist series. At start-up all are set to 1, so that by default no amplitude correction is performed.

The correction routine records a Nyquist series and performs a discrete Fourier transform on the recorded length signal for each frequency. The value of **NyqLcorr!()** is modified according to the amplitude of the returned signal. The value in **NyqLcorr!()** is used to calculate the amplitude of the signal written into

the **DACout%()** array for the next recording. This process is repeated until the amplitude error for all frequencies is less than $\pm 4\%$. The values of the correction array are printed to the screen in the Nyquist set up menu (Part (a) of Figure 3.4, columns labelled "Lcorr").

It could be argued that this is an unnecessary correction, especially since the length signal amplitude is taken into account when calculating muscle stiffness for all sinusoidal analysis. However even at the small amplitude oscillations used in sinusoidal analysis the nonlinearity of the muscle is still apparent. The Nyquist plots of Insect muscle fibres are especially sensitive to the amplitude at which they are recorded (see Chapter 4 for more details).

In the example shown little amplitude error occurs, the largest is a 6.1% error at the frequency 1.3kHz. In this case the correction has made very little improvement to the recording quality. However when higher frequencies are specified or a slower motor attached to the apparatus, this correction procedure is more important. The correction values can also detect mechanical resonance problems in the apparatus.

3.2.6 Other recordings

From the main program screen of the muscle program, pressing Shift-F12 calls the subprogram **SignalParameters**. This displays a full screen menu in which the operator can define the properties of each phase in a recording. The program allows up to 20 different phases to be specified in terms of muscle length (**Offset!()** array), sample interval (**Sint%()** array) and sample number (**Snum%()** array). Each phase is assigned a row on screen. The cursor keys move the cursor to any field on the screen. Values can be updated by inputting a new value manually from the keyboard or changed incrementally using the Page-Up and Page-Down keys. For sinusoidal oscillations, the user can specify the amplitude, offset, frequency and number of cycles in the trace. In ramp length changes the ramp rate can be set.

Most menu changes are made in a friendly way. For example if the duration of a phase (in seconds) is altered, the **Sint%()** value is adjusted automatically. When physically impossible entries are made, a warning beep is given and the nearest value possible is substituted. Examples of this are frequencies specified that are too high, ramp rates which would last for longer than the duration of the phase and offsets which are beyond the range of the DAC.

Though this menu is more complex than the Nyquist or Step set-up menus, it is very versatile. A recording can be set-up from any combination of steps, ramps or sinusoids. Some of the more commonly used recordings can be

selected using the function keys. The pre-programmed parameter sets include fast steps, T1-T2 recordings, staircase recordings and recordings designed for motor calibration. Pressing the relevant function key will make all the necessary changes to the phase array values. This makes it more convenient to change recording styles during an experiment.

3.2.7 Datalab communication

Interfacing the Datalab to the PC presented an unexpected problem. The card used for the GPIB interface was compatible with BASICA and GW-Basic, but unfortunately pre-dates QuickBASIC. QuickBASIC differs from the former languages in the length of its string descriptors. The subroutines on ROM expect a 2 byte string descriptor, not the QuickBASIC 3 byte descriptor. A further complication is the address of card in PC memory. The card has a switch enabling the user to set the ROM segment address to any 64K page boundary. Unfortunately the subroutines on the ROM make calls to subroutines in page &hC000. For this reason if the card is set to any page other than &hC000 the ROM routines cannot possibly function.

Despite the ROM problem, the page switch will allow the registers necessary for GPIB communication to relocate successfully. I chose to write my own subroutines to send values directly to the registers on the bus controller chip. To do this it was necessary to disassemble CEC ROM and follow the code to find out how to program the controller chip TMS9914A.

Three machine code subroutines, **DLsend**, **DLreceive** and **DLchannels**, enable the computer to communicate with the Datalab. An initialisation sequence in Basic in the **Details** subprogram establishes contact with the Datalab and sets up the bus controller chip. A further subprogram called **DLdialogue** allows the user to type commands strings directly to the Datalab.

The **DLsend** and **DLreceive** subroutines, as their names suggest are simple routines which communicate short messages between the Datalab and the computer.

The **DLchannels** subroutine dumps channel data from the Datalab to arrays in the computer memory. A small array is passed to the subroutine when it is called. This array instructs how many channels to dump, the number of samples per channel and the location in memory of the arrays where the channel data is to be stored.

In normal recordings the channel data is dumped to two arrays called **Ldata%()** and **Tdata%()**. These arrays hold the length and tension channel data

respectively. The channel data is not written directly to the array memory, but is added to the values currently in memory. This simplifies the process of trace averaging, but makes it necessary to set arrays to zero before the first recording in a sequence.

3.2.8 Trace Averaging

Due to the high accuracy of the system and the repeatable nature of the majority of recordings made, it is possible to record and average a specified number of separate muscle responses to a given length signal.

This averaging results in a significant reduction in noise in the recorded data. This method of noise reduction is preferable to any kind of filtering, whether electronic or digital. A maximum of sixteen traces can be averaged in this way. This ceiling is imposed by the fact that **Ldata%()** and **Tdata%()** are two-byte integer arrays. The channel data from each run in an averaging sequence is added into these arrays and divided through by the number of runs at the end. To average more than sixteen traces would require the use of four-byte integers.

The use of signal averaging in this way, reduces noise by approximately the square root of the number of traces averaged. Using the maximum of sixteen averaging runs will result in about a four fold improvement in the signal to noise ratio. Only when very small length changes are imposed is such a number of runs necessary. Since the improvement in data quality decreases with each run, it is usually not worthwhile to perform more than five. Unlike digital and electronic filters, this method of noise reduction is not frequency dependent. Both high and low frequency noise are reduced equally well.

Ideally, for each trace in an averaging sequence, the fibre should be in the same chemical, thermal and mechanical environment. Particularly during mechanical perturbations greater than 0.5% in activating solutions, there are large changes in the concentrations of ATP, ADP and Pi within the fibre and in the solution immediately surrounding it. For this reason in such recordings there is a forced wait between averaging runs to allow the fibres chemical environment to equilibrate. The duration of the wait period is set in the **Details** menu. In recordings which involve a large amplitude stretch activation, a wait period greater than 10s can be necessary.

3.2.9 Finding zero tension

Due to the slow drift in the tension transducer circuit, frequent zeroing recordings are necessary. A zeroing trace is usually made with each recording,

although this option can be turned off in traces where the step may damage the fibre. The subprogram **Zero** performs this function.

To find zero tension a large amplitude (more than 1%) step release is recorded. Step releases of this amplitude cause the fibre to go slack. The tension samples recorded in the few milliseconds following the step are averaged and the result stored in the variable **zeroT%**. Once recordings are finished, the value in **zeroT%** is subtracted from all values in the **Tdata%()** array (similarly **zeroL%** is subtracted from **Ldata%()**). The zeroing trace alone can be executed by pressing Shift-F9. The **Zero** subprogram prints the present value of steady state tension on the screen. This can be useful when following the progress of slow activations.

When several traces are being averaged, the zeroing trace is recorded in the middle of the averaging set. Assuming a steady drift in one direction, this method gives the best estimate for the average value of **zeroT%** for all the traces. This is important when averaging many traces that last for several seconds.

3.3 Viewing traces

3.3.1 Plotting the data to screen

The main program screen is made up predominantly of a plot of the data. The data may be plotted in one of four ways. Figure 3.5 shows captured screens of all four plotting methods. All the screens are plots of the same recorded trace. Pressing the F2 key cycles the muscle program through these different plot types. The plots used most often are the length and tension against time and the tension against length plots ((a) and (c) in Figure 3.5). The sample number plot (b) is useful when finding the best values for the number of samples and sample interval when setting up the recording phases. The $\log_{10}(\text{time})$ plot is good way to view all the muscle tension processes in equal detail without needing to alter the timebase. When fitting exponentials to tension transients, a single log plot can show how well the fitted curve describes the fastest and the slowest processes simultaneously.

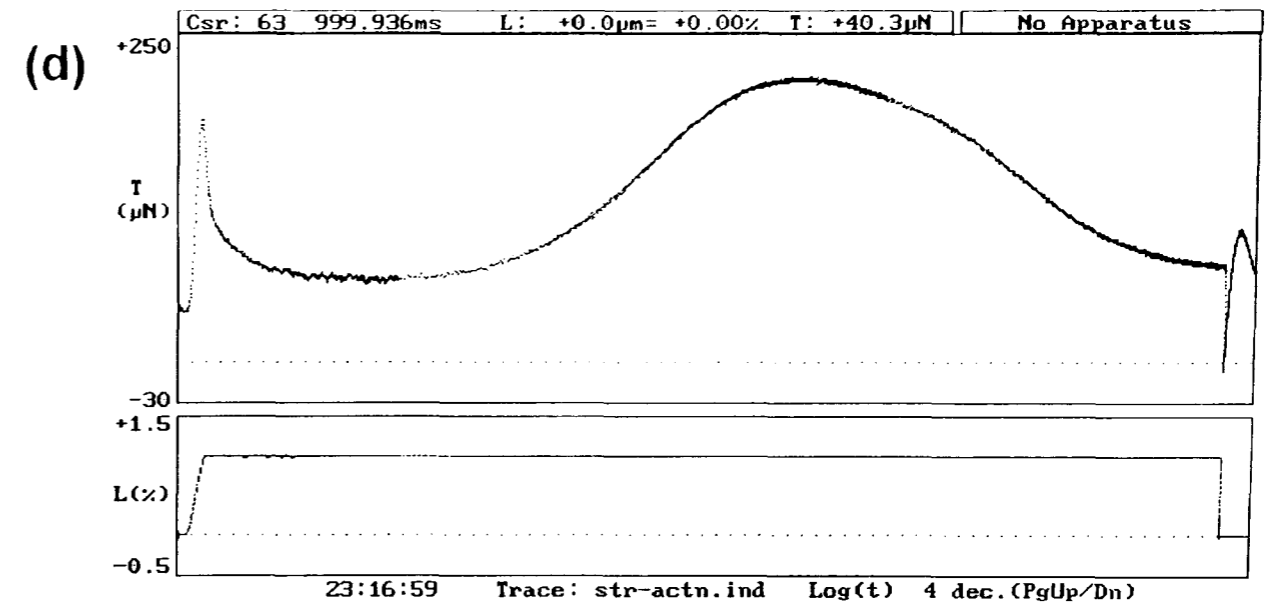
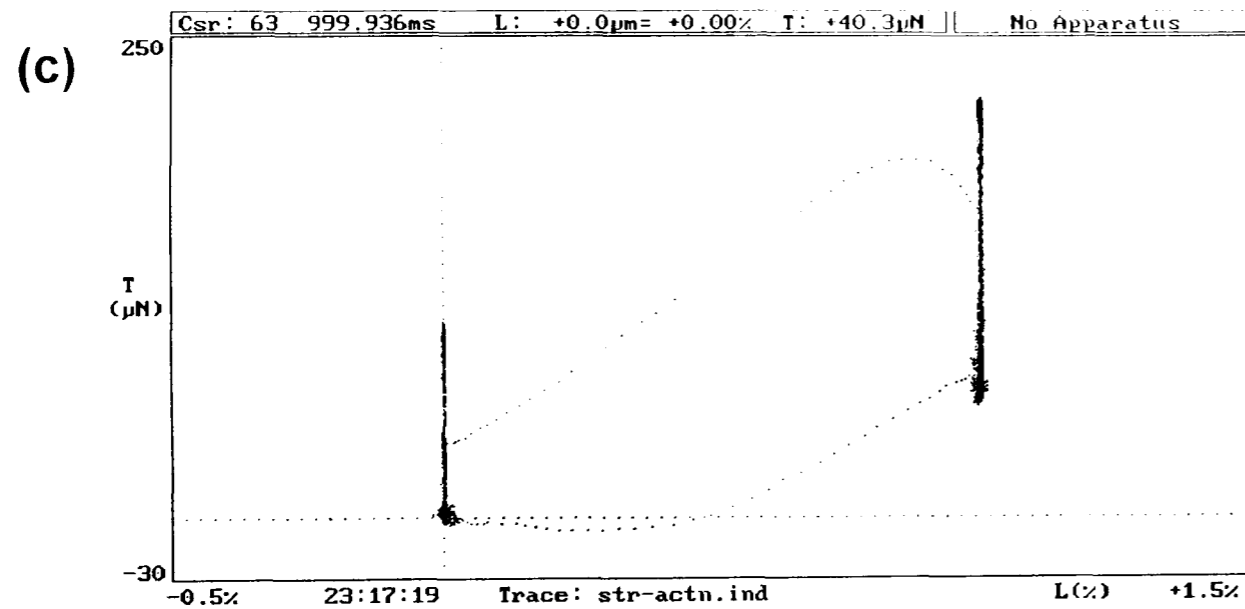
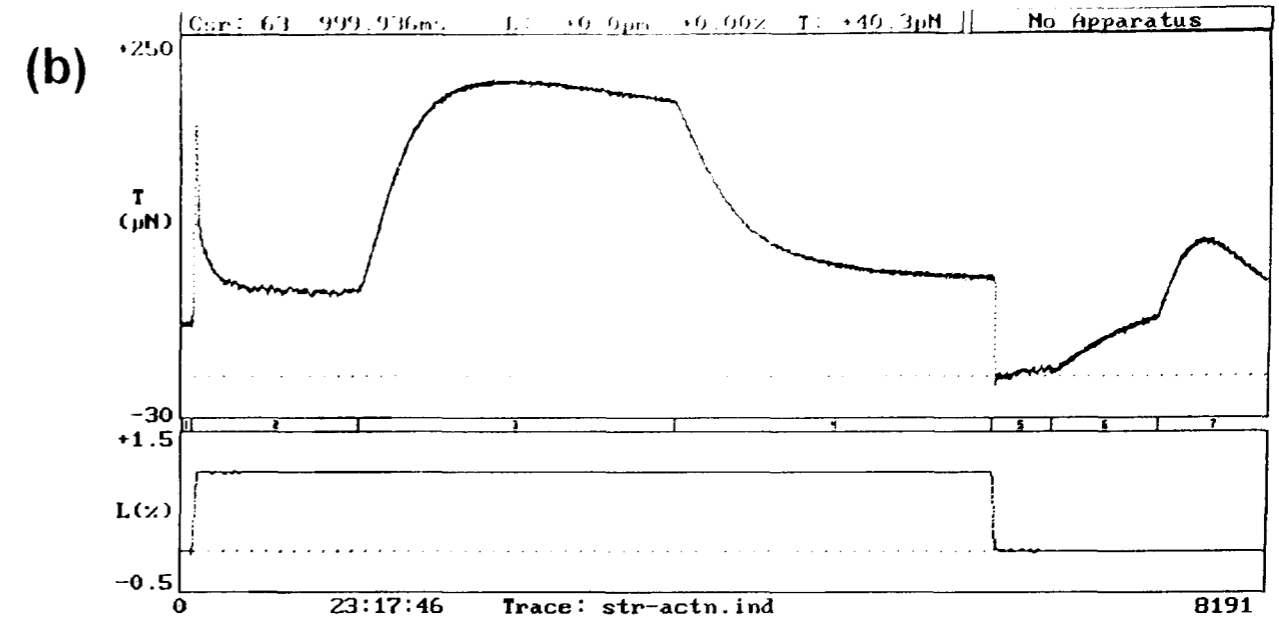
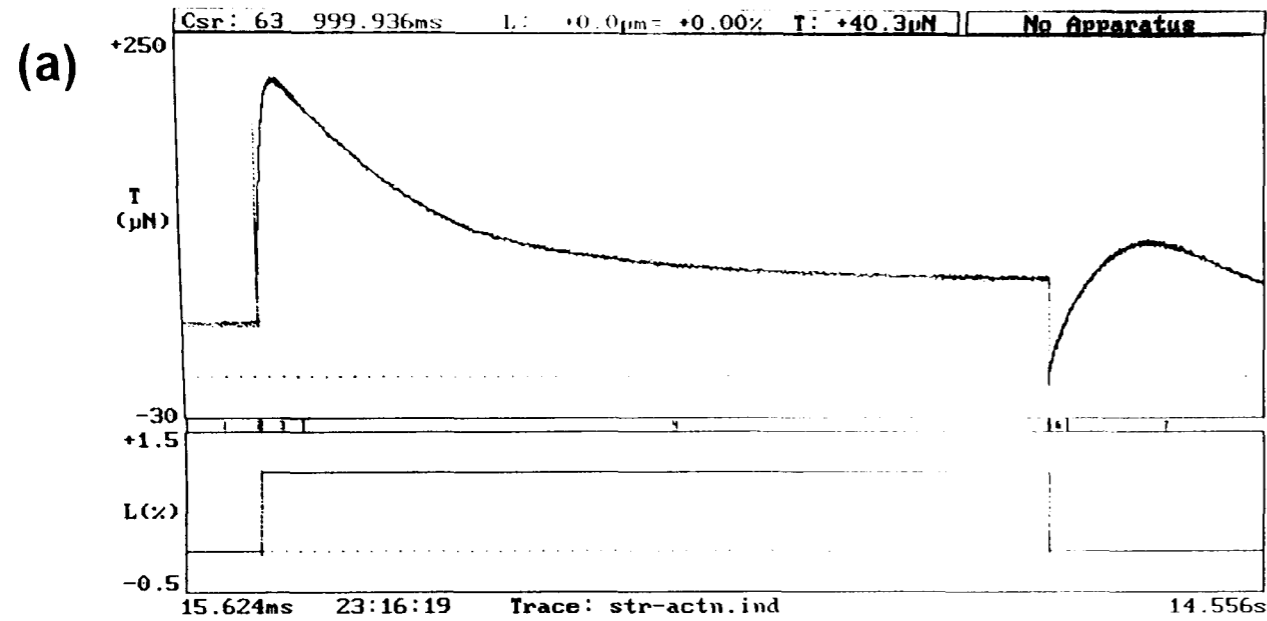


Figure 3.5: Diagram showing screens captured from the muscle program. These show the four ways that a recorded trace can be plotted to the screen. The plot types are (a) length and tension against time, (b) length and tension against sample number (c) tension against length and (d) length and tension against $\log_{10}(\text{time})$. The same data trace is displayed in all plots. All trace samples are plotted in all views except (d), where the first few points are not plotted.

A cursor cross is always present on screen (not visible in the screens shown). Information about the current cursor position is displayed on the top line of the main screen. This line shows the time, length and tension of the data highlighted by the cursor cross. The cursor can be moved in several ways. The left and right arrow keys move the cursor by one sample. This movement speed is increased when the CTRL key is also pressed. The Page-Up and Page-Down keys move the cross by a whole recording phase. The Home and End keys move the cursor to the first or last data points on screen. If a Microsoft (or compatible) mouse is present, the cursor cross can be moved to any data point on the screen by moving the on-screen pointer to the relevant data and clicking the primary mouse button. The cursor cross follows the mouse if the primary button is held on.

The plot screen can display between 2 and all 8192 data samples. There are several ways that the user can zoom-in on part of the trace. A single phase can be plotted by entering the phase number from the keyboard. The present cursor position can be made the first or last point plotted on screen by pressing "L" or "U" respectively. Clicking the primary mouse button to the left of the data plot area causes a vertical line to be drawn down the screen. If the mouse button is held closed, this line can be dragged to any point on the screen. When the button is released, the screen is re-plotted starting from this position. Similarly clicking to the right of the plot area allows the upper plot boundary to be selected. Pressing "A" on the keyboard re-plots all the data.

All the data plots are created by a single machine code subroutine called **Datplot**. The details of the plot are passed to the subroutine in a single data array. The information sent to the subroutine includes the plot type, the number of points to plot, the number of data series to plot. With each data series plotted, the subroutine must be told where in memory to find the data, where to plot on screen and the pixel colour for that series.

The subroutine automatically detects the current screen mode. This allows it to exit gracefully if it detects a text mode, and not to attempt to plot pixels that map off-screen. The subroutine works in all the commonly used graphics modes on the IBM PC (Hercules, CGA, EGA and VGA but not super-VGA). In the two graphics modes used in the muscle program, pixels are plotted directly into screen memory. This is much faster than using the pixel plotting routines available by using software interrupt 10.

3.3.2 Printing routines

The muscle program contains a simple printing routine. This routine allows graphics screens to be dumped to an Epson compatible dot-matrix printer connected to LPT1. A more complex printer interface has not been implemented for two reasons. Firstly there is no industry standard interface for dumping graphics files to printing devices. Secondly, with the now commonplace use of the Microsoft Windows as a working environment, screens from DOS applications can easily be captured and pasted into graphics packages or word processors. From here the images can be saved to disk or printed using the normal Windows procedures.

3.3.3 Data smoothing

Despite the use of low noise amplifiers the signal to noise ratio from the strain gauge amplifiers is not as high as I would like it to be. Electronic filtering could reduce the high frequency noise to much more acceptable levels. Unfortunately, as the level of analogue electronic filtering increases, the high frequency response of the circuitry decreases. This reduces the highest frequencies at which accurate stiffness measurements can be made.

An alternative to this is to filter data after capture. This has several advantages over analogue electronic filters. Firstly and most importantly, software filtering introduces no phase shift into the signal. Electronic filters introduce a shift into the signal because they only have the present signal value and its recent history to work on. However, software filters that work on previously captured data, can make use of the future signal as well as previous values when filtering a data point. The data points immediately before and after the point to be filtered are treated on an equal basis.

Many filtering algorithms can be used, the simplest to imagine being moving average filters. In a three point moving average filter, a data point is averaged with the data points on either side of it. As more points are used in the averaging filter, more smoothing is obtained. Moving average filters are fast and simple to write. Unfortunately they have the tendency to smooth out the tops of peaks in the data. During rapid length changes, sharp peaks occur in the tension data that give the experimenter information about the stiffness of the fibre. For this reason a filter that reduces the peak height would remove important information from the data.

Other more complex convolute functions exist which allow for weighting or favouring of data nearest the filtered point. This reduces the tendency to smooth

out sharp peaks in the data. A further improvement on this would be a filter that places the point on a line which best fits the data in its vicinity. The most popular numerical criterion for defining 'best fit' is that of least squares. That is the minimisation of the squared difference between the fit curve and the data.

Savitzky and Golay (1964) describe a method to perform least squares smoothing using simple integer arithmetic. This method allows a polynomial to be fit to the data to determine the best value for the central point. However it is not necessary to do any complex curve-fitting arithmetic. Savitzky and Golay publish tables of integers which when used in a weighting function give exactly the same results as fitting polynomials using least squares. Corrections necessary for some of the tables are given by Steinier *et al* (1972).

The tables include integer sets to fit a cubic or a quintic equation to the data to find the best value for the smoothed data point. The exact curves being $y = a_0 + a_1x + a_2x^2 + a_3x^3$ for the cubic and $y = a_0 + a_1x + a_2x^2 + a_3x^3 + a_4x^4 + a_5x^5$ for the quintic. The smoothing tables shows integer sets for filters from 5 to 25 points for cubic smoothing and from 7 to 25 for quintic smoothing.

The code to perform data smoothing is written in machine code, in the subroutine **Filter**. This subroutine contains the all the smoothing integer sets. When the subroutine is called, the arguments passed include the number of data points to filter, the location of the data in memory and a three letter string which specifies the filter type. For example "A13" would perform a 13 point moving average filter, whilst "Q25" a 25 point quintic smoothing filter.

The filtering process is fast. To smooth 8192 data points using a 9 point cubic filter takes less than one second on the 16MHz 286 used for experiments. Since filtering is so fast, the traces are stored on disk in the original captured form and filtered later if necessary. Traces should be stored in their original unfiltered form, since the filtering process may remove some information that is required later. When filtering is done, the filter type is added to the on-screen trace name. The presence of this addition prevents the trace being saved to disk or filtered more than once. To apply a different filter, the original data must be loaded back from the disk.

The cubic and quintic smoothing filters dramatically alters the appearance of the plotted data. Small tension changes which were previously hidden in the high frequency noise become much more clear. Improving the appearance of the recorded traces, and making small signal changes more visible are the main use of these smoothing filters. In terms of Fourier analysis and exponential fitting, the smoothing filters make no significant change to the results obtained from these analyses.

3.4 Saving and loading traces

The Basic subprograms **Savetrace** and **Loadtrace** allow traces to be saved to disk and retrieved. Length and tension channel data is written to disk in binary form. With the data from both channels (16K each) and some environment and trace information, the trace data files occupy approximately 33K each.

As well as the channel data, the following information is saved with each trace; experimenter names, muscle species name, muscle length, apparatus calibrations, number of traces averaged to create the trace and all the relevant signal description arrays.

The method Basic uses to save integer values to disk is very slow. For this reason a small machine code subroutines (**FastSave**) copies the channel data to a fixed length string which Basic then saves to disk. The subroutine **FastLoad** performs the converse action when loading the trace from disk.

The filename used to save the trace is created automatically by the save subprogram. A user-defined filename can be given the trace is saved using the Shift-F4 "Save trace" option. The filenames generated by the savetrace subprogram have the format shown in Figure 3.6.

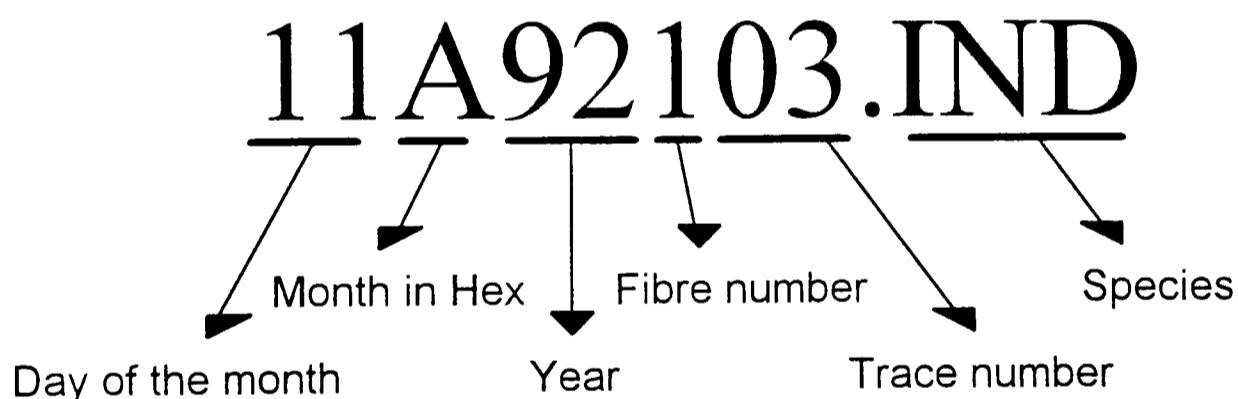


Figure 3.6: Diagram illustrating the nomenclature for muscle trace files.

This filename format appears complex. However the amount of information that can be obtained simply by viewing a directory listing makes the complexity worthwhile. Using simple masks and wild-cards, all the recordings made on one day can be listed from a directory or disk containing many files.

3.5 Exponential fitting

Accurate values for the amplitudes and rate constants of the phases in the tension signal can be obtained by fitting exponentials to the captured data. The software to fit up to five exponentials to the data was incorporated into the muscle

program. Exponential fitting is one of the more complex types of curve fitting problems, requiring an iterative procedure to estimate the parameters.

3.5.1 Introduction to Linear and nonlinear regression

Most curve fitting problems can be solved by linear regression. In this context the word *linear* can be interpreted in two ways. Firstly, it could mean that the curve to be fitted is a straight line. Secondly and more relevant here, that the curve function is linear in its parameters. Meaning that the function has no products of parameters or parameters in exponents. This distinction is very important here, because the solution to nonlinear regression problems is not nearly so straightforward as for linear.

In most regression analysis, the best fit is calculated by minimising the sum of the squared difference between the data and the fit curve, also known as the sum of the squares. That is the point at which the fitting parameters (β) are at such values that the sum of the squares $S(\beta)$ is at its global minimum.

$$S(\beta) = \sum_{i=1}^n [Y_i - f(X_i, \beta)]^2$$

For most purposes, regression analysis is described with Σ s with standard algebraic notation. The mathematics can be described equally well using matrix algebra. In fact using matrices can make the algebra considerably easier, especially when several parameters are involved or there are more than one regressor variable (multiple regression). Here matrices will be written as single letter in bold non-italic type, for example \mathbf{Y} .

In matrix notation the function to be fitted to the data (X_1, Y_1) , $(X_2, Y_2), \dots, (X_n, Y_n)$, with parameters $\beta_1, \beta_2, \dots, \beta_p$ can be written as

$$\mathbf{y} = \mathbf{X}\beta + \varepsilon$$

where:

$$\mathbf{y} = \begin{bmatrix} y_1 \\ y_2 \\ \vdots \\ y_n \end{bmatrix}, \quad \mathbf{X} = \begin{bmatrix} 1 & x_{11} & x_{12} & \cdots & x_{1k} \\ 1 & x_{21} & x_{22} & \cdots & x_{2k} \\ \vdots & \vdots & \vdots & & \vdots \\ 1 & x_{n1} & x_{n2} & \cdots & x_{nk} \end{bmatrix}, \quad \beta = \begin{bmatrix} \beta_0 \\ \beta_1 \\ \vdots \\ \beta_k \end{bmatrix} \quad \text{and} \quad \varepsilon = \begin{bmatrix} \varepsilon_1 \\ \varepsilon_2 \\ \vdots \\ \varepsilon_k \end{bmatrix}.$$

The $(n \times 1)$ vector \mathbf{y} contains the y data. The matrix containing the x data is \mathbf{X} . It has one column for each parameter and so is an $(n \times p)$ matrix. The parameter vector β is $(p \times 1)$, and the errors are in ε which is an $(n \times 1)$ vector.

the sum of the squares $S(\beta)$ reaches a minimum. It is possible to imagine a three dimensional surface plot in which the two parameters β_0 and β_1 are the horizontal axes and $S(\beta)$, the dependent variable, is the vertical axis.

The shape of this surface depends on how well the data can be described by a single exponential. With data that accurately follows a single exponential with little noise, the surface would be smooth and have a single very distinct minimum point. The position of this minimum point shows the optimal values for the two parameters, $S(\hat{\beta})$. Unfortunately, data is rarely so ideal. With more noisy data the sum of the squares surface is much less regular. The surface may contain many local minima, as well as the global minimum point. Also the global minimum itself may be a long valley, that is it may be well defined for some parameters, but not so clear for others.

Most iterative fitting algorithms work by looking at the shape of the sums of squares surface in the neighbourhood of the present parameter values, and making a best fit estimate from that information with each iteration. The different algorithms vary according to how they decide the best changes to make to the parameters with each iteration.

The simplest fitting algorithm to imagine is the *steepest descent* method. This method examines the slope of the surface at the present parameter values and moves the parameters in the direction of the steepest gradient until convergence, that is a minimum point is reached. When more than two parameters are being fit, the mechanism becomes much harder to visualise, however the mathematics is not much more complex. The direction of the vector used to change the parameters is of the form

$$-\frac{\partial S(\beta)}{\partial \beta_1}, -\frac{\partial S(\beta)}{\partial \beta_2}, \dots, -\frac{\partial S(\beta)}{\partial \beta_p}.$$

Different steepest descent methods vary according to how they define the magnitude of the step. This method is fast to converge when the surface is ellipsoidal with a single global minimum. Unfortunately when the $S(\beta)$ surface is irregular, the steepest descent method can be very slow and inefficient. The parameters may find themselves stuck in a local minimum which is not close to the best fit, or moving very slowly down a long valley. Typically the algorithm will make good progress at first, especially if the starting parameter values (β^0) are not close to $\hat{\beta}$, but become painfully slow close to convergence.

A better method to use when the surface is non-ellipsoidal and irregular is the *Linearization method*. Other names for the same method include *Gauss-Newton*, *Taylor Series*, and *Inverse-Hessian method*.

As these names suggest this method uses a Taylor series expansion of the gradient at $S(\beta)$ to make a linear approximation of the function. Only the first order terms are required to give a reasonable approximation of local curvature. The linearization method is usually faster than the steepest descent method when the parameters are close the global minimum values.

By far the most common algorithm used in nonlinear parameter estimation is a compromise between these two methods. This is the *Marquardt algorithm* (Marquardt, 1963), it combines the advantages of both the steepest descent and the linearization method. Other names that refer to the same algorithm include *Levenberg-Marquardt*, *Marquardt's compromise*, and *Maximum Neighbourhood*.

In the Marquardt algorithm parameter change direction lies somewhere between that suggested by the linearization and the direction of steepest descent. The variable λ dictates the exact direction. When the value of λ is high the parameters change in the direction close the steepest descent. When $\lambda \rightarrow 0$, the parameters change is more Gauss-Newton.

The Marquardt algorithm begins with a large value for λ . As fitting progresses the value decreases with each iteration. However the value is increased if Gauss-Newton cannot find a solution, and the iteration repeated.

3.5.3 Exponential fitting procedure

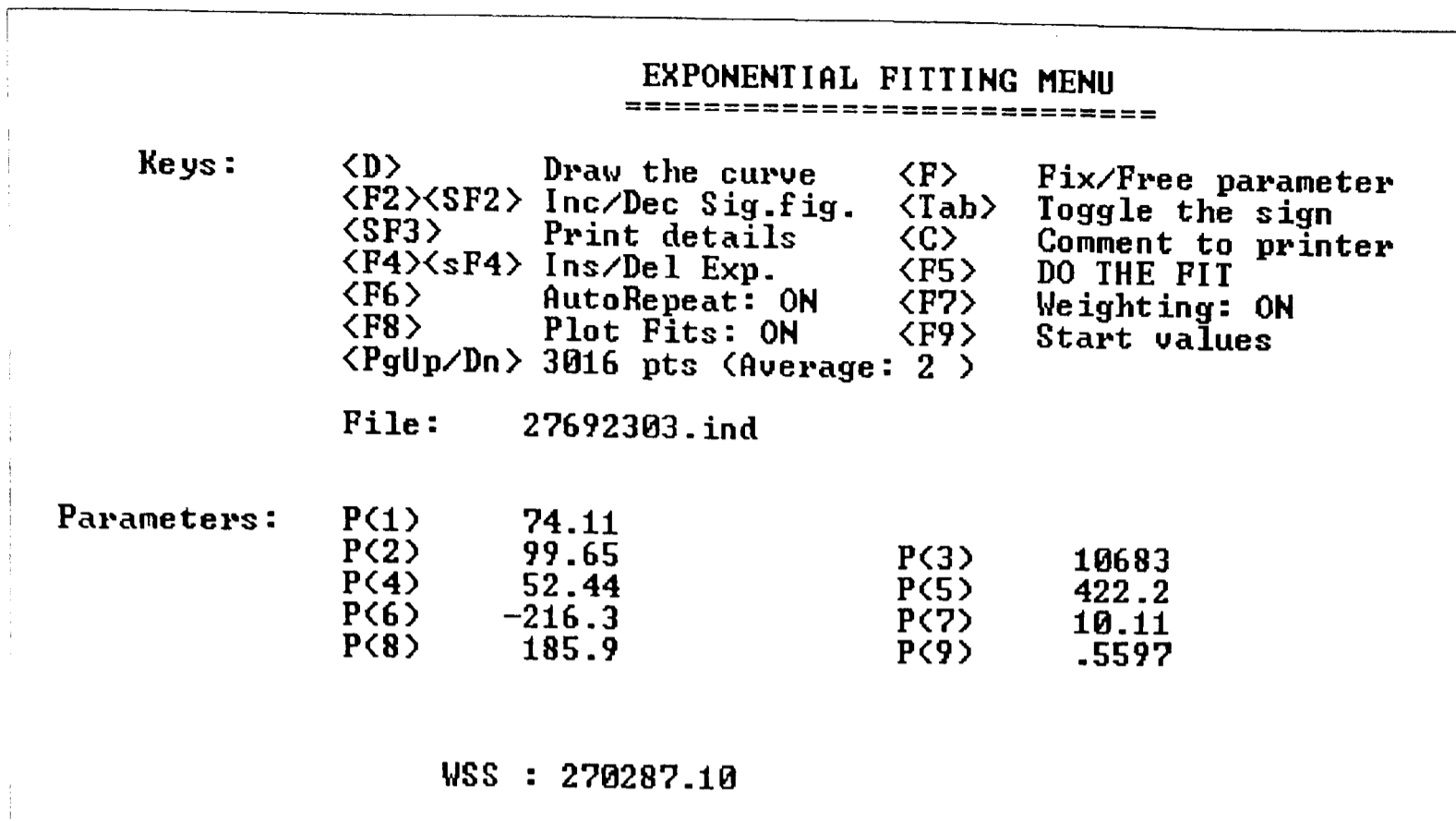
The exponential fitting menu is accessed from the main program screen by pressing F5. Before this the user must select the data points to be used for curve fitting. This is done from the main program screen by windowing the data. In the exponential fitting menu (Figure 3.7 part (a)), the user is able to set up the fitting environment.

From the fitting menu the starting parameters can be edited. The first parameter P(1) is the offset for the fit equation. The parameters below this describe the exponential processes, the exponential amplitudes on the left (units are μN) and the rate constants on the left (sec^{-1}). In the example screen shown a total of four separate exponential processes have been fit, the equation fit to the data is as follows:

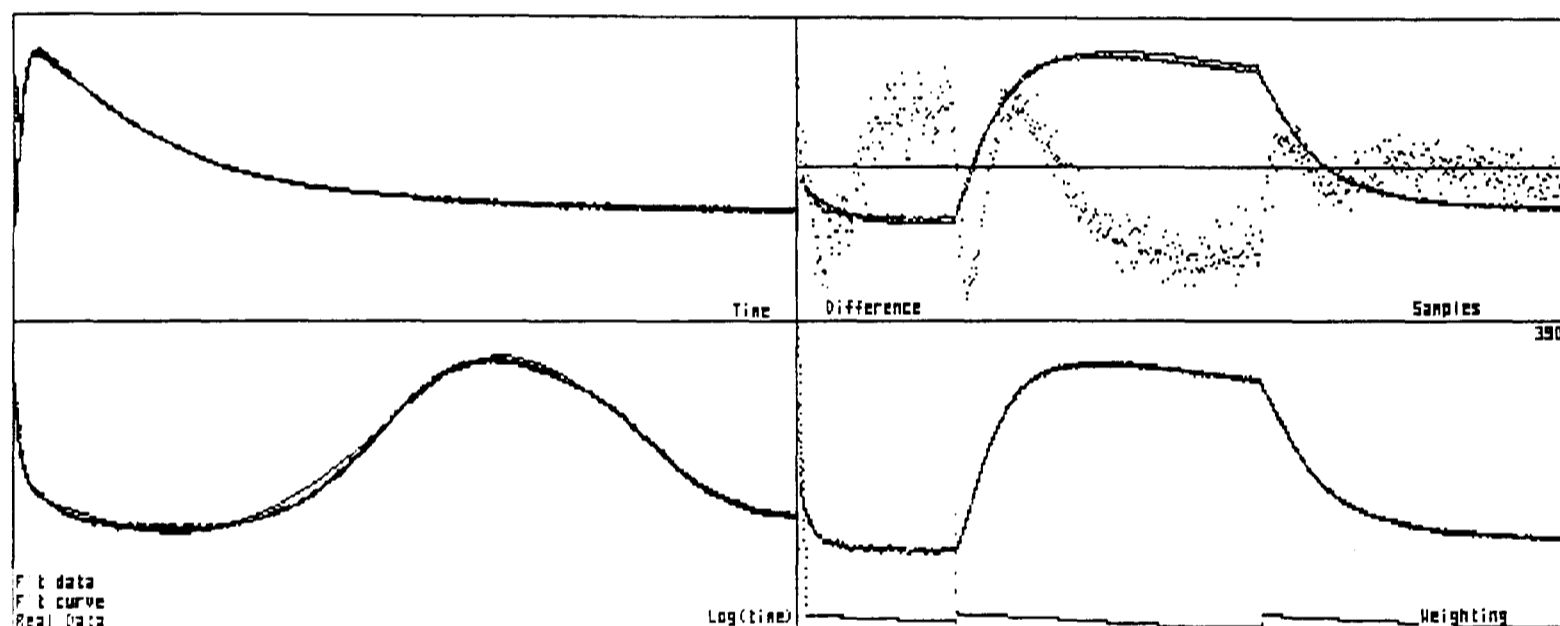
$$P(1) + P(2).e^{-P(3).t} + P(4).e^{-P(5).t} + P(6).e^{-P(7).t} + P(8).e^{-P(9).t}.$$

(a)

Software



(b)



Parameters: P(1) 1.00031 74.053680
 P(2) 0.99990 99.687538 P(3) 0.99995 10682.799805
 P(4) 0.99851 52.637203 P(5) 1.00920 417.040955
 P(6) 0.99981 -216.454971 P(7) 0.99947 10.129509
 P(8) 1.00013 185.809082 P(9) 1.00058 0.558987

#2 Time: 140.16s Points: 3016 (Ave. = 2) File: 27692303.ind
WSS : 269579.56000563 (Mean : 2.76 μ N)
Improv. : 1.000781173483 Lambda : 0.099999998

Figure 3.7: Exponential fitting. The fitting menu (a) allows the user to set the fit starting values and the extent of data averaging before fitting. (b) As the fitting algorithm progresses the parameters are printed on the screen as they are modified, and the the current curve is plotted against the data. Four separate plots are shown. The fitted curve is plotted over the data with time (upper left) and with log(time) (lower left). The upper right plot shows the data and the fitted curve plotted against sample number, along with another plot showing the difference between the data points and the curve. In the lower left plot, the data is shown along with the current weighting function applied to the data points.

Individual parameters can be fixed by moving the text cursor to the parameter and pressing "F". Repeating "F" will free a fixed parameter. Parameters fixed in this way are not adjusted during the fitting procedure. The number of data points that are sent to the fitting routine can be adjusted using Page-Up and Page-Down. Fitting a curve to a small number of data points is fast, but produces a less accurate fits than when larger data sets are used. If "Auto repeat" is selected by pressing F6, a sequence of fits is done. With each fit in the sequence more data points are sent, until the last fit where all the data is used. Pressing F5 begins the fitting procedure.

Part (b) of Figure 3.7 shows an example screen of the fitting algorithm in progress. The new parameter values are printed to the screen with each iteration. To the right of each parameter, the ratio of the parameter to its value in the previous iteration is shown. These values tend towards 1 as the fit progresses. This value shows which parameters are changing most rapidly. It can also indicate parameters which are causing difficulties in the fitting process.

During the fitting process the four data plots are regularly updated. The two plots on the left of the screen display the current curve fit plotted over the data against time (upper) and log-time (lower). The upper right plot expands the difference between the data and the fit curve (plotted against sample number). Below this the data weighting is shown, also plotted against sample number.

3.5.4 Exponential fitting software

The implementation of the Marquardt algorithm in the muscle program is modified from a version published by Schreiner *et al* (1985). The majority of the mathematical operations are done in Basic. A machine code subroutine is used to when calculating the value of the exponential processes at a given time (**ExCalFn**).

I made some minor modifications to the Marquardt algorithm. In the original algorithm the sign of any of the parameters is free to change. When fitting to muscle transients this is not useful. The rate constants will always remain positive, since these are always decays and never a growth exponentials. Secondly, sign of the amplitude of each phase will not change since this depends on direction of the length change. In fact when the algorithm attempts a sign change, a warning beep occurs and the offending parameter is highlighted temporarily. An attempted sign change in this situation indicates that the procedure has gone 'off track'. In some cases this may require some user intervention. Pressing any key during the fitting procedure will make the program return to the fitting menu after completion of the current iteration.

3.5.5 Data Weighting

Due to limitations on the highest possible sample rate, the fast phase 2 rapid relaxation process is made up of far fewer samples than are phases 3 and 4. For this reason, unless the data is weighted in some way, the phases made up of more samples will be favoured in the fitting process. The **Wgt!()** array contains a weighting value for all the data values sent to the fitting procedure. The weighting assigned to each data point takes into account the both the time interval from the previous data point and also the contribution of the data point to each of the exponential processes (based on the starting rate constant values). The data weighting function can be toggled on and off using the F7 key.

3.5.6 Exponential fitting problems and considerations

In some situations the accuracy of the starting values has a very large effect, not only on the speed of convergence but also on the accuracy of the result. However in most cases, when fitting exponentials to muscle tension transients, the default values or the result of a previous fit are good enough.

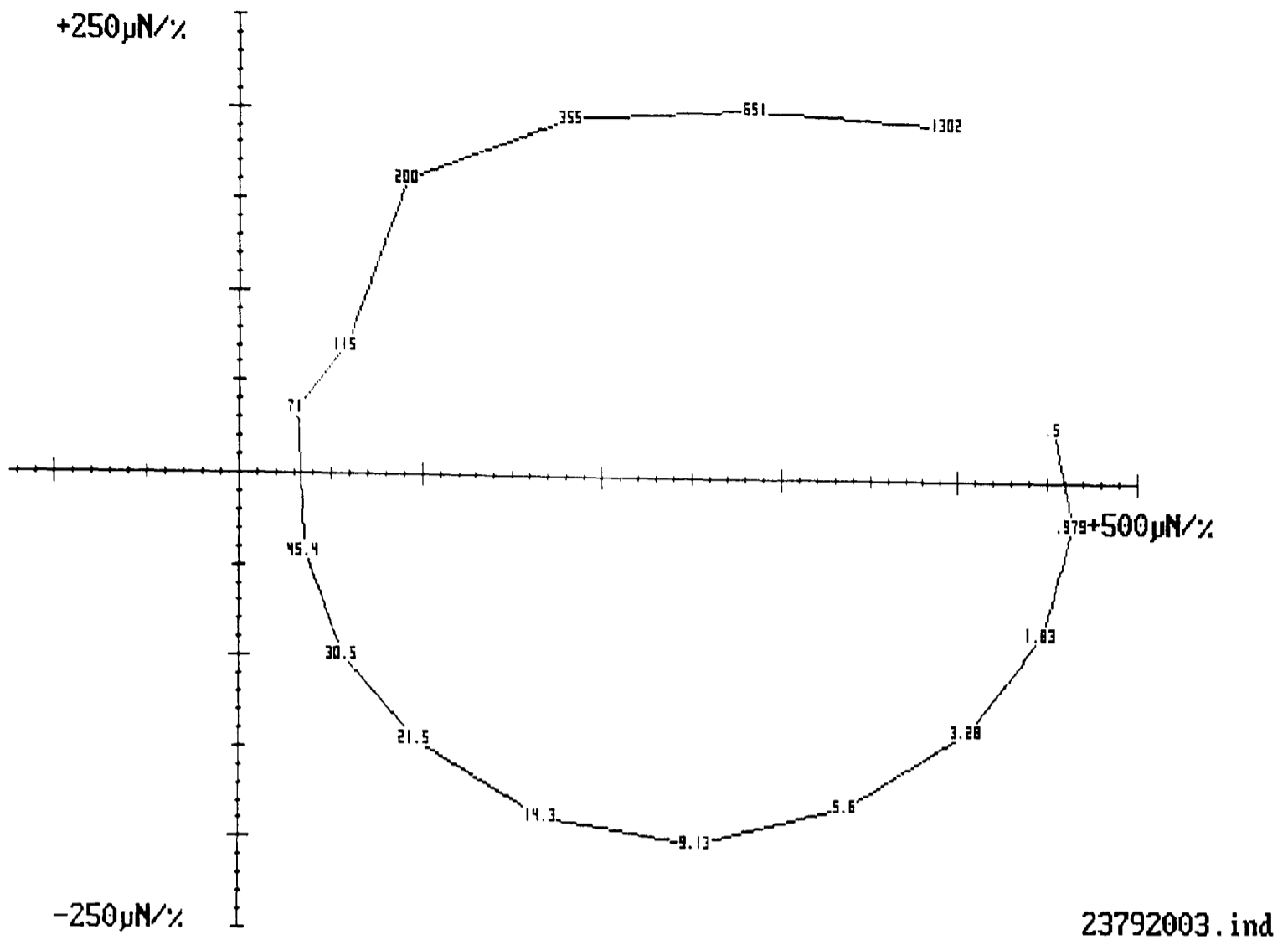
The software does not quantify goodness of fit for the exponential curves. The result of the final weighted sum of squares is not a good criterion since this value is sensitive to the weighting function applied, the amplitude of the processes being fit and the noise in the tension signal. Presently the only criterion for judging the quality of fit is the appearance of the fit curve after convergence.

3.6 Sinusoidal analysis

With a Nyquist style recording loaded, pressing F7 will invoke the Nyquist analysis. By calling the subprogram **Fourier**, a discrete Fourier transform (DFT) is performed on all the frequencies in the series. If a phase contains more than one cycle, then these cycles are averaged into one cycle before the DFT is done. This is a simple process since the number of cycles and also the number of samples in a recording phase are always numbers of the form 2^x , where x is an integer.

Using the results of the DFT performed on the length and tension signals, the phase relationship of the two signals is calculated. Using the phase shift and complex stiffness values, the In-phase and quadrature stiffnesses are calculated. The DFT results can be shown drawn over the data (optional). This demonstrates the linearity of the tension signal.

(a)



(b)

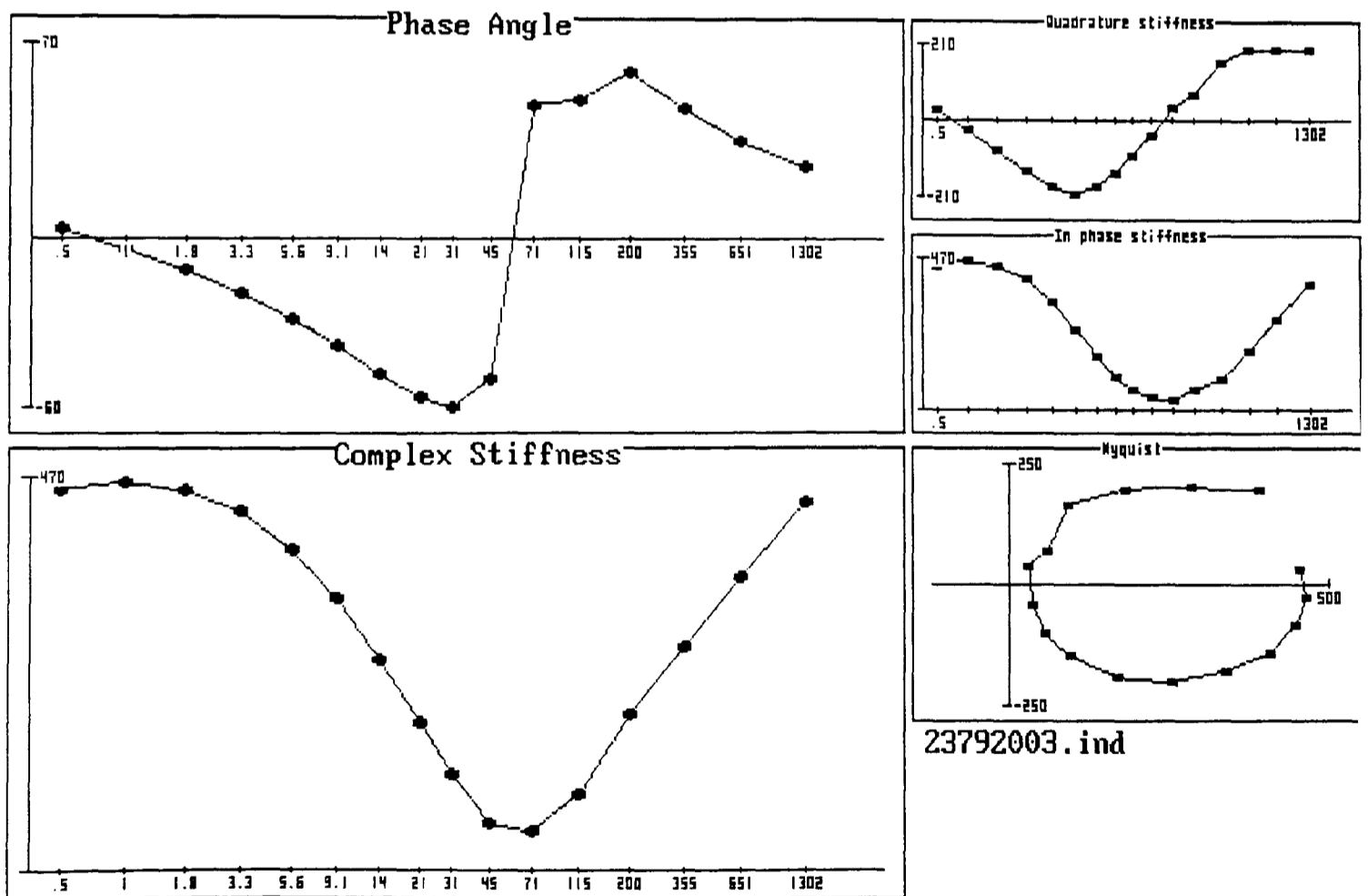


Figure 3.8: An example of the Nyquist plot and Bode plot screens. These plots describe the small signal frequency characteristics of one or more Nyquist recordings. Using a menu screen, multiple Nyquist analysis results can be stored and plotted together.

The Nyquist plot menu can store the phase shift and stiffness results for up to 16 different traces, each trace with up to 32 frequencies. This allows the results from traces to be compared on the same plot. The results of the DFT analysis can be shown in different ways.

Examples of a Nyquist plot and a Bode plot are shown in Figure 3.8 (parts (a) and (b) respectively). Both the plots shown are screens captured directly from the muscle program. In a Nyquist plot the quadrature stiffness is plotted against the in-phase stiffness. The frequency of the individual points can shown on the plot. In the Bode plot, the phase shift and complex stiffness are plotted separately against the Log(frequency). The example Nyquist plot and Bode plot shown are from the same trace.

Both the Nyquist plots and Bode plots can display the frequency responses from up to 16 traces. When using a colour monitor, each plot is shown in a different colour. This makes it simple to identify the individual plots.

3.7 Future Work

3.7.1 Curve Fitting to Nyquists

A very important, and possibly quite simple, addition to the sinusoidal analysis software would be the ability to fit a curve to Nyquist plots. Like the exponential fitting algorithm, this is a nonlinear problem. It may be possible to fit a curve by making some modifications to the present Marquardt algorithm. The ability to fit a curve to the Nyquist plot would mean that rate constants for the three major processes could be extracted from the Nyquist recordings. This would be a great improvement on the present case where only qualitative observations and comparison of Nyquist plots can be made.

3.7.2 High frequency correction

Ford *et al* (1977, Appendix F) describe a method to correct the tension signal data given the mechanical limitations of the transducer itself. This correction is important when the frequency response of the strain gauge is limiting the accuracy of high frequency stiffness measurements. At each tension data point ξ , the value is corrected depending on the velocity and acceleration of the signal, to give the corrected signal ξ_{corr} .

$$\xi_{\text{corr}} = \xi + \frac{b_t}{k_t} \dot{\xi} + \frac{m_t}{k_t} \ddot{\xi}$$

The other values required in the above equation describe the mechanical characteristics of the transducer itself. They are the damping coefficient of the transducer b_t , its effective stiffness k_t and the mass of the moving part of the transducer m_t . Ford *et al* (1977) describe how the coefficients b_t/k_t and m_t/k_t can be calculated from the resonant frequency of the transducer ν_t and the time constant of the decay of its resonance τ_t as follows.

$$\frac{m_t}{k_t} = \frac{1}{(2\pi\nu_t)^2 + (1/\tau_t)^2}$$

$$\frac{b_t}{k_t} = \frac{2}{\tau_t} \times \frac{m_t}{k_t}$$

The method recommended to find the velocity and acceleration of the signal is to use the data values immediately before and after the data being corrected. However, due to a combination of a high data rate and noise in the signal, this frequency correction simply results in a large increase in the noise in the corrected signal. This noise is caused by the unreliable way in which the velocity and acceleration of the signal are calculated.

One way to reduce this would be to apply the previously described least squared smoothing algorithm before the frequency correction. However, by far the best solution would be to modify least squared algorithm to calculate accurately the first and second derivative of the signal. Savitzky and Golay (1964) and Steinier *et al* (1972) provide the integer sets necessary to do this.

4. Materials, Methods and Controls

4.1 Introduction

This chapter serves as a general materials and methods chapter describing the techniques used for single fibre mechanical experiments. Also described are several experiments performed to investigate the optimal conditions to make single fibre recordings.

4.2 Muscle fibres

4.2.1 Flight muscle dissection

The flight muscle used in the majority of experiments was the dorsal longitudinal muscle of *Lethocerus*, the giant waterbug. *Lethocerus indicus* (Thailand) and *Lethocerus griseus* (Florida) were kept alive in the laboratory for up to a year, fed with live goldfish.

Before dissection, the waterbug was cooled on ice for two minutes to make it easy to handle. Using scissors, the head was removed, followed by the legs and wings. Using small scissors, the cuticle of the abdomen was cut close to the thorax. Here care was taken so little damage was done to the gut. The abdomen was pulled away from the thorax, at the same time removing as much gut as possible. Avoiding the flight muscle, sharp scissors were used to remove the ventral side of the thorax cuticle. Any remaining gut was removed, to avoid exposing the flight muscle to gut enzymes.

The thorax was immersed in a glycerol extraction solution. This procedure demembrates (skins) the fibre by a combination of two mechanisms. The glycerol disrupts the membrane by a process of osmotic shock, while a detergent disrupts the membrane chemically.

For the first 24 hours of demembration, the thorax was kept on ice. In this time there were solution changes at 1 hour and at 6 hours. Glycerol solutions contained 50% glycerol (v/v), 20mM potassium phosphate buffer, 1mM sodium azide, 1mM dithiothreitol (DTT), 2mM magnesium acetate and adjusted to pH 7.0. The DTT reduces oxidation of sulfhydryl groups in the myofibrillar proteins. The presence of magnesium ions reduces the enzymatic degradation of the myosin light chains (Weeds and Pope, 1977). Sodium azide reduces bacterial contamination. The extraction solution used in the first 24 hours also contained 0.5% (v/v) of the detergent Triton X-100 and the following protease inhibitors:

1 µg/ml pepstatin (Sigma, P4265), 10 µg/ml leupeptin (sigma, L2884) and 10 µg/ml trypsin inhibitor (Sigma, T9777).

After the first 24 hours in the extraction glycerol solution, the thorax was transferred to storage glycerol (without the Triton-X100 and protease inhibitors) and stored at -20°C. When required single fibres were removed from the thorax immediately before use. Thoraces varied according to how long their fibres showed good active responses, that is a low amplitude resting tension and large amplitude delayed tension rise. Typically a thorax stored at -20°C lasted between 2 and 4 months.

For a small number of experiments, *Tipula* (crane-fly) dorsal-longitudinal flight muscle was used. Due to the large numbers of these insects in the late summer, muscle could be used on the same day of capture. In the dissection the thoraces were cut in half vertically using dissecting scissors. This left two half thoraces each with a set of dorsal-longitudinal muscles exposed. For demembration, I used the same glycerol extraction buffers that were used for *Lethocerus*. The muscle tissue was left on ice for at least half an hour in the 50% glycerol buffer with 0.5% Triton-X100 before use.

4.2.2 Fibre size

For each muscle fibre type there is an optimal diameter for mechanical experiments. Since changes in tension are proportional to the cross-sectional area of the fibre, larger fibres give a larger signal to noise ratio. However when studying active muscle, diffusion rates to and from the centre of fibres of ATP and its hydrolysis products can affect the mechanical properties of the muscle.

Large fibres have a low surface area to volume ratio and can become diffusion limited. When the ATP concentration falls close to zero at the centre of the fibre, rigor cross-bridges form in these myofibrils. The presence of a small central core of diffusion limited myofibrils can have a large effect on the appearance of the tension response. The most obvious indicator of a diffusion-limited fibre is the large high-frequency stiffness of the fibre. This is seen as a large spike at the start of step length changes.

Clearly fibre size is not the only variable in the system that affects the ratio of the rate of ATPase and the diffusion rate of ATP into the fibre. Increasing the concentration of ATP in the muscle solution will increase the diffusion rate into the fibre. However the concentrations of 15mM and 20mM ATP used in experiments are already high. Alternatively the muscle ATPase can be reduced by lowering the temperature of the muscle bath. Muscle ATPase has a temperature coefficient (Q_{10}) greater than 3, whereas the diffusion rate is

proportional to the absolute temperature. For this reason a small reduction in temperature can have a large effect on the ratio of diffusion rate to ATPase. The ATP concentration and bath temperature chosen are discussed further in 4.4.2.

Lethocerus fibres are small and very uniform in their diameter. Most fibres have a diameter between 70 μ m and 90 μ m. When demembrated, these fibres remain intact and can be separated very easily. A single *Lethocerus* fibre at 15°C, saturating calcium and 15mM ATP is not limited by ATP diffusion (the accumulation rates of P_i and ADP have not been investigated). This makes the *Lethocerus* fibre a very convenient preparation for fibrillar muscle experiments.

Generally, the fibre size in the fibrillar muscle of other insects is larger. In *Tipula* flight muscle, fibres have a diameter greater than 220 μ m. Even at 20mM ATP, fully activated whole fibres are diffusion limited at 15°C. For this reason it is necessary to split fibres to a diameter closer to that of *Lethocerus*. Using sharp tungsten needles, the fibres can be pared down quite easily. The resulting bundles of myofibrils can then be treated in the same way as whole fibres. Although stray myofibrils do make them harder to handle than the discrete *Lethocerus* fibres.

4.2.3 Attaching fibres to the apparatus

The method of fibre attachment is a very important consideration in single fibre mechanical experiments. In the ideal fibre mounting system, all myofibrils in the fibre should contribute equally to the measured tension and undergo the same length changes when the motor position changes. Also, there should be no compliance at the mount itself. The quality of fibre attachment will be close to this *in vivo*, but repeating this on the apparatus is not simple.

Two methods were used to attach fibres to the apparatus. In the majority of experiments, fibres were glued directly to the apparatus hooks. In some experiments, aluminium clips were used to mount the fibres.

4.2.3.1 T-clips

Small T-shaped pieces of aluminium foil (T-clips) were made from 20 μ m aluminium foil. The clips were cut using a fine-ended scalpel under a dissecting microscope as described by Molloy, 1988. In the glycerol extraction buffer, the T-clips were attached to each end of the fibre before transfer to the apparatus bath.

Attaching the T-clips to the muscle fibre is a delicate procedure that takes some practice before it can be done reasonably reliably. While the fibre is resting on the clip, first one then the other arm of the clip are folded over it. Then a small force is applied to the top of the clip to squeeze the fibre. It is this process that

determines how well the fibre is gripped. If the fibre is not gripped well it will pull free of the clip when under little tension on the apparatus. Conversely if too much force is applied to the clip, the fibre will be damaged and will also break away from the clip when the fibre is under tension.

Between these extremes the fibre can be gripped sufficiently well to perform most types of muscle experiment. However the highest tensions are rarely as high as those achieved when the equivalent fibre is glued to the apparatus. One advantage that T-clips have over gluing is that fibres can be easily removed intact. For electron microscopy of mechanically tested fibres, T-clips are the better system of attachment. T-clips must be used if the fibres are shorter than 4mm as is the case for some small *Tipula*.

4.2.3.2 Cellulose nitrate glue

Cellulose nitrate glue was used to stick fibres directly to the apparatus hooks. The glue was made by dissolving cellulose nitrate centrifuge tubes in acetone. The best ratio is approximately three volumes of acetone to one volume of cellulose nitrate. Though due to evaporation, it is necessary to add acetone from time to time to maintain the viscosity. If the glue is too viscous it does not adhere well to the fibre, which will pull free under tension. With too much acetone, the glue can run along the surface of the fibre.

Fibres were cut to the required length allowing another 2mm for looping around the hooks. They were transferred to the muscle bath which contained the 50% glycerol 50% glycerol storage buffer. The ends of the fibre were looped around the glass hooks 2 or 3 times. With the fibre raised out of the muscle bath, the tension micromanipulator was used to pull the fibre to give it some tension. The corner of a tissue was used to remove excess solution where the fibres wrap around the hooks. This improves adherence of the glue to the fibre. Using the end of a flexible piece of wire, cellulose nitrate glue was added to each end of the fibre to secure it to the apparatus. The flexible wire made it possible to touch the glass hook on the tension transducer, without the fear of it disappearing across the laboratory. As little as possible glue was used, firstly so that the glue dried quickly, minimising the amount of time the fibre spent exposed to the air, and secondly so as not to reduce too much the frequency response of the strain gauge due to added mass. On drying the glue turns white, at this point the fibre was returned to the muscle bath. After experiments the fibres were removed by dissolving the glue with acetone.

The use of glycerol in the muscle bath greatly reduces the amount of damage done to the fibre when it is exposed to air. Under laboratory temperature and humidity, water evaporation from the 50% glycerol storage buffer will stop at

when the volume of glycerol reaches 75%. Above 75% this solution is hygroscopic. Therefore when the fibre is exposed to air it does not dry out, but its solution content reduces by a maximum of 25%.

The mechanical performance of glued fibres is better than that of fibres mounted using T-clips. The fibres can withstand much higher tensions before failing. This is because comparatively little damage is done to the fibre as it is mounted. Also the glue is able to diffuse into the fibre, so myofibrils at the centre of the fibre are bonded to the apparatus with the same strength as those on the periphery.

4.2.4 Rest length

Rest length is the term that refers to the point of 0% length offset in mechanical experiments. Given the sensitivity of insect fibrillar flight muscle to small changes in the length, it is important that a consistent method is used in the definition of rest length.

For all mechanical experiments described in this thesis, rest length was defined as that fibre length which gives a tension of $10\mu\text{N}$ when relaxed. This is the first measurement to be made on the fibre. The value of steady state tension is measured by giving a step release to find zero tension. Because some slow elongation of the fibre as it is put under tension (stress relaxation) the fibre is given a few seconds to reach a steady tension value before tension is measured.

A length-tension plot of a slow 5% ramp applied to a single relaxed *Lethocerus* fibre is shown in Figure 4.1. The plot shows that for tensions between $5\mu\text{N}$ and $40\mu\text{N}$ the relationship with length is linear. Below $5\mu\text{N}$ the tension approaches zero more slowly than would be predicted by this linearity. The reason for this nonlinearity can be seen if the fibre is viewed under high magnification. At tension values below $5\mu\text{N}$ some myofibrils are slack while others are under tension. A rest length tension of $10\mu\text{N}$ is high enough to perform small signal sinusoidal analysis on all relaxed myofibrils in the fibre. A higher value was not used because the rate of stress relaxation increases with increasing tension.

The exact tension value used to define rest length could conceivably take into account the diameter of the fibre. However this would unnecessarily complicate experiments in which the fibre diameter generally remains within a narrow range.

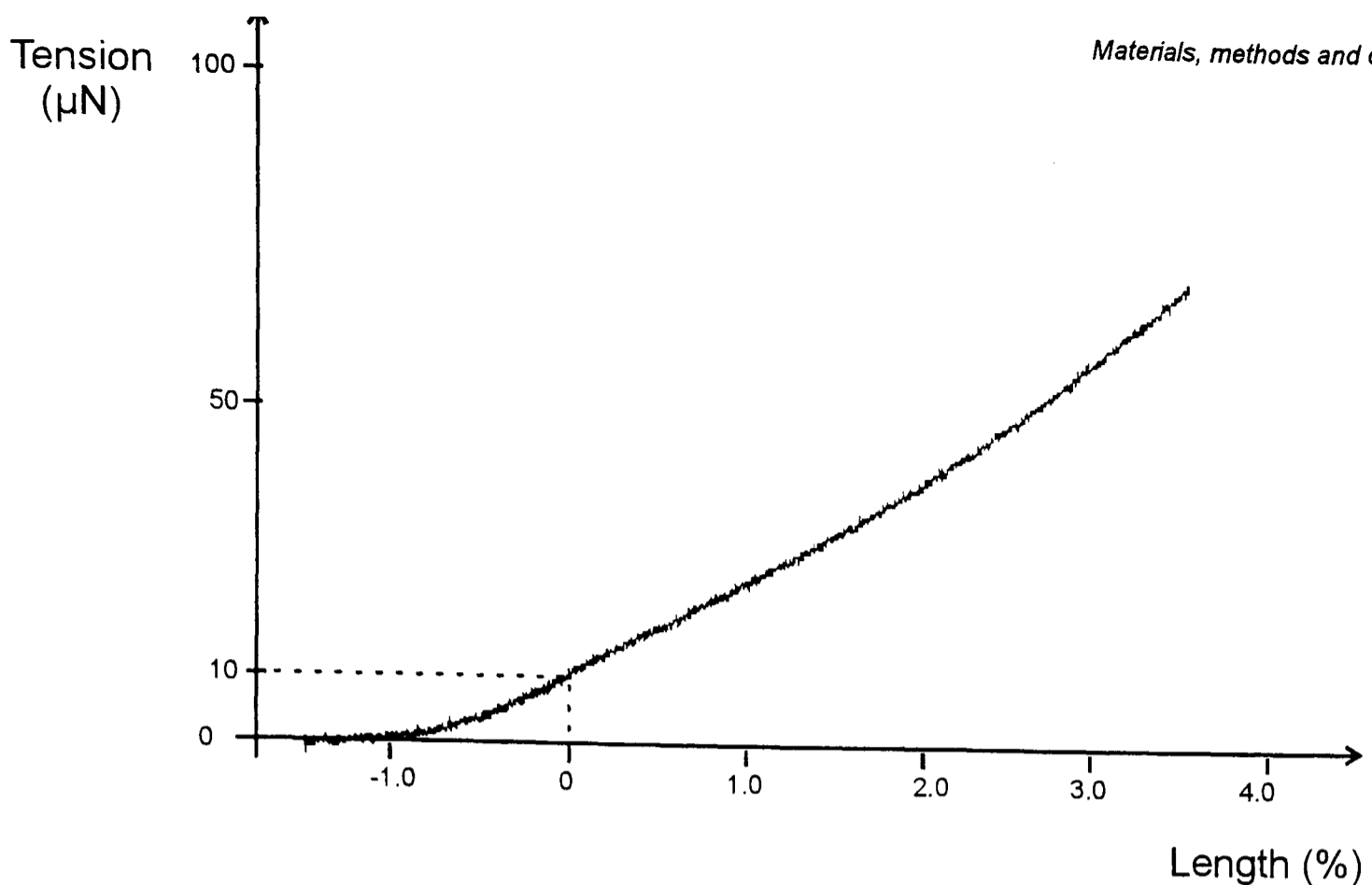


Figure 4.1: The tension trace describes the definition of rest length used for mechanical experiments on single fibres. Rest length is that fibre length which gives a steady tension of $10\mu\text{N}$ in relaxing solution. The tension trace was recorded by applying a slow 5% ramp length change ($0.25\%/s$) to a relaxed *Lethocerus* flight muscle fibre, starting with the fibre slack.

4.2.5 Mounted fibre lifetime

Mounted fibres have given large amplitude stretch activation after five hours on the apparatus, when maintained at 15°C using the solutions described in Table 4.1 That is not to say that the mechanical characteristics of the fibre remain constant in this time. The amplitude of the processes contributed by cross-bridges slowly reduces with time. That is the amplitude of stretch activation and the stiffness in active and rigor conditions all decrease. Relaxed stiffness does not seem to decrease, indeed in some instances an increase in relaxed stiffness has been recorded after two hours or more on the apparatus.

The cause of these changes will be a combination of several factors. Stress relaxation occurs in all mounted muscle fibres. One factor which certainly contributes to stress relaxation is compliance at the fibre mount. Generally the rate of stress relaxation is higher in fibres attached with T-clips than those glued to the apparatus. The reduction in active response could also be due to damage at the level of the whole myofibrils, the myofilaments or the cross-bridges.

For the reasons outlined above, to make quantitative comparison of recordings made on the same fibre it is important that the time interval between

the recordings is as short as possible. The results of experiments described in this and the other chapters, were all recorded within one hour of mounting the fibre on the apparatus. The majority of experiments were complete within half an hour. To reduce fibre damage caused by rapid step stretches, where possible non-recorded length changes were made using slow ramps. For example when a step length change is recorded without the return to rest length the motor position is ramped to zero once sampling has finished.

4.3 Solutions

4.3.1 Constituents

Unless otherwise stated all chemicals were obtained from Sigma. The constituents of the solutions were calculated using a PC computer program based on the algorithm by Perrin and Sayce (1967). The program **SOLUTION.EXE** calculates the quantities of various stock solutions necessary to give the specified final concentrations and ionic strengths for each solution. These values are calculated using a table of binding equilibria given in the input file. All the muscle solutions have ionic strength of 150mM and pH 7.0 at 15°C. The details of the constituents are given in table 4.1.

Solution	Added Constituents (mM)								Some resulting constituents (mM)	
	Na ₂ -ATP	Mg-acetate	EGTA	Ca-CO ₃	P _i buffer	Histidine	Glutathione	K-propionate	Mg-ATP	Free Ca ²⁺
Relaxing	15.00	13.90	5.00	-	-	15.00	5.00	45.65	12.62	-
Activating - no added P _i	15.00	13.50	5.00	5.24	-	15.00	5.00	46.57	12.39	0.032
Activating + 20mM P _i	15.00	14.25	5.00	5.24	20.00	-	5.00	7.15	12.40	0.032
Rigor	-	-	5.00	-	-	15.00	5.00	130.48	-	-
Ca ²⁺ - Rigor	-	-	20.00	22.5	-	15.00	5.00	82.90	-	2.5

Table 4.1 Composition of solutions used in mechanical experiments. The ionic strength of all solutions was adjusted to 150mM by potassium propionate. All solutions were adjusted to pH 7.0.

The ionic strength of all solutions was corrected to 150mM by making up the

difference using potassium propionate. To create the Mg-ATP complex the magnesium ions in solution were added in the form of magnesium acetate. All solutions except the 20mM phosphate solution contained 15mM histidine as a pH buffer. In the phosphate solution, the P_i buffer itself served this purpose.

In the case of ATP concentration the solutions used in the work described in this thesis were carried out using an ATP concentration of 15mM. The ionic strength for all solutions is adjusted to 150mM. Using higher concentrations of ATP would leave less freedom for adjustment of other constituents without forcing ionic strength above the 150mM value. For each 1mM increase in ATP concentration there is a further increase in ionic strength of 2mM due to the associated sodium ions and approximately 1.7mM of potassium ions that are added for pH correction. Another reason for not using higher ATP concentrations is the necessity to avoid straying too far from physiological conditions.

Magnesium acetate was added to provide the magnesium ions for the Mg-ATP complex in solution.

4.3.2 Changing solutions

The bath solution was changed using two syringes in a flow-through system. Using a 250 μ l Hamilton syringe the new solution was washed into the 30 μ l muscle bath, the surplus solution removed using a second syringe.

In the ideal muscle bath design, little more than one bath volume would be required to replace the solution completely with the new solution. Unfortunately flow through the bath is non-laminar. The second best alternative is to have optimal mixing of the new solution with the current bath volume, washing through several bath volumes until the bath contains little of the original solution.

The exact volume that was washed through the muscle bath on solution changes was dependent on the type of solution change. New solution was washed through until the point where further solution caused no change in the mechanical properties of the fibre. The minimum volume used for any solution change was one full syringe (250 μ l). This is equal to more than eight bath volumes and is sufficient for most solution changes. Rigor solutions required more than one syringe volume to reduce the concentration of ATP sufficiently for the muscle to go into rigor.

4.4 Nyquist recordings

Most Nyquist recordings were made using frequencies from 1302Hz to 0.25Hz. The apparatus used was capable of higher frequencies, but would complicate the recording procedure. The phase and amplitude inaccuracies caused by the limitation of the tension transducer response time would make it necessary to make frequency corrections to the data above 1302Hz. At 1302Hz and below I measured phase and amplitude errors small enough to omit the frequency correction procedure (see Figure 2.5 for details of the strain gauge frequency response).

A lower frequency of 0.25Hz was chosen for reasons of recording speed. Though lower frequencies could be recorded, the sampling times necessary would start to have a significant effect on the Nyquist recording time, especially if pre-recording oscillation is necessary. Between these frequencies limits, the intervening frequencies are spaced logarithmically, usually with a bias towards the central frequencies.

The number of traces averaged in a single recording was dependent on the amplitude of the resulting tension signal. In some instances it was necessary to average five or more traces to obtain a high signal to noise ratio. Such high averaging was necessary where very small amplitude length changes were imposed or the fibre stiffness was very low.

4.4.1 Pre-recording oscillation

When an oscillation is applied to a muscle fibre, the tension response changes in the first few cycles. The muscle fibre requires several cycles to settle into its new oscillating state. The number of cycles that are required to reach a steady state depends on both the frequency and amplitude of the length change applied. Because most Nyquist recordings are made using small amplitude length changes only a small number of oscillations are necessary before sampling can proceed.

The need for pre-recording oscillations indicates that the oscillation steady state is different from the isometric steady state. However with low amplitude oscillations (0.2% or less) there is little or no difference between mean tension during oscillations and isometric tension suggesting that difference in the state of the muscle is very small.

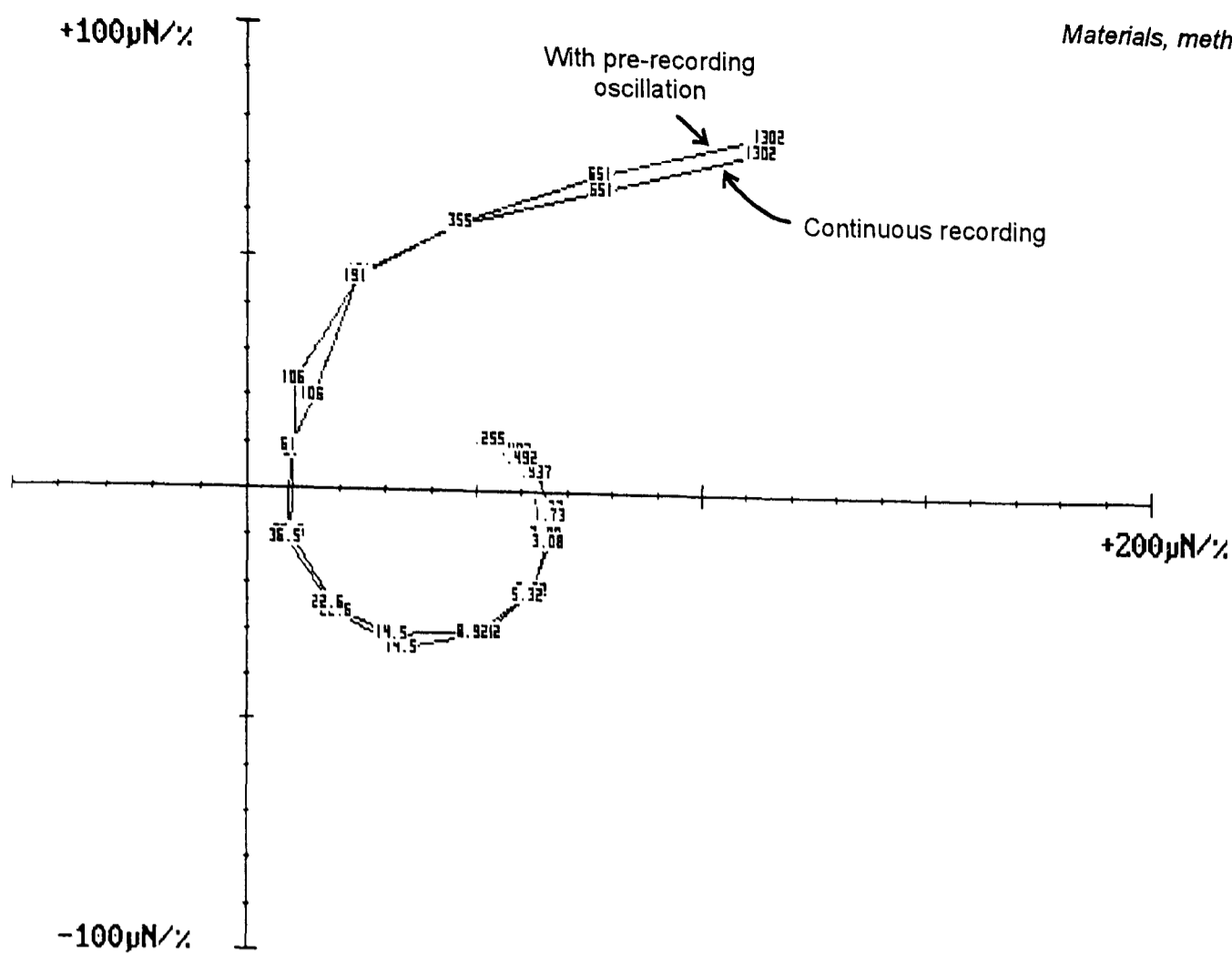


Figure 4.2: Nyquist plots showing the frequency response of a single active insect flight muscle fibre oscillated at an amplitude of 0.2%. Two recording methods were used. In one the fibre was oscillated at each frequency for 0.25s before sampling took place. In the continuous recording, all frequencies were recorded consecutively without pausing.

The Nyquist recordings described in this thesis were made using two methods. In some recordings, for each frequency the fibre was oscillated for a specified amount of time before any cycles were recorded. In this type of Nyquist recording the motor driving software was given a minimum pre-oscillation time. The muscle was oscillated for the nearest whole number of cycles over this time. Most Nyquist recordings were made at an amplitude of 0.2%. At this amplitude a pre-oscillation time of 0.2s was sufficient time for the fibre to reach a steady state. Longer periods of pre-recording oscillation made no change to the recorded Nyquist.

In the second style of Nyquist recording, a pre-recording oscillation was applied only for the first recorded frequency. Following this, all the frequencies were recorded consecutively. In such recordings, for each frequency the preceding oscillation serves as the pre-recording oscillation.

The Nyquist plot in Figure 4.2 shows that at low amplitude these two methods of recording give almost identical results. The advantage of the second method is that recordings take less than half the time. In the example shown all frequencies were sampled in less than 9.5s using the continuous method compared to 20.5s for the pre-recording method. When multiple recordings are

made to increase the signal to noise ratio, the doubling of recording speed becomes a more significant improvement to experiments.

In all Nyquist recordings the highest frequencies were recorded first, the lowest frequencies last. Nyquist plots in which the order of applied oscillations was reversed superimposed (data not shown). Application of frequencies in a random order was not tried, although the lack of any change when reversing the frequency order suggests that little or no difference would be observed. Clearly in a randomly ordered Nyquist series the fibre would need to be pre-oscillated at each frequency. This pre-recording oscillation duration is (as defined above) sufficient time for the fibre to reach its new steady (oscillating) state, so removes any effect of the previous oscillation frequency.

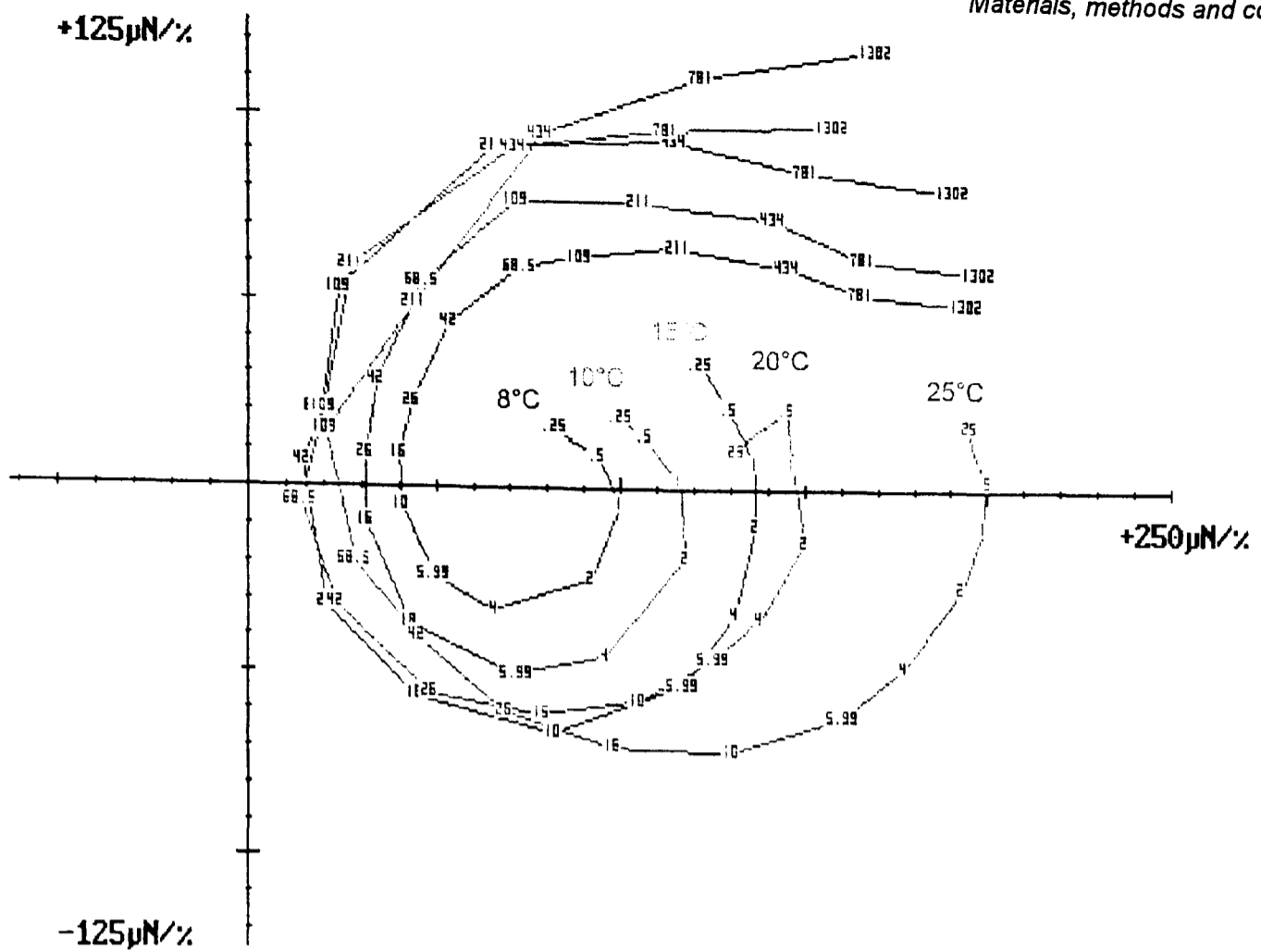
4.4.2 Temperature

The effect of temperature on the small amplitude transfer function of insect fibrillar flight muscle is shown in Figure 4.3. Data recordings were made of oscillation frequencies from 1302Hz to 0.25Hz. All recordings were made using the same fibre in activating solution (no added phosphate). After each temperature change, there was a pause of two minutes. This reduced any temperature gradients across the bath and allowed the fibre some time to reach a steady state.

As the temperature increases, the general trend is that the processes become faster and complex stiffness amplitudes larger. The greatest shift in phase angle with temperature occurs in the region of the plot with negative phase angle. That is the process with the most temperature sensitive kinetics is the work producing process. Nyquist recordings were also made at 30°C and 35°C, though these are not shown in the Figure 4.3. At these higher temperatures the fibre became diffusion limited. There was a large increase in the high frequency stiffness. Also the kinetics became slower, the phase angle plot appearing closer to that at 15°C than the one at 25°C.

The results of this experiment indicate the optimal temperature to perform Nyquist analysis using this preparation. A large amplitude tension signal is an advantage since this increases the signal to noise ratio, improving the accuracy of the analysis. This is a good reason to perform experiments at a temperature higher than 10°C.

(a)



(b)

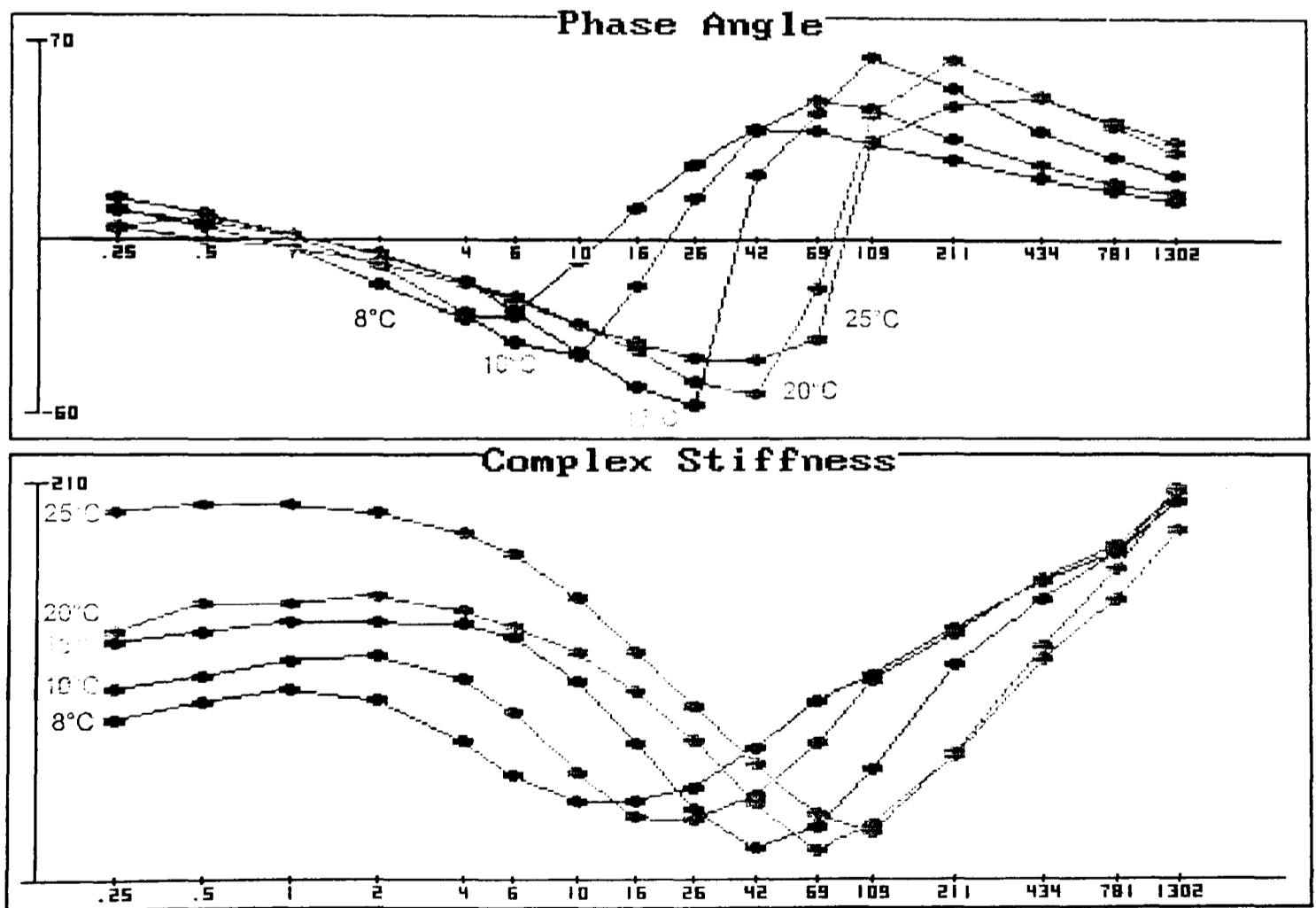


Figure 4.3: Nyquist (a) and Bode (b) plots showing the small amplitude frequency characteristics of a single *Lethocerus* flight muscle fibre at the temperatures 8°C, 10°C, 15°C, 20°C and 25°C. The oscillation amplitude was 0.2% in all recordings.

At the higher temperatures the diffusion rate of ATP and its hydrolysis products starts to become limiting. Under the conditions used in this experiment, the diffusion rate of ATP does not become limiting until 30°C. However if the fibre is activated further by recording large amplitude step stretches or by increasing the pre-stretch of the muscle, the temperature at which diffusion limitation becomes a problem is lower.

For the reasons outlined above, all mechanical experiments on single fibres other than those described here were performed at 15°C. At 15°C the amplitude of the tension signal is much larger than that recorded a few degrees cooler. However increasing temperatures above 15° increases the tendency for diffusion limitations to occur especially during large stretches.

4.4.3 Oscillation amplitude

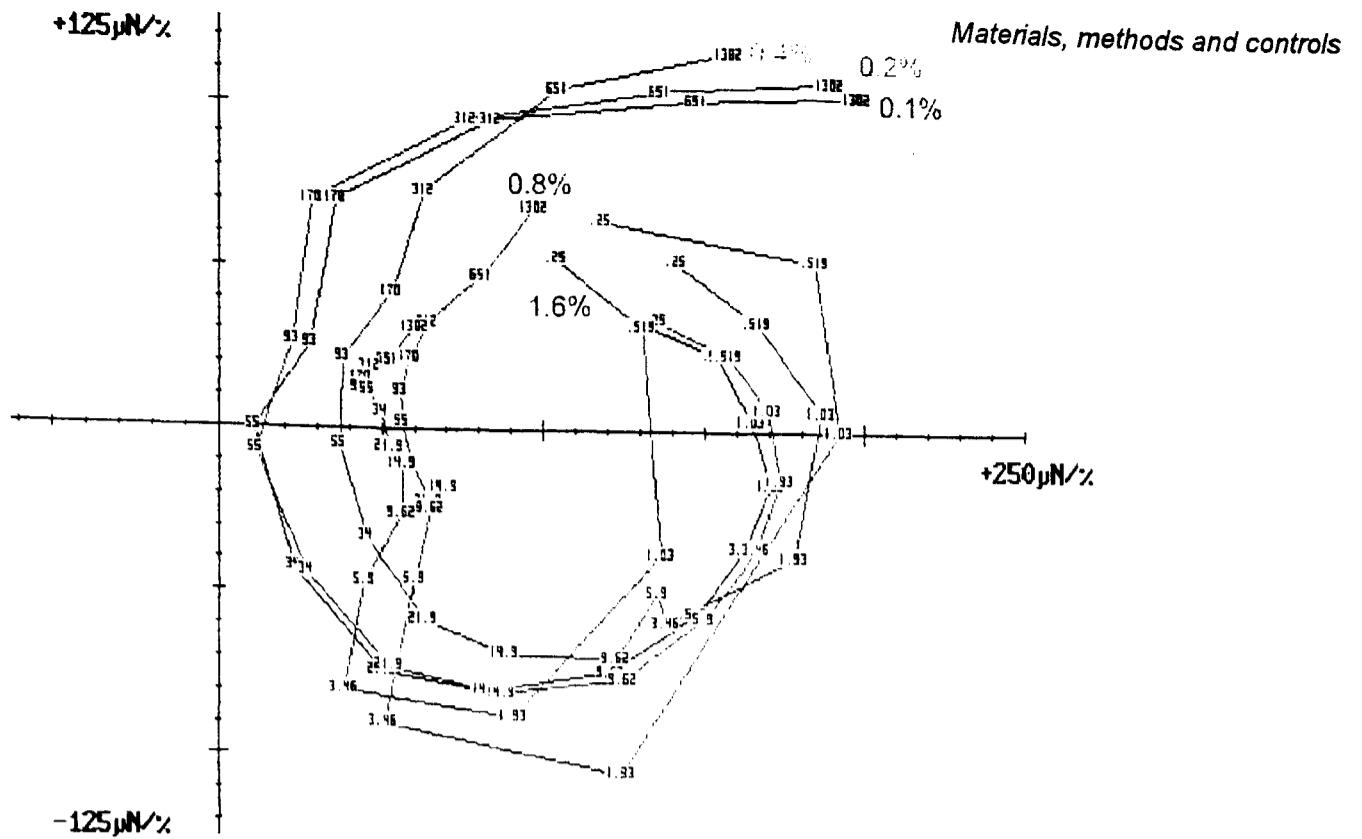
To obtain accurate results from sinusoidal analysis, the tension response must be close to linear. The Discrete Fourier transform (DFT) routine fits a single sinusoid to the tension signal. As the shape of the tension signal departs from that of a single sinusoid the results of the Fourier analysis become less accurate.

Active insect flight muscle is a nonlinear material. The response to a stretch is not a mirror image of that to a release. The main difference is in the kinetics rather than the amplitude of these two processes. The extent of this difference increases with the amplitude of the length change imposed. Unlike step length change experiments, with sinusoidal analysis the kinetics of both the stretch and the release are analysed together.

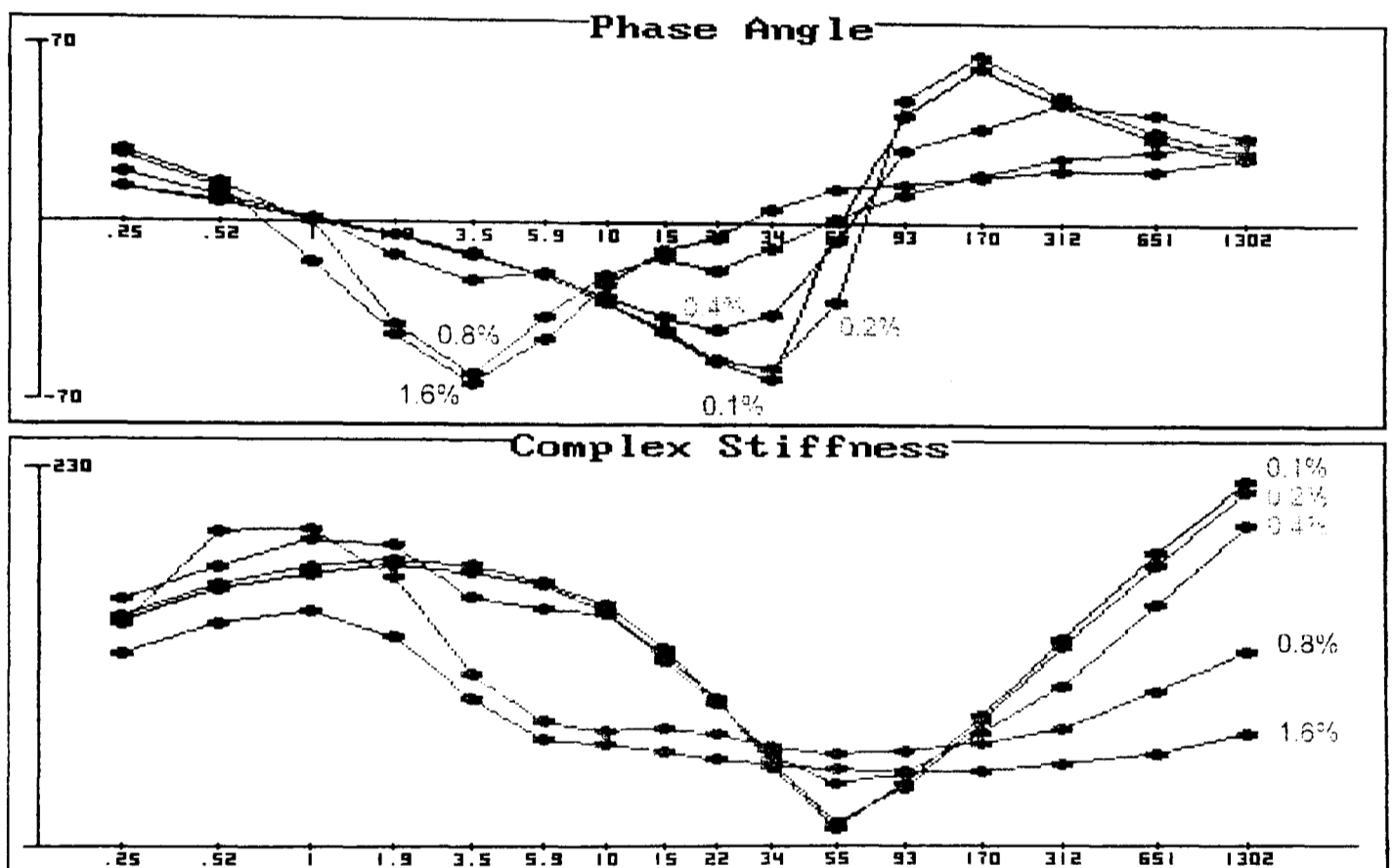
To investigate this nonlinearity a single *Lethocerus* fibre was oscillated at the following amplitudes: 0.1%, 0.2%, 0.4%, 0.8% and 1.6%. The duration of pre-recording oscillation for each frequency were 0.25s, 0.25s, 1s, 2s and 4s respectively. The length offset remained the same for all amplitudes. The fibre was held at 15°C in an activating solution with no added phosphate.

The resulting Nyquist and Bode plots are shown in Figure 4.4. The plots for 0.1% and 0.2% amplitude oscillation superimpose throughout the range of frequencies tested. However at amplitudes of 0.4% and higher, the plots change considerably. Another feature of these large amplitude sinusoidal recordings is the change in mean absolute tension.

(a)



(b)



(c)

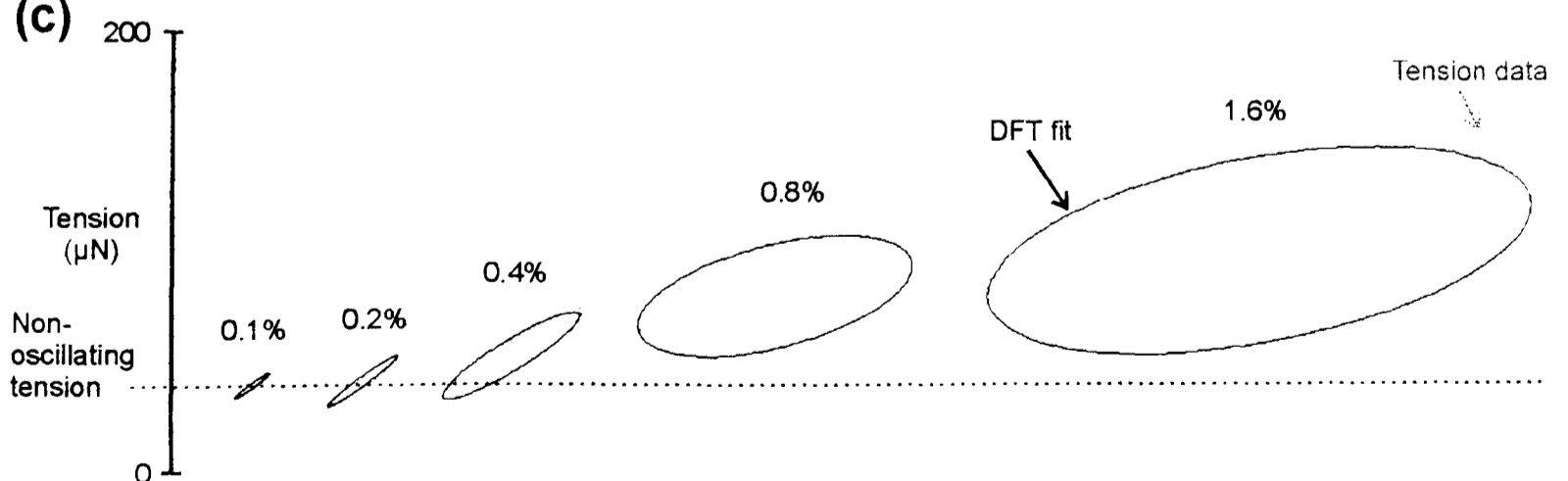


Figure 4.4: Nyquist (a) and Bode (b) plots showing the frequency characteristics of a single fibre at different amplitudes of oscillation. At 0.1% and 0.2% the plots superimpose. At 0.4% and above there are large changes in the frequency response of the muscle. (c) The 3.5 Hz data from each Nyquist series is shown as length-tension plots. The solid line shows the result of the discrete Fourier transform plotted over the data.

For a linear material, the shape of the Nyquist plot remains independent of the amplitude of the perturbation imposed (provided no damage is done to the material). The results shown for insect muscle indicate that this is the case for the amplitudes up to 0.2%. However at oscillations of 0.4% and above, the muscle is very nonlinear. It must be stressed here that since the shape of the tension waveform is less sinusoidal at the higher amplitudes, it is not possible to make accurate phase angle or stiffness measurements from the data using the DFT. The result of the DFT analysis is shown plotted over the 3.5Hz data from all the Nyquist series in part (c) of Figure 4.4.

The signal analysis of the higher amplitude is further complicated by another problem, that of *oscillation activation*. The muscle is stretch activated by the large imposed length changes, such that at certain frequencies the mean tension is considerably higher than the steady state (non-oscillating) tension. This effect can be seen in part (c) of Figure 4.4. At low amplitudes (0.1% and 0.2%) mean tension is the same at all frequencies as it is without oscillation. Therefore at these amplitudes, the Nyquist plot is analysing the active state of the fibre at its current length. At higher amplitudes, the general level of fibre activation changes depending on the frequency of oscillation. The mean tension is highest at the work producing frequencies. Because the level of activation changes with frequency in the higher amplitude recordings, interpretation of the results is further complicated. However some observations can still be made about the general changes in the shapes of the resulting plots.

The change in muscle kinetics with increasing amplitude of oscillation can be seen in the phase angle curves in the Bode plot. The most dramatic changes occur at the work producing frequencies. The frequency of maximum negative phase angle is that frequency with the most open work loops. As oscillation amplitude is increased, this frequency is reduced. The shift to a lower frequency is not a gradual one, instead it appears to occur in a discrete step.

For reasons of nonlinearity at the higher amplitudes, all other Nyquist recordings shown in this thesis were made at an amplitude of 0.2%.

4.4.4 Pre-stretch

As the pre-stretch of insect fibrillar muscle fibres is increased, the steady state tension also increases. This increase in tension is higher than that expected due to the elasticity of the passive components in this muscle, and is due to the stretch activation of the muscle fibre.

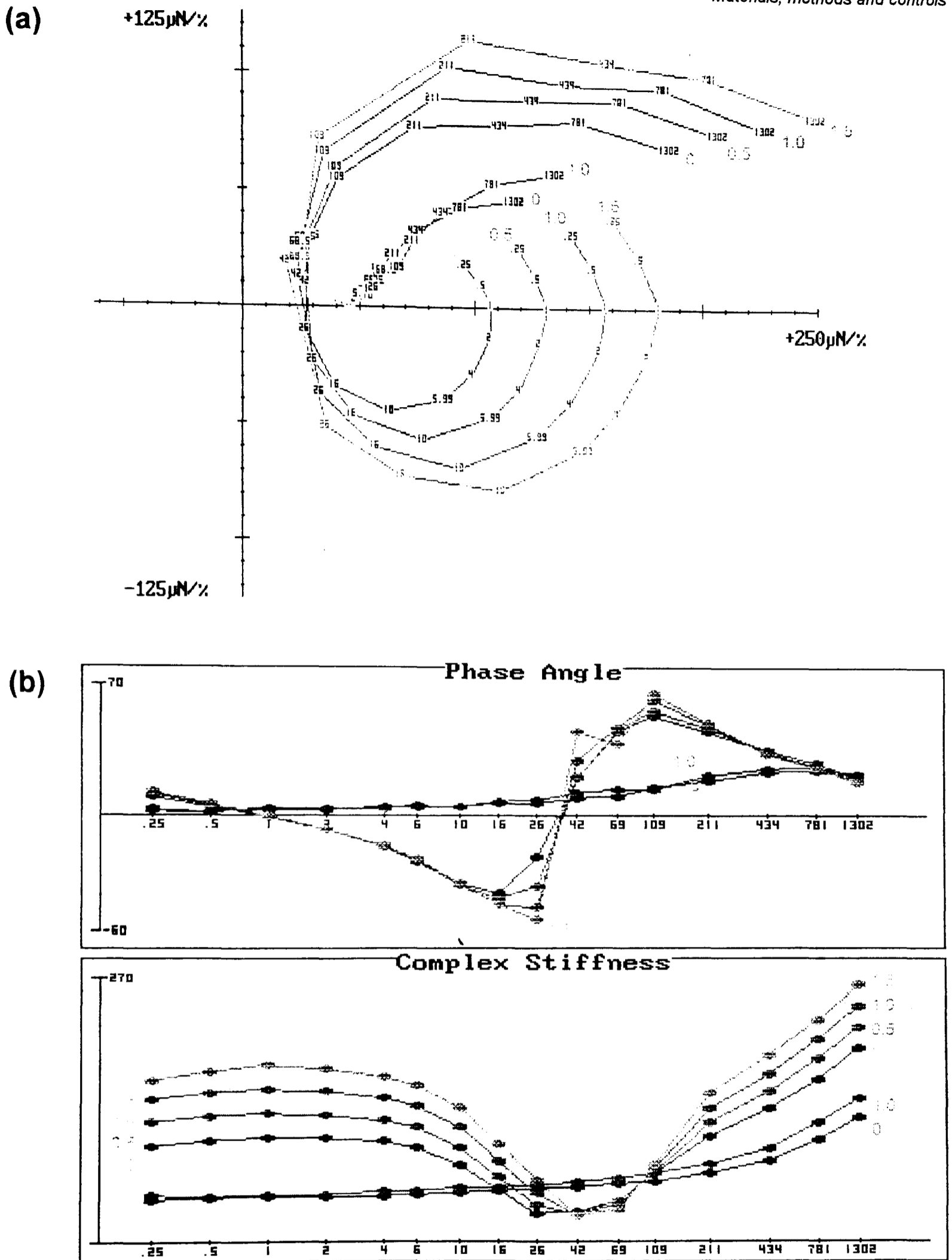


Figure 4.5: The effect of increasing pre-stretch on the small signal mechanical characteristics of active *Lethocerus indicus* flight muscle. All recordings were made at an oscillation amplitude of 0.2%, at 0% (rest length), 0.5%, 1.0% and 1.5% pre-stretch. The relaxed response is also shown at 0% and 1% pre-stretch. Increasing the pre-stretch results in a very small increase in relaxed stiffness. In the active response, increasing the pre-stretch has very little effect on phase angle, but increases muscle stiffness at all frequencies except those in a small range above the work frequencies.

The effect of increasing pre-stretch on the small signal mechanical characteristics of active insect fibrillar flight muscle was investigated using *Lethocerus indicus* fibres. The Nyquist recordings were made at an amplitude of 0.2%, at logarithmically spaced frequencies from 1302Hz to 0.25Hz. The first two recordings were made in relaxing solution at rest length (0%) and at a 1% pre-stretch. The stretch was applied by adjusting the strain gauge micromanipulator. The fibre was returned to rest length and activated. Nyquist recordings were then made at 0%, 0.5%, 1.0% and 1.5% pre-stretch. The fibre was given at least 20s at each new length to reach a steady active state before the recording started.

The Nyquist and Bode plots from the resulting data are shown in Figure 4.5. In relaxing conditions, there is a small increase in fibre stiffness with pre-stretch. When active, the increase in stiffness with pre-stretch is much greater. The complex stiffness increases with pre-stretch for all frequencies except for those frequencies in the low stiffness region. At these low stiffness frequencies (42Hz, 69Hz and 109Hz), the Fourier results suggest that increasing pre-stretch has little or no effect on complex stiffness. As can be seen in the phase angle plot there is very little change in the rate constants of these small amplitude mechanical processes with stretch.

The results are entirely compatible with the idea that the process of stretch activation involves an increase in the total number of attached cross-bridges. The reason for the lack of change in the low stiffness region can be partially explained by the relaxed Nyquist response. The passive elements responsible for the high relaxed stiffness of insect muscle also contribute to the active response (White, 1983). For this reason, as the population of active attached cross-bridges increases, the active response should move proportionately further from the relaxed Nyquist. Indeed the direction of many of the frequencies point towards the position of the same frequency on the relaxed Nyquist plot. Given this reasoning, the active frequency points that are closest to the relaxed Nyquist plot will move least as the muscle is stretched.

4.5 Step length change recordings

Unlike sinusoidal analysis, in the analysis of data from step length change experiments, the stretch and the release kinetics are analysed separately. For this reason, by using step length changes, it is possible to obtain accurate estimates of fibre kinetics at large amplitude length changes. The maximum of 0.2% length changes imposed for sinusoidal analysis does not apply to step length change experiments.

Because in typical step length change experiments larger amplitude length changes were used, the already high signal to noise ratio reduced the need to perform multiple trace averaging. In most experiments between one and three traces gave a clean tension signal from which accurate rate constant and amplitude information could be extracted.

When more than one trace was averaged in a single recording, it was necessary to specify a pause time that the controlling software should wait between traces. This gave the fibre time to reach a steady state, so that all traces averaged were recorded under the same conditions. In some large amplitude length stretches a pause as long as 15s was necessary between traces.

**5. The effects of mild calpain
digestion on *Lethocerus* indirect flight
muscle.**

5.1 Introduction

The work described in this chapter, investigates the role of one particular protein in stretch activation in insect fibrillar flight muscle. The protein is troponin-H (Tn-H), a member of the troponin complex in the thin filaments of insect fibrillar flight muscle.

The troponin complex of *Lethocerus* flight muscle is almost twice the size of that found in vertebrate skeletal muscle. Bullard (1984) suggested that this large troponin complex may play a role in stretch activation by blocking potential cross-bridge binding sites. These sites only become available after the muscle is extended. This type of model for stretch activation is compatible with that of Wray (1979b) in that it would act alongside such geometric models.

Bullard *et al* (1988) gave a detailed account of the biochemistry of the troponin complex of insect flight muscle. They described three components. Troponin-C (MW 18 000Da) and troponin-T (MW 53 000Da) were isolated and shown to have similar properties to their vertebrate equivalents. Troponin-I was not observed in this study, but a heavy component, referred to as Troponin-H (Tn-H) was described in some detail. The molecular mass of Tn-H is approximately 55 000Da, although in poly-acrylamide gel electrophoresis it runs anomalously high in the 80 000Da to 90 000Da region.

5.1.1 Troponin-H

Although *Lethocerus* Tn-H has not been sequenced, the sequence is known for *Drosophila* Tn-H. Karlik *et al* (1984) have investigated the gene arrangement in the 88F subdivision of chromosome 3 in *Drosophila*. This small region in the right arm of chromosome 3 contains the genes for several myofibrillar proteins, including the *act88F* flight muscle actin gene. Karlik *et al* describe five antigenically related proteins, from a 20 kilobase region in the 88F subdivision, three of which accumulate only in the indirect flight muscles.

Three of the five proteins, referred to as proteins 127, 128 and 129 (from their positions on a 2D PAGE), have MW 35 000Da and are tropomyosin isoforms. The remaining two, proteins 33 and 34, are flight muscle specific proteins of apparent MW 78 000Da and 70 000Da respectively. All five of the proteins are generated from just two transcribed regions, by multiple overlapping mRNAs. The two regions are Tm 1 which encodes the tropomyosin isoforms 127, 129 and Tn-H 34, Tm 2 encodes tropomyosin 128 and Tn-H 33.

The difference in mass between troponin-H (33 and 34) and the tropomyosin isoforms (127, 128 and 129), is due to the addition of a particularly unusual sequence of amino acids at the carboxy end. These carboxy-terminal portions of the proteins contain a very high proportion of proline. This is unusual because tropomyosins, being α -helical, do not contain this amino acid. Approximately the last 100 amino acids consist of a repeating pattern; an acidic residue (usually glutamine) followed by a glycine, then 3 to 7 prolines and/or alanines.

Bullard *et al* (1988) showed that these heavy tropomyosins in *Drosophila* are equivalent to the Tn-H of *Lethocerus*. Monoclonal antibodies to *Lethocerus* Tn-H cross reacts strongly with these *Drosophila* proteins. The epitope shared between the two was the unusual carboxy terminal half. This is known because the antibody did not react to the other tropomyosins.

Electron micrographs of isolated thin filaments from *Lethocerus* flight muscle showed very conspicuous swellings at 39nm intervals. Observed under the same conditions rabbit striated muscle thin filaments have no such repeat, and appear uniform along their length. The 39nm distance corresponds to the repeat of the troponin-tropomyosin in the thin filament. The protrusion itself is thought to be due to the large troponin complex, particularly the Tn-H component.

The secondary structure of the carboxy terminus of the Tn-H protein is not known. However the high proline content of this part of the protein does put some constraints on its possible structure. Sometimes prolines are present in an α -helical region of a protein where they cause an abrupt change in direction of the helix. However the occurrence of so many prolines in this part of Tn-H, makes it impossible for the carboxy terminus to be α -helical. The high proline content of the carboxy-terminus is typical of proteins which have extended conformations such as collagen.

Further evidence for the presence of Tn-H in the troponin complex comes from gold/Fab labelling of Tn-H (Newman *et al*, 1992). Isolated thin filaments were labelled with gold-conjugated Fab fragment of the monoclonal antibody to Tn-H. The gold particles were 3nm in diameter, the minimum size to be clearly visible by conventional electron microscopy. Given the size and shape of the probe, the gold particles could occur no further than 8nm from the combining site, a distance which is short enough to determine a 40nm repeat in the thin filaments. The resulting micrographs showed a convincing 40nm repeat of the gold particles in the case of the *Lethocerus* flight muscle thin filament, but no correlation in the leg muscle thin filaments, where Tn-H does not occur. In some instances, in the flight muscle thin filament, two gold particles could be seen at the same place on the filament. These would correspond to the two tropomyosin-

troponin complexes on opposite sides of the filament, suggesting that the stoichiometry of Tn-H is one per tropomyosin-troponin complex.

Some preliminary unpublished data from R. Marco and J.C. Sparrow suggests that in *Drosophila* thin filaments, for every 6 actins there are: 1 arthrin, 2 tropomyosins and either 1 or 2 Troponin-H. The latter includes both the Tn-H 33 and Tn-H 34. If these values prove to be correct, the 1 or 2 Tn-Hs would be present in addition to (not replacing) the tropomyosins present in the each tropomyosin-troponin complex.

5.1.2 Calpain

Bullard *et al* (1988) suggest that previous failure to localise Troponin-H in insect flight muscle was due to the high sensitivity of this protein to proteolysis. The endogenous enzyme thought to be responsible for this proteolysis is calpain, a Ca^{2+} -activated protease present in muscle. Calpain is also known as *calcium activated protease*, *calcium activated neutral protease*, *calcium activated factor* and *calcium dependent protease* (CAP, CANP, CAF and CDP respectively). Calpain and its natural inhibitor calpastatin have been isolated from many different tissue and from many organisms (Melloni and Pontremoli, 1991).

Animal tissues contain two isoforms of calpain, classified according to their Ca^{2+} -sensitivity. Calpain I requires micromolar Ca^{2+} to be proteolytic, whereas calpain II reaches only half maximal activation at 1.2mM Ca^{2+} (Tsuji and Imahori, 1981). Calpain is a membrane associated enzyme, though most forms do not require association with a membrane surface in order to be proteolytic. *In vivo* regulation of calpain activity is not merely a function of Ca^{2+} concentration. Both calpain I and calpain II require autolysis in order to be fully activated, also the presence of the inhibitor and some membrane bound regulator proteins affect its proteolytic activity (Melloni & Pontremoli, 1991).

The natural function of calpain is not yet clear. Evidence from its preferred substrates and location in the cell, has led people to suggest that calpain has a role in protein turnover in the cytoskeleton and myofibrils. However, calpain has also been shown to exist in platelets which have neither a cytoskeleton nor significant protein turnover (Phillips and Jakábová, 1977). The physiologically uncommon levels of calcium required to fully activate calpain II suggest that it may have a role in pathological conditions where calcium levels can be very high.

5.1.3 Calpain specificity

Many reports have described the action of calpain on myofibrillar proteins and on the appearance of myofibrils. The most noticeable event in the digestion of myofibrils by calpain is that at sufficiently high levels, calpain will remove Z-lines (Reedy *et al*, 1975). At the level of digestion required to completely remove Z-lines, there was very little reduction of myosin, actin or paramyosin, suggesting that these proteins are not very susceptible to cleavage by calpain (Reddy *et al*, 1981).

The sensitivity of Tn-H to calpain digestion is very much greater than the other major myofibrillar proteins. The extent of calpain digestion necessary to digest all Tn-H results in only a very small reduction in the levels of α -actinin and Tn-T.

The unusual structure of Tn-H and the fact that it is an insect fibrillar muscle specific protein led to the suggestion that it plays a role in stretch activation (Bullard, 1984 and 1988). Bullard (1988) suggested that the potentially stiff proline rich tail end of the Tn-H molecule may extend away from the thin filament, explaining its high susceptibility to cleavage. This carboxy end of Tn-H may attach to the thick filament, where it could be involved in the mechanism of stretch activation by sensing the relative displacement of the thick and thin filaments.

Given the possible role Tn-H in stretch activation and a potential method to selectively remove the Tn-H, I decided to investigate the effect of mild calpain digestion on the stretch activation of skinned *Lethocerus* fibres.

5.2 Materials and Methods

Unless otherwise stated, the set-up of the apparatus and muscle bath solutions used were the same as those described in chapter 4.

5.2.1 Digestion conditions and solutions

Calpain used in digestion experiments was the 80K subunit of calpain II, the variety which requires calcium concentrations of more than 1mM for full activation. Although the 30K subunit is necessary for full activation, the 80K subunit alone is sufficient for proteolysis (Tsuji and Imahori, 1981). Calpain was kept in a deactivating storage solution at -20°C. The storage solution contained 10 units of calpain (Sigma, P4533), in 1ml of solution of 50% glycerol (v/v), with

2mM EGTA, 2mM mercaptoethanol, 3mM sodium azide and 5mM histidine at pH 7.0.

Without the 30K subunit, 80K subunit of calpain II requires 1.4mM Ca^{2+} to give half of its maximal activity (Tsuji and Imahori, 1981). For this reason the Ca^{2+} -rigor solution used for digestion contained 2.5mM free Calcium (calculated using the program SOLUTION using known association constants). This very high calcium concentration, readily washed out with the calcium free rigor solution and did not adversely affect the muscle's active response.

The solution used for all calpain digestions contained 2 μ l of the calpain stock and 98 μ l of Ca^{2+} rigor solution.

For the 5 minute period of digestion the temperature was raised to 25°C. This temperature gives optimal enzyme activity, above this the calpain shows increased autolysis (Dayton *et al.*, 1976). Control fibres received a 5 minute incubation at 25°C in the Ca^{2+} rigor solution without added calpain.

5.2.2 Fibre mechanics

Fibres were attached to the mechanical testing apparatus with cellulose nitrate glue. Fibres attached to the apparatus using T-clips had a tendency to slip in the clips after mild digestion, causing them to lose tension, so T-clips were not used for these experiments.

In step length change experiments all mechanical testing was done at 15°C, the bath temperature was changed to 25°C only for the digestion and control periods. First, the fibre was given a 1% stretch in relaxing solution. After 1 minute in pre-activating solution, activating solution was washed through and another 1% step stretch given to record the stretch activated response of the muscle. The fibre was put into rigor, first by washing through relaxing solution to remove calcium, then the rigor solution. The Ca^{2+} -rigor solution was then washed through. Only a small step was given (0.2%) to measure rigor stiffness to prevent damage to the fibre.

Calpain digestion rigor solution was washed through and the bath temperature set to 25°C. The fibre remained in digestion solution for 5 minutes. After digestion the bath temperature was reset to 15°C and calpain-free Ca^{2+} -rigor washed through. A 0.2% step was given to find the post-digestion rigor stiffness. Normal rigor then relaxing solution were washed through and 1% step was used to measure relaxed stiffness. The muscle was then activated and a 1% step given to record the post-digestion stretch activation. Finally, the muscle was put into Ca^{2+} -rigor and stiffness recorded again as a check for any fibre damage.

High frequency stiffness measurements were made from the step length change experiments by plotting tension against length for the period of the length change. A straight line was fitted to the data using linear regression, and the slope used to measure fibre stiffness. In the majority of recordings, the length change is 95% complete in less than 200 μ s. Unfortunately, in some active fibres this is not fast enough. In these fibres, phase 2 relaxation has begun before the length change is over. In these recordings the stiffness was measured during the first part of length change where the tension rise remains linear, by plotting length vs tension over this part of the record.

The amplitude of the stretch-activated response was calculated by subtracting the starting steady state tension (before the stretch) from the maximum tension reached between phases 3 and 4.

In the case of Nyquist analysis, the same overall procedure was used. However all steps were replaced by brief sinusoidal oscillation sweeping through a range of frequencies at an amplitude of 0.2% peak to peak. In some fibres both Nyquist and step analysis were performed. The frequencies used were in the range 1.3kHz to 0.25Hz, with a logarithmic spacing biased towards the mid-range frequencies, close to that which produces maximum work per cycle. Some of the fibres used for mechanical experiments were fixed for electron microscopy.

5.2.3 Digestions for PAGE and the Western Blot

In parallel experiments fibres were digested, using exactly the same procedure as for mechanical experiments. Digestions were done in 10 μ l droplets of Ca²⁺-rigor with calpain solution under silicone oil. The control fibres were incubated in Ca²⁺-rigor without calpain. Each droplet and fibre was used for a gel lane, in this way both the insoluble fibre matrix and any soluble proteolytic fragments could be observed. Digestions were started by dragging a single *Lethocerus* fibre into a droplet. Digestion was stopped by the addition of 2 μ l of SDS sample buffer (5 x normal concentration).

5.2.4 SDS Poly-acrylamide gel electrophoresis (PAGE)

Vertical mini-slab gels were run on a Protean (BioRad, Richmond CA) system. The separating gel was made up of 10% (w/v) acrylamide:bis-acrylamide (95%:5% respectively), 375mM Tris pH 8.8, 0.1% (w/v) SDS, 1.5mM APS, 4mM TEMED. The stacking gel was 3.75% (w/v) acrylamide, 125mM Tris pH 6.8, 0.1% (w/v) SDS, 2.3mM APS, 6.4mM TEMED. The gel was run at 200V for 40 minutes. Then stained in 40% methanol, 10% acetic acid and 0.1% Coomassie

brilliant blue-R for 2 hours. The gel was destained in 10% acetic acid for 24 hours with constant agitation. The buffer system used was that described by Laemmli (1970).

5.2.5 Western Blot

The 1D SDS gel was soaked for 40 minutes in transfer buffer. Proteins were transferred to nitrocellulose (600mA for 1.5hrs). Rinsed in transfer buffer and cut in half, one for stain, one for hybridisation. Nitrocellulose was stained in Ponceau-S for 10 minutes, washed with acetic acid, rinsed with water and left to air dry. Hybridisation procedure was as follows. The surface of the nitrocellulose was blocked with 3% BSA in TBS for 1hr, followed by multiple washes in TBS. The monoclonal antibody (MAC144) was kindly donated by Belinda Bullard. This was hybridised to the gel for 1hr at room temperature. The secondary antibody (goat, anti-rat) conjugated with horseradish peroxidase (HRP) was left for 1hr at room temperature. Horseradish peroxidase was developed using HRP stain for 5 to 10 minutes. Rinsed with water and left to air dry.

Solution constituents:

TBS 20mM Tris, 500mM NaCl, 0.01% Thimersal pH 7.5.

Transfer buffer 25mM Tris, 150mM Glycine, 20% methanol, pH 8.3.

Ponceau-S stain 0.2% Ponceau-S (Sigma, Mo) in 3% TCA, 3% sulphosalicylic acid.

HRP stain 0.017% 4-chloro-1-naphthol, 0.015% H₂O₂, 16% methanol in TBS.

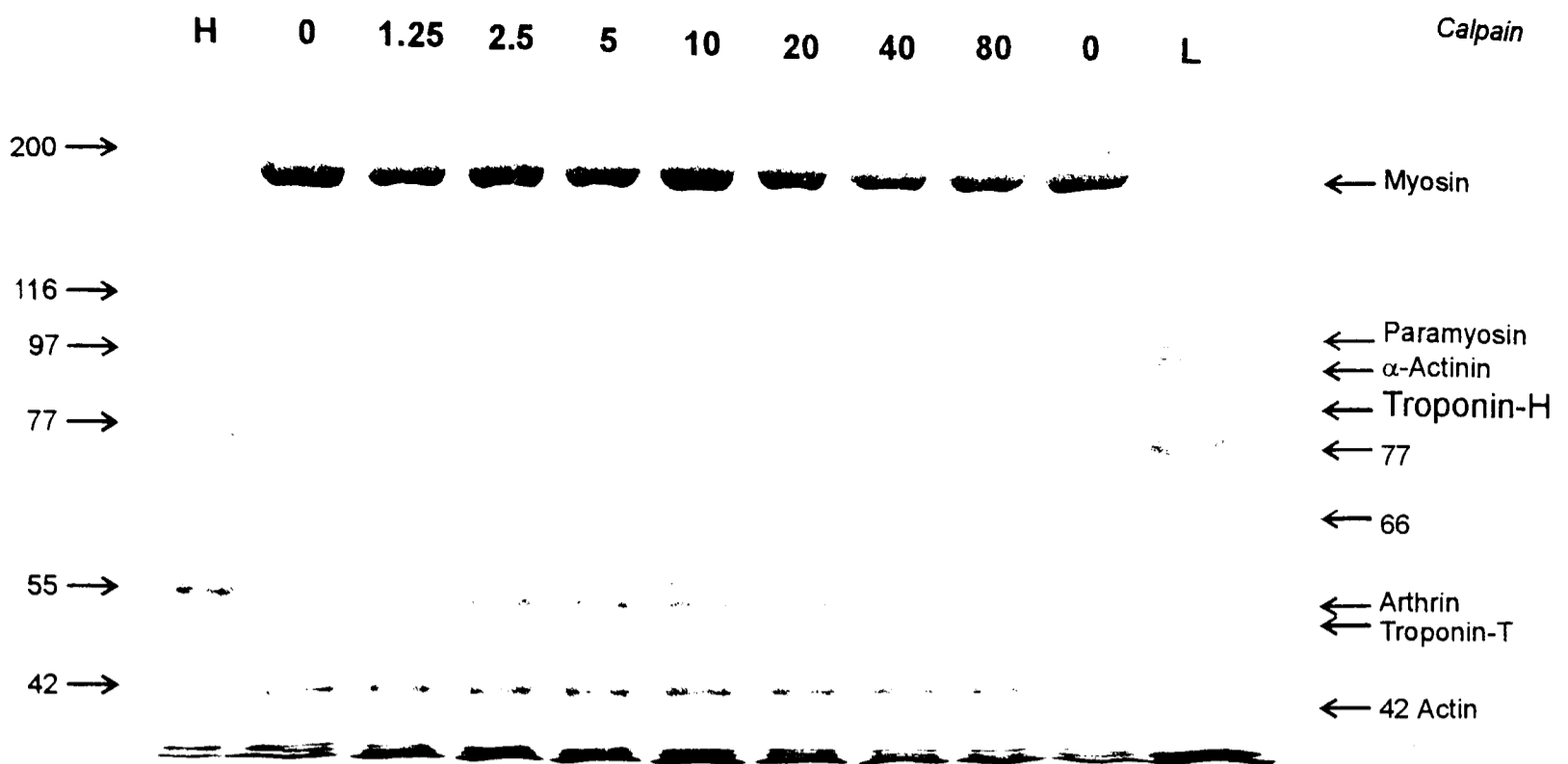


Figure 5.1: 10% SDS/polyacrylamide gel. A time series showing the progress of digestion of myofibrillar proteins by calpain. Whole fibres were digested at 25°C in Ca²⁺ rigor solution. The lane headings show the total digestion times. High (H) and low (L) molecular weight marker lanes are also shown. The Troponin-H band reduced most rapidly, it is significantly reduced at 1.25 minutes and is not visible at 2.5 minutes.

5.3 Results

5.3.1 Electrophoresis

The SDS polyacrylamide gel (Figure 5.1) shows that mild digestion with calpain removed Tn-H from whole skinned fibres in Ca²⁺ rigor solution. Under the conditions used Troponin-H appears to be highly sensitive to calpain digestion. At 1.25 minutes it is considerably reduced. At 2.5 minutes onwards it is not visible. No other protein is digested so quickly. Some of the proteins such as actin and myosin show no reduction in intensity even at 80 minutes. The arthrin band can be seen to become weaker at 20 minutes of digestion.

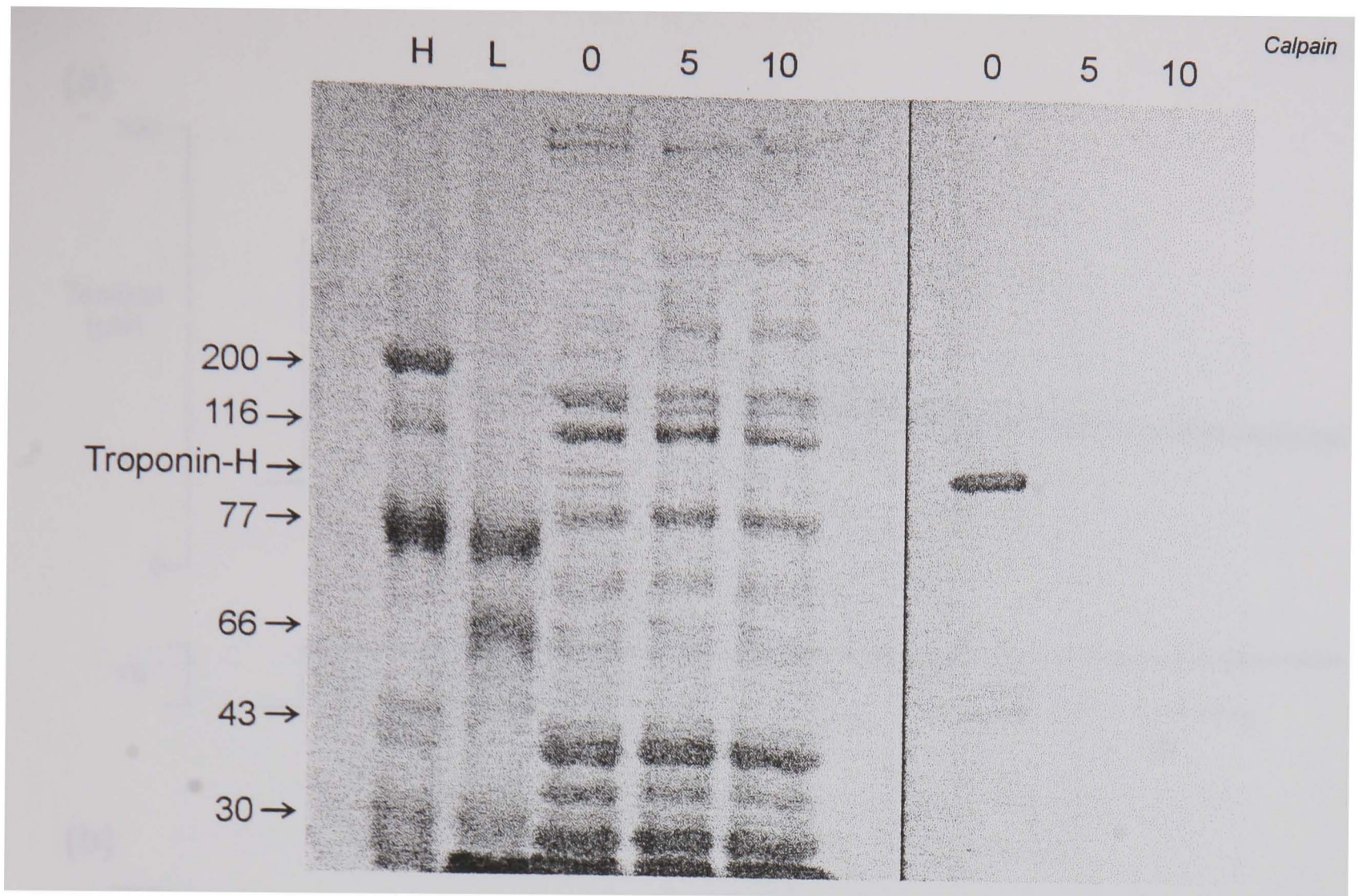


Figure 5.2: Western blot: the disappearance of Tn-H after 5 minutes of mild calpain digestion, shown using the MAC144 antibody. Whole demembranated *Lethocerus indicus* fibres were digested. The lane headings show the digestion time in minutes. The first two lanes contain high (H) and low (L) molecular weight markers.

5.3.2 Western Blot

The western Blot in Figure 5.2 confirms the result suggested by the SDS polyacrylamide gel that all Tn-H within the fibre has been digested at 5 minutes of digestion. Because of the high contrast of this method, any very small amount of Tn-H would be visible in the other lanes.

5.3.3 Step length changes

A summary of the changes in the mechanical characteristics of the fibre due to digestion is given in table 5.1. No significant change in either the relaxed or the rigor stiffness occurs. However, in the same fibres there is a significant reduction in the amplitude of stretch activation. An example step response is shown in Figure 5.3. for the tension response to a 1% step stretch before and after mild calpain digestion.

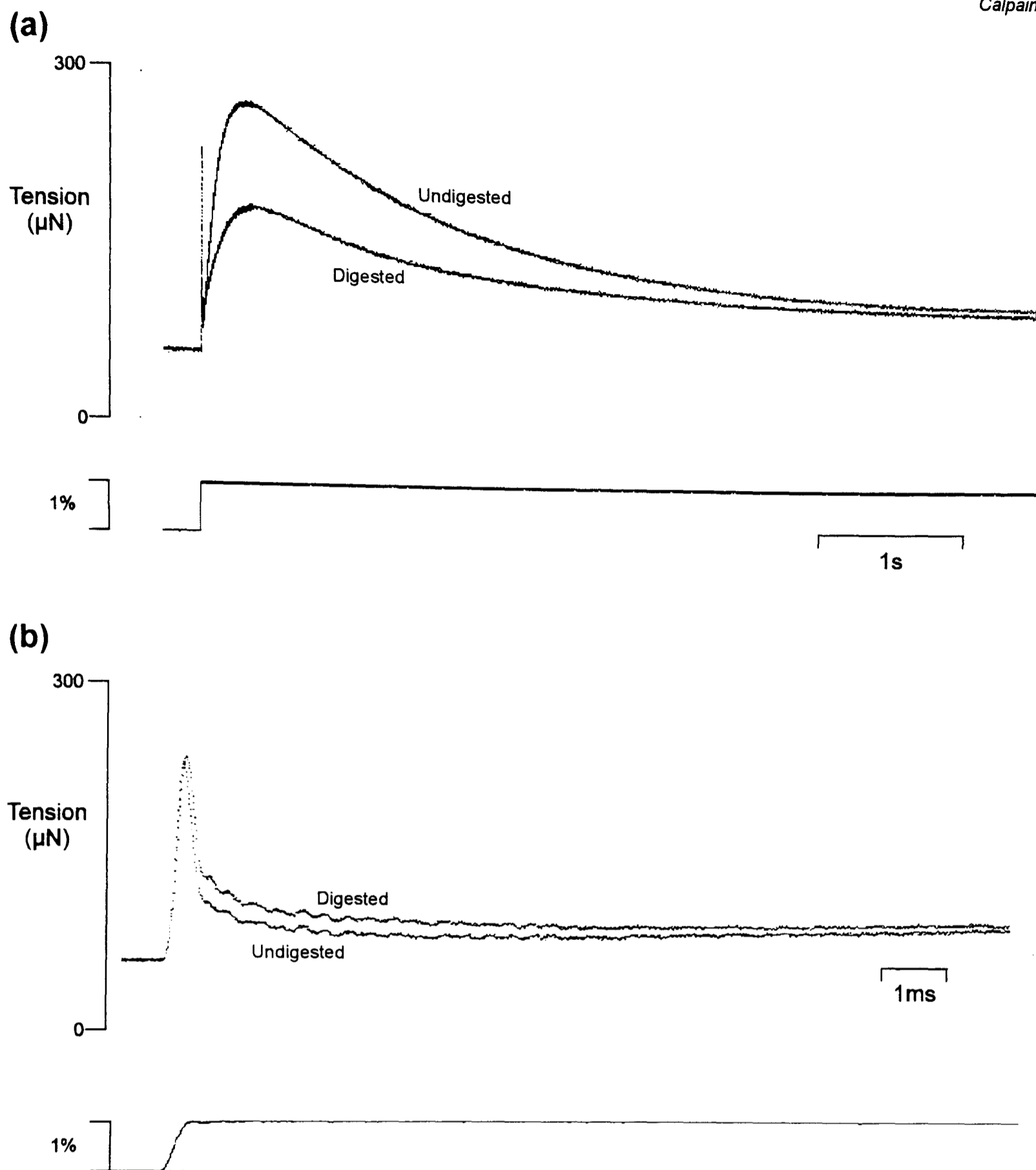


Figure 5.3. The superimposed active tension responses of a single *Lethocerus indicus* fibre before and after mild calpain digestion. The same traces are shown in (a) and (b), on different time bases. (a) There is a large decrease in the amplitude of the delayed tension after digestion. (b) The immediate stiffness of the fibre at steady state is not changed. The amplitude of the phase 2 recovery is reduced following digestion.

	Control (n=4)	Calpain digested (n=10)
Relaxed stiffness	100% ± 6%	101% ± 7%
Rigor stiffness	92% ± 1%	90% ± 2%
Active stiffness	91% ± 6%	89% ± 9%
Amplitude of stretch activation	92% ± 3%	56% ± 4% *

Table 5.1: Mechanical properties of *Lethocerus indicus* flight muscle fibres from rapid step length change experiments. The values are digested divided by undigested (mean ± s.e.m.). Measurements marked with "*" demonstrate a significant difference between the control and the digested fibres.

5.3.4 Sinusoidal analysis

In a similar way to the step length change results, the small amplitude sinusoidal analysis showed little or no change in the relaxed and rigor stiffnesses due to digestion. The before digestion and after digestion Nyquist plots at rest length (0% offset) superimpose over the whole range of frequencies (Figure 5.4). However after 1% pre-stretch, the complex stiffness of the digested fibre at all frequencies is considerable less than for the same fibre before digestion.

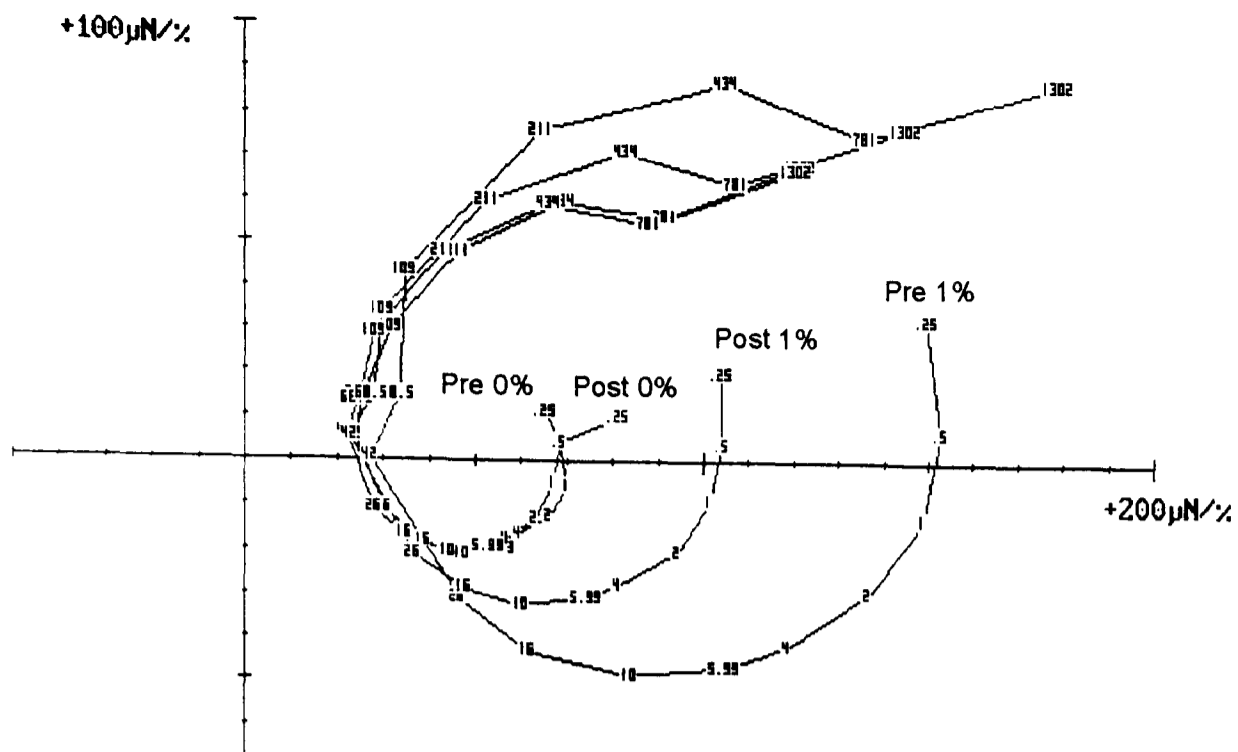


Figure 5.4: Nyquist plots of a single *Lethocerus indicus* fibre before (Pre) and after (Post) mild calpain digestion. Plots are shown at rest length (0%) and at 1% strain. The pre and post-digestion responses overlap at rest length. However at 1% stretch the digested fibre has a much lower stiffness at most frequencies, the maximum work per cycle is lower at the work producing frequencies.

5.3.5 Electron micrographs

After mechanical testing, electron micrographs were made of some of the fibres (Figure 5.5). There is no obvious difference between the fibres given mild calpain digestion and the undigested fibres either in the filament lattice or at the Z-lines. It is important to know that the integrity of the sarcomeres is unaffected by the dosage of calpain used, because calpain is known to remove some Z-line proteins (Goll *et al*, 1991), and at high enough levels will completely remove Z-lines (Reedy *et al*, 1975).

Electron micrographs of four of the digested fibres were compared to those of the control fibres, no structural damage was observed in the digested fibres.

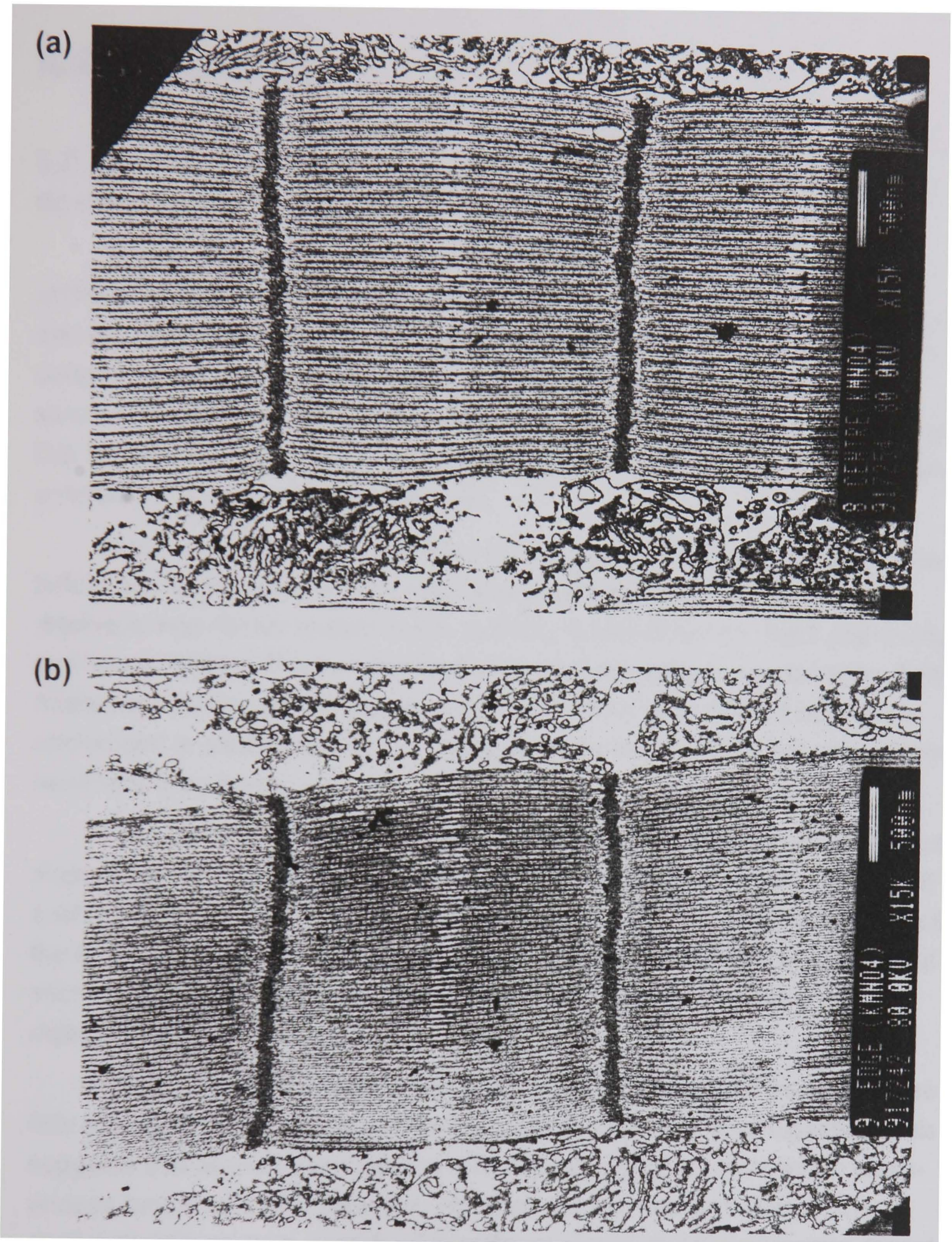


Figure 5.5: Electron micrographs of fibres used in mechanical experiments. The fibre in **(a)** was a control fibre with no calpain digestion. In **(b)** the fibre shown has been digested with calpain during a mechanical experiment. At the level of digestion used, there is no visible damage to the sarcomere.

5.4 Discussion

The SDS PAGE results (Figure 5.1) and those of the Western blot (Figure 5.2) show that at the level of digestion used, the Tn-H protein was significantly digested whereas other sarcomeric proteins remained intact.

The results (Table 5.1) show that there is no significant reduction of rigor stiffness. This indicates that there is no reduction in the number of cross-bridges that are able to bind to actin following mild calpain digestion, showing that cross-bridges remain undamaged. Secondly it shows that other structures in the sarcomere that are under tension also remain intact. These include the thick and thin filaments and also the Z-lines. Any damage to these structures would cause a reduction in measured rigor stiffness.

There is no significant difference in between the stiffness of relaxed fibres before and after digestion. The high relaxed stiffness of insect fibrillar flight relative to non-fibrillar muscle is due to the C-filaments (White, 1983 and Granzier and Wang 1993b). The protein that makes up C-filaments in insect fibrillar flight muscle is minititin (also known as projectin). The fact that relaxed stiffness is unchanged is good evidence that the C-filaments remain intact after the calpain treatment used here.

It has been suggested that stretch activation may arise from thick filament stress caused by the C-filaments (White, 1983; Granzier and Wang, 1993a). If such a mechanism for stretch activation is present in insect fibrillar flight muscle, the fact that passive stiffness is unaffected in these experiments suggests that such a mechanism, if present, should not be affected by the level of calpain digestion used.

The results of sinusoidal analysis show that at rest length there seems to be little difference between the cross-bridge activity before or after digestion. This suggests that at rest length there is a similar sized population of active cross-bridges before and after digestion. However with an imposed stretch, the undigested fibres were considerably stiffer at almost all the frequencies recorded.

The post digestion Nyquist plot at 1% stretch (Post 1%) is the response one would expect in a normal fibre if the pre-stretch were somewhat less than 1% (see Figure 4.5). A worry is that because of fibre damage, the actual inter-filament displacement imposed by the 1% pre-stretch was less in digested fibres than in non-digested fibres. A good argument against this is that because rigor and relaxed stiffness values showed no significant change, the mechanical damage to digested fibres must be minimal.

To summarise, the SDS PAGE and the Western blot show that the level of calpain digestion used removes most of the Tn-H in the fibre without grossly affecting other contractile proteins. The electron micrographs show that any myofibrillar disruption is minimal. The maintenance of relaxed and rigor stiffnesses indicate that the mechanical integrity of the sarcomere remains and that a similar number of cross-bridges can bind in digested compared to undigested fibres. However after mild calpain digestion, stretch activation measured as the difference between the maximum force in the delayed tension phase and pre-step tension, is much reduced.

Together these findings imply that Tn-H has a major role in the stretch activation of *Lethocerus* flight muscle, but that one or more other mechanisms probably exist in parallel with this mechanism.

5.4.1 Passive stiffness and stretch activation

As well as insect fibrillar flight muscle, vertebrate cardiac muscle also gives a large amplitude stretch activated response. One factor that these muscle types have in common is the very high passive stiffness compared to that of non-stretch activated muscle. This has led to the idea that high passive stiffness in some way increases the amplitude delayed tension seen in striated muscle.

The fact that high passive stiffness and stretch activation are common to these muscle types does not necessarily confirm the causal relationship that is often assumed. These muscles also have in common the fact that they both work cyclically with relatively short length changes. Given these conditions it may well be the case that a high passive stiffness makes the muscle more efficient and does not necessarily imply a role in the mechanism of stretch activation.

The work of Tawada and Kawai (1990) is often quoted as evidence that increasing muscle stiffness increases the stretch activation of the muscle. Performing what may be the converse experiment to that described here, they cross-linked about 20% of cross-bridges to the thin filament in rabbit psoas muscle. This gave the fibres more insect-like mechanical characteristics, notably an increase in relaxed stiffness and a large enhancement of oscillatory work output.

It is important to note that the link added here is between the cross-bridges and the thin filament, whereas that in insect fibrillar flight muscle is located in the C-filaments at the ends of the thick filaments. This of course does not account for the possibility that Tn-H may link the two filaments similarly to the cross-link added in the Tawada and Kawai experiment.

Unfortunately there is one line of evidence that is not in favour of the idea that Tn-H spans gap between the two filaments. A molecule that formed a permanent link between thick and thin filaments would contribute to the relaxed stiffness. However digestion of Tn-H shows no significant change in the passive stiffness of the fibre. This suggests that if Tn-H has a permanent attachment to the thick filament then the link must be "slack" or very compliant. By completely removing thin filaments, Granzier and Wang (1993a) have demonstrated that the low frequency passive stiffness of *Lethocerus* fibres is entirely due to tension in the thick and C-filaments. This is further evidence that if Tn-H forms a link between the filaments then it is not under tension in the passive fibre at rest length.

5.4.2 Possible roles for Tn-H in stretch activation

The calpain digestion experiments described here do not indicate any mechanism for the stretch activation mechanism. However, it is possible to make some suggestions based on the location of Tn-H and its properties. All the potential roles for Tn-H in stretch activation described here assume stretch activation to be a cross-bridge recruitment process.

5.4.2.1 Tn-H and the Wray model

One way Tn-H could act is such that the mere size of the protein prevents a large proportion of cross-bridges from binding to the thin filament. This is a model that could work in the same way as Wray's model (1979). Stretching the muscle allows the cross-bridge access to the thin filament, which before the stretch was obscured by the large Tn-H molecule. This kind of model is similar to the steric blocking model for thin filament regulation by troponin-tropomyosin.

One of the arguments against the Wray model is the instability of the low activation state (see section 1.4.1). In order to maintain this low activation state the relative longitudinal displacement of the filaments must remain within a narrow range (see Figure 1.5). Also a small twist in a filament, either thick or thin, can have a large affect on the size of the force producing cross-bridge population on that filament.

What the model requires is evidence that the position of the filaments relative to each other is well controlled throughout the sarcomere. It is not likely that having the filaments constrained at the Z-lines and at the M-lines is enough to prevent filament rotation in the overlap region.

An alternative way in which Tn-H could control the relative positions of the filaments is by cross-linking the two filaments. The link across could control the

position of the filaments, and prevent twisting. In this way it would enhance the Wray mechanism by maintaining the register (or lack of it) of the thick and thin filament repeats. This idea is compatible with some of the results of this work. However not the value of steady state tension. If this was the real function of Tn-H in the sarcomere, then cleavage of the Tn-H would result in a large rise in tension, as filaments twist into configurations where more cross-bridges can attach.

5.4.2.2 Tropomyosin displacement

Troponin-H forms part of the tropomyosin-troponin complex (Bullard *et al*, 1988). Clearly this is the best location for a protein if it is to interact mechanically with the thin filament regulatory complex.

In synchronous muscle the presence of calcium ions bound to Tn-C is sufficient to displace the tropomyosin from the thin filament groove, exposing the cross-bridge binding sites and allowing full activation. This is not the case in insect fibrillar muscle. The addition of saturating calcium to a relaxed fibre gives a very small tension rise, the absolute value may be as little as 10% that achieved when the fibre is stretched.

It is possible that the presence of calcium ions is not sufficient to displace the tropomyosin from its position in the thin filament groove. However Tn-H could make a mechanical link to the thick filament. Now with a small stretch of the fibre, the Tn-H could cause a displacement of the tropomyosin.

5.4.2.3 Direct interaction with the Cross-bridge

The Tn-H link between the two filaments could act on the cross-bridges themselves. There is some similarity between the sequence of the carboxy terminus of Tn-H and that of the amino terminus of MLC-2 in *Drosophila* (Bullard *et al*, 1988). This gives Tn-H a potential binding site on the cross-bridge head. If Tn-H does bind to the cross-bridge in this way, stretching the fibre could pull cross-bridges closer to the thin filament, increasing the probability of attachment. This could also be the mechanism by which the cross-link in the Tawada and Kawai experiment increases the delayed tension observed.

Since stretch activation in insect flight muscle has evolved several times (Cullen, 1974), it is quite likely that different mechanisms of stretch activation exist in different species of insect. Indeed the mechanical characteristics of activated muscle varies between the different orders of insects, as does the presence of proteins that cross react to *Lethocerus* Tn-H antibody (Peckham *et al*, 1992).

However, the results described in this chapter show that Tn-H plays a role in the mechanism of stretch activation in *Lethocerus* flight muscle.

6. Insect flight muscle **cross-bridge kinetics.**

6.1 Introduction

This chapter describes experiments which investigate how insect flight muscle cross-bridge kinetics vary with the concentration of P_i and the amplitude of step length perturbations.

By subtracting the passive tension component, the T_1 - T_2 curves of the remaining active component of *Lethocerus* flight muscle are plotted. Using the mathematical model proposed by Huxley and Simmons (1971) to account for the rapid tension recovery after a fast step, it is possible to make estimations of the size of the cross-bridge working stroke.

The relationship of the rate constant for the phase 2 rapid tension recovery with step size is well known (Huxley and Simmons, 1971). Here I describe a study in which the relationships of the rates constants for phases 2, 3 and 4 with step size are all investigated in insect flight muscle. Both synchronous and asynchronous flight muscles were used in this study.

Increasing the concentration of P_i reduces steady state tension. Following a step stretch the amplitude of phase 3 is reduced and the rate constant is increased as the concentration of P_i is increased (White and Thorson, 1972). Here this effect is characterised over a range of step sizes.

The effect of interfilament displacement on the amplitudes and rate constants for the phases 2, 3 and 4 are investigated. Are these parameters determined solely by the size of step applied or is the initial filament displacement also important? If the latter is true, the nature of this relationship with distortion may shed some light on the mechanism of stretch activation.

6.2 Materials and methods

The flight muscle fibres used in these experiments came from three species of insect: the hemipteran bug *Lethocerus indicus*, the Dipteran *Tipula* (cranefly) and the noctuid moth *Noctua pronuba* (Large yellow underwing). The *Lethocerus* and the *Tipula* both have asynchronous muscle, whereas that of the *Noctua pronuba* (order Lepidoptera) has synchronous flight muscle (Cullen, 1974).

All experiments were performed at 15°C and at an ionic strength of 150mM (as described in Chapter 4). All mechanical rate constants were estimated using

the nonlinear least squares algorithm described in section 3.5.4. With the exception of the first T_1 - T_2 experiment described here, fibres were mounted by gluing them directly to the apparatus hooks with cellulose nitrate glue as described in 4.2.3.2.

6.2.1 T_1 - T_2 with passive component subtracted

To make the T_1 - T_2 records, a single *Lethocerus indicus* fibre was given a series of fast steps and releases ranging from 0.1% to 1% in amplitude. The same sequences of steps and releases were recorded in both relaxing and activating solutions. All step length changes were complete within 210 μ s.

The duration of time at each length offset was very short, 10ms for stretches and 8.3ms for releases. This provides enough time to record a tension signal to which a single exponential function can be fitted. A slightly longer period of time was given on the stretches to capture all of the slower phase 2 at the larger stretches.

Between these steps, a pause of 5s was given to allow the muscle to reach a steady state. This is particularly important in the case of the larger stretches where some initial delayed tension changes must be given time to return to the steady pre-step tension.

In order to generate a T_1 - T_2 curve that demonstrates the characteristics of the active component of the muscle (the cross-bridges), the recordings made in relaxing solution were subtracted from the active transients. The tension values for T_0 , T_1 and T_2 were read using the muscle program. The rate constant for phase 2 was estimated by fitting a single exponential decay to phase 2.

6.2.2 Changes in r_2 , r_3 and r_4 with step size and $[P_i]$

Sequences of varying amplitude step stretches and releases were applied to the flight muscle of *Lethocerus*, *Tipula* and *Noctua pronuba*. Recordings were of sufficient duration that phase 4 was completely or almost completely finished. Allowing the muscle to reach a new steady state in this way increases the accuracy of the exponential fit to phase 4.

With the *Noctua pronuba* (synchronous) fibre length changes ranged from -0.6% (release) to +3.5% (stretch). With the two asynchronous flight muscle fibres smaller ranges were used. This is because these fibres have a higher passive stiffness which reduces the offset at which mechanical damage starts to occur. The *Tipula* fibre was tested over the range -0.4% to +1% and *Lethocerus* from -1% to +1%.

In both *Tipula* and *Lethocerus* fibres, a range of concentrations of P_i was used. The P_i activating solutions used in these experiments were made by combination of two stock activating solutions with 0mM added phosphate and 20mM added phosphate. Both solutions had an ionic strength of 150mM, their constituents are described in Table 4.1.

Experiments with *Tipula* were performed in activating solutions containing 0mM, 3.3mM and 10mM P_i . Since a single exponential did not fit well to the rapid tension recovery of these records, two exponential functions were fitted to phase 2, and one each to phases 3 and 4. The small signal characteristics of *Tipula* flight muscle was investigated at a range of concentrations of P_i , in the frequency range 1.3kHz to 0.5Hz.

Activated *Lethocerus* muscle experiments were performed in 0mM, 1mM, 3.1mM and 10mM P_i solutions. The records were made starting with the activating solution with no added P_i . Several bath volumes of solution were washed through with each solution change to be sure that as little as possible of the previous solution remains in the bath. Records were not made for at least 30s after the solution was washed through. This ensured that the bath temperature had stabilised and that the new solution has diffused into the fibre. In the case of the *Lethocerus* records, after the last 10mM P_i recordings, a second sequence of steps at 0mM P_i was recorded.

6.2.3 Comparison of kinetics at 0% and 1% strain

To investigate the effect of fibre strain on the parameters of the four phases of the tension recovery a series of step length change records were made. The same amplitude of step length change was applied at both rest length (0%) and at 1% pre-strain. This experiment could be performed by making a sequence of step length change recordings at rest length, then applying a 1% strain using the micro-manipulator on the tension gauge then repeating the same step sequence at this new strain. Unfortunately without the aid of a sarcomere length detector, it is difficult to know how much stress relaxation has occurred during the few minutes necessary to record the steps at 1% strain. To reduce the possibility of error due to stress relaxation the 0% (rest length) and the 1% (strained) recordings were made consecutively in a series of double step experiments.

Each record began with the step from rest length, this length offset is maintained for 10s. Next the fibre was given a ramped length change to change the fibre strain to exactly 1% above rest length, the length remained at this value for a 12s period to allow the fibre to reach a new steady state. From this new offset, the original step was repeated and recorded for a further 10s. Irrespective

of the size or direction of the first step, the fibre was always returned to 1% above rest length before the second step was applied.

In this study due to the long duration of the recordings, the order of the step length changes was randomised. The step length changes (in percent of fibre length) were made in the following order: 0.1, -0.4, 0.6, -0.1, -1, -0.6, 0.4, 0.2, -0.8, 0.8, -0.2, 1, 1.4, 1.8, and finally 2.2. As can be seen from this order, it is not truly random in that the largest four step sizes were performed last. This was a precaution taken in case these larger steps caused any loss of steady state tension at rest length. This would indicate that the fibre had been damaged.

6.3 Results

6.3.1 T_1 - T_2 Active minus passive

The active and relaxed tension signals are plotted in Figure 6.1a. Separate plots are shown for stretches (upper) and releases (lower). In the larger releases, tension drops to zero. The tension signal does not overshoot far beyond the zero tension line indicating that the frequency response of the strain gauge is high.

The length signal can be seen in Figure 6.1c. Note that in each of these plots, two time bases are used. The length of time at each new length is 10ms for stretches and 8.3ms for releases. Between each of these steps there is a recovery period of 5s.

The length-tension plots for the same data are shown in part (b). Here the plots are separated into the active and the passive responses. Note that in the active response, the T_1 and T_2 curves can be seen in the untransformed original data.

Tension transients resulting from the subtraction of the passive response from the active are shown in Figure 6.1. part (b). As in part (a), the data is plotted with sample number. The resulting T_1 - T_2 curve (Figure 6.1. part (a)) is not like the Huxley-Simmons (1971) curve. The most noticeable difference is the fact that the T_2 curve crosses the vertical axis with negative gradient rather than the zero gradient found by Huxley and Simmons. The displacement at which the T_2 curve reaches zero tension is close to -14nm. The T_1 curve is close to linear, although some curvature is present. The T_1 curve crosses zero tension at -8nm.

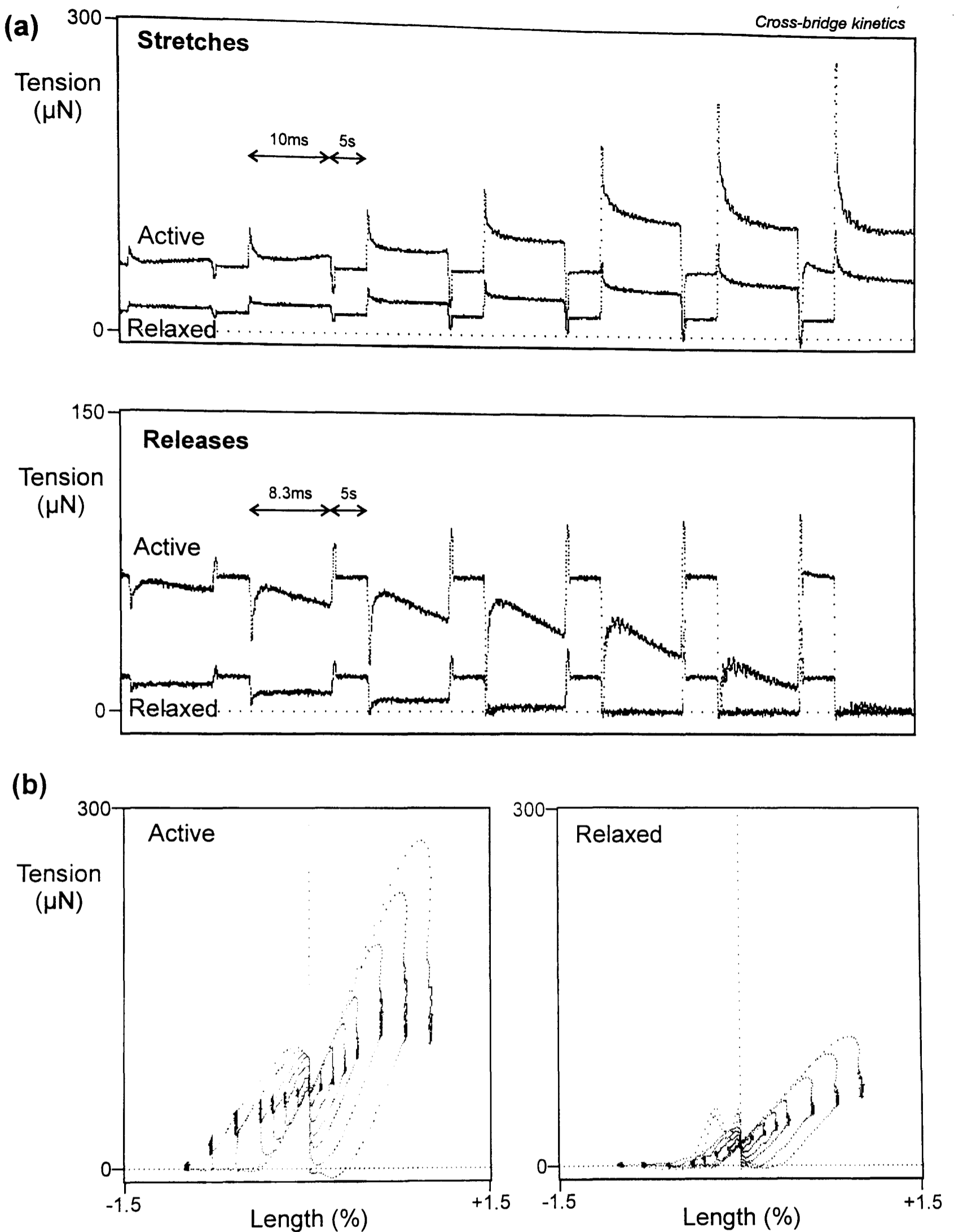


Figure 6.1: Active and relaxed *Lethocerus indicus* flight muscle given a series of steps of increasing amplitude. **(a)** In the tension traces, the data is plotted against sample number, not against time. All length changes are complete within $200\mu\text{s}$. The length of time at each length offset is 8.3ms in the releases and 10ms in the stretches. Between steps a pause of 5s was given to ensure that the fibre had reached steady state. **(b)** The same data is shown in length-tension plots. The active and relaxed traces are plotted separately. In the active plot the T_1 - T_2 curves are visible within the data.

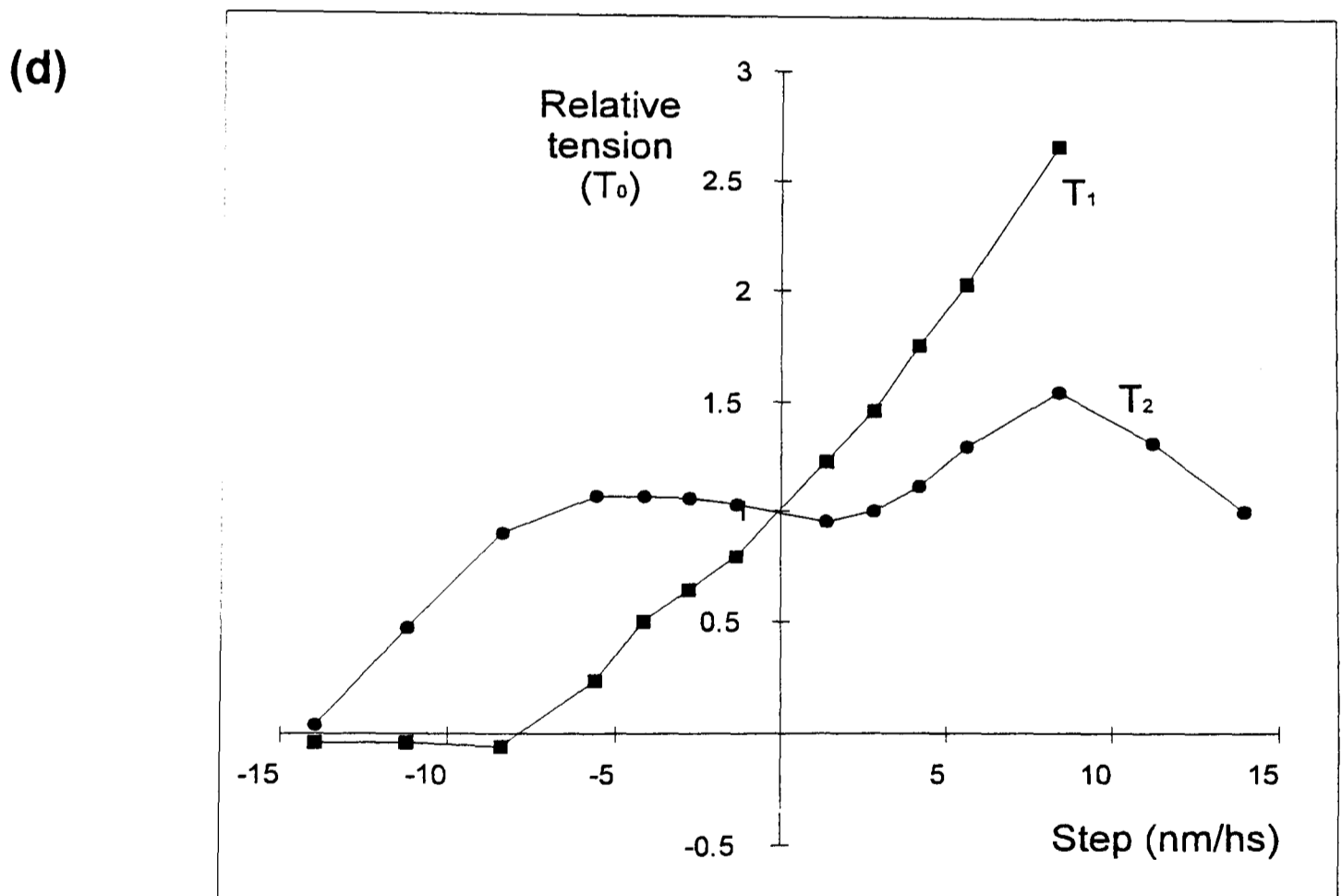
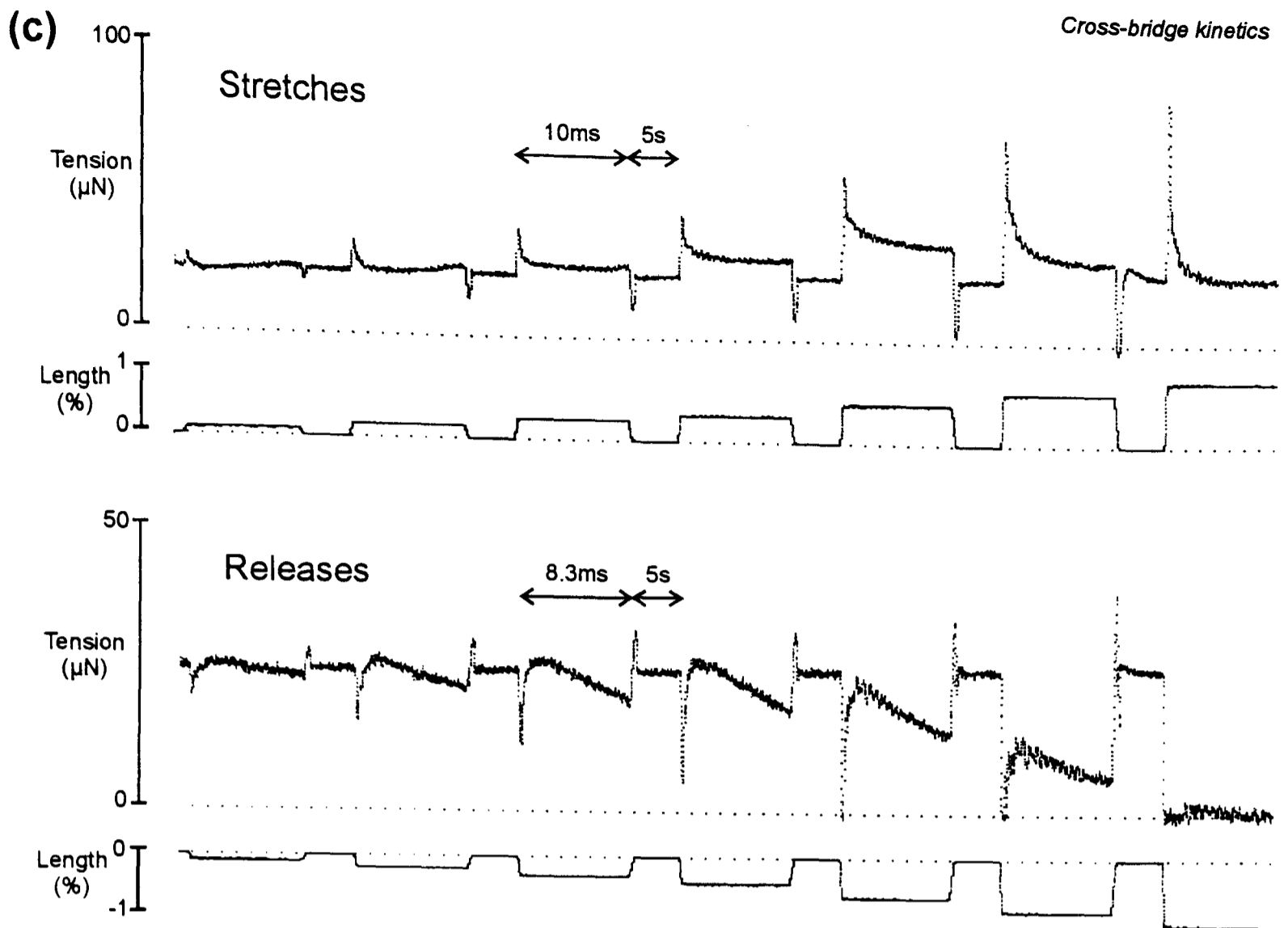


Figure 6.1 (continued): A T_1 - T_2 plot generated from the data shown in Figure 6.1a. **(c)** The traces shown are the result of subtracting the relaxed response from the active. **(d)** The T_1 - T_2 plot for the active component in *Lethocerus indicus* flight muscle differs from that of vertebrate striated muscle. The T_2 curve crosses the vertical axis with a negative gradient. The step units were converted to nanometres per half sarcomere (nm/hs) assuming a sarcomere length of $2.8\mu\text{m}$.

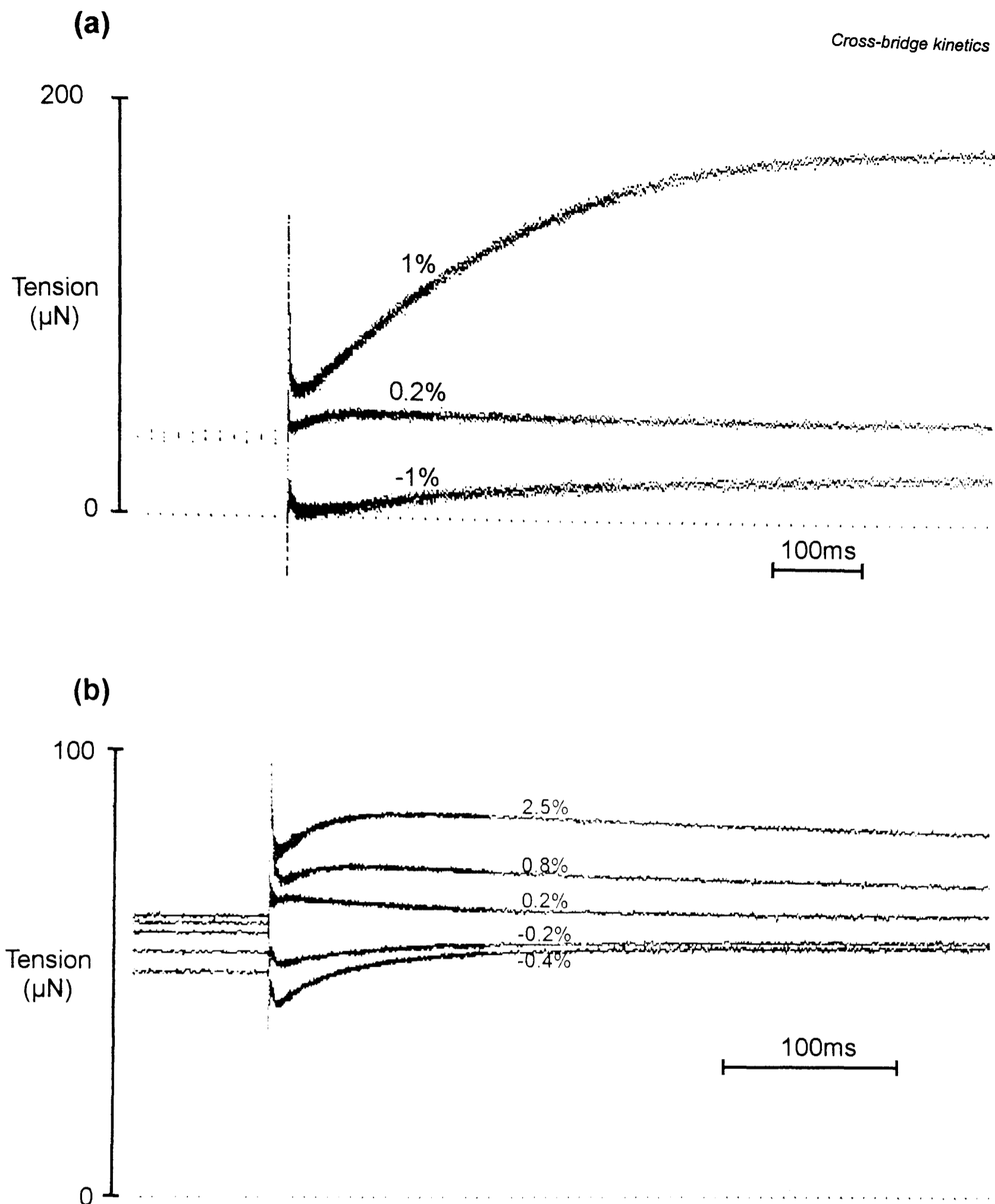
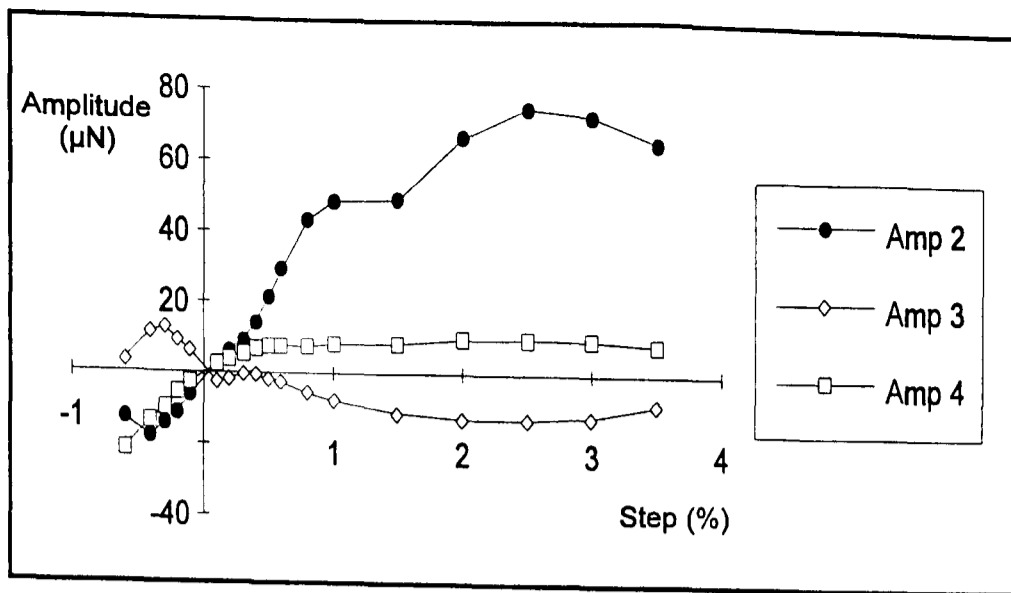
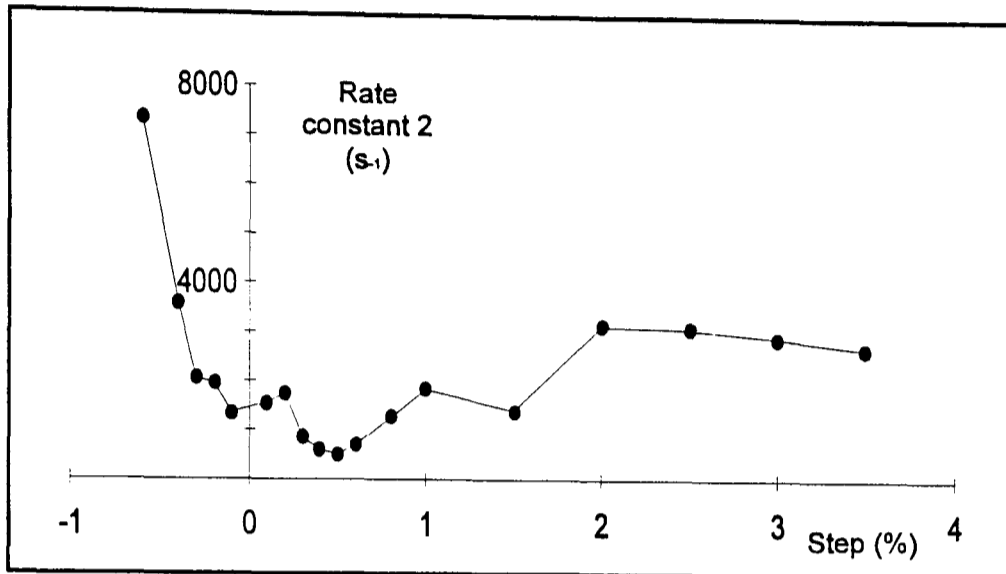


Figure 6.2: Tension transients showing the change in rate constants of phase 3 (delayed tension) with step size in activated insect flight muscle. Both sets of traces show the response of a single activated fibre in a solution with no added phosphate. The transients in (a) are *Lethocerus indicus* (asynchronous), while in (b) the moth *Noctua pronuba* (synchronous). With increasing step size the rate constant for delayed tension reduces dramatically.

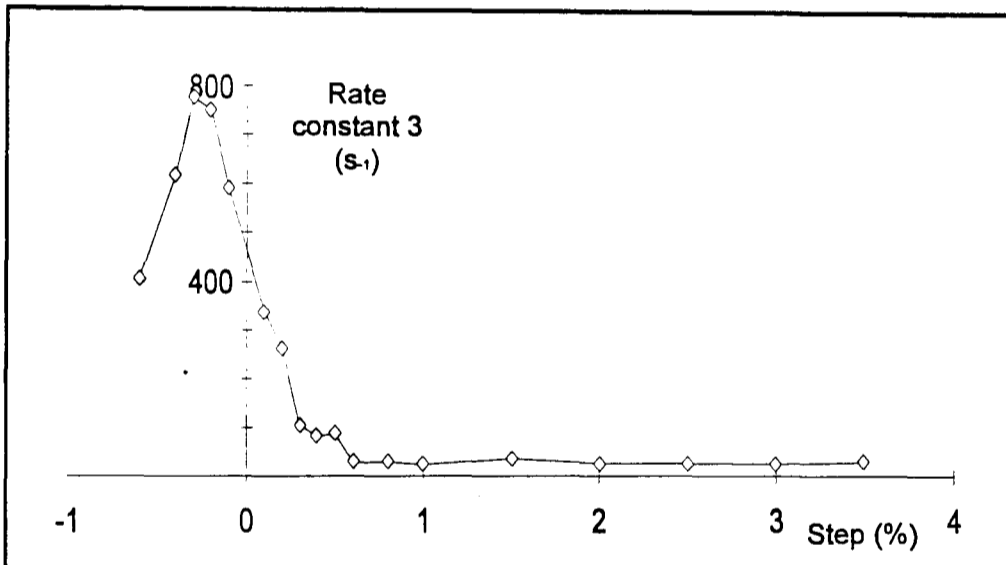
(a) Amplitudes



(b) Phase 2



(c) Phase 3



(c) Phase 4

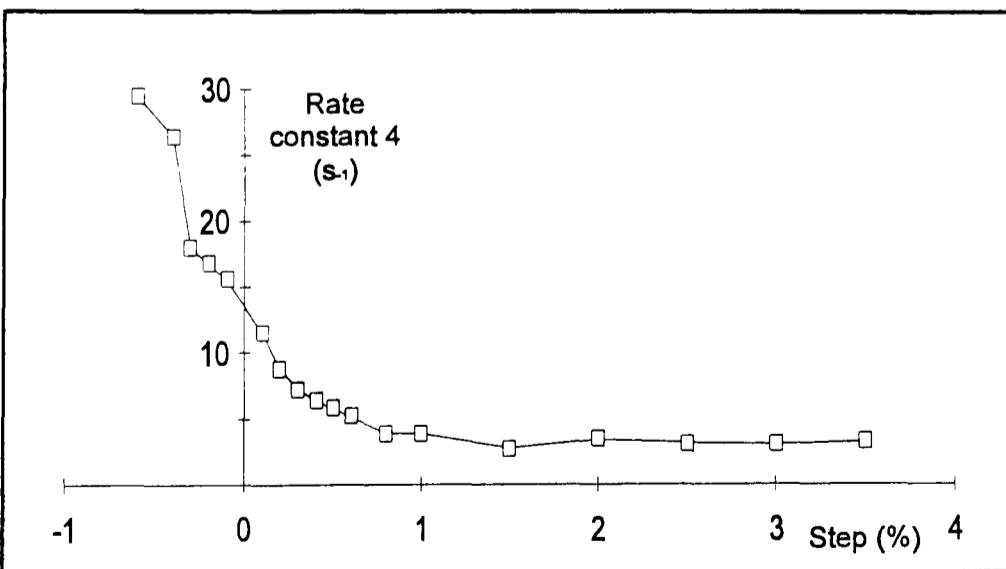


Figure 6.3: The amplitudes and rate constants of phases 2, 3 and 4 for the activated synchronous flight muscle of the moth *Noctua pronuba* (Large yellow underwing). Three summed exponentials were fitted to the data using a nonlinear least squares procedure.

6.3.2 Step size and r_2 , r_3 and r_4

In the tension transients of Figure 6.2 it can be seen that the rate constants for phases 3 and 4 both decrease with increasing step size. This was found to be true for both the asynchronous muscle of *Lethocerus indicus* (a) and the synchronous muscle of *Noctua pronuba* (b). Also with increasing step size, the amplitude of both phases 3 and 4 increase. The results of the curve fits to the transients of *Noctua pronuba* are summarised in Figure 6.3. These show that the relationship of the rate constants for phases 3 and 4 have a similar relationship to step size as phase 2 i.e. slow for large stretches, fast for smaller stretches and very much faster for releases.

6.3.3 The effect of P_i on the step size dependence of r_2

The results of this study are summarised in Figure 6.4. Some of the tension transients used to create the plot are shown in part (a). The plot shows that there little or no change in the rate constant for the phase 2 recovery with increasing concentration of P_i .

Due to the lower steady state tension in the higher phosphate solutions, the step releases larger than 0.4% resulted in tension falling to zero, so no curves could be fitted to these transients.

6.3.4 The effect of P_i on the T_1 - T_2 curves

The affect of P_i on the T_1 - T_2 curves can be observed in Figure 6.5. It must be recognised that the high frequency characteristics of glued fibres such as this one are not as good as those of T-clip preparations such as that described in Figure 6.1. The presence of the glue on the end of the strain gauge reduces its frequency response.

Despite this, stiffness changes can be observed. The effect of increasing P_i is to reduce the gradient of the T_1 curve. This suggests that the there is a reduction in the number of attached cross-bridges at the higher concentrations of P_i used.

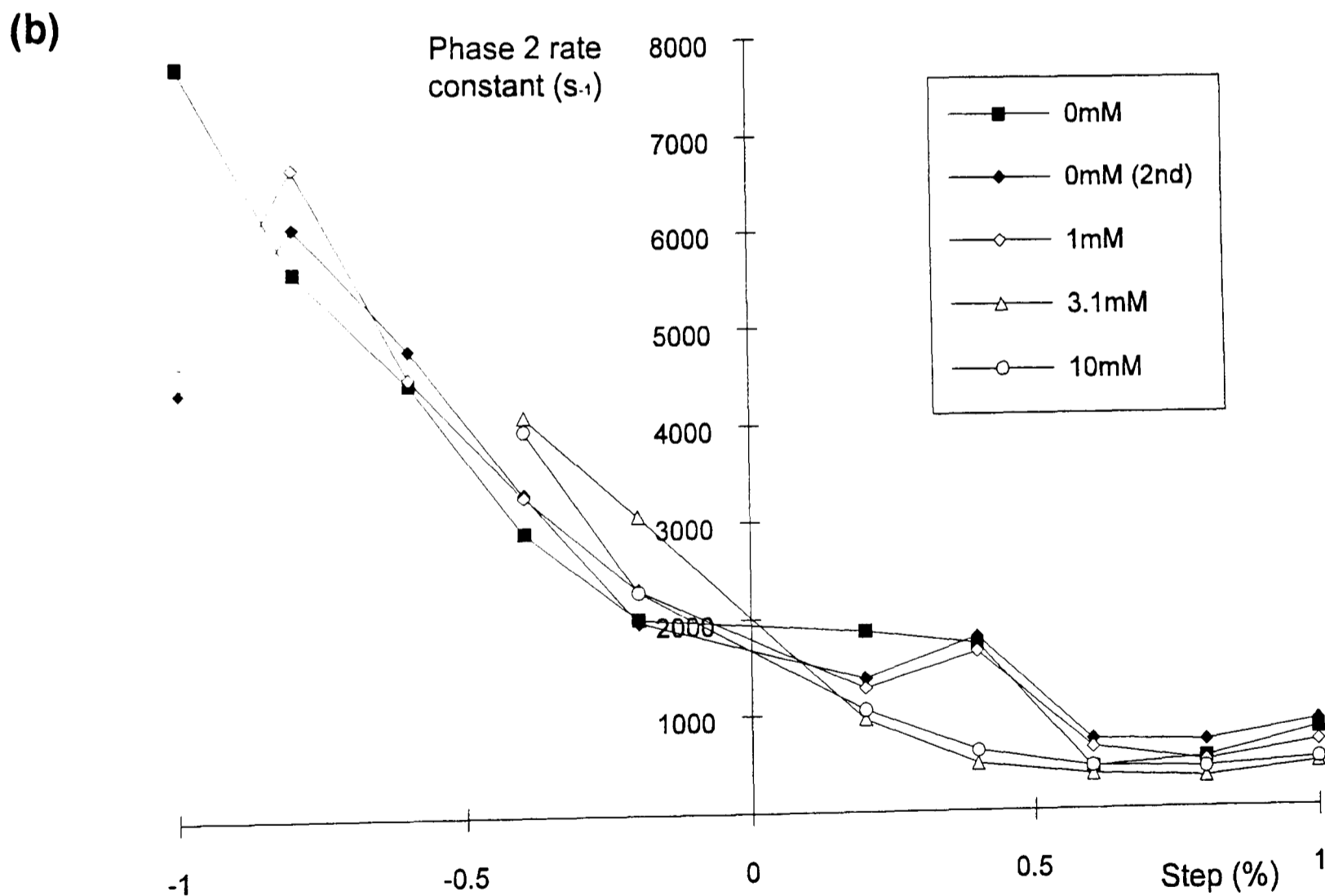
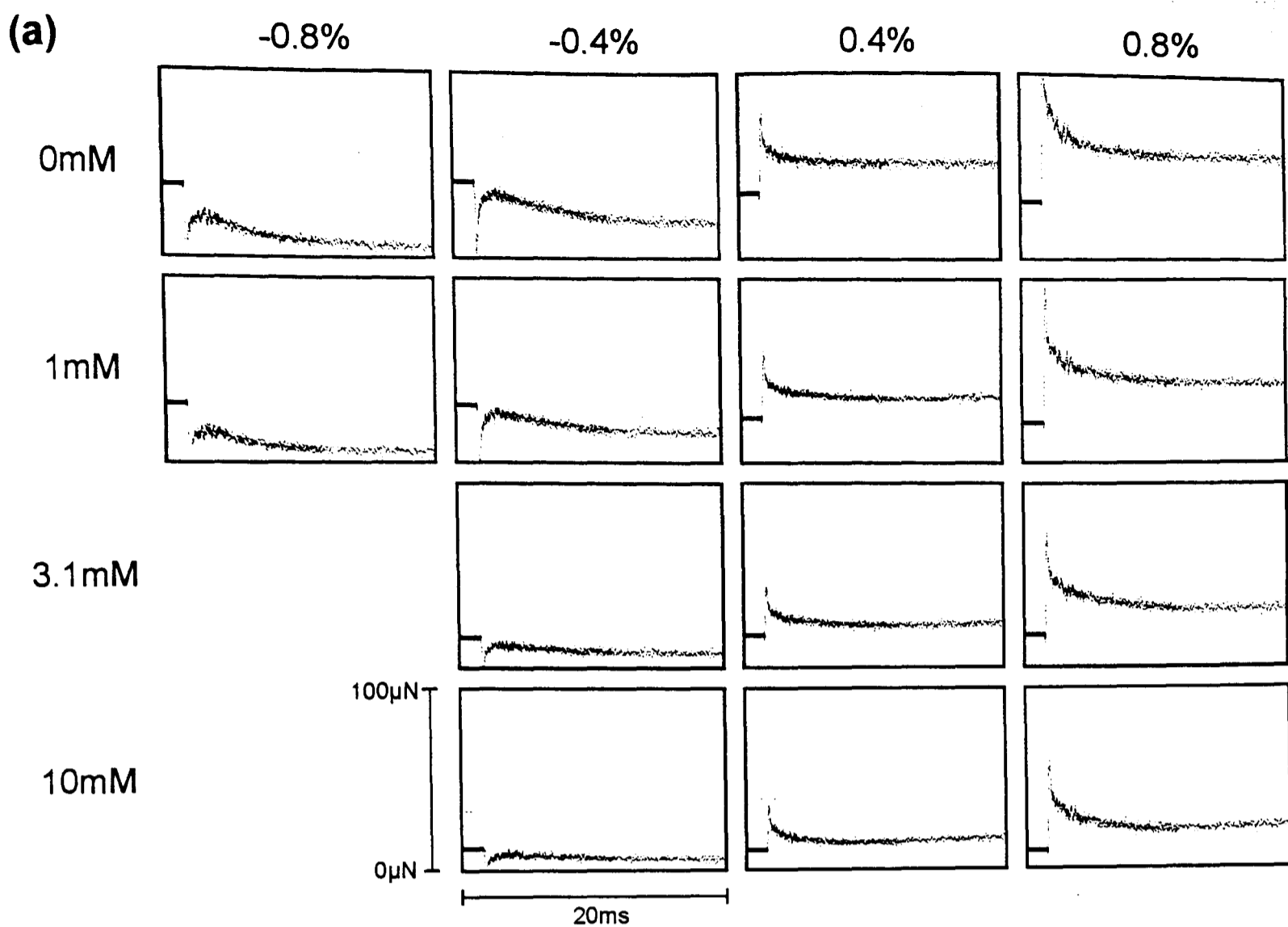


Figure 6.4: The effect of the concentration of inorganic phosphate (P_i) on the rate constant of the rapid recovery phase in activated *Lethocerus indicus* flight muscle. **(a)** Some of the tension transients are shown, all on the same scale (each box is 20ms wide, full scale tension ranges from $0\mu\text{N}$ to $100\mu\text{N}$, solid line indicates resting tension). The larger releases were not possible in 3.1 and 10mM P_i due to lack of tension. **(b)** Rate constants were estimated by least squares fitting three exponentials to phases 2, 3 and 4. Rate constant plotted against step size shows no effect of P_i . This indicates that P_i release step is not associated with the working stroke.

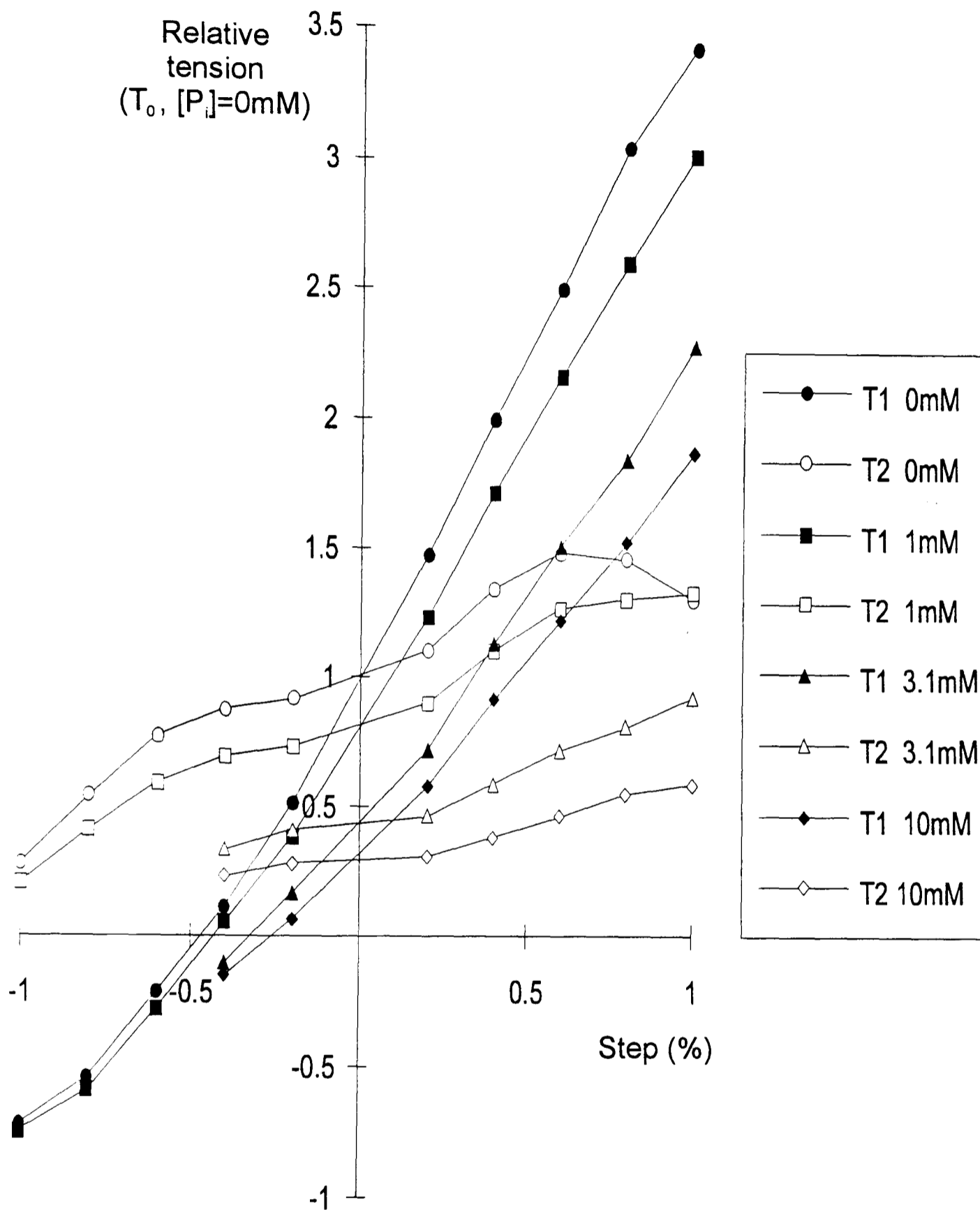


Figure 6.5: The T_1 - T_2 curves for an activated *Lethocerus indicus* fibre at different concentrations of added inorganic phosphate (P_i). All tensions are plotted relative to T_0 with no added phosphate. The instantaneous stiffness of the fibre (T_1 , solid symbols) decreases with increasing P_i .

6.3.5 The effect of P_i on the step size dependence of r_3 and r_4

As was shown previously (White and Thorson, 1972), with increasing P_i concentration, the rate constants for both phases 3 and 4 following a stretch become faster (Figure 6.6). The results described here show that in contrast, for step releases, the rate constant of phase 3 becomes slower with increasing concentration of added P_i .

It is worth noting that the amplitude of phase 4 for releases in the higher P_i solutions was very low. This reduces the accuracy of the fit and in some cases made fitting an exponential impossible. The amplitudes and rate constants for phase 3 and phase 4 estimated for these data are shown in Figure 6.8 and Figure 6.9 respectively.

The *Tipula* rate constants for phase 4 could not be fitted satisfactorily in the higher P_i solutions, due to the presence of a brief Schädler's oscillation following the delayed tension rise (Schädler *et al*, 1971). This oscillation is greatest at large stretches in the 10mM P_i solution. It was not possible to prevent the curve fitting procedure from fitting phase 4 to this rapid reduction in tension rather than the more gradual tension decline of phase 4.

In *Tipula* flight muscle in the presence of millimolar quantities of P_i there is a slight increase in r_3 as the step size increases (see Figure 6.7). For steps greater than 0.2%, r_3 becomes faster as the concentration of added P_i increases.

6.3.6 The Effect of P_i on the Nyquist plot

The small amplitude frequency response of the fibre at different concentrations of P_i is shown in Figure 6.10. The most striking effect of increasing the concentration of P_i is to reduce the complex stiffness of the fibre at all frequencies tested. This result is consistent with a reduction in the number of attached cross-bridges as P_i increases. There is also a small increase in the frequency of maximal work per cycle.

6.3.7 The kinetics of *Lethocerus* flight muscle at 0% and 1% strain

An example experimental record is shown in Figure 6.11a. The pair of T_1 - T_2 curves for 0% (rest length) and 1% (strained) are plotted in Figure 6.11b. Despite steady state tension more than doubling after the 1% strain, the gradient of the T_1 curve shows only a very small increase.

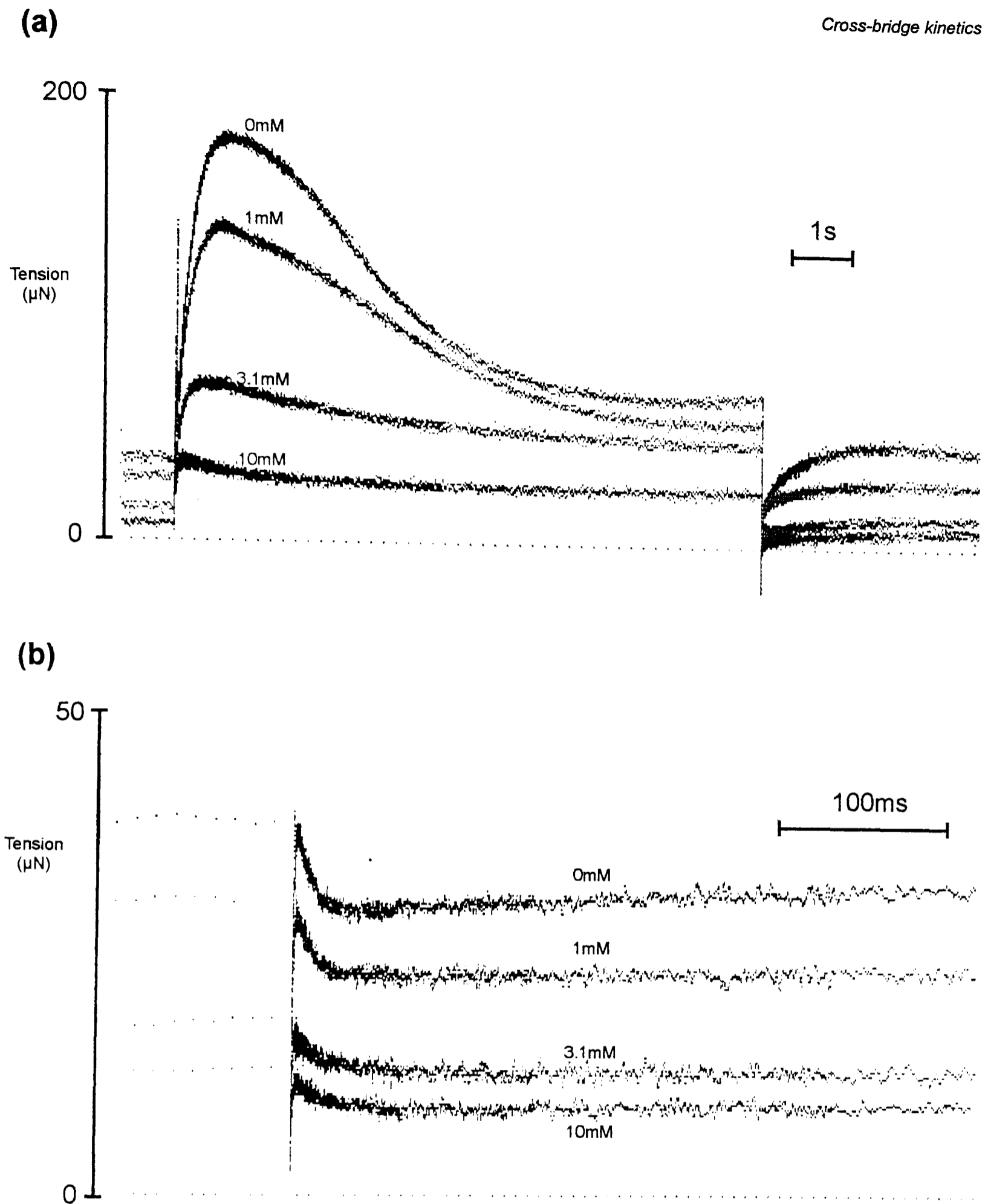


Figure 6.6: A series of traces demonstrating the effect of inorganic phosphate (Pi) on the delayed tension changes in *Lethocerus indicus* flight muscle. (a) After a 1% stretch the delayed tension rise (phase 3) becomes faster and lower in amplitude with increasing Pi. Indeed at 10mM Pi, phase 3 is too fast to be seen clearly on the timebase used. (b) On a step release (-0.4%) the phase 3 process is faster. As in (a) the amplitude of phase 3 reduces with increasing Pi. However the rate constant can be seen to be faster in the traces with lower Pi. For clarity the traces in (b) were filtered using a 15-point quadratic least squares smoothing filter.

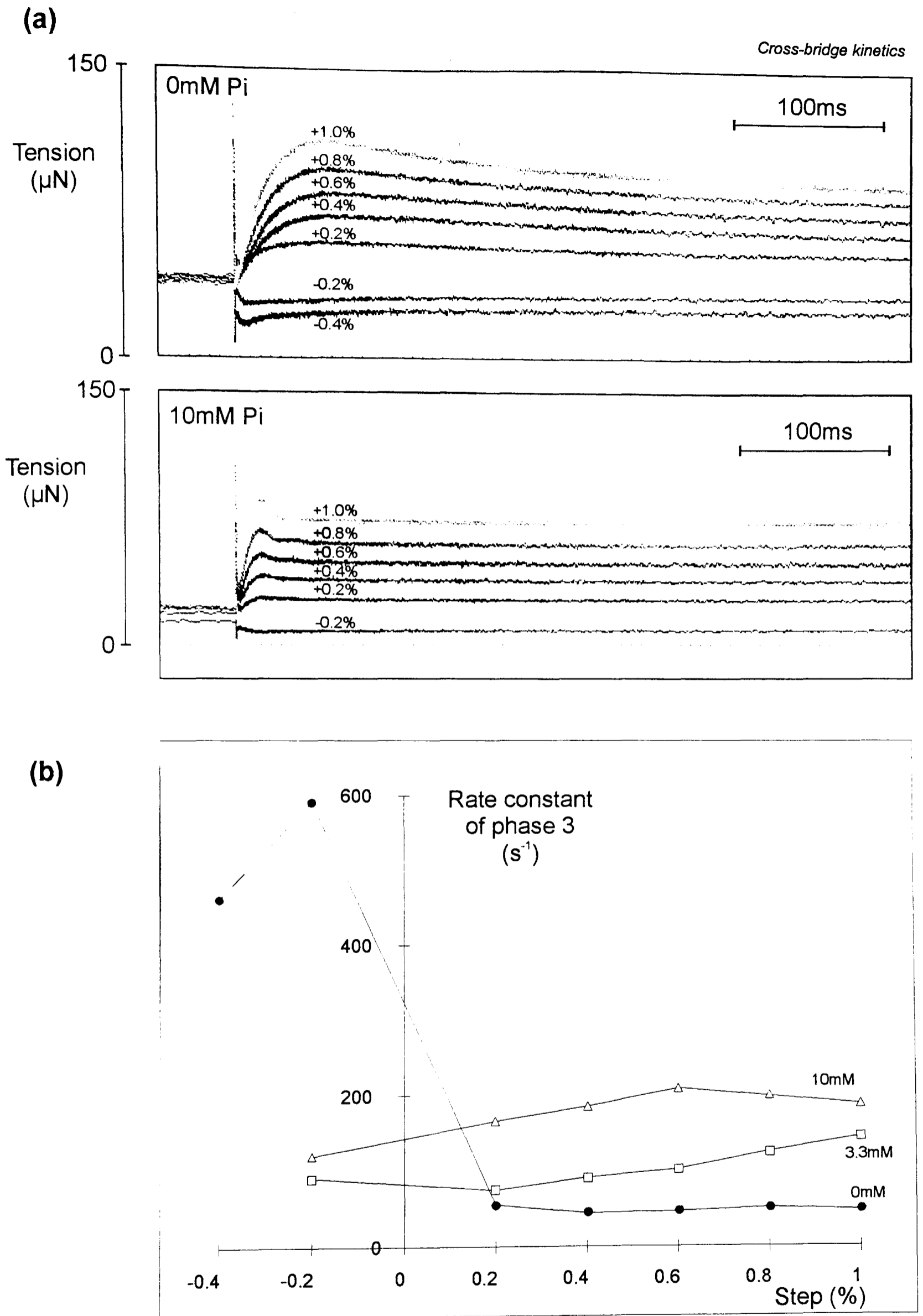


Figure 6.7: The relationships between step size, the concentration of inorganic phosphate (P_i) and the rate constant of the delayed tension (r_3) in *Tipula* (crane-fly) flight muscle. **(a)** Tension transients show that the r_3 becomes slower with increasing step size in low phosphate conditions, but changes little in the higher phosphate solution. **(b)** The rate constant for the phase 3 as estimated by fitting three exponential functions to the data.

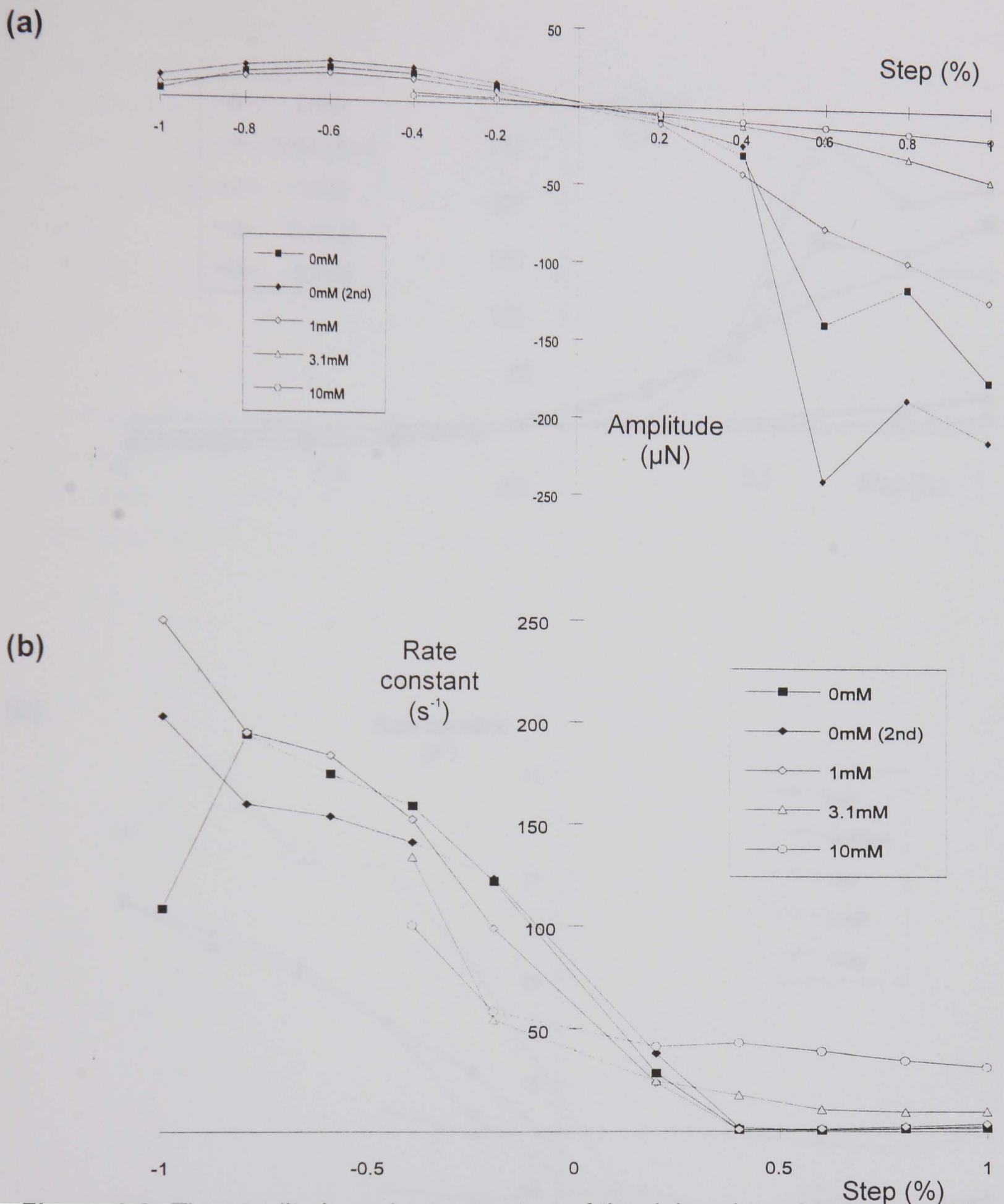
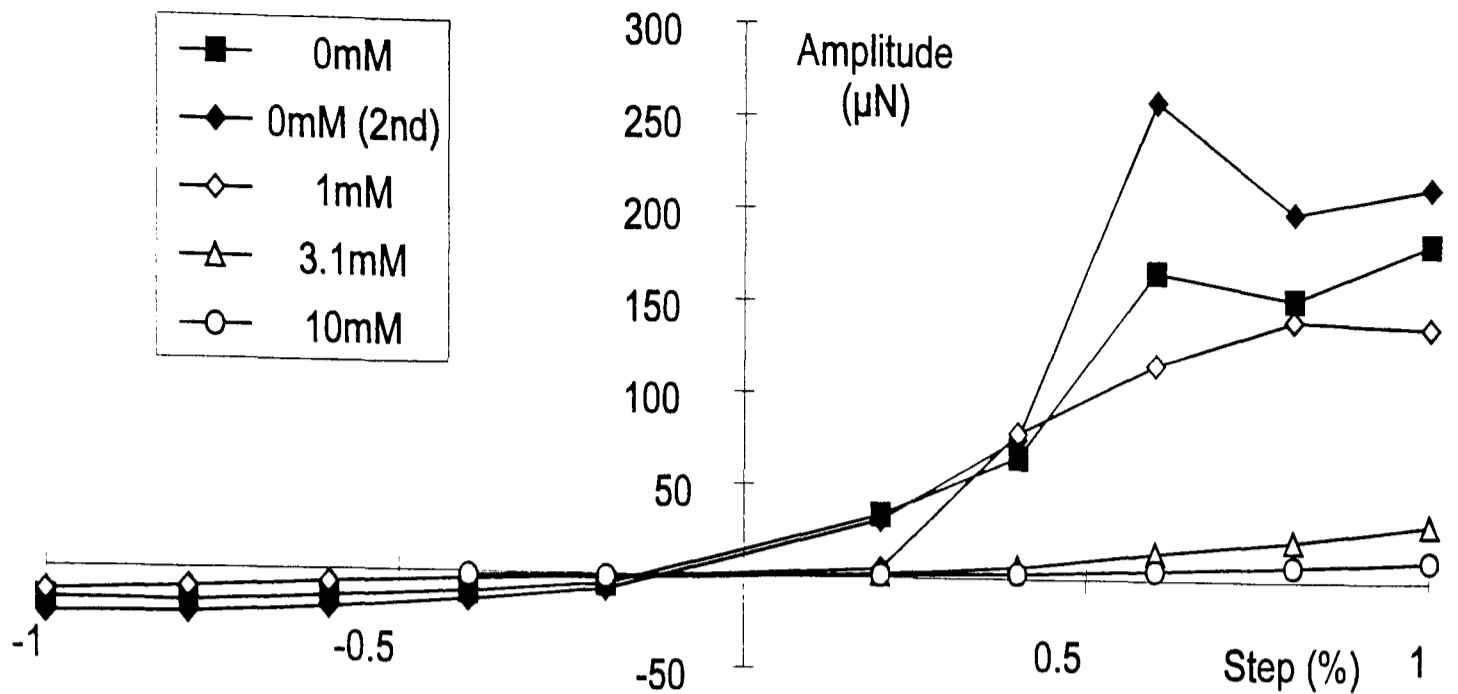


Figure 6.8: The amplitude and rate constant of the delayed tension (phase 3) in *Lethocerus indicus* flight muscle at different concentrations of inorganic phosphate (P_i) and at a range of step sizes. Plotted are the results from a nonlinear least squares fitting procedure, three exponentials were fitted to phases 2, 3 and 4 of each trace. **(a)** The amplitude of phase 3 reduces considerably with increasing concentration of P_i . **(b)** The rate constant of phase 3 is fastest on the large releases becoming slower on the stretches. The degree of change is dependent on the concentration of P_i . With no added P_i , a release of 0.4% has a rate constant of 140s^{-1} , a 1% stretch gives 1s^{-1} to 2s^{-1} . The same steps in 10mM added P_i gives 100s^{-1} to 31s^{-1} respectively.

(a)



(b)

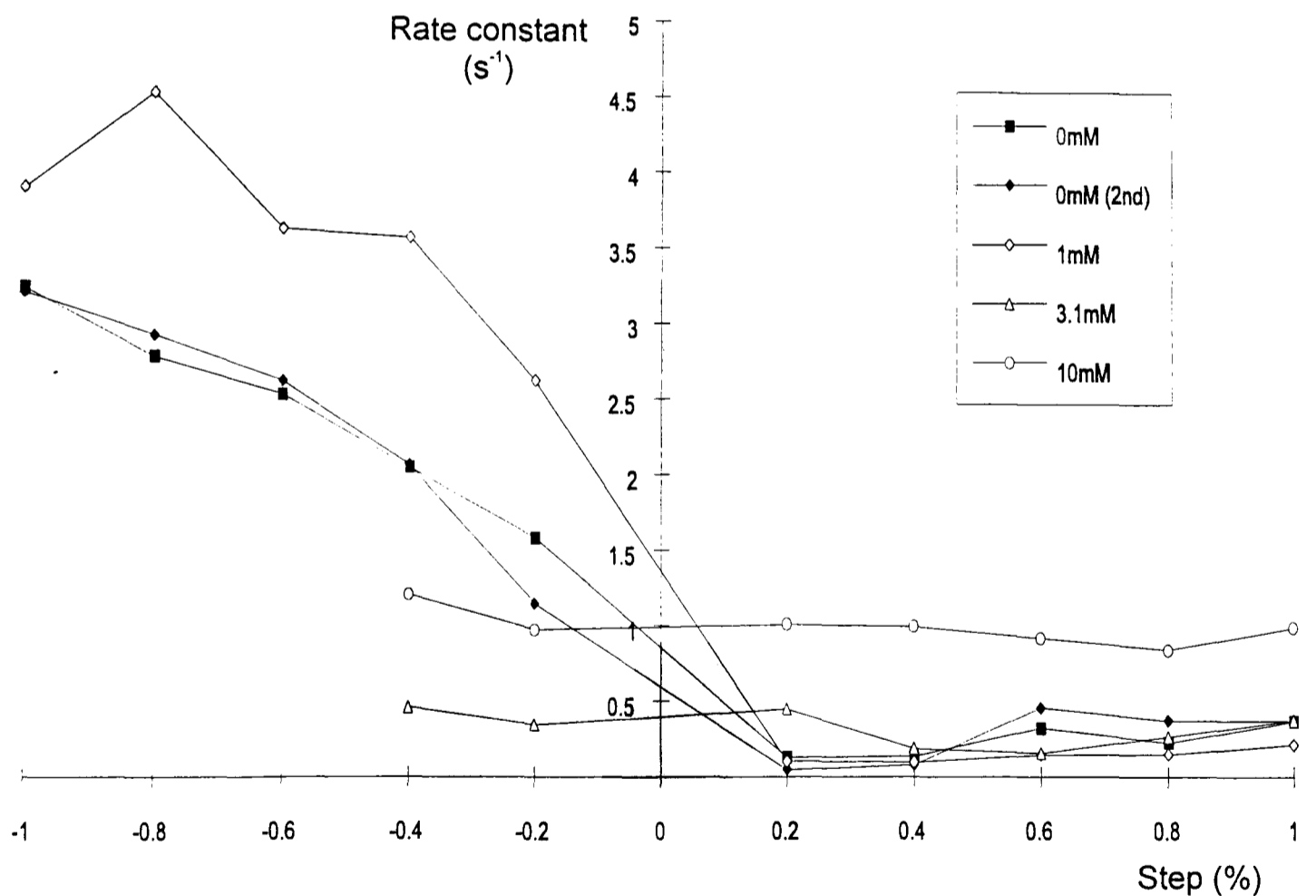


Figure 6.9: The amplitude and rate constant of phase 4 in *Lethocerus indicus* flight muscle at different concentrations of inorganic phosphate (P_i). **(a)** The amplitude of phase 4 decreases with increasing P_i . **(b)** With low or zero levels of added phosphate, the rate constant for phase 4 decreases with increasing step size. At the highest level of P_i used, the rate constant shows little or no relationship to step size.

The results of fitting three exponential functions to phases 2, 3 and 4 of both the 0% and 1% transients are plotted in Figure 6.12. In these plots the "Step" axis does not include the 1% strain applied, for example a 0.2% step will be plotted at 0.2% irrespective of whether the step occurred before or after the 1% strain. This simplifies the comparison of the parameter curves before and after the applied strain.

The rate constant for phase 2 shows no detectable trend with the change in strain. The amplitude of phase 2 is slightly greater following the 1% strain.

The rate constants for both phase 3 and 4 also prove to be quite insensitive to the level of strain on the fibre. However the amplitude of phases 3 and 4 show a horizontal shift. In the region of stretches from 0.2% to 0.8% there is a large increase in the amplitude of phases 3 and 4 at 1% strain. This horizontal shift of the amplitude curves 3 and 4 is in the region of 0.2% to 0.3% of the fibre length.

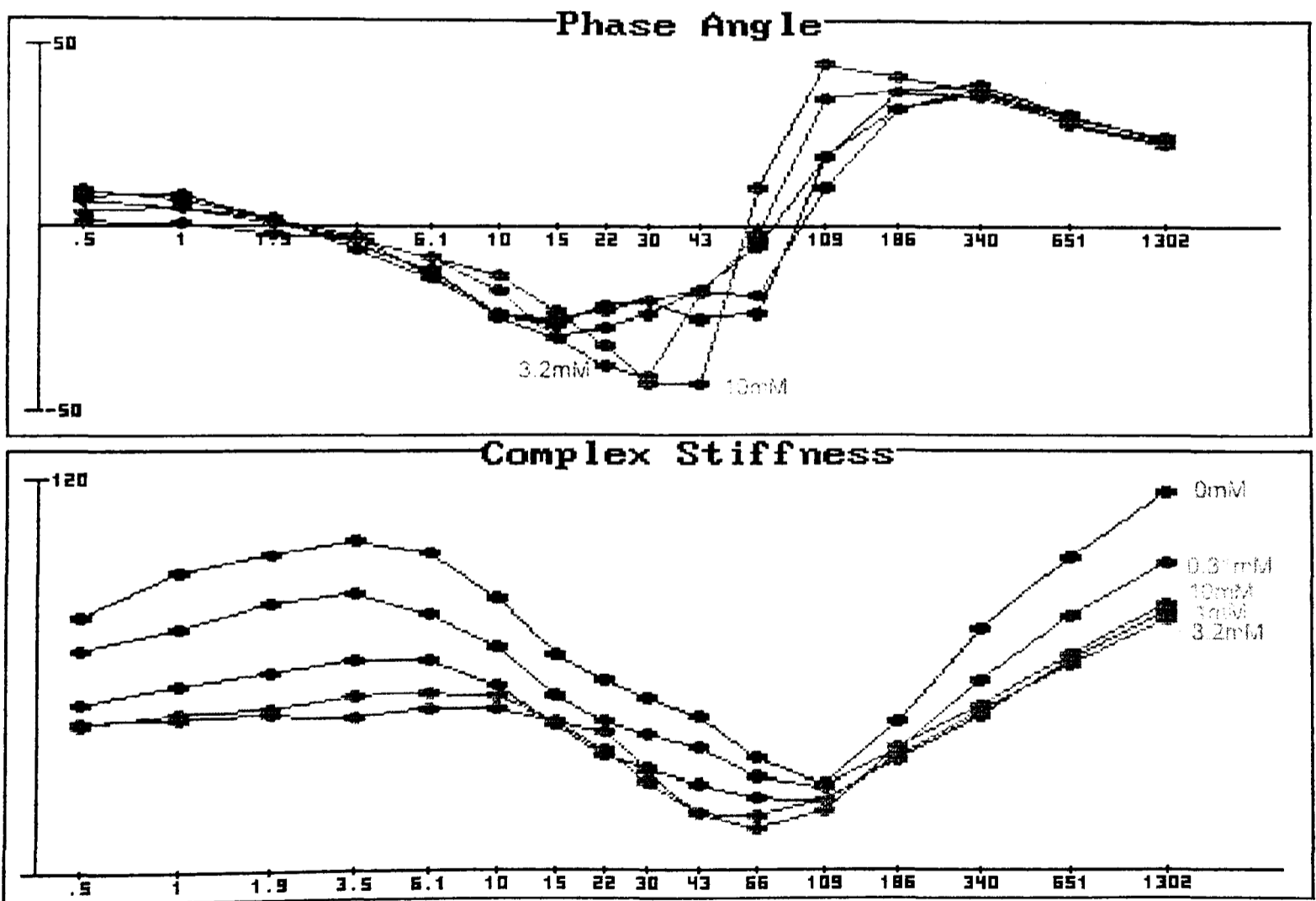
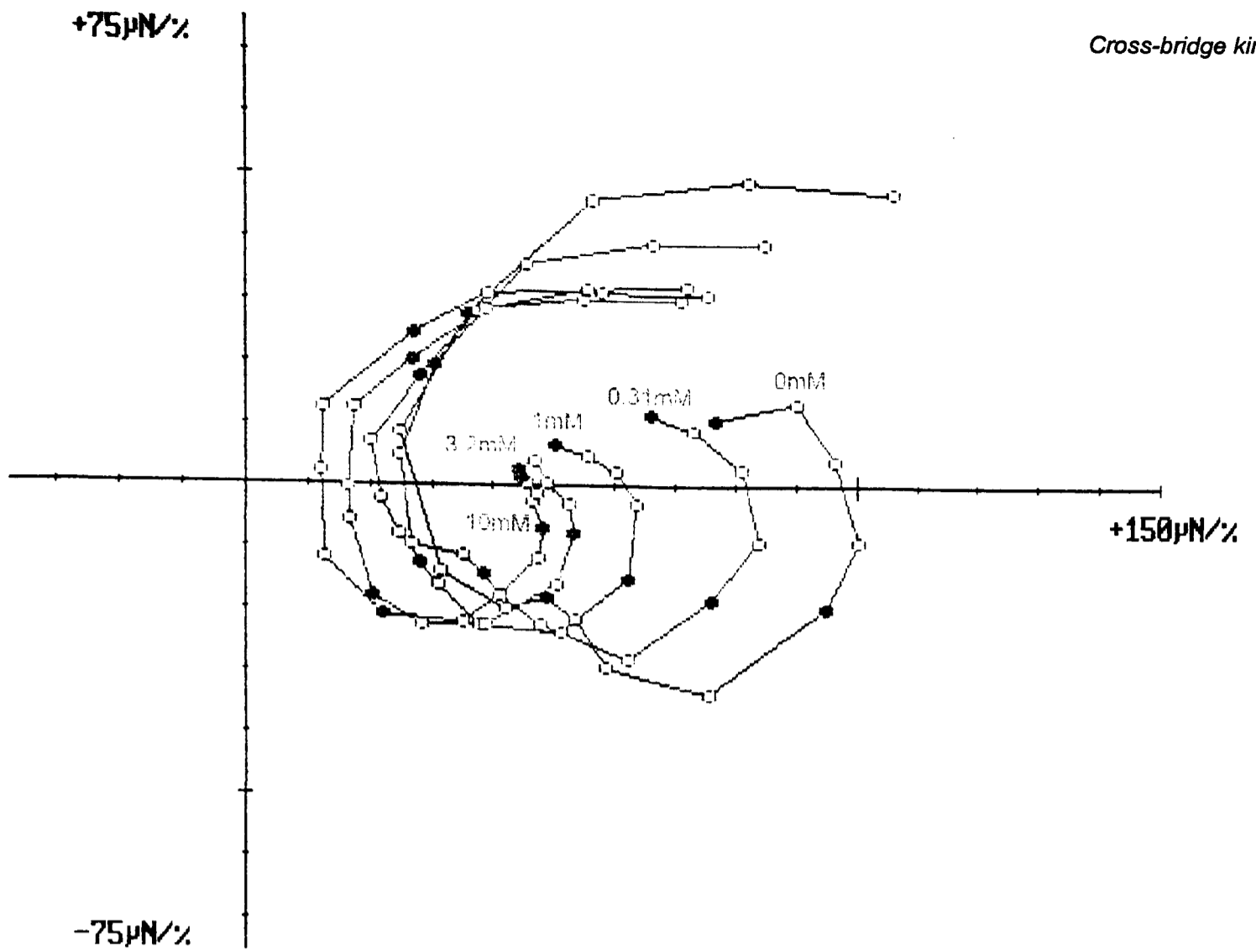


Figure 6.10: Small signal analysis of activated *Tipula* flight muscle at a range of concentrations of P_i . The change in the mechanical characteristics with increasing P_i is complementary to the results of the step length change experiments, though the effect is smaller. With increasing phosphate the amplitude of all processes are reduced. The largest negative phase angle (corresponding to phase 3 in step experiments) occurs at increasing frequencies at the higher concentrations of P_i (3.1mM and 10mM).

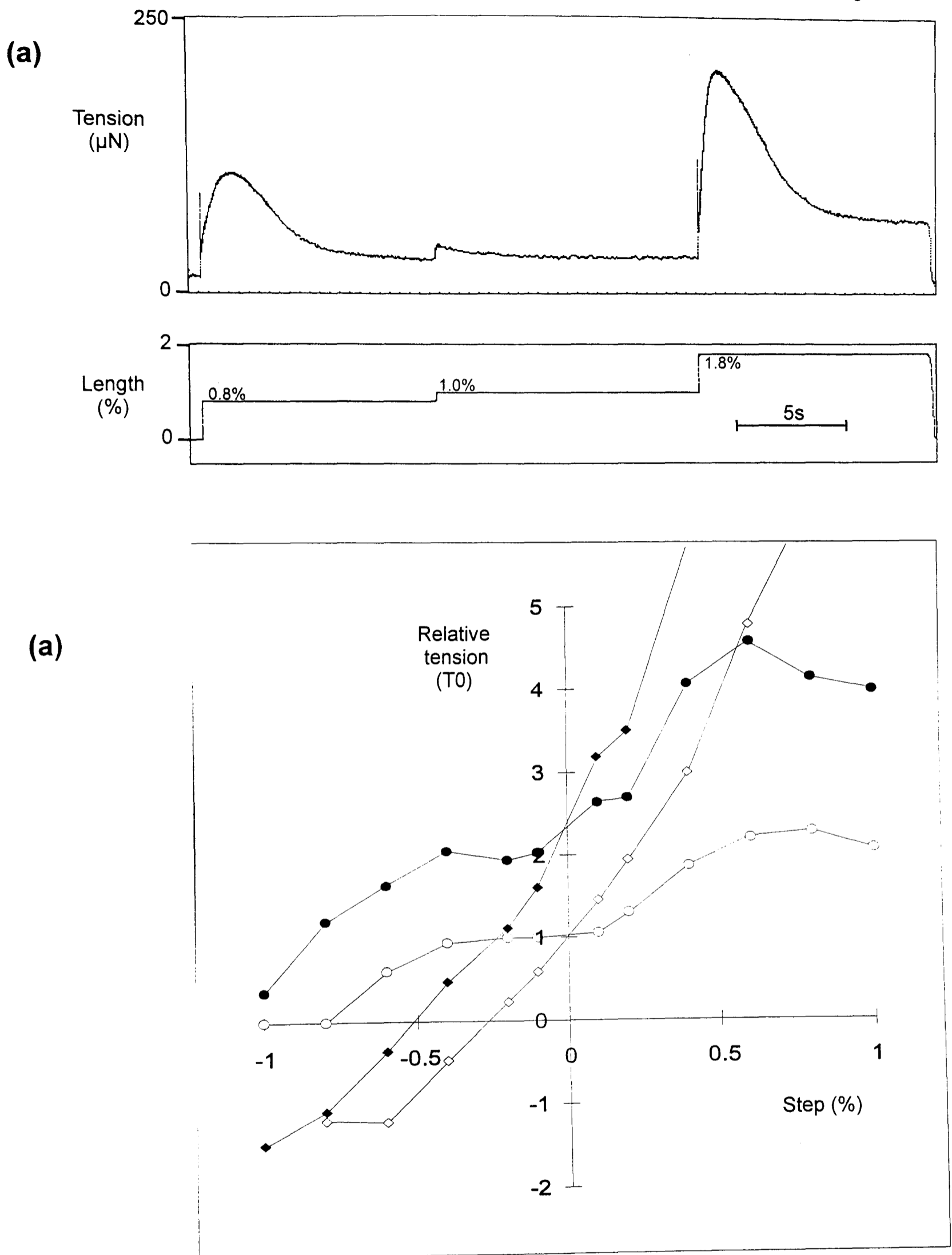
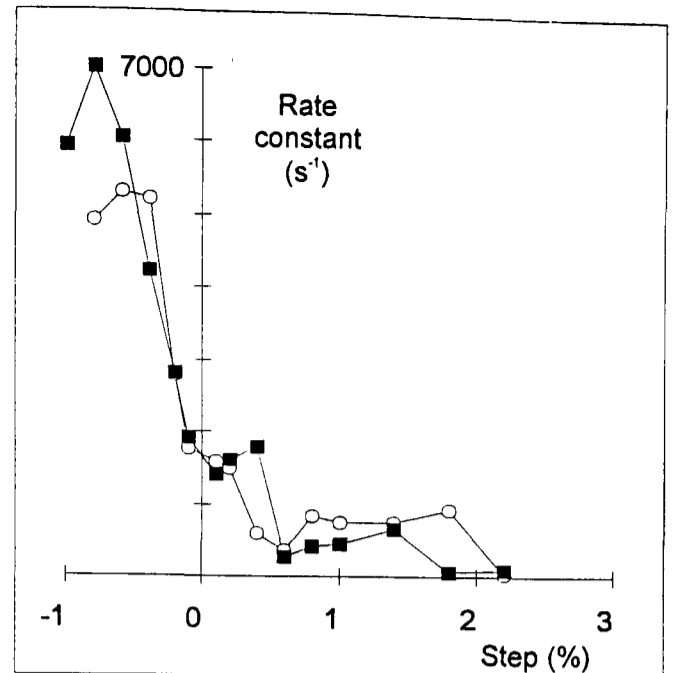
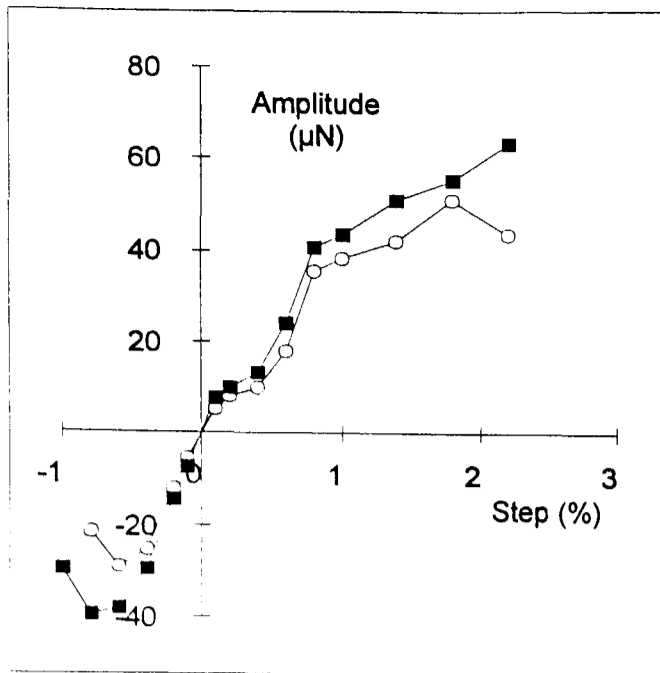
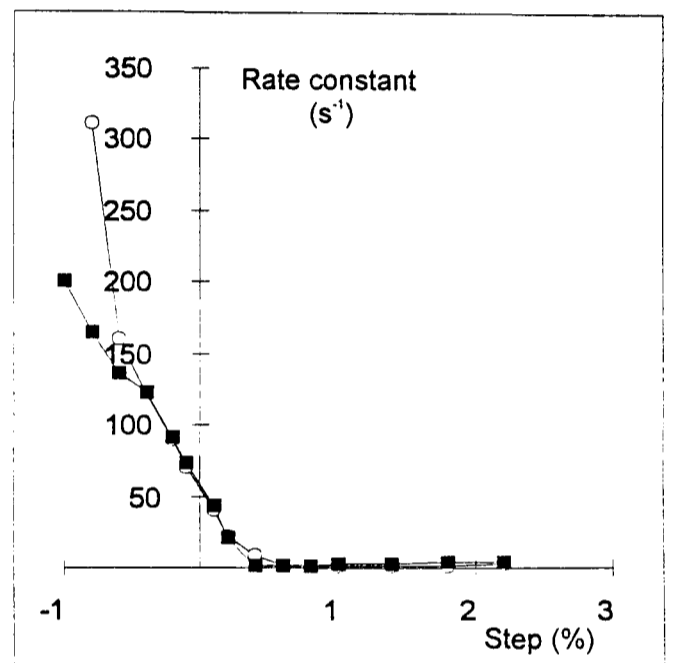
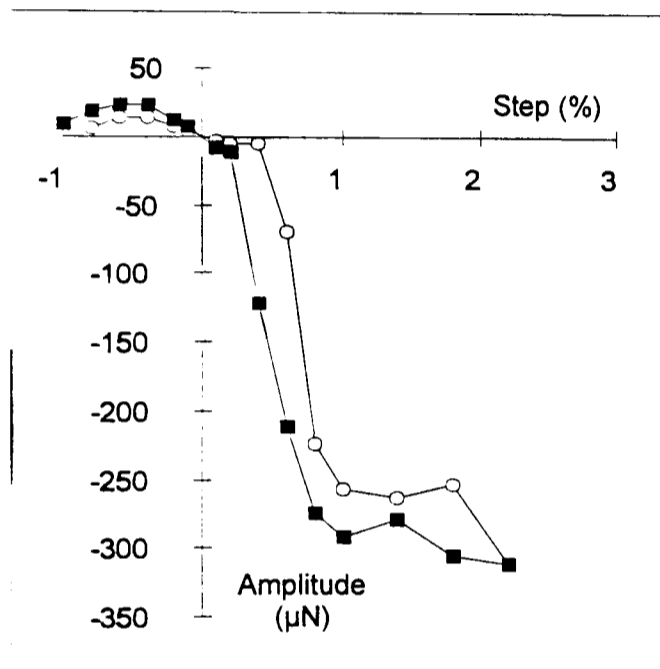


Figure 6.11: The T_1 - T_2 curves recorded at 0% and at 1% pre-stretch. **(a)** For each step size, the step was applied at rest length (0%), then the fibre pre-stretch was adjusted to 1% above rest length. Once at steady state (12s later) the same step size was repeated. **(b)** The T_1 - T_2 curves are plotted relative to T_0 at 0% pre-stretch. The curves with filled symbols are those recorded at 1% pre-stretch. The T_1 curves (diamonds) show that there is very little increase in stiffness after the 1% pre-stretch.

Phase 2



Phase 3



Phase 4

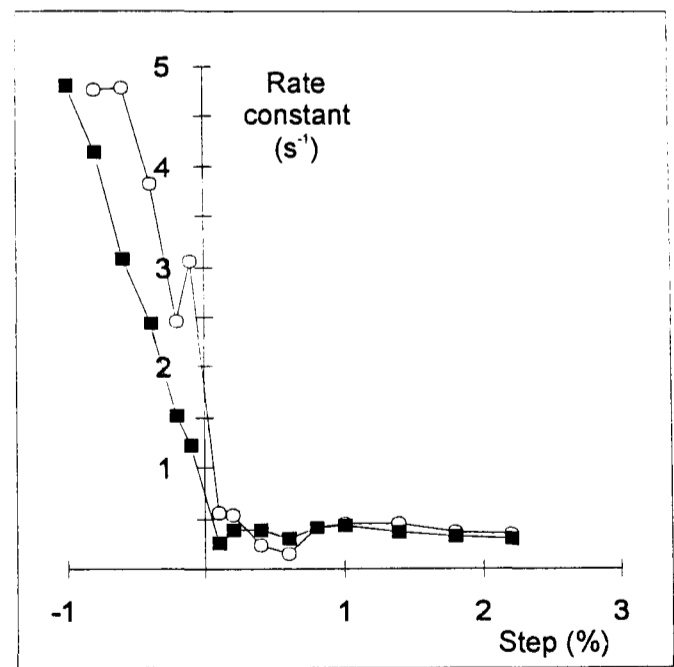
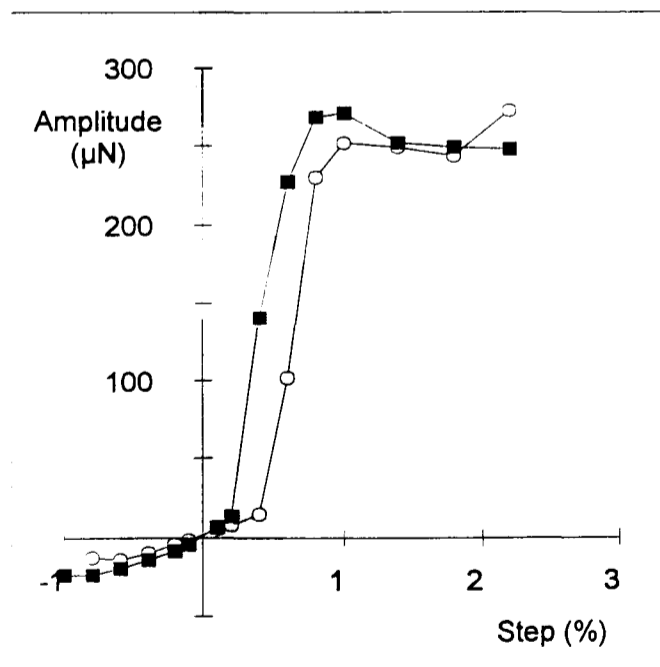


Figure 6.12: The amplitudes and rate constants for phases 2, 3 and 4 for a single activated *Lethocerus indicus* flight muscle at 0% (circles) and at 1% pre-stretch (filled squares).

6.4 Discussion

6.4.1 The active component T_1 - T_2

In many ways the T_1 - T_2 curves shown in Figure 6.1d resembles that of in vertebrate skeletal muscle as described by Huxley and Simmons (1971). Their mathematical modelling of the rapid recovery (phase 2) provides a framework in which it is possible adjust the parameters that define the shape of the T_2 curve.

To estimate the value of α in their equations, a term required by the modelling process, the rate constants fitted to phase 2 at all step sizes were plotted against step size (Figure 6.13). The Huxley-Simmons model shows that the curve should have an equation of the type:

$$r = \frac{r_0}{2} (1 + e^{-\alpha y}).$$

The value used for r_0 was 2750s^{-1} , this being an estimate of the region where the r_2 curve crosses zero step size (see Figure 6.13). The curves for two values of α are plotted over the data. The curve of the original Huxley-Simmons value for α of 0.5nm^{-1} does not describe the data well. The rate constants are too high on the releases. The other curve ($\alpha=0.2\text{nm}^{-1}$) is a much better fit to the data. However rate constants measured for larger displacements do not fit the shape of curve very well. They were ignored when estimating the goodness of fit for a particular value of α .

Using the Huxley-Simmons model it is possible to generate theoretical T_1 - T_2 curves for given values of working stroke h , cross-bridge stiffness K , and α . Using their equation (16),

$$T_2 = K \left(y_0 + y - \frac{h}{2} \tanh \frac{\alpha \cdot y}{2} \right),$$

The value of y_0 is the release size at which the T_1 curve reaches zero tension. For the insect muscle studied here, y_0 is 8nm . That is the same value as that used by Huxley and Simmons.

Using the same values for the constants α and K used by Huxley and Simmons, but changing the value of the working stroke h , it is possible to generate a T_2 curve with the negative gradient characteristic shown by the insect data. The result of changing the working stroke from 8nm to 11nm is shown in Figure 6.14 along with the original Huxley and Simmons T_2 and T_1 curves.

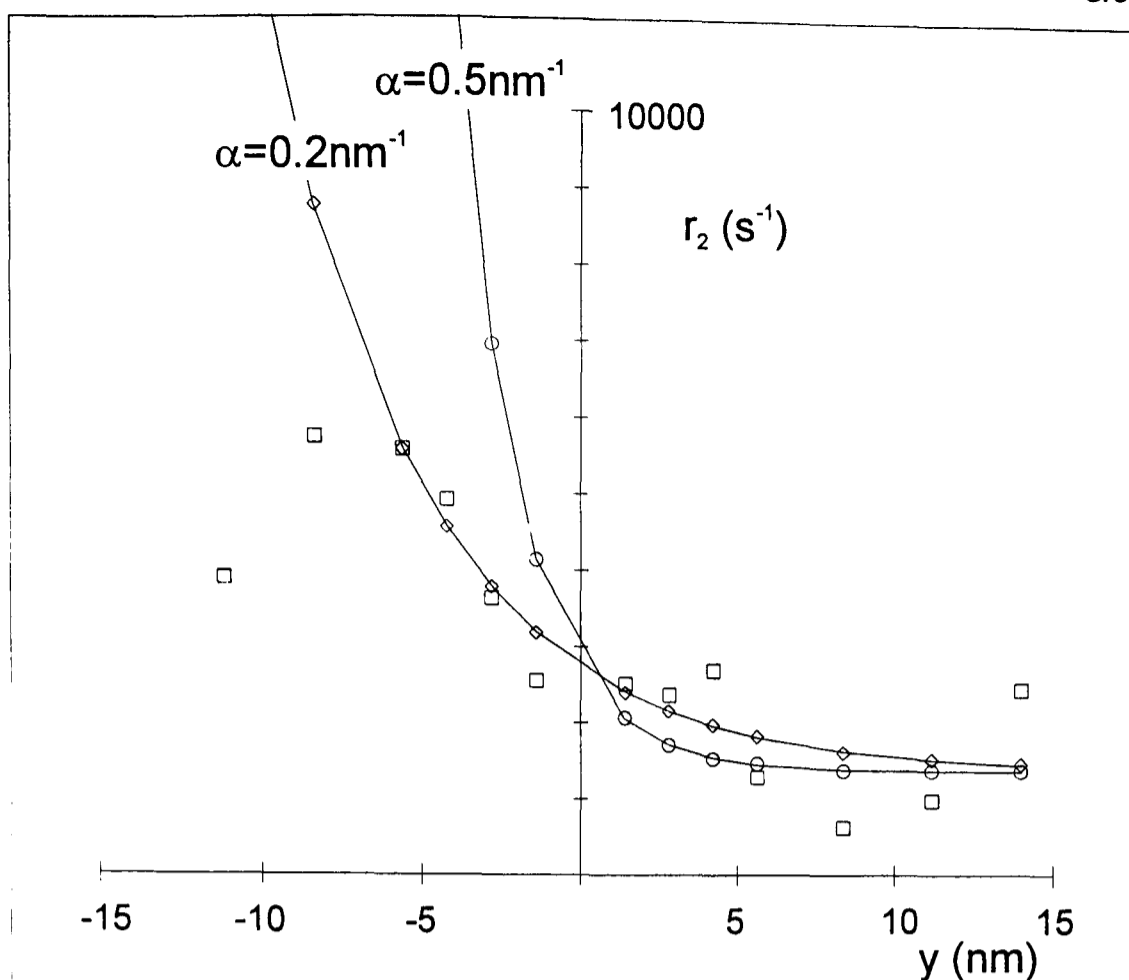


Figure 6.13: Calculation of α based on the relationship between step size and the rate constant of the rapid recovery phase. The rate constant (black squares) was estimated using a nonlinear least squares fitting procedure. The value of α which best fits the equation $r=(r_0/2)(1+e^{-\alpha y})$ to the data is considerably lower than that of Huxley and Simmons (1971). Curves of $\alpha=0.5\text{nm}^{-1}$ (circles) and $\alpha=0.2\text{nm}^{-1}$ (diamonds) are shown ($r_0=2750\text{s}^{-1}$ for both curves).

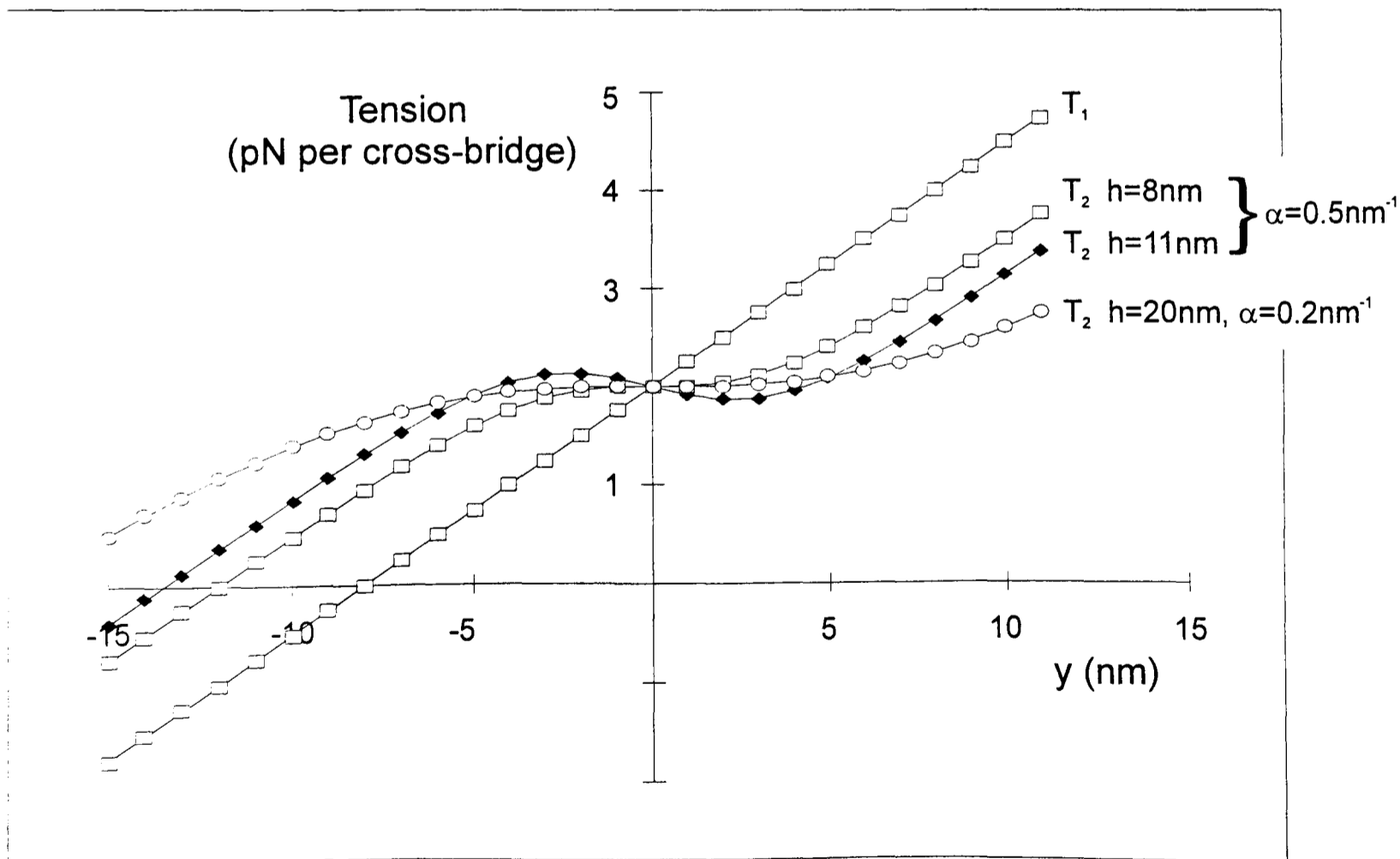


Figure 6.14: T_1 - T_2 plots showing the output of the Huxley and Simmons (1971) model of the rapid recovery phase. The T_2 plots show the output of the model given different values of the working stroke (h) and for α .

The relationship between the rapid tension recovery rate constant and the imposed step size led to the estimation α of to be 0.2nm^{-1} for insect fibrillar flight muscle. This is less than half the value that was estimated by Huxley and Simmons to describe the vertebrate skeletal muscle r curve. With the value of the working stroke set a 8nm , using the new value for α to generate a T_2 curve results in a curve which crosses the vertical axis with a positive gradient. In order to generate a T_2 curve with a negative gradient at small step sizes, it is necessary to use a value for the working stroke greater than 20nm . The T_2 curve generated for $h=20$ and $\alpha=.2\text{nm}^{-1}$ is shown in Figure 6.3.

If the estimation of α is accurate, then this modelling suggests that the cross-bridge working stroke must be over 20nm to account for the existence of the negative gradient region of the T_2 curve. One consequence of such a large value for the working stroke is that the position of the point where T_2 reaches zero tension is shifted along the axis. The experimentally determined T_2 curve reaches zero tension at a release size close to 14nm . This characteristic of the T_2 is more similar in appearance to the curve generated by $\alpha=.5\text{nm}^{-1}$ and $h=11$ than it is to curves described by $\alpha=0.2\text{nm}^{-1}$ and $h>20\text{nm}$. In the light of this, it is reasonable to assume that the estimate of α is too low.

To explain the shape of the insect fibrillar muscle T_1 - T_2 plot in terms of the Huxley-Simmons 1971 mathematical model it is necessary to conclude that the working stroke in insect muscle is longer than it is in vertebrate muscle. To reproduce the negative gradient of the T_2 curve at the vertical axis, the cross-bridge working stroke must be at least 11nm , assuming $\alpha=0.5\text{nm}^{-1}$, and must be set to closer to 20nm when the value used for α is 0.2nm^{-1} .

This issue will be addressed more fully in Chapter 7, where the stochastic cross-bridge modelling provides a more complete explanation of how the shape of the T_2 curve changes with work-stroke size. In particular, this model removes the need for the assumption, of the Huxley-Simmons equations, that at t_0 the two states are equally populated.

6.4.2 Phosphate and the step size dependence of r_3 and r_4

The relationships of r_3 and r_4 with step size have the same characteristics in both synchronous and asynchronous insect flight muscle. Both of the rate constants r_3 and r_4 maintain roughly constant values at stretches greater than 0.3% . However for the smaller stretches there is an increase, and for releases the increase in rate constant can be an order of magnitude or more.

The cross-bridge model described in chapter 7 is able to reproduce these characteristic r -step size plots for phases 3 and 4. The general mechanism of

how this takes place is the following. Following the step length change there is a redistribution of cross-bridges amongst the two states on either side of the work stroke transition. Following this redistribution there is a surplus of cross-bridges in one state and a “lack “ of cross-bridges in the other state. Due to the definition of the free energy profiles of these two states (and in the vast majority of similar models) the “surplus” cross-bridges must detach via a route that is not the work stroke step. This is because the work-stroke transition is particularly energetically unfavourable for these cross-bridges.

For this reason the routes for the redistributing cross-bridges after the rapid tension recovery phase is different depending on whether a stretch or a release was applied. Due to the different routes of cross-bridge redistribution, depending on whether the length change was a stretch or a release, it is not surprising that the rate constants for these processes are different.

That P_i increases r_3 and r_4 on stretch and reduces them on releases may be explained if the P_i release step is located between the steps that set the rate constants for phases 3 and 4. However I have not yet done model simulations with varying P_i concentration.

6.4.3 Phosphate and the step size dependence of r_2

Figure 6.4 shows that if the concentration of P_i has an effect on the relationship of phase 2 with step size, then this effect is very small.

It is widely believed that in vertebrate striated muscle, the power stroke step is the P_i release step from the AM.ADP. P_i state (Hibberd *et al*, 1985; Dantzig *et al*, 1992). If this is the case in insect fibrillar muscle, the rate constant for phase 2 should be sensitive to the concentration of P_i , especially for step stretches. If P_i release corresponds to the cross-bridge work stroke, the stretch r_2 would be most sensitive to P_i concentration because it is in the stretches where the cross-bridges would be moving from the AM.ADP state to the AM.ADP. P_i state. If P_i release is concomitant with force generation, the rate of r_2 on stretch should become much more rapid with increasing P_i concentration. If anything the reverse of this trend seems to occur, stretch r_2 values being lowest in the higher P_i .

From this it can be concluded that in insect fibrillar flight muscle the P_i release step occurs at a different time from the work stroke step. This conclusion has also been drawn from oxygen exchange studies on insect fibrillar flight muscle by Lund *et al* (1987), who suggest that P_i release occurs in a step following the work stroke step.

6.4.4 The effect of P_i on the fibre stiffness

The fibre stiffness reduces with increasing P_i . This is indicated by the reduction in the slope of the T_1 curve in Figure 6.5, and also the reduction in the complex stiffness in the sinusoidal analysis shown in Figure 6.10. The decrease in fibre stiffness indicates that the number of attached cross-bridges is lower in the higher P_i solutions. This reduction in the number of attached cross-bridges suggests that the P_i release step occurs before or in the same step as force generation. If P_i release followed force generation as suggested by Lund *et al* (1987), an increase in P_i concentration would encourage the cross-bridges back into the force producing states, resulting in an increase in fibre stiffness with increasing P_i .

6.4.5 Fibrillar muscle kinetics at 0% and 1% strain

This is a comparison between the tension transients of active *Lethocerus indicus* flight muscle at rest length and at 1% pre-stretch. The T_1 - T_2 curves are shown in Figure 6.11. The most striking observation to be made in this plot is that at 1% pre-stretch, even though the fibre is producing twice the tension, the immediate stiffness is not much higher. If this is the case, and assuming that all attached states are of equal stiffness, this implies that the same number of cross-bridges are attached at the steady state following the pre-stretch as were attached at the rest length steady state.

The results of fitting three exponential functions to the steps before and after the applied pre-stretch are plotted in Figure 6.12. The first thing to note is that none of the graphs contain 1% displacements. Such a result would indicate that the filaments had a rigid mechanism for detecting inter-filament displacement, such as the match-mismatch model. On stretches the rate constants show no apparent relationship with pre-stretch. There is some separation of the r_3 and r_4 plots on the step releases, though this may be due to the fibre tension dropping close to zero in the rest length steps.

The most significant horizontal offset can be seen in the amplitudes of phases 3 and 4 in the stretch range 0.2% to 0.8%, though this offset is 0.3% at most. This observation is more compatible with models of stretch activation in which a flexible link is extended (such as C-filaments or Tn-H) rather than the rigid filament geometry favoured by Wray.

7. A stochastic model of cross-bridge cycling and stretch activation

7.1 Introduction

This chapter is concerned with computer simulation of cycling cross-bridges. It describes a multiple state model devised to simulate the mechanical and biochemical properties of striated muscle.

The relative displacement of a cross-bridge and its potential binding site on the thin filament is referred to as distortion. In this model some of the reaction rate constants are distortion dependent, both to emulate certain mechanical and biochemical properties of muscle and also to obey the laws of thermodynamics.

The same software includes three model types. In the first, a vertebrate skeletal muscle model, the distribution of distortions is uniform. The second and third models investigate two ways to generate a stretch activated response. The match-mismatch model suggested by Wray (1979) is simulated by setting the distortion of most cross-bridges within a small range of the distortions available. Finally strain activation is investigated in a model in which the stability of all attached states is dependent on strain on the muscle.

Simulating cross-bridge dynamics in this way provides much more insight into possible molecular mechanisms than can a series of equations on paper. Using this model it is simple to observe the effect of a change in a single rate constant on the dynamics of the whole system.

7.1.1 Cross-bridge models

Since Huxley published his model in 1957, virtually all cross-bridge models have incorporated many of the same ground rules. One particular aspect of the 1957 two state model that has been included in the majority of proposed cross-bridge models is the concept of distortion dependency of the rate constants. The rate constants of the Huxley 1957 model are shown in Figure 1.1. The most fundamental property of the distortion dependencies used in this and all subsequent multi-state models is that cross-bridges must be encouraged to remain attached at positive force, and should detach quickly at negative forces.

After Huxley and Simmons (1971) suggested that attached cross-bridges existed in at least two mechanically distinct states, several multiple state models have been published. The two models on which the model presented here is based are that of Eisenberg, Hill and Chen (1980) and Pate and Cooke (1989). Particularly the free energy values of the states in this model were taken from these papers. However, unlike these models, the model presented here was

developed to study what is required for a multi-state model to recreate not only phase 2 but also phases 3 and 4 of the muscle tension transients.

In 1974 Terrell L. Hill published a set of "rules" that must be followed if a muscle model is to be thermodynamically possible. This formalism was used to define the free energy profiles of the attached states in the model as well as the relationship between the forward and backward rate constants in all steps.

7.2 A novel algorithm for stochastic modelling

The method by which the step direction is chosen is a very important consideration in a model such as this. **Figure 7.1a** shows the conventional approach to this problem. Given the three rate constants moving out of a particular state, it is possible to calculate the probability in time t that this step will occur. These probabilities are assigned their own region in the space 0 to 1. If a computed random number falls in that region, then that step is chosen. It can be seen that if a large value is chosen for t (5ms in the example shown) then a step could be taken in the majority of iterations, making the model run quickly. Unfortunately the problem with large values of t is that it becomes more likely that two (or more) steps could occur within that time.

Because assigning probabilities to two or more steps starts to become very complex, it is usually not done. Instead the value of t is chosen so that the probability of two steps is low in the most rapid parts of the scheme. Even so this method cannot rule out this possibility. With a small t (1ms in the example), the majority of iterations predict no state change. This is computationally expensive because a large number of random numbers must be generated before a single state change is performed. This means that to simulate one second of data with a few hundred cross-bridges in the model is a very slow process.

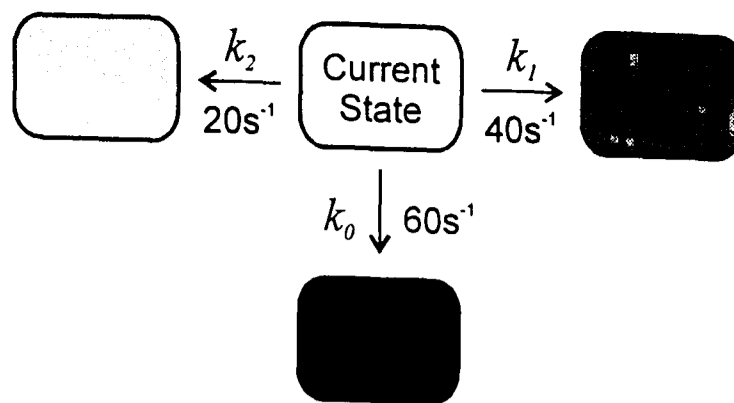
In my model I used a different approach. Rather than have a fixed iteration time, I used the random number generator to predict a "next step time" for each of the three possible directions. Now the random number generator provides a simulation of **when** the event occurs rather than whether it has occurred at a specified time.

Considering each step independently, the exponential curves for step i (1, 2 & 3) out of the current state have the following equation:

$$S_i = \exp(-k_i t),$$

where k_i is the rate constant and S_i is the state population (tending from 1 to 0).

Model:



Model

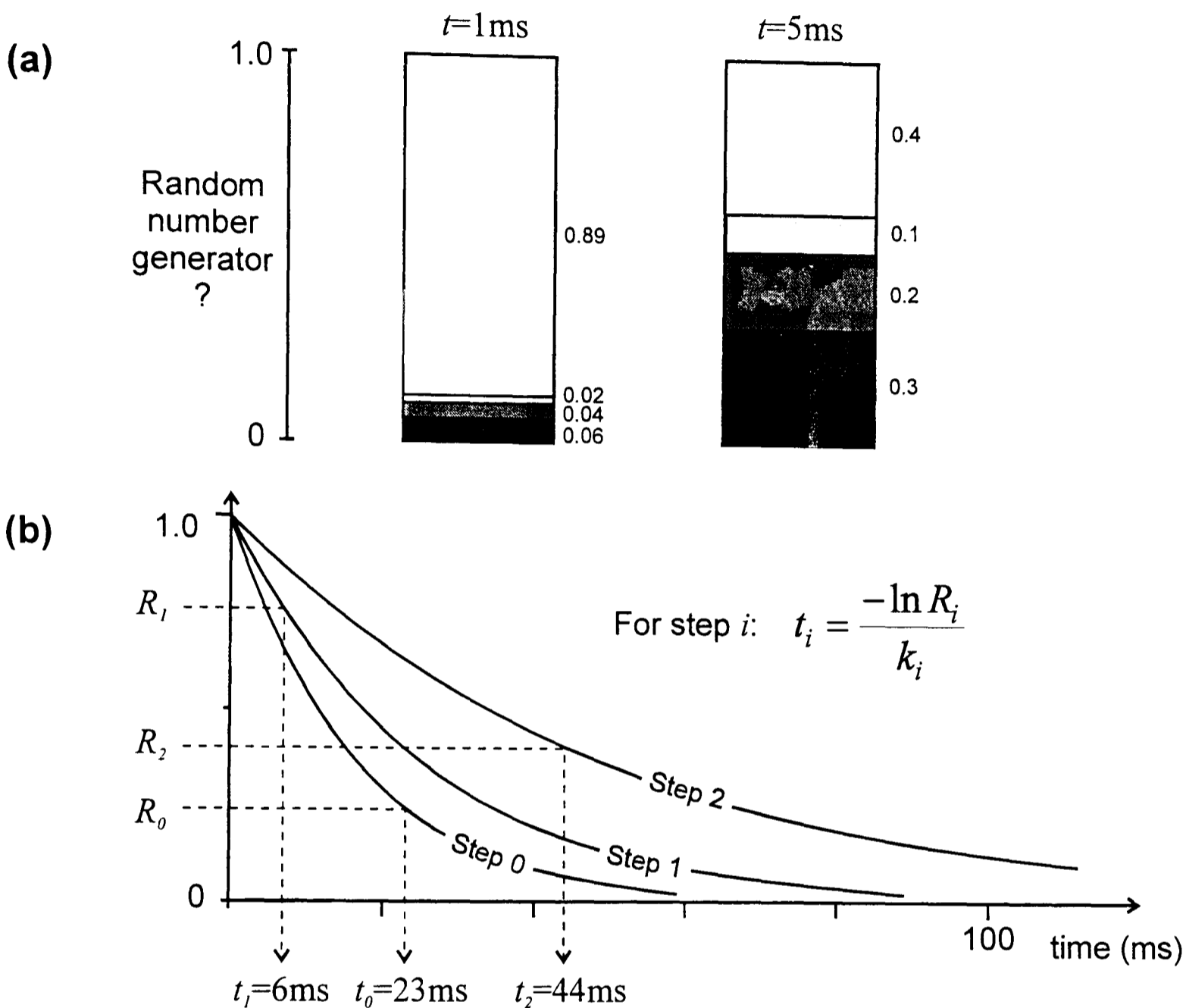


Figure 7.1: Two approaches for modelling a single step in a complex chemical pathway. In the example shown the model must choose one of three possible steps. (a) In the first method, a small time interval (t) is chosen. The probability that each step occurs within time t is calculated. Each step is allocated its own a region of the range 0 to 1. A random number is generated ($0 < R \leq 1$, uniform distribution). If the value of R falls within the range allocated to a step, then that step is chosen. The value chosen for t must be sufficiently small that the probability of performing two steps within that time is low. Although this is the conventional method it is slow and sometimes inaccurate. (b) The second approach uses the random number generator to provide a time value for each possible step. In this example the three random numbers $R_0=0.2516$, $R_1=0.7866$ and $R_2=0.4148$ provide the step times using the equation shown. The step chosen by the model is that with the smallest time value (in this instance step 1).

Therefore a random number between 0 and 1 (R_i) can be used to estimate a step time t_i simply by rearranging the equation:

$$t_i = \frac{-\ln R_i}{k_i}.$$

The method is described in Figure 7.1. A new random number is generated for each of the three time values. The fastest time value is the step chosen. Using this system each cross-bridge must have its own time variable to store the time of the last state change.

In terms of processor time this method is very efficient. One third of all random numbers generated result in a cross-bridge step.

7.2.1 Storing time information for each element in the model

This model algorithm makes the iteration time very flexible. That is the algorithm can be called to run for any finite length of time, independent of the values of the rate constants in the system. So for example the program can plot tension every microsecond or every ten seconds.

There is one pitfall that must be avoided, particularly when short iteration times are chosen (that is iteration times where only a small number or no state changes occur). When a calculated step time over-shoots the iteration end time, the algorithm must exit in the state it was in at that end time. That is it must not perform the last step since this occurs after the specified end time.

So what should be done with the step that was calculated, but not performed before the algorithm was exited? It is very important that this step is not discarded and recalculated in the next call. Doing this would “select against” quite valid slow steps in the sequence if they overshoot an end-time boundary. This step calculation **must** be stored and used in the next call. When the algorithm is exited the current and the next state must both be stored for each element in the model. In this way a the transition time for a slow step may span many iterations. After each iteration, the time value for each element must store the calculated time point for the transition from the current state to the next state.

In this way the algorithm is not biased towards faster step rates. Also, but of less importance, saving calculated steps in this way increases the efficiency of the model.

7.2.2 Verification of the model mechanism

Since I was not able to find previous models that used such a mechanism, it was necessary to show that the procedure used is a valid one. To show that the model follows the same curve as the analytical solution in a simple system would be a good indication that the method is valid.

Although a simple two-state system would give a good indication of the validity of the model, this would by-pass one crucial part of the model mechanism. That is the occasions where the model must chose between different possible step directions. Clearly the simplest model which incorporates this is a linear three state model. The model used is shown in Figure 7.4(a). The rate constants for the steps in the system are shown as a , b , c , and d . The number of elements in states 1, 2 and 3 are n_1 , n_2 and n_3 respectively. The total number of elements in the system is N , where $N = n_1 + n_2 + n_3$.

The differential equations for this system are:

$$\frac{dn_1}{dt} = n_2a - n_1b$$

$$\frac{dn_2}{dt} = n_1b + n_3c - n_2a - n_2d$$

$$\frac{dn_3}{dt} = n_2d - n_3c.$$

Since all elements in the system sum to N , it is possible to find the solution by solving the two equations dn_1/dt and dn_3/dt .

Since $n_2 = N - n_1 - n_3$,

$$\frac{dn_1}{dt} = (N - n_1 - n_3)a - n_1b$$

and

$$\frac{dn_3}{dt} = (N - n_1 - n_3)d - n_3c.$$

Expanding,

$$\frac{dn_1}{dt} = -(a + b)n_1 - an_3 + aN$$

and

$$\frac{dn_3}{dt} = -dn_1 - (d + c)n_3 + dN.$$

These expressions can be written in matrix form as follows:

$$\begin{bmatrix} dn_1/dt \\ dn_3/dt \end{bmatrix} = \begin{bmatrix} -(a+b) & -a \\ -d & -(d+c) \end{bmatrix} \begin{bmatrix} n_1 \\ n_3 \end{bmatrix} + \begin{bmatrix} aN \\ dN \end{bmatrix}.$$

The general solution to a matrix expression such as this is written as (Chiang, 1984):

$$\begin{bmatrix} n_1(t) \\ n_3(t) \end{bmatrix} = - \begin{bmatrix} -(a+b) & -a \\ -d & -(d+c) \end{bmatrix}^{-1} \begin{bmatrix} aN \\ dN \end{bmatrix} + A_1 \begin{bmatrix} v_{11} \\ v_{21} \end{bmatrix} e^{\lambda_1 t} + A_2 \begin{bmatrix} v_{12} \\ v_{22} \end{bmatrix} e^{\lambda_2 t}.$$

This expression shows that the solutions to this system is for states 1 and 3 are made up of two exponential processes with an offset value. The offset value, often called the long run solution (LRS) is given by the solution of the first two matrices in the expression. This provides the function value at $t = \infty$. The rate constants for the two exponential processes are given by the eigenvalues ($-\lambda$). The amplitudes of each exponential are given by an amplitude term (A) and the eigenvectors $\begin{bmatrix} v \\ v \end{bmatrix}$.

Solving the LRS matrices gives the following:

$$\begin{bmatrix} n_1(t) \\ n_3(t) \end{bmatrix} = \frac{N}{ad + bd + bc} \begin{bmatrix} ac \\ bd \end{bmatrix} + A_1 \begin{bmatrix} v_{11} \\ v_{21} \end{bmatrix} e^{\lambda_1 t} + A_2 \begin{bmatrix} v_{12} \\ v_{22} \end{bmatrix} e^{\lambda_2 t}.$$

The eigenvalues, which provide the rate constants in the solution, are obtained by finding the values of λ which satisfy the following:

$$\begin{bmatrix} -(a+b) - \lambda & -a \\ -d & -(d+c) - \lambda \end{bmatrix} = 0.$$

This provides the two values,

$$\lambda = \frac{-(a+b+c+d) \pm \sqrt{(a+b+c+d)^2 - 4(ac+bd+bc)}}{2}. \quad (7.1)$$

To find the eigenvectors, it is necessary to reduce the number of terms. This is done by simplifying the eigenvectors. The eigenvectors $\begin{bmatrix} v_{11} \\ v_{21} \end{bmatrix}$ and $\begin{bmatrix} v_{12} \\ v_{22} \end{bmatrix}$ can

be replaced with $\begin{bmatrix} 1 \\ \theta_1 \end{bmatrix}$ and $\begin{bmatrix} 1 \\ \theta_2 \end{bmatrix}$, where $\theta_1 = v_{11}/v_{21}$ and $\theta_2 = v_{12}/v_{22}$.

The eigenvectors can now be found using the relationship

$$\begin{bmatrix} -(a+b) & -a \\ -d & -(c+d) \end{bmatrix} \begin{bmatrix} 1 \\ \theta \end{bmatrix} = \lambda \begin{bmatrix} 1 \\ \theta \end{bmatrix}.$$

This yields two equations, either of which can be used to find the two values for θ , these are:

$$\theta = \frac{-d}{\lambda + c + d} \quad \text{and} \quad \theta = \frac{\lambda + a + b}{-a}. \quad (7.2)$$

The equations for the curves n_1 and n_3 can be written:

$$\begin{aligned} n_1(t) &= LRS_1 + A_1 e^{\lambda_1 t} + A_2 e^{\lambda_2 t} \\ \text{and} \quad n_3(t) &= LRS_3 + A_1 \theta_1 e^{\lambda_1 t} + A_2 \theta_2 e^{\lambda_2 t}. \end{aligned} \quad (7.3)$$

Given the values for the eigenvectors, it is possible to obtain the values for the amplitude constants A_1 and A_2 from what we know about the initial conditions of the system.

$$\begin{aligned} \text{When } t = 0, \quad n_1(0) &= LRS_1 + A_1 + A_2 \\ \text{and} \quad n_3(0) &= LRS_3 + A_1 \theta_1 + A_2 \theta_2. \end{aligned}$$

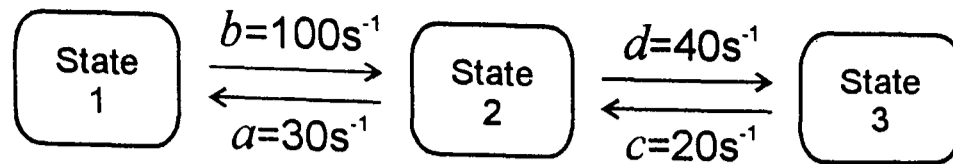
This provides equations for the amplitude components as follows:

$$\begin{aligned} A_2 &= \frac{n_3(0) - LRS_3 - (n_1(0) - LRS_1)\theta_1}{(\theta_2 - \theta_1)} \\ A_1 &= n_1(0) - LRS_1 - A_2 \end{aligned} \quad (7.4)$$

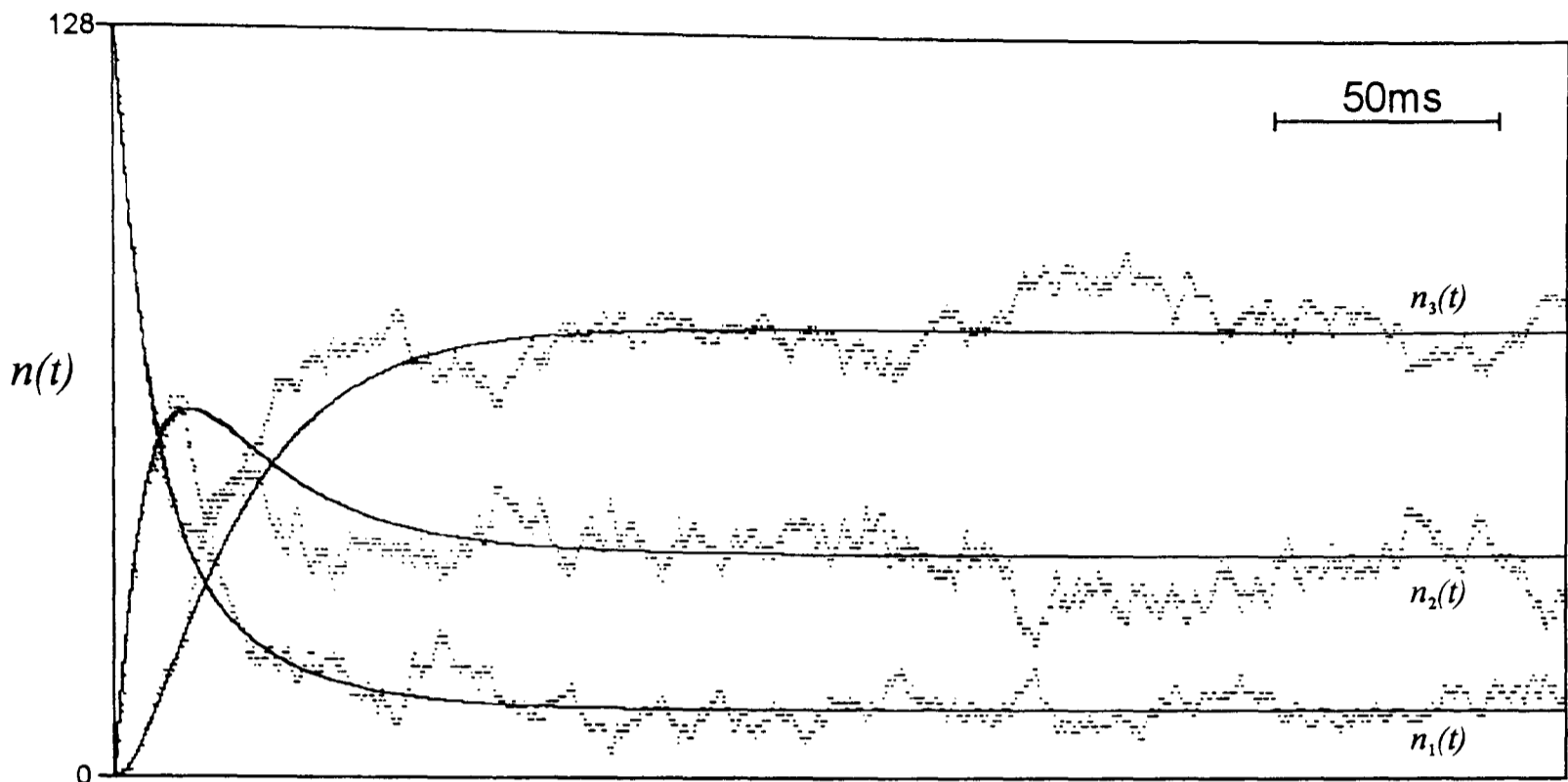
Using the solution described above it is possible to plot the output of the model over the theoretical curves, shown in Figure 7.2(b) and (c). These curves are plotted using the output of equation 7.3, using the results of equations 7.1, 7.2, and 7.4. When the number of elements in the simulation is high, the output of the stochastic model follows the theoretical curve very closely. This was the case using different values for the rate constants. The results in Figure 7.2 show that the model output follows the line provided by the analytical solution. The error or noise in the model output decreases with increasing number of elements in the model.

(a) Model

Model



(b) 128 elements



(c) 8192 elements

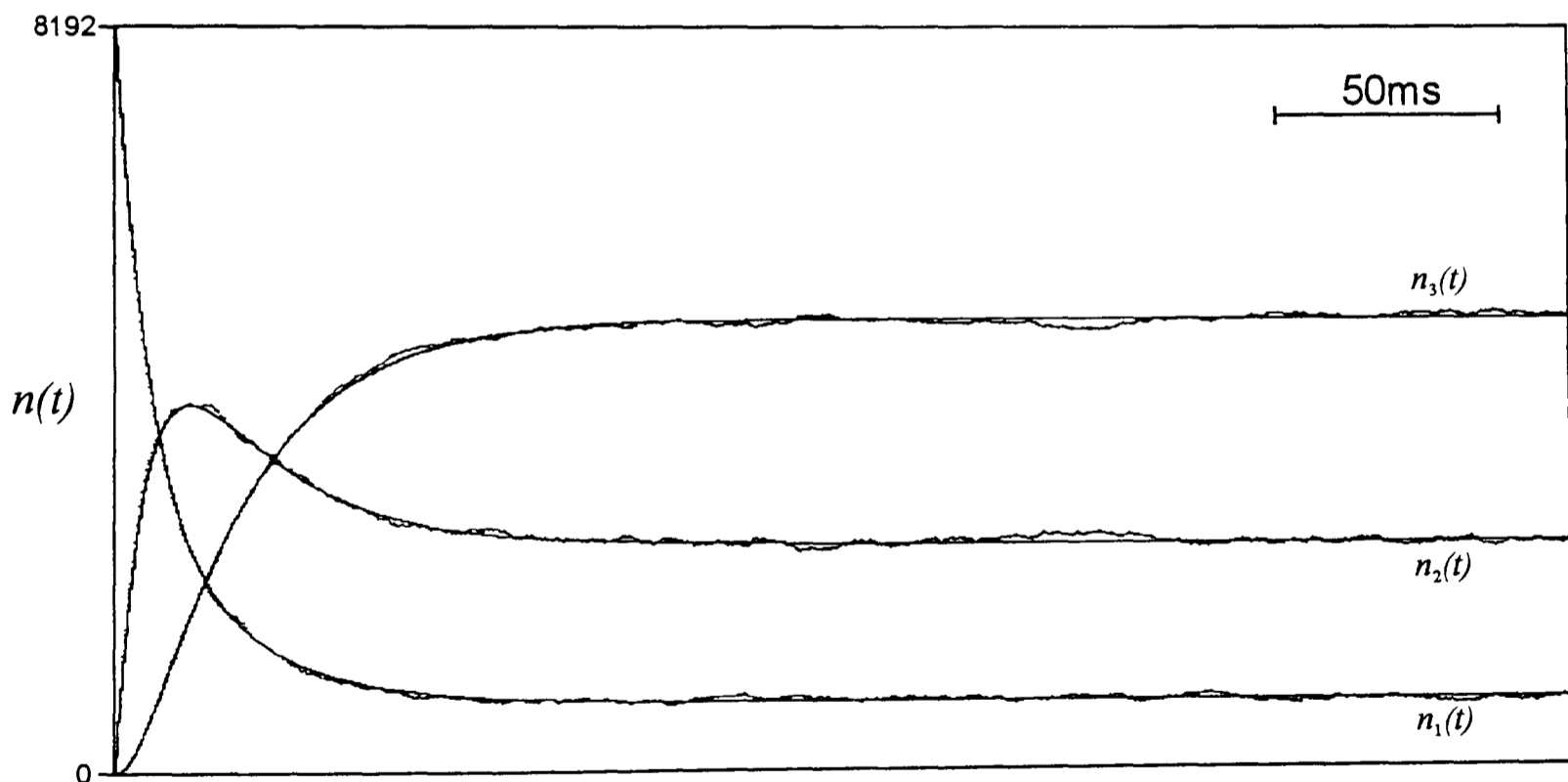


Figure 7.2: The approach to equilibrium of a simple three state system shown as both an analytical solution and a stochastic simulation. The model and the values of the rate constants used are shown in (a). At $t=0$ all elements in the system are in state 1. Two model runs are shown using 128 elements (b) and 8192 elements (c). The analytical solution is indicated by a solid line, the stochastic model output plotted as single points. The stochastic simulation uses the same mechanism as that used in the muscle model. That the simulation superimposes the theoretical curves is a good indication that the model method is a valid one. The simple program used to generate the plots (MOD-METH.BAS) is included on the diskette.

7.3 Software

The biochemical scheme used in the model is shown in Figure 7.3. Although a total of eight states are used, when the model is running some of these states contain very few or no cross-bridges. The scheme was made symmetrical to simplify the programming. By keeping the scheme rectangular in this way, a cross-bridge at any state position has to choose one out of the three possible step directions.

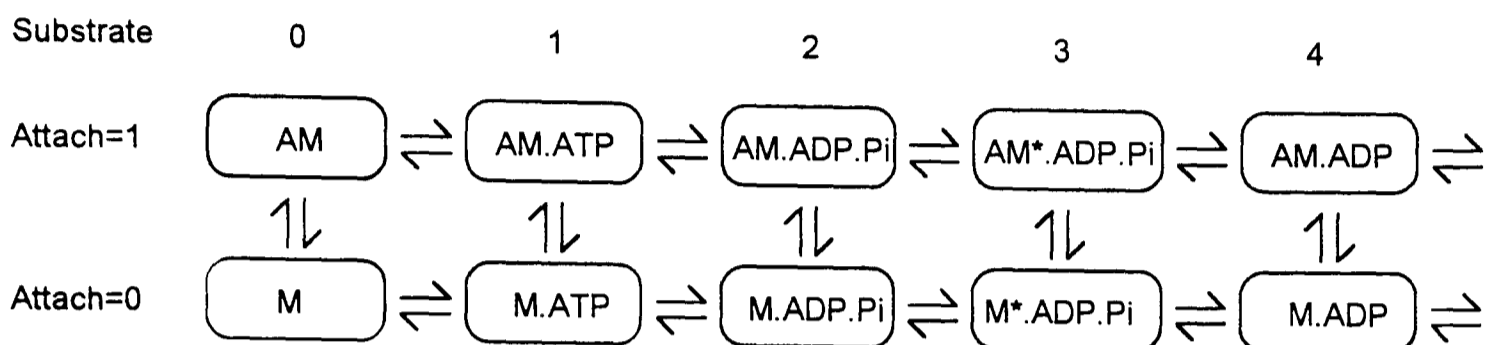


Figure 7.3 The biochemical scheme showing all cross-bridge states used in the model. The software refers to each state using a substrate and an attachment value.

7.3.1 The Stoch subroutine

All the state stepping is performed within the `Stoch` subroutine. This routine is passed four arrays, an example call line is shown below:

```
CALL Stoch (Steps&(0,0),X%(1,0),k!(0,0,0,0),Xtime!(0)).
```

The `X%()` array describes the state of all cross-bridges in the model. For each cross-bridge this array stores information about the biochemical state (0 to 4), the current attachment status (1 for attached, 0 for detached) and the current distortion values. Possible distortions range from -5nm to 20nm. Distortions are calculated in angstroms (Å) providing a total of 251 possible cross-bridge distortions.

The `k!(0,0,0,0)` array holds the rate constant look-up table. For a particular cross-bridge the rate constant is found based on the criteria of biochemical state, current distortion, attachment status and the step direction.

For each cross-bridge, the sequence of events is as follows. Three random numbers are generated, and provide time values for the three possible steps from the current state. The step with the fastest time is taken. This step time is added to the cross-bridge time in the `Xtime!()` array and the cross-bridge state is

updated in the `X%` () array. This process is repeated until the cross-bridge time passes the current iteration end time (stored in `Xtime!` (0)).

On exit the `Steps&` (0 , 0) array returns the total count for each step in the model. This information is useful for showing flux in the model which is not always apparent by looking at the state totals or distortion distributions. The current cross-bridge state and also the next state (already calculated) are held in the `X%` () array. The time for the next step for each cross-bridge is stored in the `Xtime!` () array.

7.3.1.1 Random number generation

Computer algorithms cannot output truly random numbers. Indeed since computers are machines designed to create perfectly repeatable output, it is not a trivial matter to make them generate output which appears random (pseudo-random). Although programming languages supply their own generators, these can often be the cause of problems. They are typically 15 bits wide and often have a short repeat period.

In order to produce "trustworthy" random numbers, I wrote a random number generator within the model machine code. The choice of random number generator algorithm is a crucial consideration when writing a model. Although this model is based on a very efficient algorithm, a large proportion of processor time is still spent in the random number generation routine.

In this model I have incorporated the algorithm suggested by Zaman and Marsaglia (1991). This algorithm allows the very fast generation of random numbers of any size. It uses a combination of two different types of generator to give an extremely long period (10^{356}). The first is a *subtract with borrow generator*, this provides the long period while satisfying conventional randomness tests. The second is the more conventional *congruential generator* with multiplier 69069 and base 2^{32} . The results of these two are XOR'ed to provide the final 32-bit value used in the model. This algorithm has the added bonus of never outputting zero. This avoids the infuriating situation of a "Division by zero" error halting the computer just before the end of a long simulation.

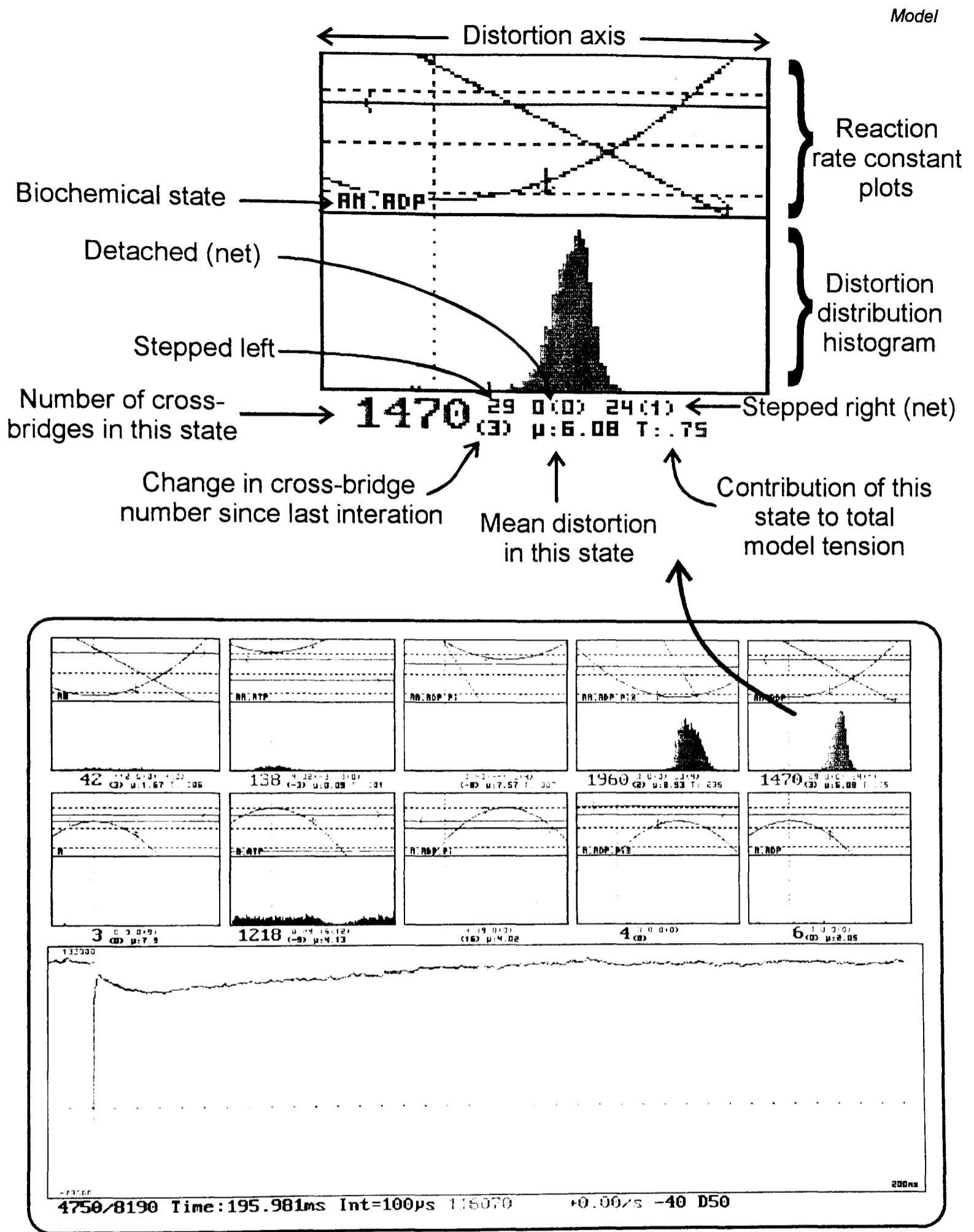


Figure 7.4: The cross-bridge model run screen. The screen was arranged to provide as much information as possible about the state of the model. The top half of the screen gives information about each biochemical state. The detail of one state is expanded (upper). The two plots show the rate constants and the distortion distribution, both plotted against distortion. Below each state plot is statistical information about the most recent model iteration. The lower half of the screen plots the progress of the model with time. Here the model tension is plotted. The number of attached cross-bridges or stiffness, strain and ATPase can also be plotted.

Like all pseudorandom number generators, the algorithm requires a seed to start. This provides a mechanism to prevent the same sequence of numbers each time the program is run. Two 32bit values are passed to the `Rinit` routine from the BASIC calling procedure. In the model program, two zeros are passed to this routine. On receiving two zeros, the PC clock time and date are combined and used as a seed.

The random number generator was tested in two ways. Firstly, using the same seed values, the code produced the same sequence of numbers as a program described by the original authors. Secondly the distribution of the random number output was shown to be uniform by performing a five digit poker test.

7.3.2 The model run screen

The model run screen is shown in Figure 7.4. Small distortion distribution histograms are updated with each iteration. When the program begins, all cross-bridges are in the M.ADP.Pi state so the user must wait until the model has reached a steady state. The following is a brief description of the keys that can be used to control the running model.

The iteration duration can be altered by a factors of ten by pressing the `<->` and `<+>` keys. The program will not allow iteration times that will require more than 20 seconds to complete.

Pressing the `<F>` key allows the user to select full screen plots of cross-bridge distortions, free energy profiles or rate constants. A full screen cross-bridge distribution plot is shown in Figure 7.5. This type of plot is useful for showing the populations and distortion distributions of all states in the model in one plot.

The model current status can be saved at any point by pressing `<S>`. The `<X>` key will restore this saved state. A step length change (nm) can be given at any point by pressing `<P>`. A sequence of steps can be started (e.g. T1-T2 experiment) with `<T>`. The `<V>` key begins a force-velocity sequence.

The `<A>` key turns on and off the ATPase, stiffness and perturbation value plots. The `` key moves to a text based screen so that the model can be run in the background in Microsoft Windows. The model type can be selected using `<M>`.

The length and tension values can be saved at any point by pressing `<O>`. These output files can be loaded into the muscle program, where curve fitting and analysis of tension values can be made.

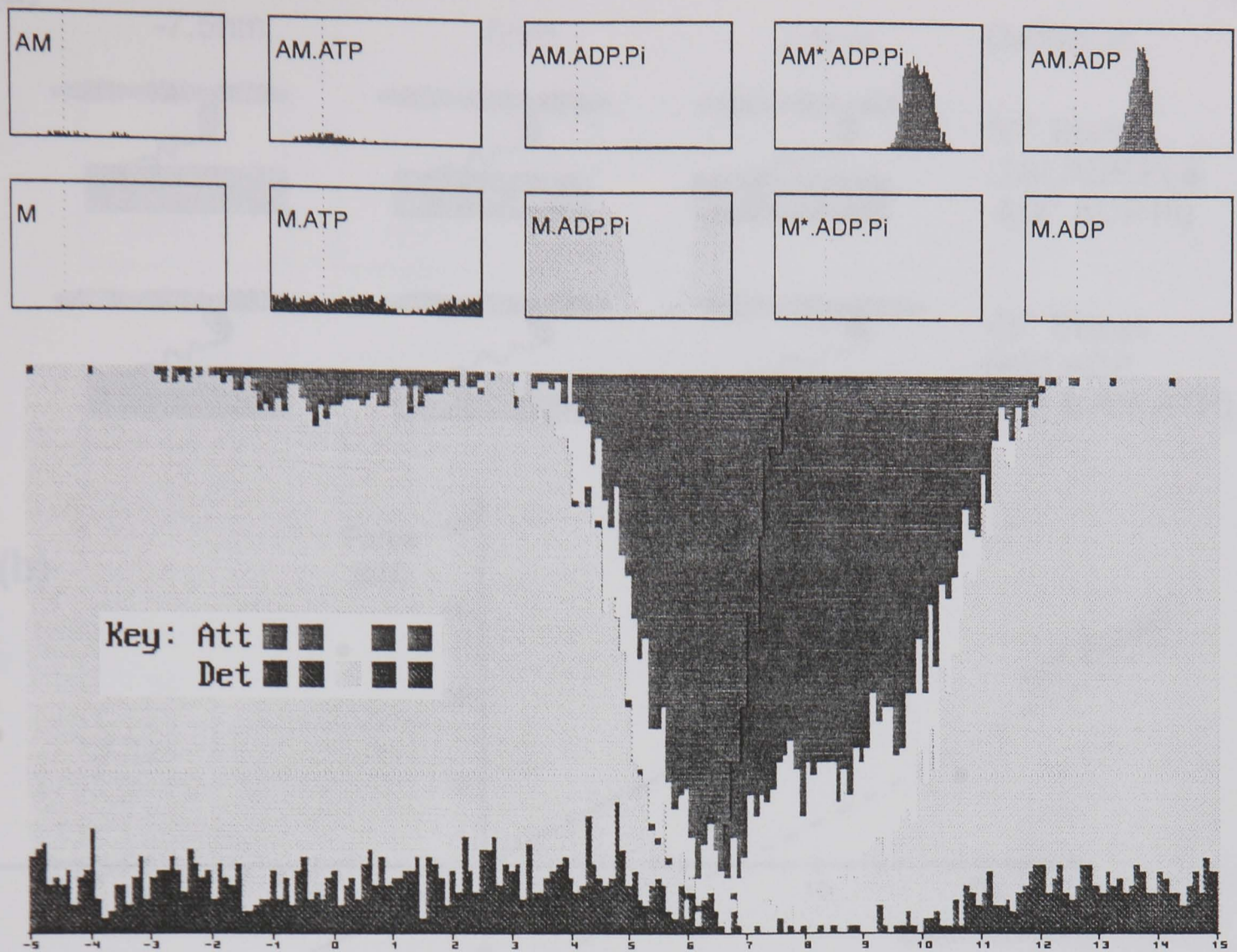
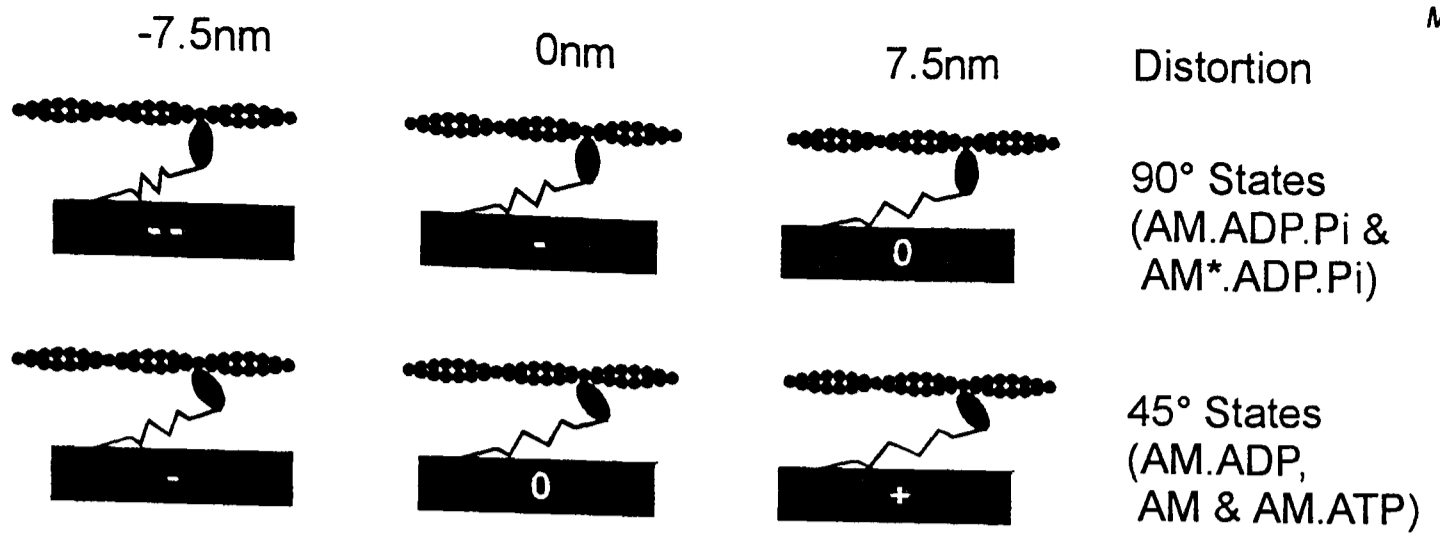


Figure 7.5: The distortion distribution of all cross-bridges in the model can be incorporated into a single diagram. Here the individual state distortion distributions (small upper plots) are shown as one single plot. This provides a concise way of describing the state of the model at any point during a simulation.

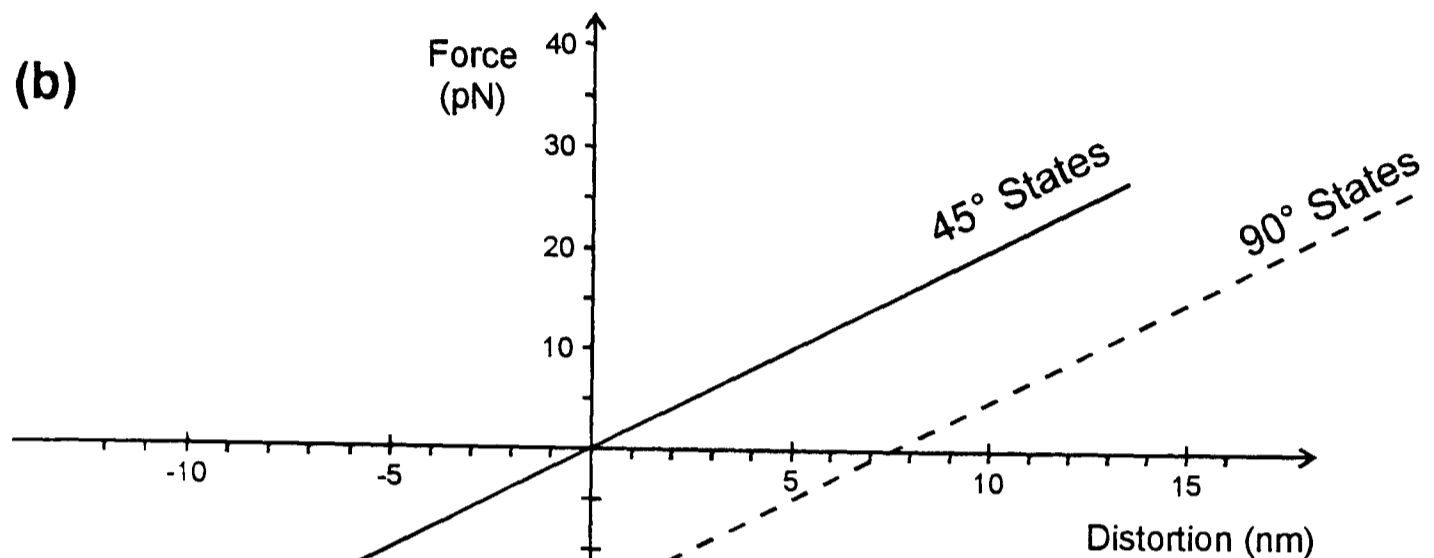
7.4 Model parameters

Like most models of this kind, the assumption is made that each cross-bridge has the capability to bind to just one site on one actin filament. No filament overlap considerations are made in this model, complete overlap is assumed. Also no activation (Ca^{2+}) parameters are included, the model is assumed to be fully activated. Cross-bridges are assumed to be completely independent force generators, binding site competition or co-operative binding are not considered.

(a)



(b)



(c)

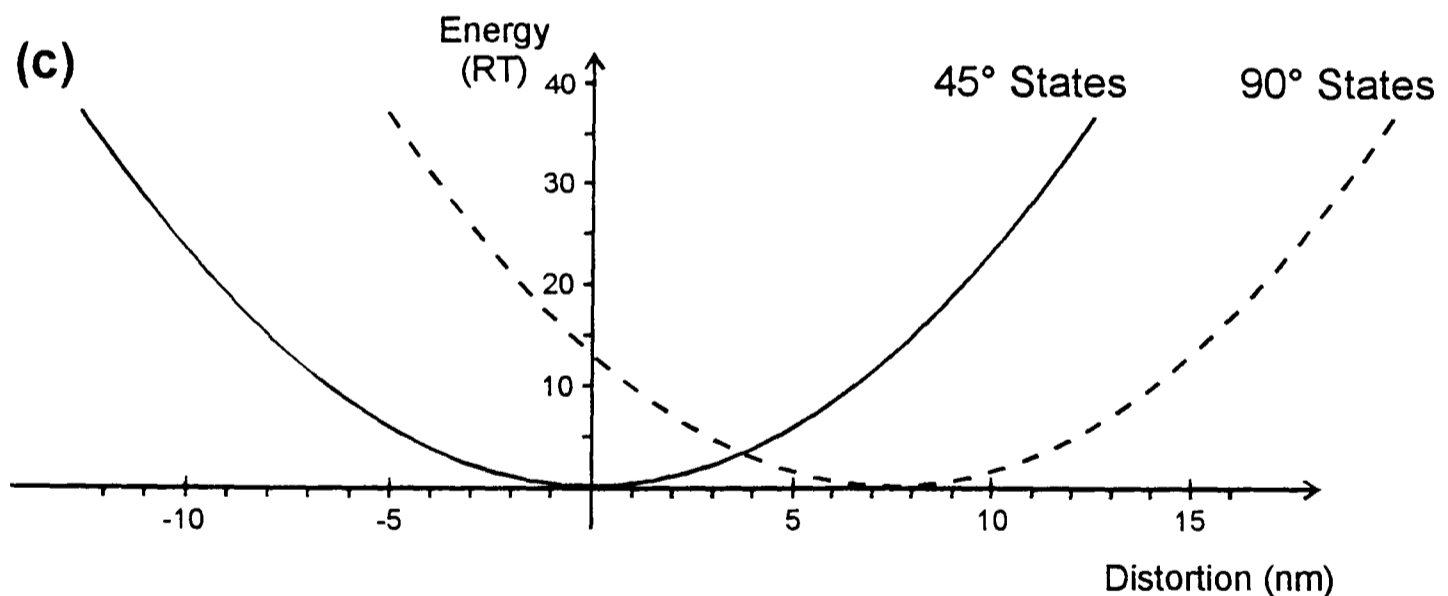


Figure 7.6: Mechanical characteristics of the attached cross-bridges in the model
(a) An attached cross-bridge can occur in either a 90° state (upper row) or a 45° state (lower row). In a typical cycle, a cross-bridge binds in the 90° state, then goes through a "power stroke" transition to the 45° state. Distortion describes the relative sliding between the two filament types. Each mechanical state is shown at three distortion values with a qualitative indication of the force contributed ("-", "0" or "+"). **(b)** The cross-bridge stiffness is 2.0pN/nm in all attached states. The 45° states produce zero inter-filament force at zero distortion. For the 90° states zero force occurs at a distortion of 7.5nm. **(c)** The mechanical (not chemical) free energy of the 45° and 90° states is the energy required to extend or compress the elastic component of the cross-bridge ($E=Kx^2/2$, where K =cross-bridge stiffness and x =distortion).

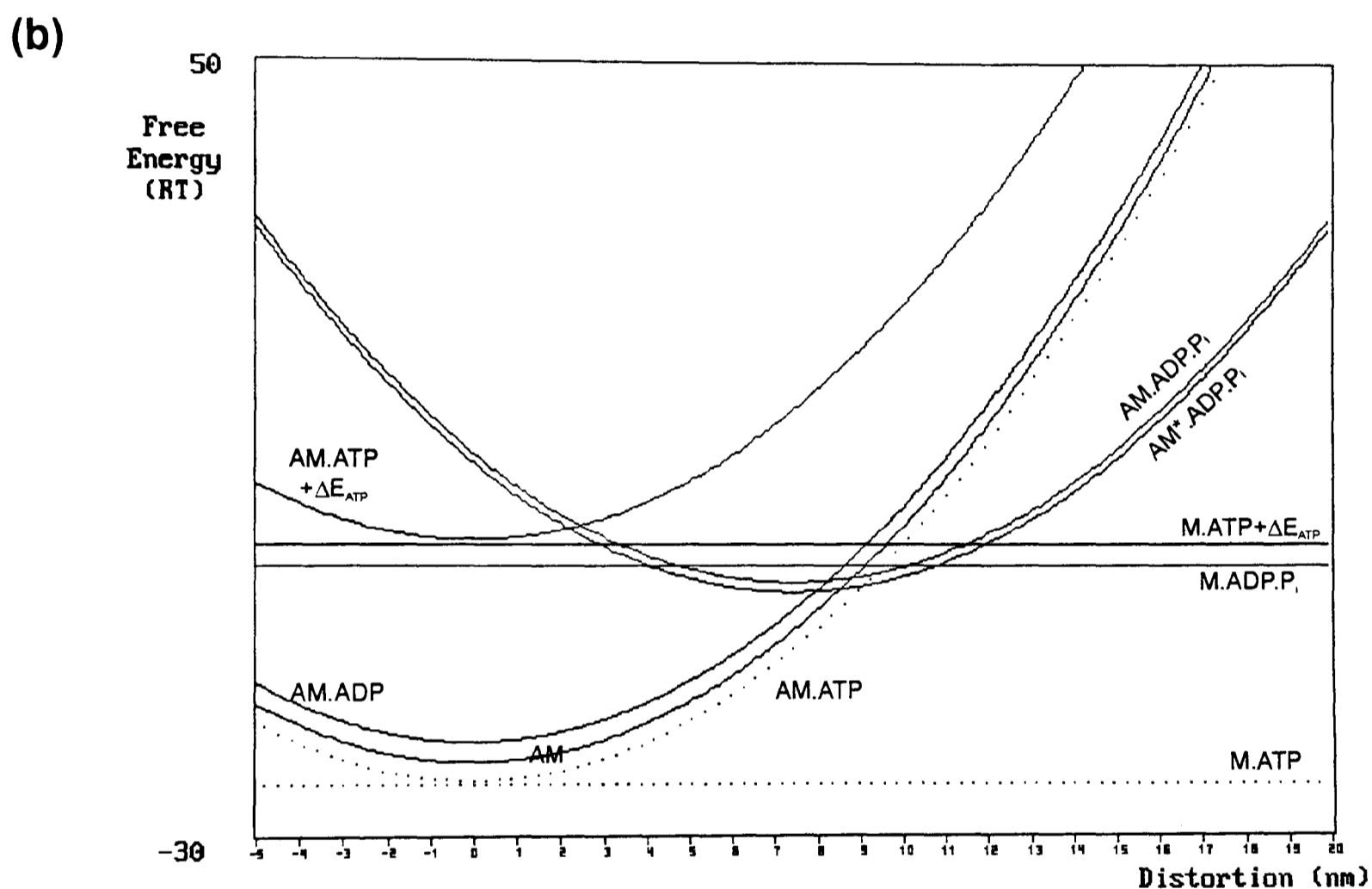
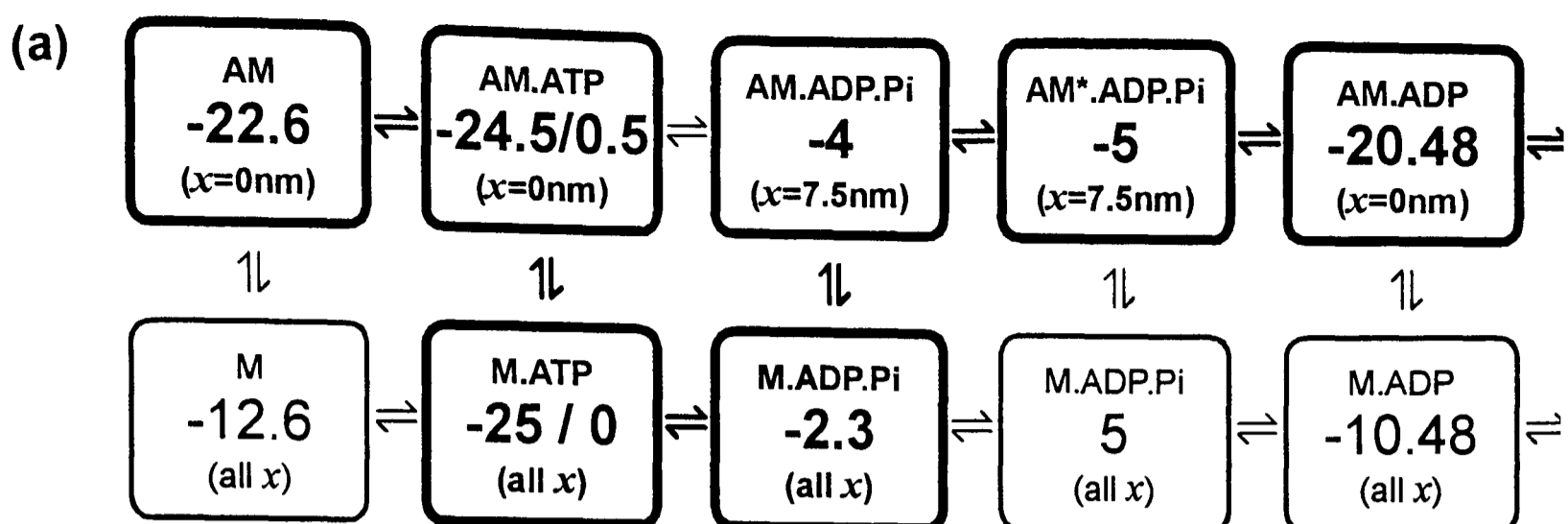


Figure 7.7: The free energy values (RT) of all biochemical states in the model.

(a) The values for the attached states (upper four) are the minimum values which occur when the cross-bridge is under no force. (b) The distortion dependency of the free energy of all states. The attached states are parabolic since they include the work to extend or compress the elastic element in the cross-bridge. Each of the "ATP" states has two plots. One includes the chemical energy provided by ATP (solid line plots), the other does not (dotted line).

7.4.1 Free energy profiles

The free energy of attached cross-bridge states is distortion dependent due to the contribution of the energy required to extend or compress the elastic component of the cross-bridge (Hill, 1974). The relationship of this “mechanical” free energy with distortion is described in Figure 7.6. Note that the free energy contribution of the chemical status of the cross-bridge is not included in this diagram. The stiffness of all attached states is assumed to be 2.0pNnm^{-1} .

The distortion value at which the force exerted by the cross-bridge is zero depends on whether the state is considered to be a 90° or a 45° state. The states preceding the work stroke are 90° states (AM.ADP.Pi and AM*.ADP.Pi). Because these states exert zero force at a distortion of 7.5nm , their free energy minimum is at this distortion value. In this way cross-bridges are more likely to bind in this region of distortion. All other attached states are 45° states, with zero force at 0nm distortion.

The free energy of each biochemical state in the model was based on the values used by Pate and Cooke (1989). The values used are described below in units of RT where K is the cross-bridge stiffness (2.0pNnm^{-1}) and x is the cross-bridge distortion. These values are plotted against distortion in Figure 7.7.

Attached:	$G_{\text{AM.ATP}}(x)$	$= .5 + Kx^2$
	$G_{\text{AM.ADP.Pi}}(x)$	$= -4 + K(x - 7.5)^2$
	$G_{\text{AM*.ADP.Pi}}(x)$	$= -5 + K(x - 7.5)^2$
	$G_{\text{AM.ADP}}(x)$	$= E_{\text{AM.ADP.Pi}}(x - 7.5) + \text{Log}_e(0.00019 * [\text{Pi}])$
	$G_{\text{AM}}(x)$	$= E_{\text{AM.ADP}}(x) + \text{Log}_e(4000 * [\text{ADP}])$
Detached:	$G_{\text{M}}(x)$	$= -12.6$
	$G_{\text{M.ATP}}(x)$	$= 0$
	$G_{\text{M.ADP.Pi}}(x)$	$= -2.3$
	$G_{\text{M*.ADP.Pi}}(x)$	$= 5$
	$G_{\text{M.ADP}}(x)$	$= -10.48$
ATP hydrolysis:	ΔG_{ATP}	$= 25$

The ligand concentrations used in the model are 1mM Pi , $30\mu\text{M ADP}$ and $5\text{mM Mg}^{2+}\text{ATP}$.

Some states are included that were not present in the Pate and Cooke model. The detached states M , $M^*.ADP.Pi$ and $M.ADP$ are included in the model because maintaining symmetry in the model simplifies the programming. These states were given relatively high free energy values to ensure that they were very rarely occupied. The free energy values of these states was set to ten more than the value of the equivalent attached state.

7.4.2 Rate constant values

The relationship between the forward and backward rate constants (R) between states a and b must satisfy the following at all distortions (x), where E is the free energy (Hill, 1974):

$$\frac{R_{ab}(x)}{R_{ba}(x)} = \exp\left(\frac{E_a(x) - E_b(x)}{RT}\right).$$

The following description of the rate constants starts from the working stroke rates and continues around the cycle. Generally distortion dependencies where they occur were kept as simple as possible.

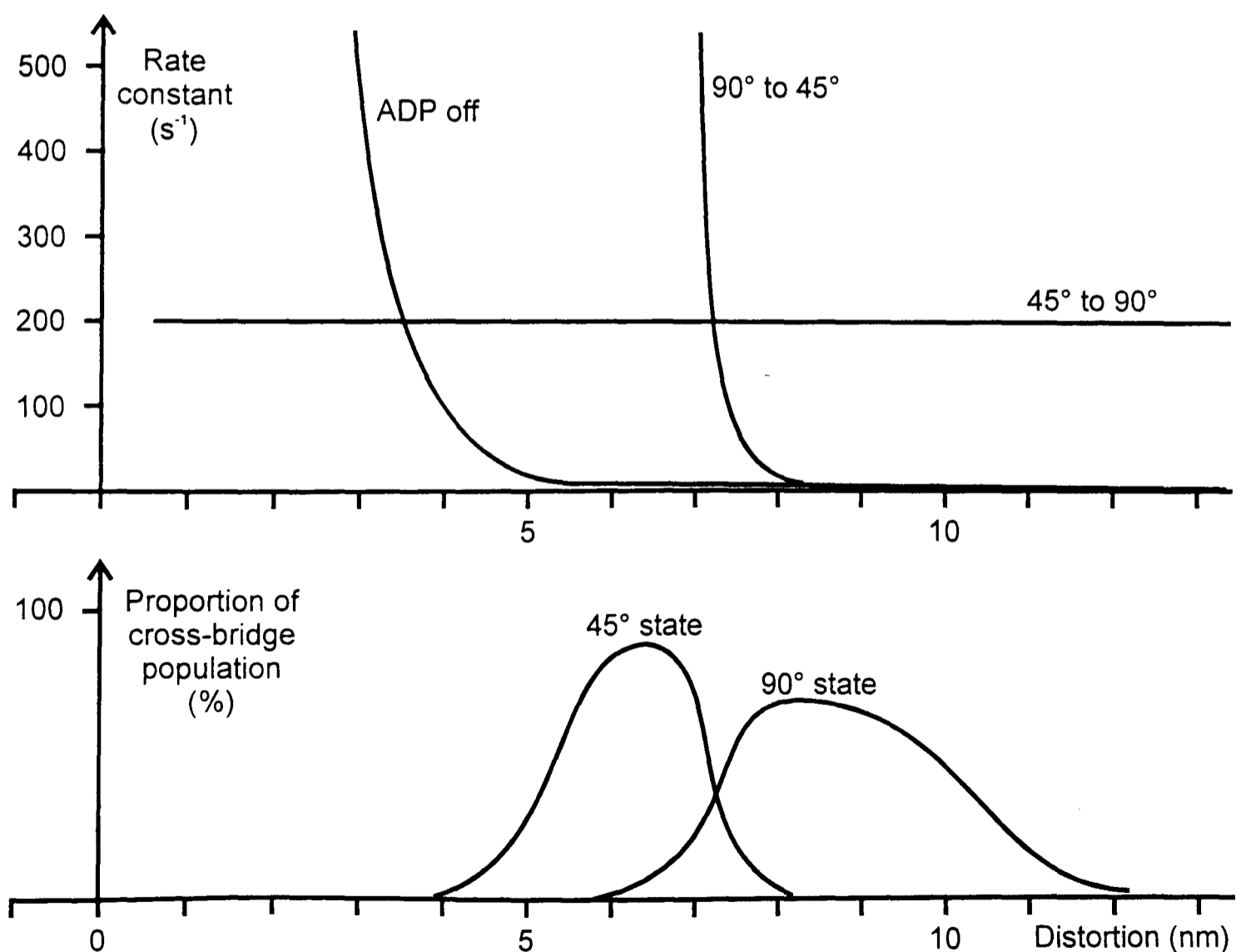


Figure 7.8: Plots of the rate constants and the steady-state populations of the $AM^*.ADP.Pi$ (90°) state and the $AM.ADP$ (45°) state. Both the rate constants and the cross-bridge populations are plotted on the same distortion scales.

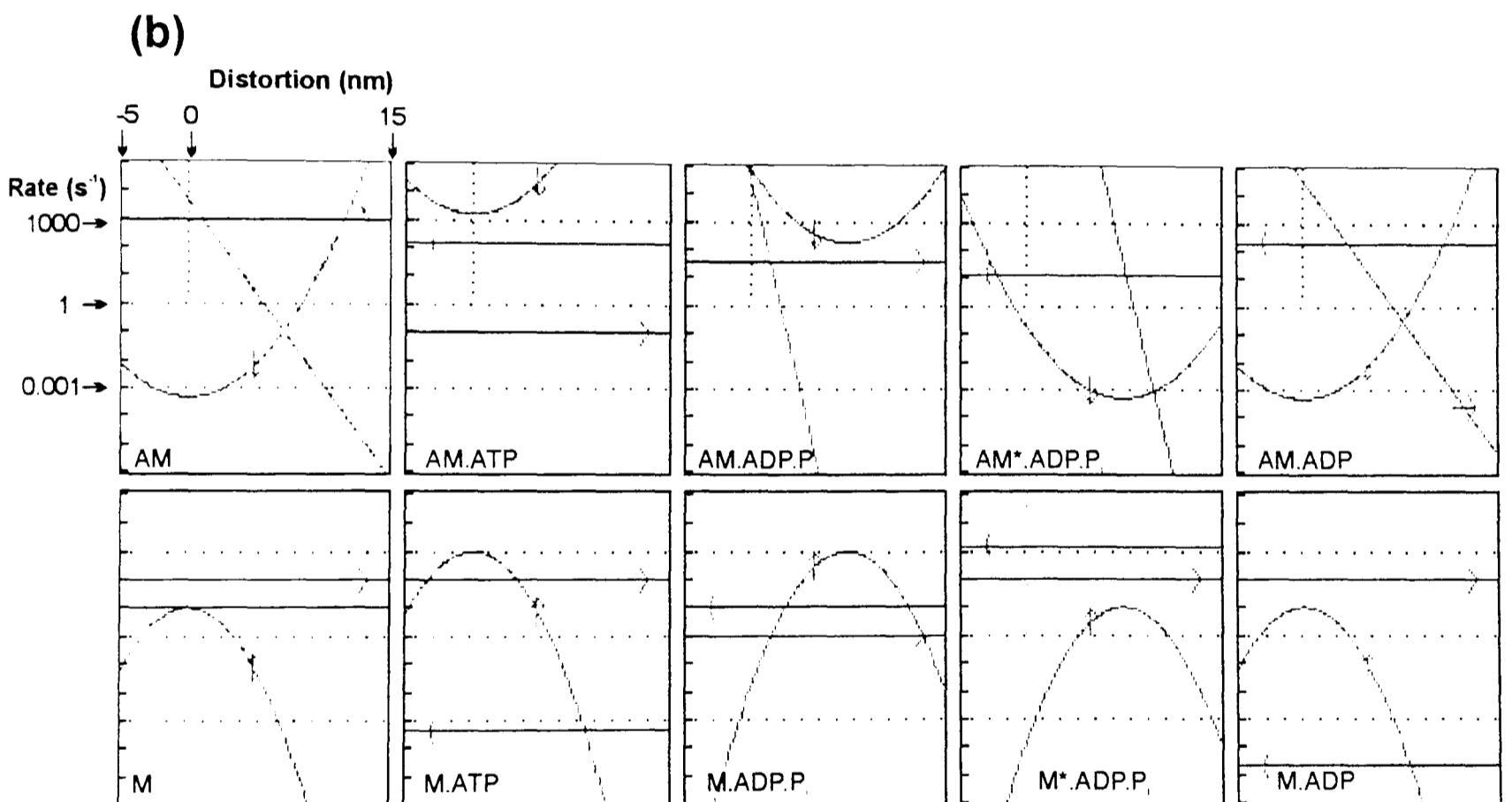
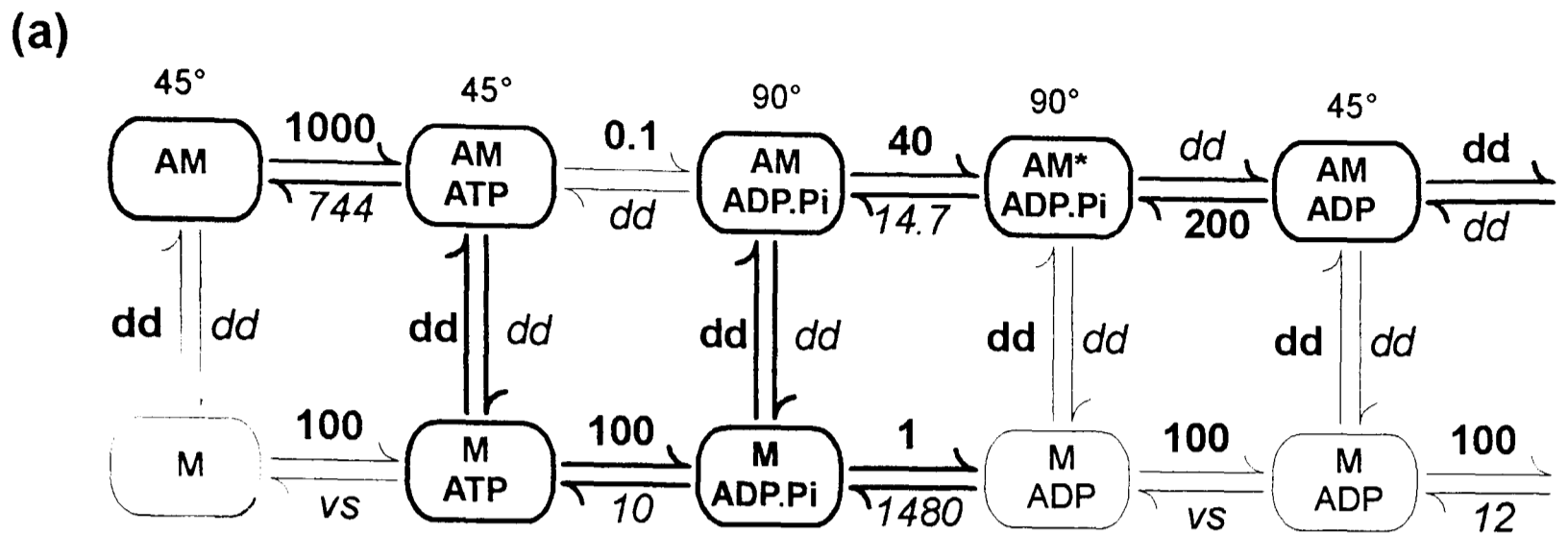


Figure 7.9: The rate constants (s^{-1}) defined in the model. (a) For each forwards/backwards reaction pair, one rate constant is defined initially (**bold**), the reverse rate constant (*italics*) is calculated given the defined rate constant and the free energy change of the reaction. This calculation is made for all distortion values. (Abbreviations "dd" distortion dependent, "vs" very slow). (b) The distortion dependency of all reactions. For each biochemical state the rate constants for the three possible step directions are plotted against distortion. Each state has a rate constant for attachment or detachment (green), a step left (red) and a step right (blue). In each plot, the step direction is indicated by a small arrow.

7.4.2.1 Work stroke AM*.ADP.Pi (90°) ⇌ AM.ADP (45°)

Huxley and Simmons (1971) proposed that the rapid tension recovery following a step is due to a redistribution of cross-bridges amongst the cross-bridge states of the working stroke. In this model the work stroke is a single step between the AM*.ADP.Pi and the AM.ADP states.

The measured rate constant for the rapid recovery phase is the sum of these two rate constants. So that the model reproduces the relationship between this rate constant and step size the rate constant for 45° to 90° was made distortion independent at 200s^{-1} . This rate constant dominates the experimentally determined rate constant (r_2) after rapid stretch (200 to 300s^{-1} Huxley and Simmons, 1971). Experimentally this rate constant does start to increase again with larger steps, though this is probably due to cross-bridges being pulled off (Chapter 6).

Once this is defined, the forward working stroke (90° to 45°) is calculated automatically according to the free energy difference at all distortions. Since the parabolic free energy profiles of the two states have minima at different distortion values ($x=0$ for 45° and $x=7.5\text{nm}$ for 90°), the resulting forward working stroke rate constant is steeply distortion dependent, being extremely fast at negative distortions. These rate constants are plotted in detail in Figure 7.8, together with the steady state distortion distributions of the cross-bridge populations of the AM*.ADP.Pi (90°) state and the AM.ADP (45°) state.

7.4.2.2 ADP on/off rate constants

After a step release, cross-bridges in the AM.ADP.Pi (90°) state move quickly into the 45° state. Cross bridges with negative distortions (i.e. negative force) must be lost quickly, by completing the hydrolysis route (Huxley, 1957). Therefore I chose a steep distortion dependency of the ADP off rate. This ADP off rate also determines the steady state ATPase of the muscle. If this distortion dependency were too steep, cross-bridges would rarely complete the hydrolysis cycle at steady state, resulting in a very low steady state ATPase.

The ADP off rate constant is defined as follows:

$$k_{\text{ADP off}} = \exp(\ln(0.5) - 1.5(x - 7.5))$$

Using this formula it is simple to define the rate constant value at the distortion of 7.5nm (0.5s^{-1} used here) and also the gradient (when plotted logarithmically, see Figure 7.9) of the distortion dependency of the rate constant (value of 1.5).

In a single step working stroke model such as this one, it is important that a reaction step with this kind of distortion dependency immediately follows the first 45° state. Firstly, at steady state, the populations of the AM*.ADP.Pi and AM.ADP states should remain high in order to produce a phase 2 on both stretches and releases. To achieve this the ADP off rate constant should be slow relative to the reverse work stroke at the distortion values of the steady state AM.ADP population (see Figure 7.8). Secondly, on releases, cross-bridges with negative distortions in the AM.ADP state must be detached quickly. Only with a very steep rate constant-distortion relationship for the ADP release step can these two criteria be satisfied.

The energy drop of $2.12RT$ for ADP release (at $30\mu\text{M}$ ADP) makes the reverse step (ADP on) rate constant slower by a factor of 8.33 at all distortions.

7.4.2.3 Attachment/detachment rate constants

For all attachment/detachment rate constant pairs, the attachment rate is defined first. The detachment curves are determined by the software given the attachment rate constant and free energy profiles.

All attachment rate constants are defined with a Gaussian distortion dependency, with the maximum attachment rate at the distortion with zero force (free energy minimum). The equation used is the following,

$$k_x = k_{max} \cdot \exp\left(\frac{-(x - \mu_x)^2}{2\sigma_x^2}\right).$$

The Gaussian mean (μ_x) is 0nm for 45° states and 7.5nm for 90° states. The standard deviation (σ_x) of all attachment profiles is 1.6nm.

The k_{max} is the maximum attachment rate at the centre of the Gaussian distribution. The maximum attachment rate constants used in the model are 10s^{-1} for M, 10s^{-1} for M*.ADP.Pi and 10s^{-1} for M.ADP.

The two significantly populated detached states M.ATP and M.ADP.Pi are both given maximum attachment rate constants of 10^5s^{-1} , to give a rapid attachment/detachment equilibrium (Stein *et al*, 1979; Brenner *et al*, 1986).

7.4.2.4 Detached M.ATP \leftrightarrow M.ADP.Pi

The two significantly populated detached states, M.ATP and M.ADP.Pi, were given the free energy values as those used by Pate and Cooke, 1989. The free energy difference of $2.3RT$ between these two states results in a factor of ten difference between the forward and backward rate constants. This forces 90% of relaxed cross bridges into the M.ADP.Pi where they can attach quickly if in the

attachment distortion range. The hydrolysis rate constant is set to 100s^{-1} , resulting in a 10s^{-1} reverse step.

7.4.2.5 AM.ADP.Pi \leftrightarrow AM*.ADP.Pi

Experimental evidence suggests that there is a rapid equilibrium (Brenner *et al.*, 1986) between M.ADP.Pi and AM.ADP.Pi. This is incorporated into the model.

If the attached state in this rapid equilibrium steps directly into the work stroke, this introduces a problem. After a step stretch cross-bridges with high distortions (i.e. those that were already in this state before the stretch) will very quickly detach due to the rapid attachment/detachment equilibrium and their energetically unfavourable distortions. Experimental evidence suggests that there is little change in stiffness at the end of phase 2 compared to steady state (Ford, Huxley and Simmons, 1977).

Also if these two rapid equilibria share a common attached state, the AM.ADP.Pi state, the redevelopment of tension following release (phase 4) would be extremely rapid. Incidentally this provides a simple way to reproduce the staircase results of Lombardi (1992), but would result in the loss of phases 3 and 4 from the resulting transients.

For these reasons an isomerisation state was added to the model moving the work stroke step away from the rapid equilibrium attachment/detachment step. Relatively slow rate constants are given to this step providing a mechanism to produce phases 3 and 4 following a step stretch in the model tension transients.

The rate constant for the forward isomerisation step is 40s^{-1} , giving a reverse value of 14s^{-1} .

7.4.3 Cross-bridge distortion distribution

The distribution of cross-bridge distortions in the model is uniform by default. The total number of cross-bridges is an integer multiple of total number of distortion values so that there is an equal number of cross-bridges at each distortion. No filament overlap considerations are made in this model.

A special case is the Wray model distribution. Here a non-uniform distribution of distortions is created, providing a way to simulate the match-mismatch model.

7.4.4 ATPase

The model ATPase is measured by counting the total number of cross-bridges stepping from AM and M states to the AM.ATP and M.ATP states. Cross-bridges performing the opposite step are subtracted from this total. In this way the model ATPase reflects the rate of loss of ATP from solution. This total ATP count is accumulated and plotted every 5ms (or every iteration if this is longer). This maximum plot frequency is set due to noise in the plot when higher plot rates are used. The value of ATPase shown (s^{-1}) is corrected for the total number of cross-bridges in the model.

7.5 Model output

All the simulation results shown here were produced using the computer model with a total of 16281 cross-bridges. Although the capability to alter the ligand concentrations has been included in the code, these parameters were not changed. Instead the results shown here describe simulations of length change experiments that can be performed on muscle.

7.5.1 Model T_1 - T_2 curves

Since the model is based on a single step work stroke transition one of the most fundamental requirements is that the model can reproduce the phase 2 properties of striated muscle. This should include not only the T_1 - T_2 relationship but also the change in the rate constant of phase 2 with step size.

Three different model T_1 - T_2 curves are plotted in Figure 7.10b. These curves were produced by loading the tension transients produced by the model (Figure 7.10a) into the muscle program where the tension values at the ends of phases 1 and 2 could be measured accurately.

As modelled using the equations of Huxley and Simmons (1971) in Chapter 6, the plot here shows the T_1 - T_2 curves resulting from using different values for the working stroke (h values used were 6nm, 7.5nm and 9nm). The cross-bridge stiffness used in each of these simulations was $2.0pNm^{-1}$. It can be seen that the stochastic model is able to reproduce the change in the gradient of the T_2 curve as it crosses the vertical axis. As the size of the work stroke increases the T_2 curve gradient becomes negative, just as predicted by the Huxley-Simmons equations.

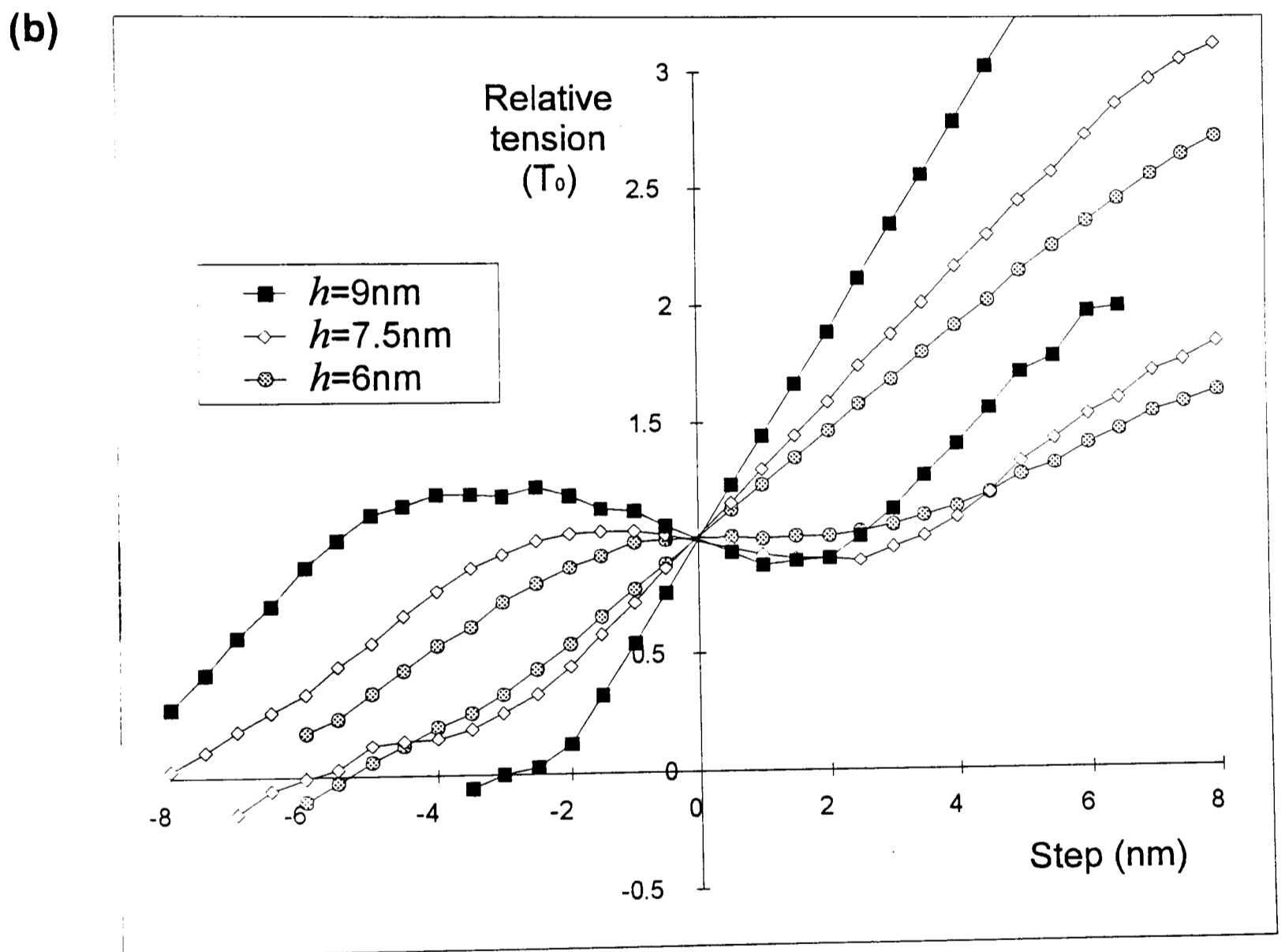
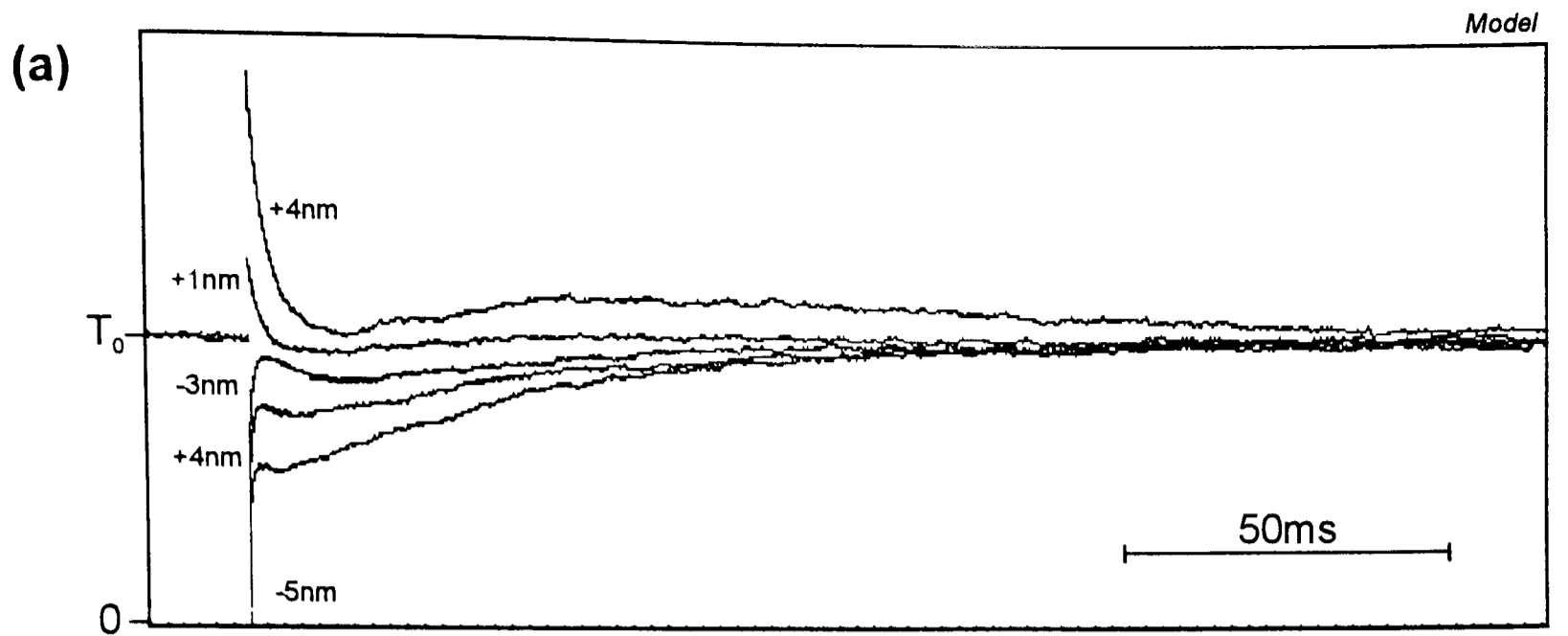


Figure 7.10: Some tension transients and the T_1 - T_2 curves from model simulations (a) Some example model output traces. These transients also demonstrate that the rate constants for all three phases (r_2 , r_3 and r_4) become faster with decreasing step size. (b) The model is able to reproduce the T_1 - T_2 curves observed in rabbit and insect fibrillar flight muscle. The T_1 - T_2 curves are plotted for three different values for the work-stroke (h). These plots show that the gradient of the T_2 curve at the vertical axis becomes negative as the work-stroke is increased as predicted by the mathematical modelling of Huxley and Simmons (1971). The change in work-stroke also alters the “symmetry” of the T_2 curve.

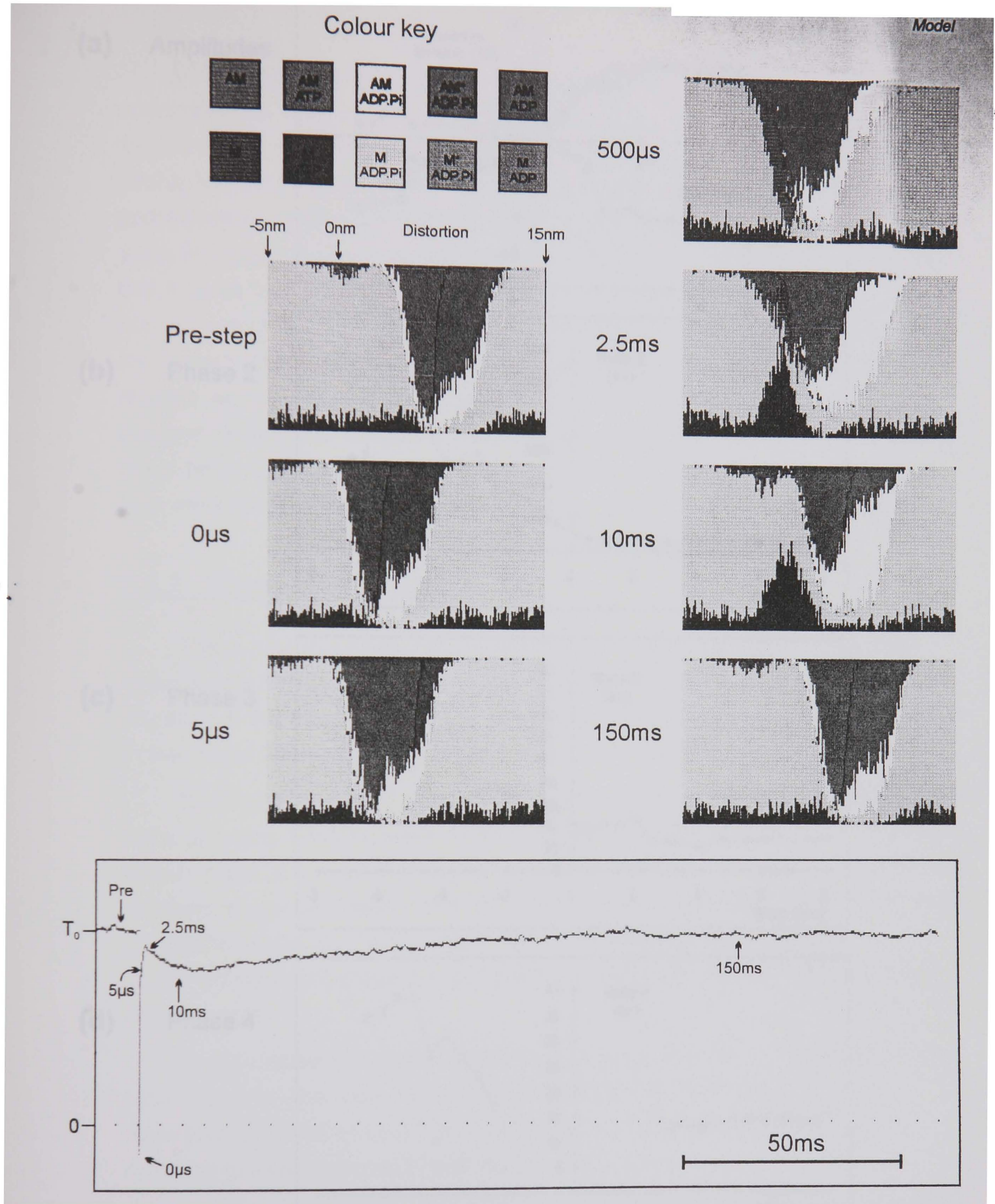
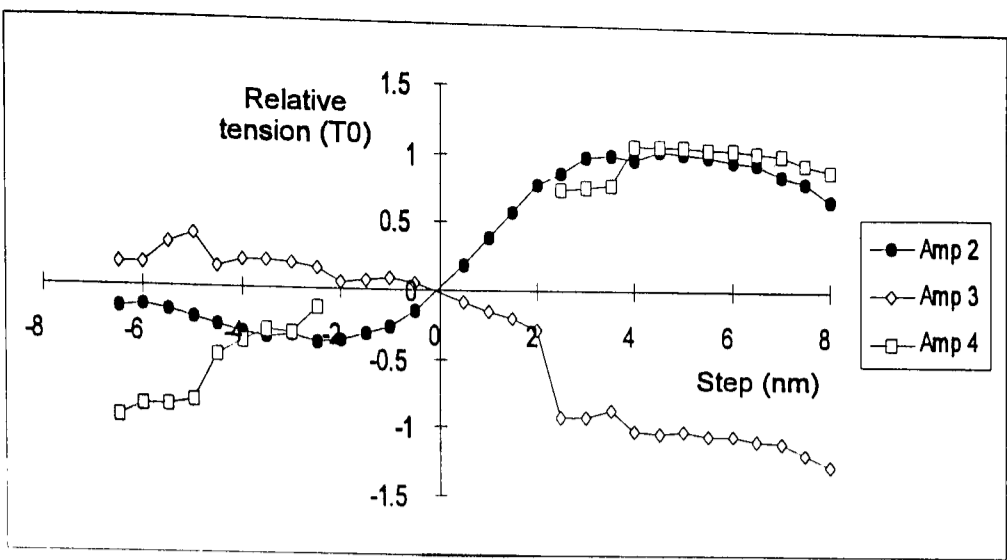
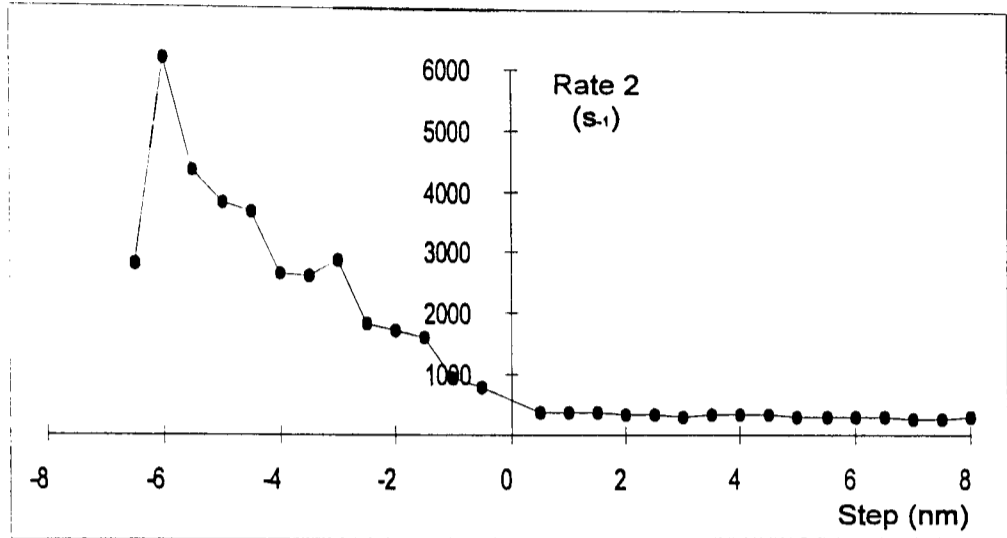


Figure 7.11: A model run simulating the four tension phases resulting from a step release of vertebrate skeletal muscle. The tension trace (lower) is model output generated by applying a 4nm release. Zero tension is indicated by the dotted line. The number and distribution of cross-bridges in each state is shown for several time points in a series of small plots. Each state is represented by a colour as described in the colour key.

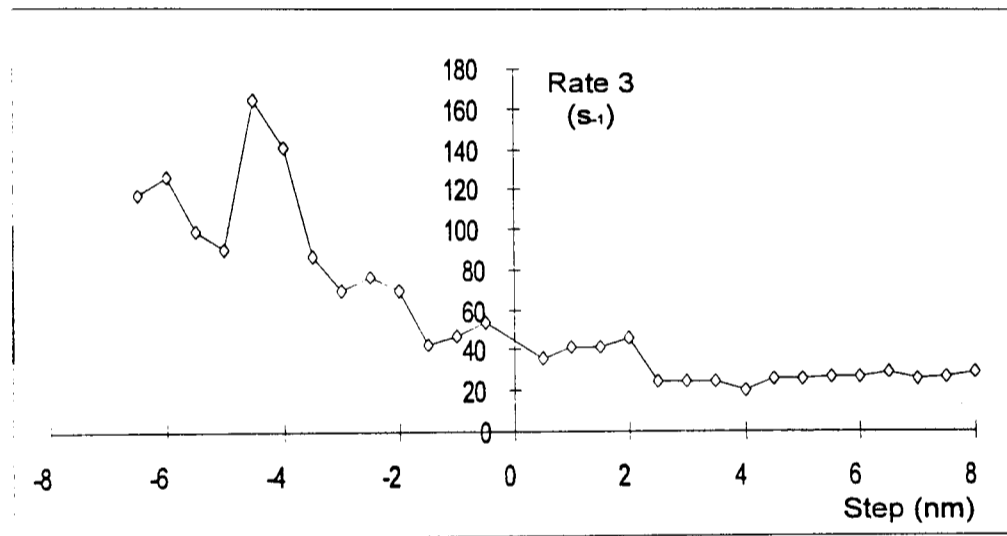
(a) Amplitudes



(b) Phase 2



(c) Phase 3



(d) Phase 4

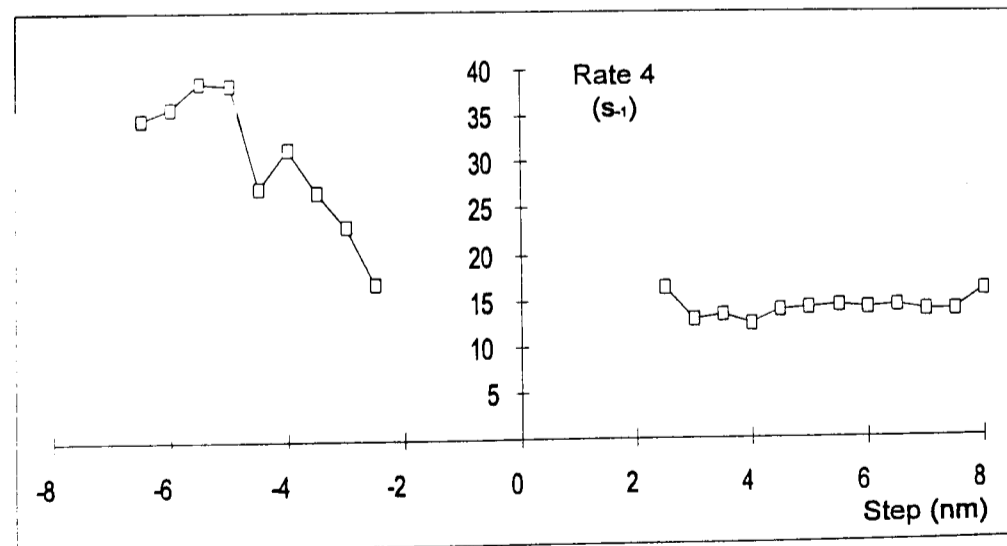


Figure 7.12: The amplitudes and rate constants of phases 2, 3 and 4 of the vertebrate skeletal muscle model at different step sizes. The values were obtained by fitting three summed exponentials to the model output using the nonlinear least squares procedure in the muscle program. In the step range -2.5nm to +2.5nm, the amplitude of phase 4 was too small to fit a curve accurately. In this range only two exponentials (phases 2 and 3) were fitted.

Of the 16281 cross-bridges in the model approximately 3000 occupy the two working stroke states at steady state. However the actual population of each of the two states at steady state was dependent on the value used for the work-stroke. With a working stroke of 7.5nm the steady state populations are approximately 1390 in the AM.ADP.Pi (90°) state and 1740 in the AM.ADP (45°) state. Being not far from equally populated this results in a simulation T_2 curve that is quite "symmetrical". A work stroke of 6nm results in steady state populations of 615 cross-bridges in the 90° state and 2840 in the 45° state. The low number of cross-bridges in the 90° state results in low amplitude phase 2 on release, so that the release T_2 curve remains close to the T_1 curve. Conversely the 9nm work-stroke simulation has 2050 cross-bridges in the 90° state and 895 cross-bridges in the 45° degree state, resulting in a large amplitude phase 2 on step releases and small amplitude following a stretch.

7.5.2 Step length changes

The model accurately reproduces all of the tension transients observed when a step length change is applied to striated muscle (both stretch and release). A detailed description of the changes in the populations of all the states in the model following a step release is shown in Figure 7.11.

Before the step release was applied, the model was allowed to reach steady state by letting it run for one second. The steady state cross-bridge distribution is shown in the "pre-step" distribution. At steady state there are approximately equal numbers of cross-bridges in the AM*.ADP.Pi and the AM.ADP states. At all times during the sequence the majority of cross-bridges remain in the detached M.ADP.Pi state since they are at distortions where attachment is energetically unfavourable.

At the instance of release (0 μ s) the whole distribution is shifted to the left (4nm release). The cross-bridges in the AM*.ADP.Pi 90° state are now at distortion values where the transition to the AM.ADP 45° state is very rapid, resulting in a rapid phase 2 (see the 5 μ s distribution).

The excess of cross-bridges in the M.ADP state at unfavourable distortions (less than 5nm) move out at a rate limited by the ADP off rate constant. This process gives rise to the phase 3 on release (2.5ms to 10ms). Tension returns to the pre-step value with new cross-bridges attaching and occupying the 90° state (phase 4, 10ms to 150ms). On release steps, the rate constant of phase 4 is determined by the rate constant for the step AM.ADP.Pi to AM*.ADP.Pi.

A series of steps were given at 0.5nm intervals from -6.5nm to +8nm. Each step started from steady state and the resulting transients were recorded for 0.5s.

These transients were loaded into the muscle program where three exponential functions were fitted to phases 2, 3 and 4 in exactly the same way as is done with experimental tension traces. The relationship of the fitted exponential amplitudes and the rate constants are shown in Figure 7.12. The same tension transients were used to create the T_1 - T_2 curves in Figure 7.10b, some of the tension transients are shown in Figure 7.10a.

On a step stretch the phases 3 and 4 are a result of different processes than those on step release. After a stretch, cross-bridges from the AM.ADP 45° state build up in the AM*.ADP.Pi 90° state (phase 2). Newly attaching cross-bridges occupy the now energetically favourable but poorly populated distortions of the AM*.ADP.Pi state (from 4nm to a maximum of 12nm, depending on the size of the imposed stretch). This process gives rise to phase 3 on stretch, and the rate constant is determined by that of the step AM.ADP.Pi to AM*.ADP.Pi. This is the same rate constant that determines the observed rate constant for phase 4 on step releases. Finally phase 4 on stretch is the result of cross-bridges at unfavourably high distortions in the AM*.ADP.Pi 90° state (mostly originally from the AM.ADP 45° state) going through the AM*.ADP.Pi to AM.ADP.Pi isomerisation and detaching.

7.5.3 Force-velocity

The force-velocity relationship plotted in Figure 7.13 was generated by applying series on constant velocity releases in the model program. Tension was measured using the muscle program. The slopes were generated by applying a 0.1nm step release with each iteration (the smallest possible perturbation in the model). Different velocities were generated by altering the iteration duration.

7.5.4 Lombardi Staircase Experiment

A staircase of step releases were applied to the model to compare the output with the results of Lombardi *et al* (1992). Each step in the sequence was 4nm in size and 8ms in duration.

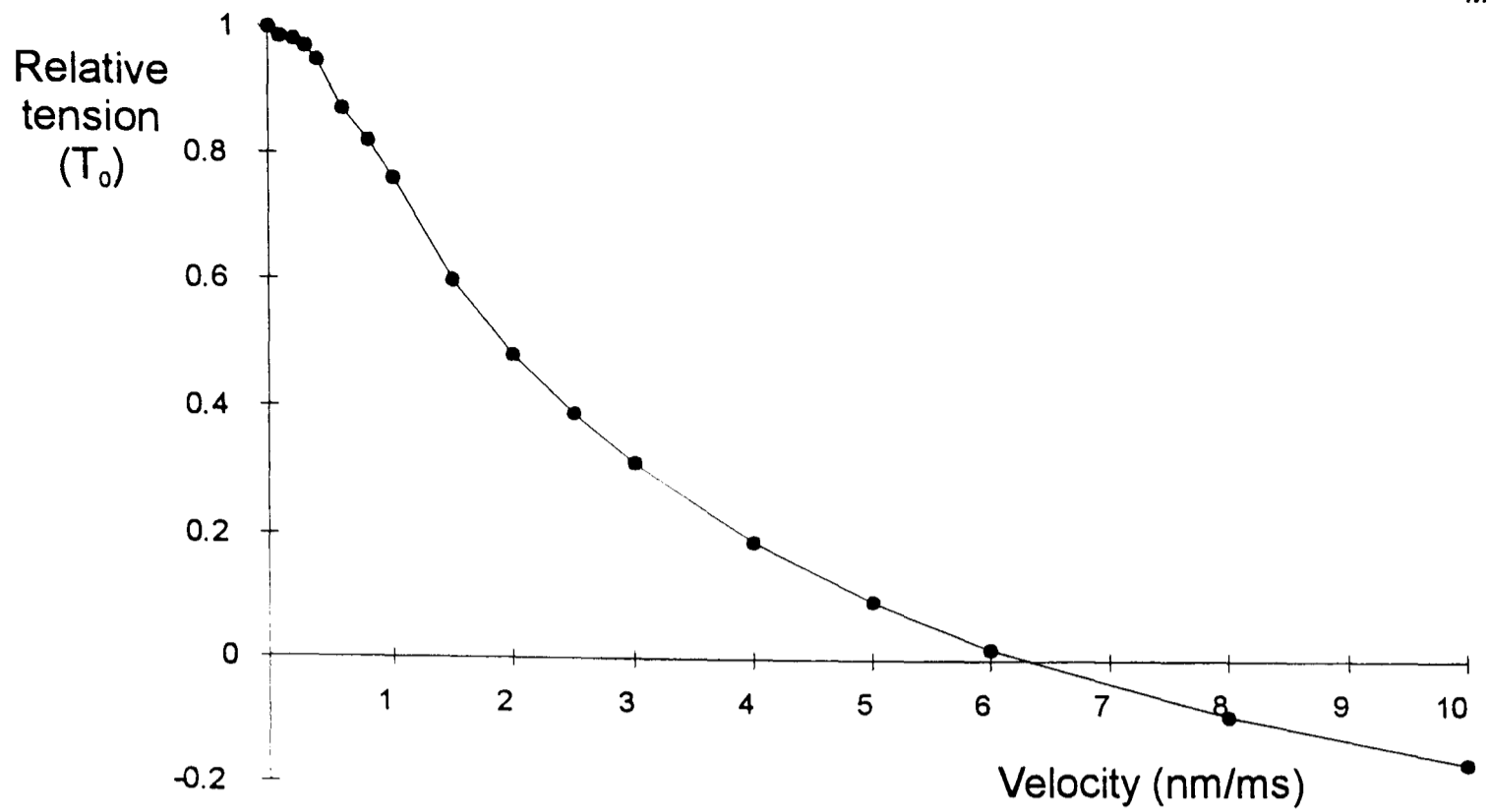


Figure 7.13: The force-velocity curve of the vertebrate skeletal muscle model.

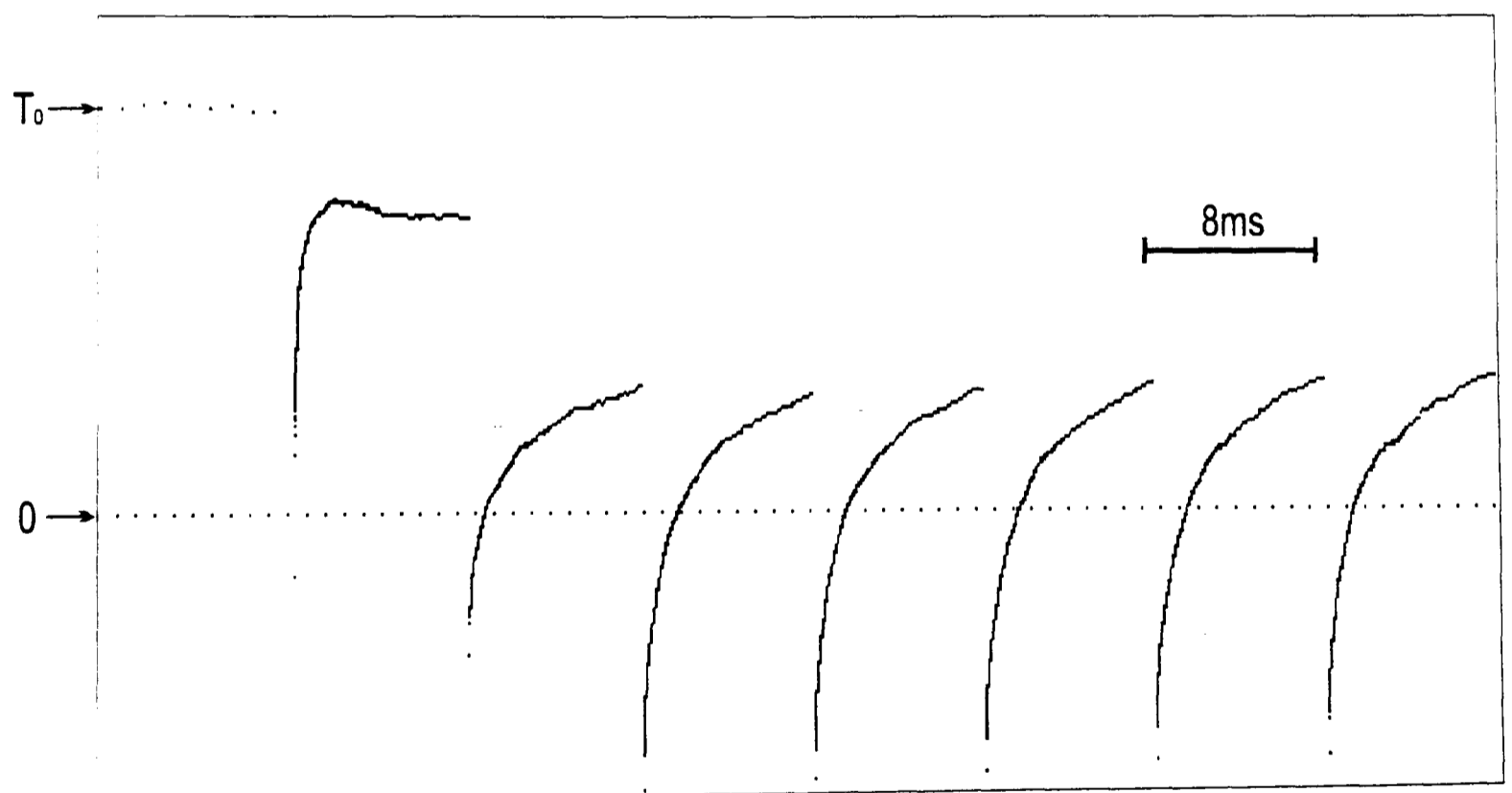


Figure 7.14: Lombardi staircase simulation.

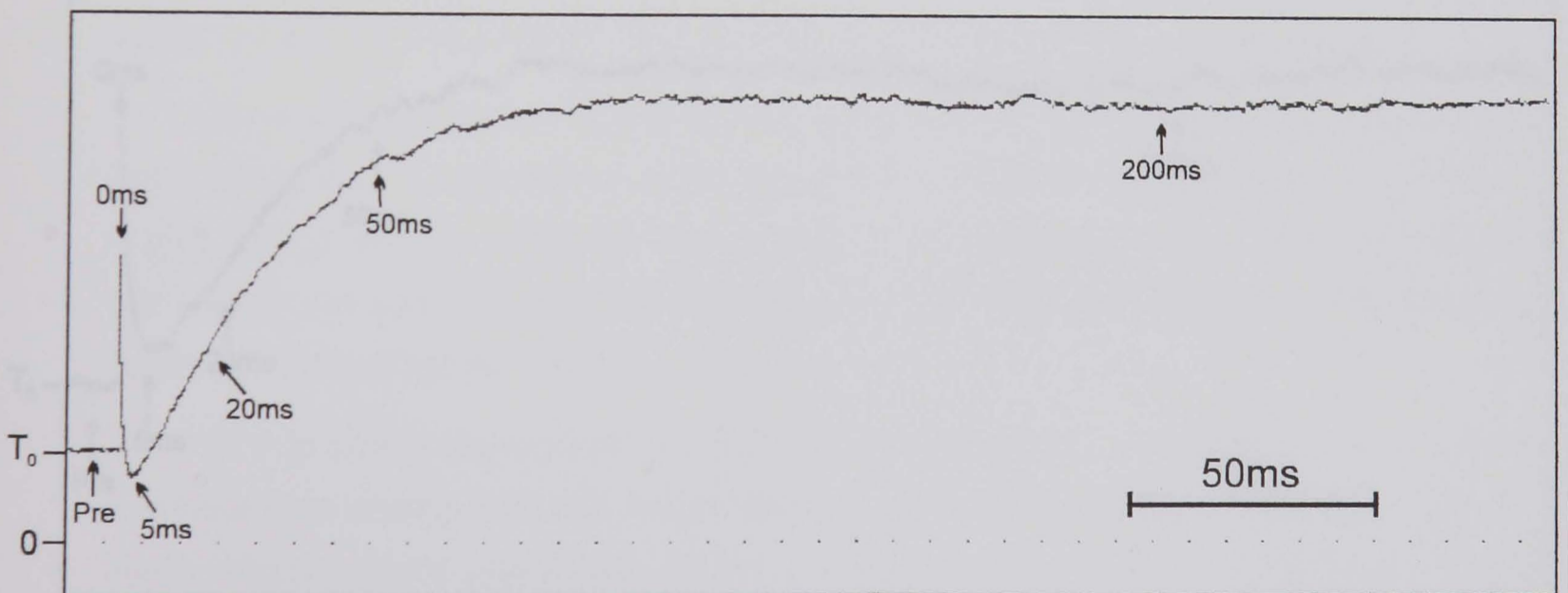
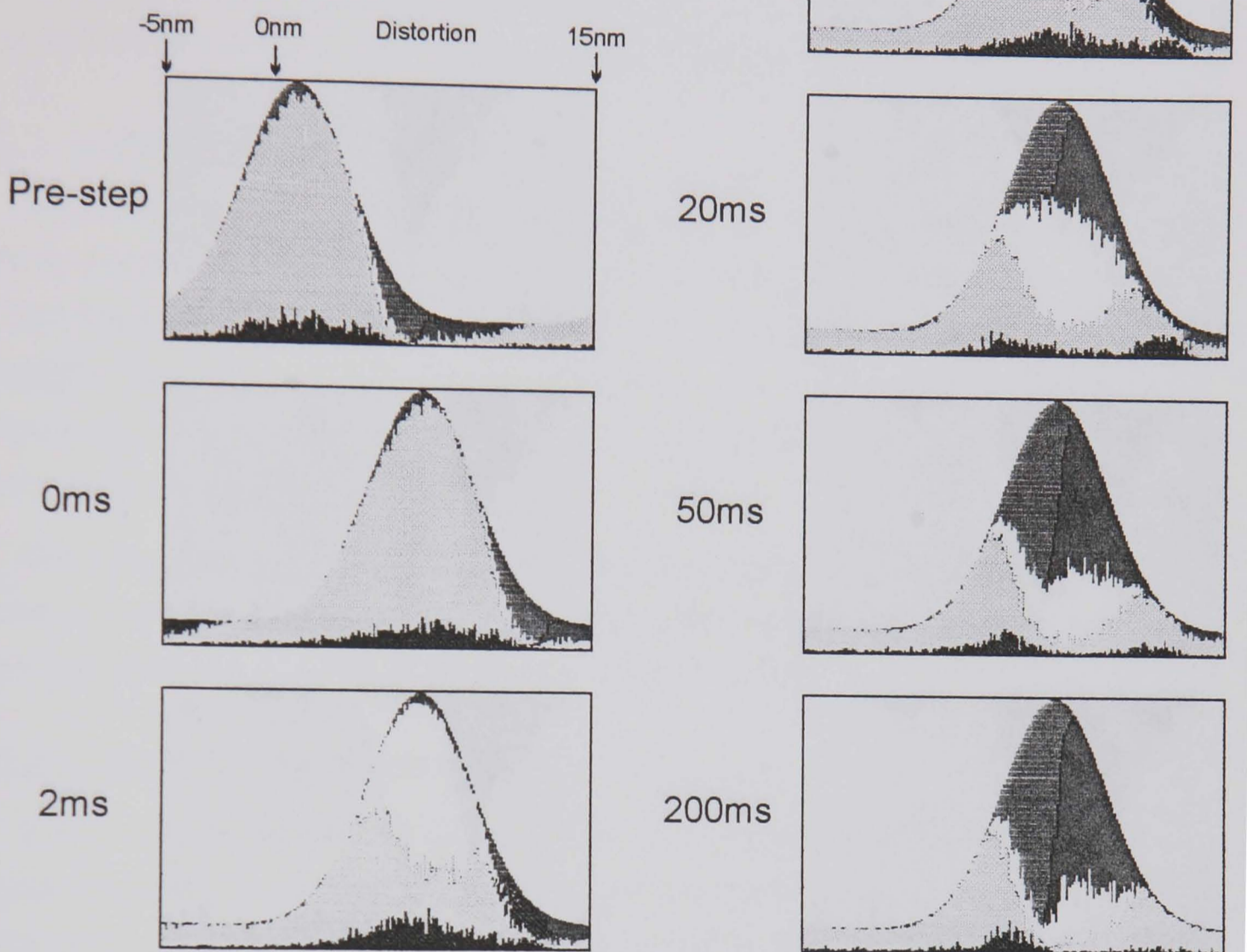
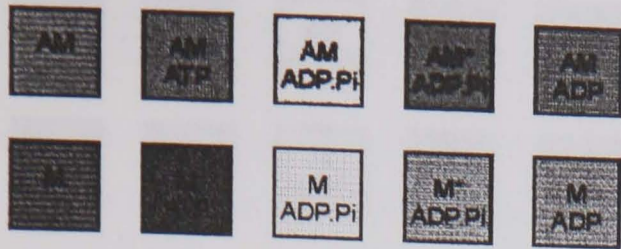


Figure 7.15: A model simulation of stretch activation based on that proposed by Wray (1979b). Distortion distribution is defined such that 80% of cross-bridges occupy a Gaussian distribution centred about zero distortion (standard deviation 2.5nm). Since most attached bridges occur in the distortion range 5nm to 10nm, only a small proportion of bridges can attach. The 6nm stretch results in a very large increase in the number of cross-bridges in this high attachment distortion range.

Colour key

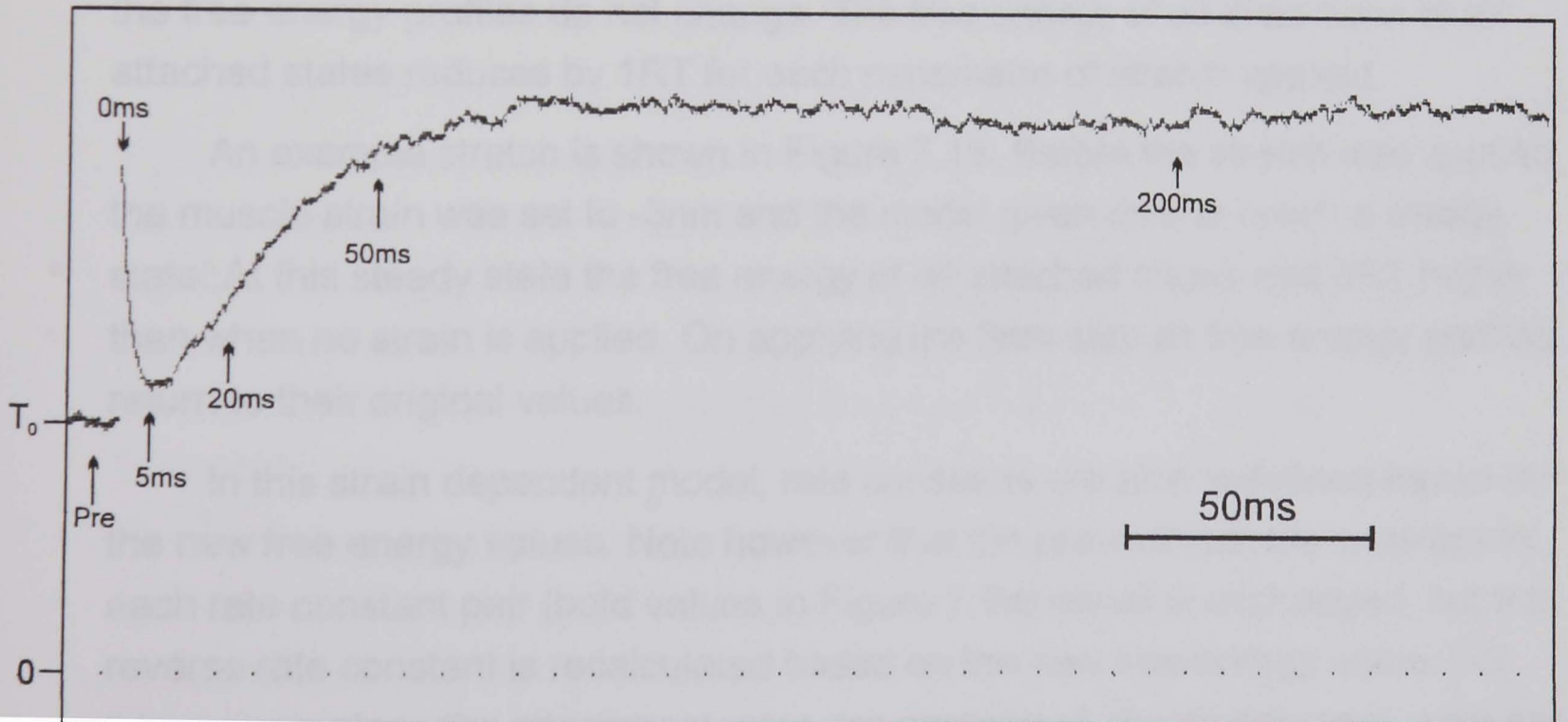
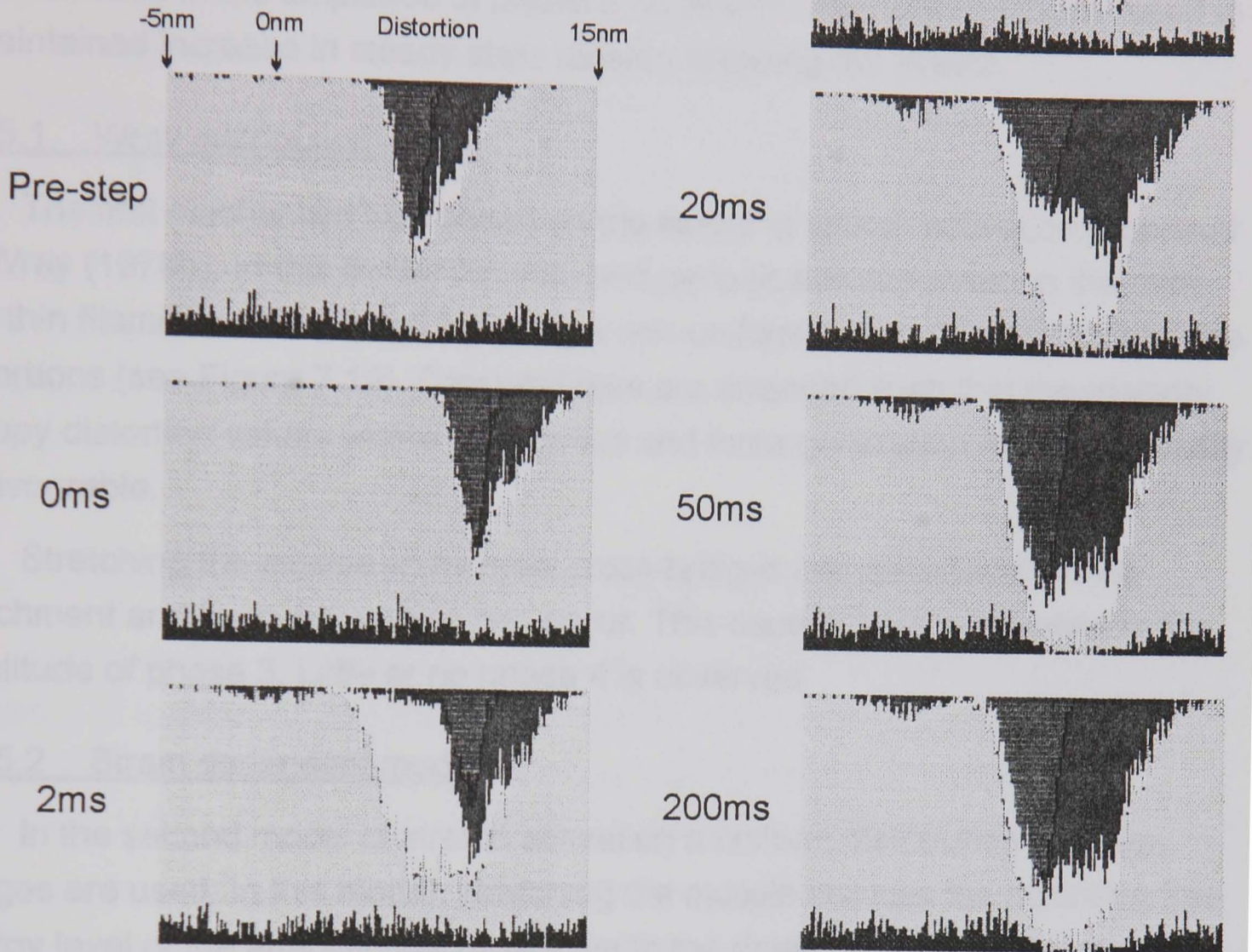
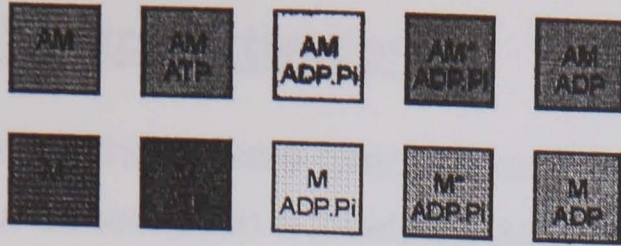


Figure 7.16: A model run demonstrating a stretch activation response in a model with uniform distortion distribution. In this model positive strain on the muscle lowers the free energy of all attached states relative to detached states at a rate of $1RT\text{nm}^{-1}$. In this way the attached population increases with strain. The step applied was 3nm.

7.5.5 Stretch activation

Two methods were used to model the characteristics of the stretch activation observed in activated insect fibrillar flight muscle. Both methods result in an increase in the amplitude of phase 3 on stretch. Also both methods result in a maintained increase in steady state tension following the stretch.

7.5.5.1 Wray distribution model

The first mechanism was based on the model of stretch activation proposed by Wray (1979b). In this model the matched periodicities observed on the thick and thin filaments is simulated by using a non-uniform distribution of cross-bridge distortions (see Figure 7.15). Cross-bridges are arranged such that the majority occupy distortion values where attachment and force generation are energetically unfavourable.

Stretching the muscle shifts most cross-bridges into distortions where attachment and force generation can occur. This causes a large increase in the amplitude of phase 3. Little or no phase 4 is observed.

7.5.5.2 Strain dependent model

In the second model of stretch activation a uniform distribution of cross-bridges are used. In this model, stretching the muscle reduces the minimum free energy level of the attached states relative to the detached states. The shape of the free energy profiles do not change. The free energy of all distortions of all attached states reduces by $1RT$ for each nanometre of stretch applied.

An example stretch is shown in Figure 7.16. Before the stretch was applied, the muscle strain was set to -3nm and the model given time to reach a steady state. At this steady state the free energy of all attached states was $3RT$ higher than when no strain is applied. On applying the 3nm step all free energy profiles return to their original values.

In this strain dependent model, rate constants are also redefined based on the new free energy values. Note however that the pre-defined rate constant in each rate constant pair (bold values in Figure 7.9a) remains unchanged, but the reverse rate constant is recalculated based on the new free energy value. For this reason, since the attachment rates are predefined, the detachment rates are the only rate constants to change with strain. All other rate constants in the model remain unchanged.

7.6 Discussion

This model is able to reproduce the characteristics of the four phases observed in tension transients in both step stretch and release experiments on activated striated muscle.

Although all states in the model are described biochemically, it is quite likely that the biochemical identities of some states in the model are not accurate. Clearly for the model to reproduce realistic tension transients, the mechanical characteristics of each state and the rate constants between them are the important factors, rather than the biochemistry of each state. This is particularly true here because the main focus of this study has been the accurate reproduction of tension transients, rather than the sensitivity to changes in the various ligand concentrations.

7.6.1 Huxley and Simmons (1971) characteristics

In this model, one of the fundamental assumptions made is that the rapid recovery of tension following step length changes (phase 2) is due to a redistribution of cross-bridges between two attached states (Huxley and Simmons, 1971). The step between these two states is the force generating step.

Since this is the force generating step, it is important that the model is able to match well the characteristics of phase 2. The model reproduces T_1 - T_2 that are very similar to those seen in muscle (Figure 7.10).

In the right conditions the model T_2 curve can have a gradient of zero where it crosses the vertical axis (as seen in vertebrate skeletal muscle) or can demonstrate the negative gradient observed in the insect fibrillar muscle when the relaxed component of the tension response is subtracted out (Chapter 6, Figure 6.1d). An increase in the size of the work stroke results in this negative gradient as was also demonstrated by the Huxley-Simmons equations in Chapter 6.

One prediction that the Huxley-Simmons equations could not make is that the "symmetry" of the T_2 curve could be altered by changing the work stroke. The vertical distance of the T_2 curve from the T_1 curve is the same as the amplitude of phase 2. This amplitude is a function of the shapes and relative positions of the free energy parabolas of the two work stroke states and also the population sizes of the two work stroke states. The definition of the Huxley-Simmons equations was such that the two states were exactly equally populated at t_0 . No such restriction is placed on this stochastic model, with the result that the actual steady

state populations are dependent on the relative positions of the two free energy parabolas.

The insect fibrillar flight muscle T_2 curve plotted in Figure 6.1d not only has a negative gradient across the vertical axis but is also demonstrates a larger amplitude of phase 2 on release in relative to stretch. The interpretation of the shape of this T_2 curve based on the Huxley-Simmons equations was that insect muscle must have a larger amplitude working stroke to account for the negative gradient where the curve crosses the vertical axis. Unfortunately this mathematical modelling could not produce an accurate description of the T_2 curve since the Huxley-Simmons equations are limited to the assumption of equal populations of the 90° and 45° states, forcing symmetry in the amplitude of phase 2 on stretches and releases. In the stochastic model, it is the 9nm work-stroke T_2 curve that best matches that seen in insect flight muscle. This T_2 curve reproduces not only the negative gradient of the T_2 at the vertical axis but also the asymmetry of the T_2 curve.

However, it is important to note that the shape of the T_2 curve is determined not only by the relative displacement of the free energy parabolas along the distortion axis, as defined by the amplitude of the work-stroke. The shape of the parabolas, determined by cross-bridge stiffness, and the vertical position of the curves, determined by the chemical free energy of each state, also play a role. For this reason an increase in the cross-bridge stiffness could also explain the negative T_2 gradient observed in the insect flight muscle, though it is not clear whether this would also result in the asymmetry of the populations of the two states.

The apparent difference in T_1 gradient is due to the fact that all the plots are normalised to their own T_0 value. If plotted relative to the same T_0 , all the T_1 curves have the same gradient. The T_0 of the curve where $h=6\text{nm}$, is approximately twice that of the curve where $h=9\text{nm}$. Although the numbers of attached cross-bridges remains roughly the same, in the 6nm case most cross-bridges are in the 45° state whereas in the 9nm simulation most attached cross-bridges occupy the lower force producing 90° state.

Secondly it is important to note that these T_1 curves describe the tension value 100ns after the length change. For this reason the change in tension contributed by the weak binding AM.ADP.Pi will cause an increase in the T_1 gradient that is impossible to measure in real fibres.

The mechanical rate constant for phase 2 (fit using a least squares procedure) is plotted against the imposed step size in Figure 7.12b. The shape of this curve is similar to that observed in single fibre experiments (Huxley and Simmons, 1971; Chapter 6, Figure 6.4).

The rate constant is the sum of the forward and backward rate constants of the work stroke step. The range of distortions where the model work stroke rate constants influence that of phase 2 depends on both the size of the imposed step and its direction. For a step stretch the mechanical rate constant observed for phase 2 is due to the value of the reverse work stroke rate constant (AM.ADP 45° state to AM*.ADP.Pi 90° state) in the region $x \geq 7.5\text{nm}$. This is the range in which 45° cross-bridges will move into the 90° state, causing the observed tension drop. On releases the forward work stroke rate constant at distortion values $x \leq 7.5\text{nm}$ will influence the mechanically observed rate constant.

Like muscle tension transients, the model phase 2 is best fit using more than one exponential function. This is because the cross-bridges are redistributing among the 45° and 90° states at very different rates depending on their distortion.

Since in muscle r_2 changes little with increasing size of step stretch, the reverse work stroke rate constant was made independent of distortion. This results in a very highly distortion dependent forward work stroke rate constant.

Given the definitions of the free energy profiles used in the model, it is only with this type of relationship that it is possible to reproduce the r_2 -step size characteristics observed in muscle. Similar rate constants are defined by Eisenberg *et al* (1980), their model also reproduces the r_2 -step size characteristics. The complex work stroke rate constants of Pate and Cooke (1989) will not reproduce this relationship. Their rate constants would produce an r_2 that is fast on releases, faster still on stretch with the slowest transients close to the zero step size axis.

7.6.2 Step length changes

When defining the rate constants in the model, considerable attention was paid to those which would give rise to realistic phases 3 and 4 in the tension transients. That the model can reproduce these phases can be seen in the tension transients shown in Figure 7.10a, and in more detail for a single step release in Figure 7.11.

Following the 4nm step release, almost all cross-bridges that were in the AM*.ADP.Pi state move into the AM.ADP 45° state (500μs in Figure 7.11), producing the phase 2. In order to produce a phase 3 and 4 at this stage, these force producing cross-bridges must detach faster than new cross-bridges can bind and restore the original tension. This is accomplished by making the rate constant for the isomerisation step AM.ADP.Pi to AM*.ADP.Pi slow relative to the ADP off rate constant of the low distortion AM.ADP cross-bridges.

Following a stretch, 45° cross-bridges are forced into 90° state. Due to the high distortion of these cross-bridges, the mechanism for producing phases 3 and 4 cannot be the same as that for release. For the cross-bridges at the high distortions in the 90° state, detachment must occur via the reverse isomerisation step (AM*.ADP.Pi to AM.ADP.Pi), since the hydrolysis path is energetically unfavourable. Since the forward isomerisation step is more rapid, new cross-bridges bind and create force (phase 3) more quickly than these high distortion 90° cross-bridges detach (phase 4).

Since these phases are due to different processes on stretch and release the rate constants are sensitive to step direction Figure 7.12. The relationship of these rate constants with step size is very similar to that observed in insect fibrillar flight muscle (see Chapter 6, Figures 6.4, 6.8 & 6.9) and has also been demonstrated in synchronous insect flight muscle (see Chapter 6, Figure 6.3). Note that in the latter figure stretches up to 3.5% in amplitude are included. Assuming a sarcomere length of 2.6μm, the model step range of -6.5nm to +8nm is equivalent to the range -0.5% to +0.6% in this figure.

The observed rate constant for phase 4 on release and phase 3 on stretch are both determined by the same rate constant in the model, namely the isomerisation step AM.ADP.Pi to AM*.ADP.Pi. The observed rate constants for phase 3 on stretch and phase 4 on release are of similar value in insect fibrillar flight muscle (see Chapter 6, Figures 6.3, 6.8 & 6.9).

7.6.3 Muscle shortening and ATPase

The model shows the right characteristic shape of force-velocity curve, including the reduced gradient close to zero velocity. Two rate constants in the system affect the value of V_{max} . Firstly the ADP off rate constant defines how quickly low distortion (low or negative force producing cross-bridges) can detach via the hydrolysis route. Secondly the forward isomerisation rate constant affects the rate at which the higher force producing cross-bridge distortions can be occupied by newly attached cross-bridges.

The model ATPase is measured by counting the total number of cross-bridges stepping from AM and M states to the AM.ATP and M.ATP states. Cross-bridges performing the opposite step are subtracted from this total. In this way the model ATPase reflects the rate of loss of ATP from solution. The total ATP count is accumulated and plotted every 5ms (or every iteration if this is longer). This maximum plot frequency is set due to noise in the plot when higher plot rates are used. The value of ATPase shown (s^{-1}) is corrected for the total number of cross-bridges in the model.

The majority of cross-bridges in the model are in the M.ADP.Pi state, since they are at distortions where attachment is unfavourable. This is a model limitation due to the fact that only one actin site is considered for each cross-bridge. This is probably unrealistic, since in muscle a cross-bridge may have a choice of more than one actin site, possibly on more than one actin filament. For this reason the model isometric ATPase has a lower value than that of muscle ($0.8s^{-1}$).

At the onset of shortening at V_{max} (from steady state), there is a burst of high ATPase peaking at approximately 30 times the steady state value. This reflects the rapid loss of cross-bridges from the force producing states as they detach via the hydrolysis route. Once tension has reached its new value, the ATPase remains considerably high, a factor of 6 greater than the steady state value. Such a large increase in ATPase is not observed in muscle (Kushmerick and Davies, 1969). This larger increase in ATPase on shortening is a feature of all models in which the cross-bridge must pass through the AM then AM.ATP states before detaching during shortening.

The staircase of 4nm step releases of 8ms duration shown in Figure 7.14, shows that the model is not capable of reproducing the tension transients observed by Lombardi *et al* (1992). If the model is to reproduce these transients, the rate constant for the isomerisation step AM.ADP.Pi to AM*.ADP.Pi must be made considerably faster in the region of distortions $7nm \leq x \leq 11nm$. This would allow new cross-bridges to attach quickly and go through the work stroke step.

It has been demonstrated by Chen and Brenner (1993) that the model of Eisenberg *et al* (1980) is capable of reproducing the Lombardi staircase result without modification to any of the rate constants. This is because in this model cross-bridge attachment is very rapid (the rate constant α_{NI} in the range $60\text{\AA} \leq x \leq 100\text{\AA}$), and cross-bridges attach directly into the 90° state of the work stroke.

If this modification were made to the model described here, the Lombardi result could be repeated. However this would be at the expense of the accurate reproduction of phases 3 and 4 in the model. Note that the Eisenberg model will not produce a phase 3 on stretch or release. Also the Eisenberg model phase 4 will be unrealistically fast on both step stretches and releases.

If a slow step occurs between cross-bridge attachment and the work stroke step in muscle, how could the Lombardi result come about? One possible mechanism could be that cross-bridges in the 45° state of the working stroke can “slip” to a more energetically favourable actin site during rapid shortening (Brenner, 1990). Such a step would by-pass ATP hydrolysis, which could also reduce the model’s high ATPase observed during shortening.

7.6.4 Stretch activation

The model is able to reproduce the high amplitude and maintained rise of tension in phase 3 observed in insect fibrillar flight muscle in two ways. Firstly using a non-uniform distortion distribution (Wray, 1979b) and secondly by linking the free energy of all attached states to the value of the muscle strain.

In both models the starting tension is much lower than the isometric tension observed in the vertebrate skeletal muscle model (the default mode of operation of the model). In the Wray model this is achieved by starting with the majority of cross-bridges at distortions where attachment is unlikely. In the strain dependent model, the model is at a steady state at -3nm strain before the step is applied. Due to the method of activation of this model, a starting strain of -3nm results in the free energy of all attached states (at all distortions) being 0.3RT higher relative to the default model values. The applied 3nm step restores the free energy of all attached states to the default model values, so the delayed tension rise is similar to the initial activation observed in the skeletal muscle model.

The non-uniform distortion distribution in the Wray model restricts the range over which delayed tension rises can be observed. When a second 6nm stretch is applied following the delayed tension rise seen in Figure 7.15, a large amplitude phase 2 followed by a phase 4 takes the tension level close to that observed before the first stretch. No phase 3 is present in this second step due to the rate at which cross-bridges are detaching. The relaxed stiffness in insect fibrillar flight muscle (not incorporated into the model) would not be sufficient to mask out periodic changes steady state tension that would be observed if this type of distortion distribution were present in insect fibrillar flight muscle.

In typical insect fibrillar flight muscle fibre preparations a staircase of four or five 1% stretches will each result in a delayed tension rise. Of the two stretch

activation models described here, only the strain dependent model can repeat this result.

Neither of the models produce a phase 4 like that seen in insect fibrillar flight muscle. Following a stretch in low phosphate conditions (such as in this model) insect fibrillar flight muscle shows a large amplitude phase 3 and a phase 4 that can be more than half the amplitude of the phase 3.

The phase 4 following a stretch observed in the model tension records shown in Figure 7.10 is a consequence of high distortion cross-bridges in the $AM^*.ADP.P_i$ 90° state detaching after slowly going through the reverse isomerisation step to $AM.ADP.P_i$. In these records the phase 4 is caused by cross-bridges that were attached before the length change occurs. Because only a very small proportion of cross-bridges are attached before stretch in both stretch activation mechanisms modelled here, any phase 4 observed will be very small. In the transients shown here phase 4 is not detectable in the noise of the tension signal.

This suggests that in muscle the phase 4 following stretch activation is due to a process that is affecting the larger population of newly attached cross-bridges, rather than a redistribution of the those attached before the stretch. A very likely candidate for this is a build up of P_i in the fibre. The increase in ATPase due to the stretch activation causes P_i to be produced faster than it can diffuse out of the filament lattice.

7.6.5 Future work

Some parameters in the model need to be adjusted. Firstly the energy provided by ATP is currently too high. Secondly, and more importantly the cross-bridge stiffness and work-stroke values in the model are higher than the values suggested by measurements made using optical tweezers. These experiments suggest a value of cross-bridge stiffness not less than 0.38pN/nm (Molloy *et al*, 1995), although a stiffness value greater than 1pN/nm seems unlikely. Also the cross-bridge work stroke may be as low as 5nm.

The model results described here have concentrated on the tension response to mechanical length changes. There has been no attempt to model the effects of changing any of the ligand concentrations, even though the program already contains the code to modify the energy profiles of each state depending on the concentrations of ATP, ADP and P_i . Modelling the tension transients due to the rapid release of caged compounds (ATP and P_i) would allow the chemical state of the mechanical states in the system to be refined further.

The effect of P_i on the mechanical characteristics of insect fibrillar flight muscle described in chapter 6 poses a particularly interesting problem which could be investigated using this model. That increasing P_i seems to reduce the number of attached cross-bridges while not affecting r_2 suggests that the P_i release step occurs before force generation. This affect could be reproduced in the model by replacing the isomerisation step of newly attached cross-bridges with the P_i release step, and making the force producing step an isomerisation event. This would reproduce changes in the stretch values of A_3 and r_4 that occur with increasing P_i . However if P_i release occurred early in the attachment pathway some of the P_i effects would not be reproduced. The increase in stretch r_3 with increasing P_i would not occur. Also, the release kinetics of phases 3 and 4 would not be sensitive to P_i concentration, though in insect flight muscle they are clearly altered by P_i . The effects of P_i on the mechanical characteristics of insect fibrillar flight muscle are clearly complex. It may be the case that a model structure such as this is not able to reproduce all of the effects of P_i , without taking into account factors such as ligand diffusion rates into and out of the fibre.

References

- ABBOTT, R. H. & CAGE, P. E. (1978). Periodicity in insect flight muscle stretch activation. *Journal of Physiology* **289**, 32P-33P.
- AUBER, J. & COUTEAUX, R. (1963). Ultrastructure de la strie Z dans des muscles de diptères. *Journal de Microscopie* **2**, 309-324.
- BRENNER, B., CHALOVICH, J. M., GREENE, L. E., EISENBERG, E. & SCHOENBERG, M. (1986). Stiffness of skinned rabbit psoas fibers in MgATP and MgPP_i solution. *Biophysical Journal* **50**, 685-691.
- BRENNER, B. (1990). Muscle mechanics and biochemical kinetics. In *Topics in Molecular and Structural Biology 13: Molecular Mechanisms in Muscle Contraction*, ed. Squire, J.M., pp77-149. Macmillan Press Ltd.
- BULLARD, B. (1984). A large troponin in asynchronous insect flight muscle. *Journal of muscle Research and Cell Motility* **5**, 196.
- BULLARD, B., LEONARD, K., LARKINS, A., BUTCHER, G., KARLIK, C. AND FYRBERG, E. (1988). Troponin of Asynchronous Flight Muscle. *Journal of Molecular Biology* **204**, 621-637.
- CHIANG, A. C. (1984). *Fundamental methods of mathematical economics; 3rd ed. International student edition*. McGraw-Hill.
- CULLEN, M. J. (1974). The distribution of asynchronous muscle in insects with particular reference to the hemiptera: an electron microscope study. *Journal of Entomology*, **49**, 17-41.
- DANTZIG, J. A., GOLDMAN, Y. E., MILLAR, N. C., LACKTIS, J., & HOMSHER, E. (1992). Reversal of the cross-bridge force generating transition by photogeneration of phosphate in rabbit psoas muscle fibres. *Journal of Physiology* **451**, 247-278.
- DREW, K. (1984). Control of muscle experiments using the I.B.M. personal computer. M.Sc. thesis (York).
- EISENBERG, E., HILL, T. L., & CHEN, Y. (1980). Cross-bridge model of muscle contraction. Part I. *Biophysical Journal* **29**, 195-227.
- FABIATO, A. & FABIATO, F. (1975). Dependence of the contractile activation of skinned cardiac cells on the sarcomere length. *Nature* **256**, 54-56.

- FORD, L. E., HUXLEY, A. F. & SIMMONS, R. M. (1977). Tension responses to sudden length change in stimulated frog muscle fibre near slack length. *Journal of Physiology* **269**, 441-515.
- GOLL, D. E., DAYTON, W. R., SINGH, I. & ROBSON, R. M. (1991). Studies of the α -Actinin/Actin interaction in the Z-disk by using calpain. *Journal of Biological Chemistry* **266**, 8501-8510.
- GORDON, A. M., HUXLEY, A. F. & JULIAN, F. J. (1966). The variation in isometric tension with sarcomere length in vertebrate muscle fibres. *Journal of Physiology* **184**, 170-192.
- GRANZIER, H. L. M. & WANG, K. (1993a). Interplay between passive tension and strong and weak binding cross-bridges in insect indirect flight muscle. *Journal of General Physiology* **101**, 235-269.
- GRANZIER, H. L. M. & WANG, K. (1993b). Passive tension and stiffness of vertebrate skeletal muscle and insect flight muscles: the contribution of weak cross-bridges and elastic filaments. *Biophysical Journal* **65**, 2141-2159.
- HAEBERLE, J. R., COOLICAN, S. A., EVAN, A. & HATHAWAY, D. R. (1985). The effects of a calcium dependent protease on the ultrastructure and contractile mechanics of skinned uterine muscle. *The Journal of Muscle Research and Cell Motility* **6**, 347-363.
- HIBBERD, M. G., DANTZIG, J. A., TRENTHAM, D. R. & GOLDMAN, Y. E. (1985). Phosphate release and force generation in skeletal muscle fibers. *Science* **228**, 1317-1319
- HILL, A. V. (1938). The heat of shortening and the dynamic constants of muscle. *Proceedings of the Royal Society of London, Series B* **126**, 136-195.
- HILL, T. L. (1974). Theoretical formalism for the sliding filament model of contraction of striated muscle. Part I. *Progress in Biophysics and Molecular Biology* **28**, 267-339.
- HUXLEY, A. F. (1957). Muscle structure and theories of contraction. *Progress in biophysics and Biophysical Chemistry* **7**, 255-318.
- HUXLEY, A. F. & LOMBARDI, V. (1980). A sensitive force transducer with resonant frequency of 50kHz. *Journal of Physiology* **305**, 15-16P.
- HUXLEY, A. F. & NIEDERGERKE, R. M. (1954). Interference microscopy of living muscle fibres. *Nature* **173**, 973-976.

- HUXLEY, A. F. & SIMMONS, R. M. (1971). Proposed mechanism of force generation in striated muscle. *Nature* **233**, 533-538.
- HUXLEY, H. E. (1953). Electron microscope studies of the organisation of the filaments in striated muscle. *Biochimica et Biophysica Acta* **12**, 387-394.
- JEWELL, B. R. & RÜEGG, J. C. (1966). Oscillatory contraction of insect fibrillar muscle after glycerol extraction. *Proceedings of the Royal Society of London, Series B*, **164**, 428-459.
- KABSCH, W., MANNHERZ, H. G., SUCK, D., PAI, E. F., & HOLMES, K. C. (1990). Three dimensional structure of the complex of skeletal muscle actin and bovine pancreatic DNase 1 at 6A resolution *Nature*, **347**, 37-44.
- KARLIK, C. C. MAHAFFREY, J. W., MICHELLE, D.C. & FYRBERG, E.A. (1984). Organisation of contractile protein genes within the 88F subdivision of the *D. melanogaster* third chromosome. *Cell* **37**, 469-481.
- KAWAI, M & BRANDT, P. W. (1980). Sinusoidal analysis: a high resolution method for correlating biochemical reactions with physiological processes in activated skeletal muscles of rabbit, frog and crayfish. *Journal of Muscle Research and Cell Motility* **1**, 279-303.
- KUSHMERICK, M. J. & DAVIES, R. E. (1969). The chemical energetics of muscle contraction. II. The chemistry, efficiency, and power of maximally working sartorius muscles. *Proceedings of the Royal Society (London), Series B* **174**, 315-353.
- LAEMMLI, U. K. (1970). Cleavage of structural proteins during the assembly of the head of bacteriophage T4. *Nature*, **227**, 680-682.
- LAKEY, A, FERGUSON, C, LABEIT, S, REEDY, M, LARKINS, A, BUTCHER, G, LEONARD, K, BULLARD, B (1990). Identification and localisation of high molecular weight proteins in insect flight and leg muscle. *Embo (European Molecular Biology Organisation) Journal* **9**(11): 3459-3468.
- LEHMAN, W. (1977). The dual system of calcium activation in arthropod muscles. In: *Insect Flight Muscle* edited by R. T. Tregear. Amsterdam, North Holland, p. 277-283.
- LOMBARDI, V. PIAZZESI, G. & LINARI, M. (1992). Rapid regeneration of the actin-myosin power stroke in contracting muscle. *Nature* **355**, 638-641.
- LOVELL, S. J., KNIGHT, P. J. & HARRINGTON, W. F. (1981). Fraction of myosin heads bound to thin filaments in rigor fibrils from insect flight and vertebrate muscles. *Nature* **293**, 664-666.

- LYMN, R. W. & TAYLOR, E. W. (1971). Mechanism of Adenosine Triphosphate Hydrolysis by Actomyosin. *Biochemistry* **10**, 4617-4623.
- LUND, J., WEBB, M. R. & WHITE, D. C. S. (1987). Changes in the ATPase activity of insect fibrillar flight muscle during calcium and strain activation probed by phosphate-water oxygen exchange. *Journal of Biological Chemistry* **262**, 8584-8590.
- MARQUARDT, D. W. (1963). An algorithm for least squares estimation of nonlinear parameters. *Journal of the Society for Industrial and Applied Mathematics* **2**, 431-441.
- MELLONI, E. & PONTREMOLI, S. (1991). The calpain-calpastatin system: structural and functional properties. *Journal of Nutritional Biochemistry* **2**, 467-476.
- MOGAMI, K., FUJITA, S. C. & HOTTA, Y. (1982). Identification of *Drosophila* indirect flight muscle myofibrillar proteins by means of two-dimensional electrophoresis. *Journal of Biochemistry* **91**, 643-650.
- MOLLOY, J. E. (1988). Active insect fibrillar flight muscle, its mechanical performance and cross-bridge kinetics. D.Phil thesis, (York).
- MOLLOY, J. E., KYRTATAS, V., SPARROW, J. C. & WHITE, D. C. S. (1987). Kinetics of flight muscles from insects with different wingbeat frequencies. *Nature* **328**, 449-451.
- MOLLOY, J. E., BURNS, J. E., KENDRICK-JONES, J., TREGGAR, R. T. & WHITE, D. C. S. (1995). Force and movement produced by a single myosin head. *Nature* submitted.
- NEWMAN, R., BUTCHER, G. W., BULLARD, B. & LEONARD, K. R. (1992). A method for determining the periodicity of a troponin component in isolated insect flight muscle thin filaments by gold/Fab labelling. *Journal of Cell Science* **101**, 503-508.
- PARDUE, M. L., AYME-SOUTHGATE, A., VIGOREAUX, J., SAIDE, J., & BENIAN, G. (1993). Projectin, flightin and MP20: three "new" proteins associated with the contractile apparatus. *Biophysical Journal* **64**, A1.
- PATE, E. & COOKE, R. (1989). A model of crossbridge action: the effects of ATP, ADP and P_i. *Journal of Muscle Research and Cell motility* **10**, 181-196.
- PECKHAM, M., CRIPPS, R., WHITE, D. & BULLARD, B. (1992) Mechanics and protein content of insect fibrillar flight muscle. *Journal of Experimental Biology* **168**, 57-76.

- PENNYCUIK, C. J. & REZENDE, M. A. (1984). The specific power output of aerobic muscle, related to the power density of the mitochondria. *Journal of Experimental Biology*, **108**, 377-392.
- PERRIN, D. D. & SAYCE, I. G. (1967). Computer calculation of equilibrium concentrations in mixtures of metal ions and complex species. *Talanta*, **14**, 833-842.
- PHILLIPS, D. R. & JAKÁBOVÁ, M. (1977). Ca²⁺-dependent protease in human platelets. *The Journal of Biological Chemistry* **252**, 5602-5605.
- PODOLSKY, R. J., NOLAN, A. C., & ZAVELER, S. A. (1969). Cross-bridge properties derived from muscle isotonic velocity transients. *Proceedings of the National Academy of Sciences (USA)* **64**, 504-511.
- PROVENCHER, S. W. (1976). An eigenfunction expansion method for the analysis of exponential decay curves. *The Journal of Chemical Physics* **64**, 2772-2777.
- RAYMENT, I., RYPNIEWSKI, W. R., SCHMIDT-BASE, K., SMITH, R., TOMCHICK, D. R., BENNING, M. M., WINKELMANN, D. A. & HOLDEN, H. M. (1993). Three-Dimensional structure of myosin subfragment-1: A molecular motor. *Science*, **261**, 50-57.
- REDDY, M. K., ETLINGER, J. D., RABINOWITZ, M., FISCHMAN, D. A. & ZAK, R. (1975). Removal of Z-lines and alpha-actinin from isolated myofibrils by a calcium-activated neutral protease. *Journal of Biological Chemistry* **250**, 4278-84.
- REEDY, M. K. (1968). Ultrastructure of insect flight muscle. *Journal of Molecular Biology*, **31**, 155-176.
- REEDY, M. C., BULLARD, B., LEONARD, K. & REEDY, M. K. (1991). Localisation of troponin components in insect flight muscle. *Journal of muscle research and Cell Motility* **12**, 112.
- REEDY, M. K., LEONARD, K. R., FREEMAN, R. AND ARAD, T. (1981). Thick myofilament mass determination by electron scattering measurements with the scanning transmission electron microscope. *Journal of Muscle Research and Cell Motility* **2**, 45-64.
- RÜEGG, J. C., STEIGER, G. J. & SCHÄDLER, M. (1970). Mechanical activation of the contractile system in skeletal muscle. *Pflug. Arch. ges. Physiol.* **319**, 139-145.

- RÜEGG, J. C., TREGGAR, R. T. (1966). Mechanical factors affecting the ATPase activity of glycerol extracted insect fibrillar muscle. *Proceedings of the Royal Society of London, Series B.* **165**, 497-512.
- SAIDE, J. D., CHIN, BOW, S., HOGAN, SHELDON, J., BUSQUETS, TURNER, L. (1990). Z-band proteins in the flight muscle and leg muscle of the honeybee. *Journal Of Muscle Research And Cell Motility* **11**(2), 125-136.
- SAVITZKY, A. & GOLAY, M. J. E. (1964). Smoothing and differentiation of data by simplified least squares procedures. *Analytical Chemistry* **36**, 1627-1639.
- SCHÄDLER, M. STEIGER, G. J., & RÜEGG, J. C. (1971). Mechanical activation and isometric oscillations in insect fibrillar muscle. *Pflügers Arch.* **330**, 217-229.
- SCHREINER, W., KRAMER, M., KRISCHER, S. & LANGSAM, Y. (1985). Nonlinear least-squares fitting. *PC Technical Journal*, May issue, 170-190.
- SQUIRE, J. M. (1992). Muscle filament lattices and stretch activation: the match mismatch model reassessed. *Journal of Muscle Research and Cell Motility* **13**, 183-189.
- STEIGER, G. J. (1971). Stretch activation and myogenic oscillation of isolated contractile structures of heart muscle. *Pflügers Archiv. ges. Physiol.* **330**, 347-361.
- STEIGER, G. J. (1977). Stretch activation and tension transients in cardiac, skeletal and insect flight muscle. In *Insect Flight Muscle: Proceedings of the Oxford Symposium.* (ed. R. T. Tregear). pp221-268. Amsterdam: North Holland.
- STEIN, L. A., SCHWARZ, R. P., CHOCK, P. B., & EISENBERG, E. (1979). Mechanism of actomyosin adenosine triphosphatase. Evidence that Adenosin 5'-triphosphate hydrolysis can occur without dissociation of the actomyosin complex. *Biochemistry* **18**, 3895-3909.
- STEINIER, J., TERMONIA, Y. & DELTOUR J. (1972). Comments on smoothing and differentiation of data by simplified least square procedure. *Analytical Chemistry* **44**, 1906-1909.
- STEPHENSON, D. G. & WENDT, I. R. (1984). Length dependence of changes in sarcoplasmic calcium concentration and myofibrillar calcium sensitivity in striated muscle fibres. *Journal of Muscle Research and Cell Motility* **5**, 243-272.
- TAWADA, K. & KAWAI, M. (1990). Covalent cross-linking of single fibres from rabbit psoas increases oscillatory power. *Biophysical Journal* **57**, 643-647.

- THORSON, J. AND WHITE, D. C. S. (1969). Distributed representations for actin-myosin interaction in the oscillatory contraction of muscle. *Biophysics Journal* **9**, 360-390.
- TSUJI, S. & IMAHORI, K. (1981). Studies on the Ca²⁺-activated neutral proteinase of rabbit skeletal-muscle. 1. The characterisation of the 80K and the 30K subunits. *Journal of Biochemistry* **90**, 233-240.
- WANG, K. & WRIGHT, J. (1988). Architecture and the sarcomere matrix of skeletal muscle: immunoelectron microscopic evidence that suggests a set of parallel inextensible nebulin filaments anchored at the Z-line. *Journal of Cell Biology* **107**, 2199-2212.
- WANG, K., MCCARTER, R., WRIGHT, J. BEVERLY, J. & RAMIREZ-MITCHELL, R. (1993). Viscoelasticity of the sarcomere matrix of skeletal muscles. *Biophysical Journal* **64**, 1161-1177.
- WEEDS, A. G., POPE, B. (1977). Studies on the chymotryptic digestion of myosin. Effects of divalent cations on proteolytic susceptibility. *Journal of Molecular Biology* **111**, 129-157.
- WHITE, D. C. S. (1983). The elasticity of relaxed insect fibrillar flight muscle. *Journal of Physiology*, **343**, 31-57.
- WHITE, D. C. S. & DONALDSON M. M. K. (1975). Mechanical and biochemical cycles in muscle contraction. *Energy Transformation in Biological Systems (Ciba Foundation Symposium)* pub. ASP, Amsterdam pp. 341-353.
- WHITE, D. C. S. & THORSON, J. (1972). Phosphate starvation and the nonlinear dynamics of insect fibrillar flight muscle. *The Journal of General Physiology* **60**, 307-336.
- WRAY, J. S. (1979a). Structure of the backbone in myosin filaments of muscle. *Nature* **277**, 37-40.
- WRAY, J. S. (1979b). Filament geometry and the activation of insect flight muscles. *Nature* **280**, 325-326.
- ZAMAN, A. & MARSAGLIA, G. (1991). A new class of random number generators. *Annals of Applied Probability* **6**, 462-480.

**THESIS
CONTAINS
TAPE
CASSETTE**

**PLEASE CONTACT THE
UNIVERSITY IF YOU WISH TO
SEE THIS MATERIAL.**